ACTIVE AND PASSIVE TUMOR TARGETING VIA MICELLAR DENDRITIC CONSTRUCTS

by

Burcu Sümer Bolu

B.S., Chemistry, Boğaziçi University, 2006

M.S., Chemistry, Boğaziçi University, 2009

Submitted to the Institute for Graduate Studies in
Science and Engineering in partial fulfillment of
the requirements for the degree of
Doctor of Philosophy

Graduate Program in Chemistry

Boğaziçi University

ACTIVE AND PASSIVE TUMOR TARGETING VIA MICELLAR DENDRITIC CONSTRUCTS

APPROVED BY:

Assoc. Prof. Rana Sanyal ……

(Thesis Supervisor)

Prof. Amitav Sanyal ……

(Thesis Co-Advisor)

Prof. İlknur Doğan ……

Assoc. Prof. Devrim Gözüaçık ……

Prof. Sevgi Güngör ……

Prof. Nesrin Özören ……

DATE OF APPROVAL: 14.06.2017

ACKNOWLEDGEMENTS

First and foremost I would like to thank my thesis supervisors Assoc. Prof. Rana Sanyal and Prof. Amitav Sanyal for accepting me into their lab, introducing me to the magnificient world of nanochemistry, helping me through my research whenever I am stuck and shaping me into a scientist who's hoping to produce inspiring work as theirs one day.

I would like to extend my thanks to my thesis advisors and members of my thesis committee Prof. İlknur Doğan, Prof. Fethi Şahin, Prof. Nesrin Özören, Prof. Sevgi Güngör and Assoc. Prof. Devrim Gözüaçık for their careful and constructive review of the final manuscript.

I would like to express my gratitude to all of my lab mates as well as my family.

Finally I would also want to thank the graduate scholarship program by The Scientific and Technological Research Council of Turkey (TÜBİTAK) (2211-D) for supporting me during my PhD education. I would like to thank TUBITAK, Scientific and Technological Research Council of Turkey (Project 107T623), and BU/BAP, Bogazici University Scientific Research Fund (Project 8252) for contributing the funding and resources contributed to this thesis.

ABSTRACT

ACTIVE AND PASSIVE TUMOR TARGETING VIA MICELLAR DENDRITIC CONSTRUCTS

Among many other nanotherapeutics, polymeric micellar systems are emerging as a very important class of nano-pharmaceuticals due to their ability to improve pharmacokinetics and bio-distribution of chemotherapy drugs as well as to reduce related systemic toxicities. In this thesis three such systems are presented in terms of synthesis, characterization and *in vitro* activity. In the first one, drug conjugated micellar constructs are fabricated using triblock dendron-polymer conjugates where a hydrophilic linear polyethylene glycol (PEG) chain is flanked by well-defined hydrophobic biodegradable polyester dendrons bearing an anti-angiogenic drug, combretastatin-A4 (CA4). Variation in dendron generation is utilized to obtain a library of micellar constructs with varying sizes and drug loadings. For the second project a cRGDfK targeting group was introduced to micelle shell to achieve active targeting cancer cells over-expressing αυβ3/αυβ5 integrins. Non-toxic, biodegradable, and modularly tunable micellar delivery systems were generated using two dendron-polymer based components. Either an AB type dendron-polymer construct or an ABA type dendron-polymer-dendron conjugate was used as primary construct; along with an AB type dendron-polymer containing a cRGDfK targeting group. In the final section another micellar delivery system was generated with conjugated Trastuzumab antibody which is used as treatment against tumor cells expressing HER2 receptors. Incorporation of this therapeutic antibody to nano drug delivery systems can improve its target specificity further. As a result three systems were generated with different drug release profiles ranging between days to hours depending on loading strategy. Polyester dendron cores rendered them acid labile as well as stable in terms of CMC. Their sizes were in the range of EPR controllable by core components as needed. Furthermore complex targeting groups were introduced to improve the cell uptake profiles further. In conclusion generated micellar platforms exhibited suitable physical and biological characteristic indicating their potential as drug delivery systems.

ÖZET

MİSEL OLUŞTURAN DENDRİTİK YAPILARLA AKTİF VE PASİF TÜMÖR HEDEFLEME

Polimerik misellerden oluşan ilaç taşıyıcı sistemler taşıdıkları ilaçlarının farmakokinetik özelliklerini ve biyodağılımlarını iyileştirilebildikleri için önemli bir nano-farmasötik sınıfı olarak öne çıkmaktadırlar. Bu tezdeyse üç farklı misel sisteminin sentez, karakterizasyon ve *in vitro* aktiviteleri sunulmuştur. Birinci sistemde ilaç konjuge edilmiş misel yapılar triblock dendron-polimer-dendron konjugatları kullanılarak oluşturulmuştur. Bu konjugatlarda hidrofilik lineer polietilen glikol zincirlerinin her iki tarafına anti-anjiojenik combretastatin-A4 ilacı taşıyan, iyi tanımlı, hidrofobik, biyobozunur, polyester dendronlar bağlanmıştır. İkinci projedeyse bir cRGDfK hedefleyici grubu miselin yüzeyine bağlanarak αvβ3/αvβ5 integrinlerini aşırı ekpresse eden tümör hücrelerinin aktif olarak hedeflenmesi planlanmıştır. Yine toksik olmayan, biyobozunur ve moduler olarak değiştirilmeye uygun bir miselli taşıma sistemi iki tür dendron-polimer bileşeni kullanılarak üretilmiştir. Birincil tür olarak ya AB tipinde dendron-polimer ya da ABA tipinde dendron-polimer-dendron kullanılmıştır. İkincil tür olaraksa cRGDfK hedefleyici grubu içeren AB tipindeki dendron-polimer kullanılmıştır. Son projedeyse HER2 reseptörünü ekspres eden tümörlerin tedavisinde kullanılan Trastuzumab antikoru konjuge edilmiş bir misel yapılı taşıma sistemi geliştirilmiştir. Bu terapötik antikorun nano ilaç taşıma sistemine eklenmesiyle bu sistemin hedef spesifisitesi daha da arttırılmıştır. Sonuç olarak bu tezde ilaç salım dinamikleri günlerle saatler arasında değişebilen üç farklı misel sistemi geliştirilmiştir. Poliester dendronlar sayesinde sistemler asidik ortama hassas hale getirilmiş ve düşük CMC değerleri sağlanmıştır. EPR etkisinden faydalanmak için uygun olan misel boyutlarının çekirdek yapısına bağlı olarak değiştirebildiği gösterilmiştir. Ayrıca kompleks hedefleyici grupların eklenmesiyle sistemlerin hücre içine alım profilleri iyileştirilmiştir. Sonuç olarak tez kapsamında ilaç taşıma sistemleri için uygun fiziksel ve biyolojik özellikler sergileyen misel platformları üretilmiştir.

TABLE OF CONTENTS

ACKNOWLEDGEMENTS iii
ABSTRACT iv
ÖZET v
TABLE OF CONTENTS vi
LIST OF FIGURES x
LIST OF TABLES xv
LIST OF ACRONYMS/ABBREVIATIONS xvi
1. INTRODUCTION 1
1.1. Advantages of Nanomedicine 1
1.2. Nanomedicine against Cancer 2
1.3. Nanoparticle Design for Successful Systemic Drug Delivery to Tumors 7
1.4. Effect of PEGylation 8
1.5. Commonly used Polymer in DDS Platforms 11
1.6. Effect of Nanoparticle Design on Pharmacokinetics and Biodistribution 14
1.7. Nanoparticle extravasation and retention in tumor environment 17
1.8. Active Targeting and Cellular Internalization of NPs 24
1.9. Stimuli Responsive Controlled Drug Release 32
1.10. Therapeutic Potential of Polymeric Micelles 35
1.11. Modification Potential of Polymeric Micelles 37
1.12. Dendrimers, Dendrons and Their Conjugates as Nanotherapeutics 47
1.13. Micelles with RGD and Trastuzumab Targeting Groups 54
2. COMBRETASTATIN A-4 CONJUGATED ANTI-ANGIOGENIC MICELLAR DRUG DELIVERY SYSTEMS USING DENDRON-POLYMER CONJUGATES 62
2.1. Introduction 62
2.2. Experimental Section 65
2.2.1. Materials 65
2.2.2. Instrumentation 65
2.2.3. Synthesis and Characterization of G1-PEG (1), G2-PEG (2) and G3-PEG (3) 66

2.2.4. Synthesis and Characterization of Combretastatin-azide (4) 66
2.2.5. Synthesis and Characterization of Comb-G1-PEG (5) 67
2.2.6. Synthesis and Characterization of Comb-G2-PEG (6) 67
2.2.7. Synthesis and Characterization of Comb-G3-PEG (7) 68
2.2.8. Micelle Preparation and Characterization 68
2.2.9. pH Dependent Release of CA4 from Micelles 69
2.2.10. Serum Stability of Comb-G3-PEG micelles 69
2.2.11. Cell Lines 70
2.2.12. *In vitro* Cell Viability Assay 70
2.2.13. Endothelial Cell Tube Formation Assay on HUVECs 71
2.2.14. Nile Red Internalization in HUVECs 71
2.3. Results and Discussion 72
2.3.1. Synthesis and Characterization of Drug-conjugated Dendron-Polymer Conjugates 72
2.3.2. Critical Micelle Concentrations 73
2.3.3. Size and Molecular Weight of Micelles 75
2.3.4. pH Dependent Drug Release from Micelles 76
2.3.5. Determination of *in vitro* Cytotoxicity of Drug Conjugates on HUVECs 77
2.3.6. Micelle Internalization by HUVECs 78
2.3.7. Endothelial Cell Tube Formation Assay on HUVECs 79
2.4. Conclusions 81
3. DESIGNING DENDRON-POLYMER CONJUGATE BASED TARGETED DRUG DELIVERY PLATFORMS WITH A 'MIX-AND-MATCH' MODULARITY 82
3.1. Introduction 82
3.2. Experimental Section 85
3.2.1. Materials 85
3.2.2. Instrumentation 86
3.2.3. Synthesis and Characterization of G4OX 86
3.2.4. Synthesis of Primary Constructs mPEG2K-G4OX (2K) and G4OX-PEG6K-G4OX (6K) 87
3.2.5. Synthesis of cRGDfK by SSPS 87

3.2.6. Synthesis of NHS-PEG3.5K-G4OX 87
3.2.7. Synthesis of cRGDfK-PEG3.5K-G4OX 88
3.2.8. Micelle Preparation 88
3.2.9. Loading of Docetaxel into Micelles 88
3.2.10. Determination of Docetaxel Content 89
3.2.11. Determination of Critical Micelle Concentration (CMC) 89
3.2.12. Determination of Micelle Size and Dilution Stability by DLS 89
3.2.13. Determination of Micelle Size by TEM 90
3.2.14. pH Dependent Docetaxel Release from Micelles 90
3.2.15. Investigation of Serum Stability of Micelles using FRET 90
3.2.16. Cell Lines 91
3.2.17. *In vitro* Cell Viability Assay 91
3.2.18. Cellular Internalization of NR doped Micelles 91
3.2.19. cRGDfK Dependent Cell Binding Assay 92
3.3. Results and Discussion 92
3.3.1. Synthesis and Characterization of Dendron-Polymer Conjugates 92
3.3.2. Generation and Characterization of Micelles Formed from Primary and Secondary Constructs 94
3.3.3. Critical Micelle Concentrations 95
3.3.4. Micelle Size and Stability towards Dilution 97
3.3.5. pH Dependent Docetaxel Release from Micelles 100
3.3.6. *In vitro* Cellular Internalization of Targeted and Non-targeted Micellar Constructs 102
3.3.7. *In vitro* Cellular Viability Assays 104
3.3.8. *In vitro* Cell Viability Assay with Docetaxel Loaded Micelles 105
3.4. Conclusion 107
4. TRASTUZUMAB TARGETED MICELLAR DELIVERY OF DOCETAXEL USING DENDRON-POLYMER CONJUGATES 109
4.1. Introduction 109
4.2. Experimental Section 112
4.2.1. Materials 112
4.2.2. Instrumentation 112
4.2.3. Synthesis and Characterization of G4OX(1) 113

4.2.4. Synthesis of Primary Constructs mPEG2K-G4OX (2) 113
4.2.5. Synthesis of NHS-PEG3.5K-G4OX (3). 114
4.2.6. Preparation of pHrodo Red conjugated Trastuzumab (4) 115
4.2.7. Preparation of non-targeted and trastuzumab targeted micelles..... 115
4.2.8. Loading of Docetaxel into Micelles 116
4.2.9. Determination of Docetaxel Content..... 116
4.2.10. Determination of mabR Content on DPT micelles 116
4.2.11. Determination of Micelle Size and Zeta Potential by DLS 117
4.2.12. pH Dependent Docetaxel Release from Micelles..... 117
4.2.13. Cell Lines. 117
4.2.14. *In vitro* Cell Viability Assay 118
4.2.15. Micelle Internalization via Fluorescence Microscopy 118
4.2.16. Trastuzumab Dependent Cell Binding Assay 119
4.3. Results and Discussion 119
4.3.1. Synthesis and Characterization of Dendron-Polymer Conjugates . 119
4.3.2. Generation and Characterization of DP and DPT Micelles 120
4.3.3. pH Dependent Docetaxel Release from Micelles..... 122
4.3.4. *In vitro* Cell Viability Assay with Docetaxel loaded Micelles..... 123
4.3.5. *In vitro* Cell Viability Assay with Empty Micelles 125
4.3.6. Internalization of DiO loaded DP and DPT micelles 126
4.4. Conclusion 129
5. CONCLUSIONS 130
REFERENCES……. 132
APPENDIX A: ADDITIONAL DATA..... 169

LIST OF FIGURES

Figure 1.1. First approved liposomal drug, Doxil®. 4

Figure 1.2. Albumin bound paclitaxel, Abraxane® as one of the first protein-drug conjugates. 5

Figure 1.3. Polymeric micellar formulation of paclitaxel, Genexol®. 7

Figure 1.4. Advantages of PEG conjugation to biotherapeutics. 9

Figure 1.5. Factors affecting blood circulation and RES interaction 14

Figure 1.6. EPR effect for passive targeting of NPs 18

Figure 1.7. Physiological factors affection NP extravasation and distribution in tumors. 22

Figure 1.8. Effect of active targeting on NP internalization 26

Figure 1.9. Blood Stimuli-responsive controlled drug release 31

Figure 1.10. Micelle formation and design flexibility 35

Figure 1.11. pH dependent micelle dissociation after cell uptake 41

Figure 1.12. Flower micelle formation via triblock copolymers. 46

Figure 1.13. Advantages of polyester dendrons 52

Figure 1.14. Mechanism of action for trastuzumab. 59

Figure 2.1. Schematic illustration of fabrication of drug loaded micellar constructs from dendron-polymer conjugates and their delivery to tumor vicinity. 64

Figure 2.2. Synthesis of CA4 bearing dendron-polymer drug conjugates. 72

Figure 2.3. Pyrene excitation spectrum of G3-PEG micelles. Inset: $I_{338}/_{334}$ *vs.* log[Conc] graph to calculate CMC value. 74

Figure 2.4. (A) CMC and (B) HLB graph of DPD and Comb-DPD series. HLB was calculated by HLB= $20M_P/(M_D+M_P)$. 75

Figure 2.5. (A) Size of micelles from volume distribution by batch mode DLS analysis. (B) TEM image of Comb-G3-PEG micelles. 76
Figure 2.6. CA4 release profiles from Comb-G3-PEG micelles. 77
Figure 2.7. Viabilities of HUVECs treated with drug containing DPD micelles and free drug and EC50 values of individual samples. 78
Figure 2.8. Nile Red internalization by HUVECs. Scale bar 100 µm. 79
Figure 2.9. Anti-angiogenic assay using HUVECs on Matrigel. (A) Number of junctions and (B) total tube lengths between HUVECs C) Representative Matrigel images. 80
Figure 3.1. Schematic illustration of AB type 2K and ABA type 6K micelles with RGD containing secondary construct for improved docetaxel delivery into tumor cells. 85
Figure 3.2. Synthesis of primary constructs mPEG2K-G4OX (2K) and G4OX-PEG6K-G4OX (6K). 93
Figure 3.3. Synthesis of secondary construct cRGDfK-PEG3.5K-G4OX. 95
Figure 3.4. Nile Red emission spectra of 2K (A) and 6K (B) micelles. 96
Figure 3.5. CMC values of 2K and 6K micelles by mg/mL (A), molarity (B) in graphical and in tabular (C) representation. 96
Figure 3.6. Effective size diameters from volume distributionin nm of 2K and 6K micelle sets with or without drug (D) encapsulation A) graphical and B) tabular representation. 97
Figure 3.7. Micelle (A) Z-average size (B) PDI values obtained after serial dilutions and (C) corresponding dilution factors. 98
Figure 3.8. Normalized FRET ratios of 2K (A) and 6K (B) micelles in graphical representation. Final FRET ratios at 30 hours are given in table (C). 99

Figure 3.9. Dry micelles and measured mean micelle diameter values from TEM. Scale bar 200 nm. 100

Figure 3.10. Percent docetaxel release profiles from 2K (A) and 6K (B) micelles in graphical representation. Final release percentages at 30 h are given in table (C). 101

Figure 3.11. Nile Red internalization experiments of NR doped 2K and 6K micelles. Scale bar 50µm. 102

Figure 3.12. Nile Red cell internalization histograms by flow cytometry of doped 2K (A) and 6K (B) micelles and Nile Red dye only at 1 hour. MFI values were presented in (C). 103

Figure 3.13. Cell Viabilities of empty 2K and 6K micelles on A549 (A), and MDA-MB-231 (B) cell lines after 48 hours of continuous incubation. 105

Figure 3.14. Cell Viabilities of Docetaxel loaded 2K and 6K micelles on A549 (A), and MDA-MB-231 (B) cell lines after 48 hours of continuous incubation. 106

Figure 3.15. Cell viabilities of docetaxel loaded 2K and 6K micelles on MDA-MB-231 cell line after 48 hours of continuous incubation (A) and 2+22 (B) hours of pulse chase incubation. 107

Figure 4.1. Trastuzumab targeted delivery of docetaxel via micelles formed from two constructs. 111

Figure 4.2. Synthesis of primary and secondary constructs. 114

Figure 4.3. Synthesis of pHrodo Red dye conjugated trastuzumab 115

Figure 4.4. Preparation of DP and DPT micelles. 119

Figure 4.5. Effective size diameters of DP and DPT micelles A) as histograms, B) in tabular form. 120

Figure 4.6. pH dependent docetaxel release. 122

Figure 4.7. Resulting cell viabilities after 48 h and 2+22 h incubation with micellar and free formulations of docetaxel. 124

Figure 4.8. Cytotoxicity of blank DP and DPT micelles as well as free trastuzumab *in vitro.* 125

Figure 4.9. Internalization of DiO doped DP and DPT micelles by MCF-7 and SK-OV-3 cell lines. Scale bar 25 µm. 127

Figure 4.10. Flow cytometry data of MCF-7 and SK-OV-3 cell lines treated with DiO encapsulated DP and DPT micelles A) in graphical representation and B) in histograms. 128

Figure A.1. The I338/334 *vs.* log Concentration graphs for DPD and Comb conjugated DPD micelles. 170

Figure A.2. (A) SLS result of G3-PEG micelles. (B) PBS-GPC results by MALLS and by in flow mode DLS of G3-PEG micelle solution. 171

Figure A.3. HUVEC cell viabilities of DPDs after 48h continuous treatment. 172

Figure A.4. Nile Red doped micelles containing 100mM and 1mM of G3-PEG,or 100mM G3-PEG polymer and Nile Red added separately without sonication 173

Figure A.5. Serum stability of Comb-G3-PEG micelles. 174

Figure A.6. Free CA4 release profile. 175

Figure A.7. ^{1}H-NMR of mPEG2K-G4OX (2K) and G4OX-PEG6K-G4OX (6K). 176

Figure A.8. ^{1}H-NMR of secondary construct cRGDfK-PEG3.5K-G4OX. 177

Figure A.9. DLS size and histograms of 2K micelles. 178

Figure A.10. DLS size and histograms of 6K micelles. 179

Figure A.11. DLS size and histograms of drug loaded 2K-X micelles. 180

Figure A.12. DLS size and histograms of drug loaded 6K-X micelles. 181

Figure A.13. Effect of secondary construct amount on MDA-MB-231 cell internalization. 182

Figure A.14. MALDI-TOF analysis of A) NHS-PEG3.5K-G4OX, B) trastuzumab and C) trastuzumab-PEG3.5K-G4OX. 183

Figure A.15. Zeta potential A) histograms and B) values 184

Figure A.16. Cell internalization data displaying separate channels. 185

LIST OF TABLES

Table 2.1. Properties of DPD and DPD-Comb Conjugates and their resulting micelles. 73

Table 3.1. Micelle Compositions and Drug Contents. 94

Table 3.2. EC_{50} values of micellar or free docetaxel for A549 and MDA-MB-231 lines. 106

Table 4.1. Zeta potential of DP and DPT micelles. 121

Table 4.2. EC50 values after 48 h incubations. 123

LIST OF ACRONYMS/ABBREVIATIONS

α-SMA	α-Smooth Muscle Actin
ACN	Acetonitrile
Asp	Poly(aspartic Acid)
ATCC	American Type Culture Collection
ATR-FT-IR	Attenuated Total Reflection Fourier Transform Infrared
AUC	Area Under The Curve
bis-MPA	2,2-Bis(Hydroxymethyl) Propionic Acid
BSA	Bovine Serum Albumine
CA4	Combretastatin A4
CAF	Cancer-Associated Fibroblasts
CCK-8	Cell Counting Kit-8
$CDCl_3$	Deuterated Chloroform
CH_2Cl_2	Dichloromethane
CMC	Critical Micelle Concentrations
cRGDfK	Cyclic Arginine-Gylcine-Aspartic acid-Phenyl alanine-Lysine
DAPI	4',6-Diamidino-2-Phenylindole
DCC	*N,N'*-Dicyclohexylcarbodiimide
DDS	Drug Delivery System
DiI	1,1′-Dioctadecyl-3,3,3′,3′-Tetramethylindocarbocyanine Perchlorate
DiO	3,3′-Dioctadecyloxacarbocyanine Perchlorate
DLS	Dynamic Light Scattering
DMAP	4-Dimethylaminopyridine
DPD	Dendron-Polymer-Dendron
ECM	Extracellular Matrix
EDCI	1-Ethyl-3-(3-Dimethylaminopropyl) Carbodiimide
EPR	Enhanced Retention and Permeability
Fab	Antibody Fragments
FDA	Food and Drug Administration
FRET	Förster Resonance Energy Transfer

FT-IR	Fourier Transform Infrared
GFLG	Glycine-Phenylalanine-Leucine-Glycine
GI	Gastro-Intestinal
GPC	Gel Permeation Chromotography
GSH	Glutathione
HER2	Human Epidermal Growth Factor Receptor Type 2
HLB	Hydrophilic Lipophilic Balance
HPMA	N-(2-Hydroxylpropyl) Methacrylamide
HPMA	Hydroxypropyl Methacrylate
HUVEC	Human Umbilical Vein Endothelial Cell
IFN	Interferon
IFP	Interstitial Fluid Pressure
Ig	Immunoglobulin
IgG	Immunoglobulin G
IgM	Immunoglobulin M
J	Coupling Constant
kDa	Kilo Dalton
LC-MS	Liquid Chromatography–Mass Spectrometry
LDP	Linear Dendritic Block Copolymer
Mab	Monoclonal Antibodies
MALDI-TOF	Matrix-assisted laser desorption/ionization-Time of Flight
MDR	Multidrug-Resistant
MeOH	Methanol
MFI	Mean Fluorescence Intensity
MHz	Mega Hertz
MMPs	Matrix Metalloproteinases
MPS	Mononuclear Phagocytic System
mRNA	Messenger RNA
MTD	Maximum Tolerated Dose
MWCO	Molecular Weight Cut-Off
NCE	New Chemical Entities
NHS	N-Hydroxy Succinimide
NIR	Near Infra-Red

NMR	Nuclear Magnetic Resonance
NO	Nitric Oxide
NP	Nano Particle
NR	Nile red
NSCLC	Non-Small Cell Lung Cancer
OS	Overall Survival
PAMAM	Poly(amidoamine)
PBLG	Poly(γ-benzyl-l-Glutamate)
PBS	Phosphate Buffer Saline
PCL	Poly(ε-caprolactone)
PDGF	platelet derived growth factor
PDI	polydispersity index
PEG	Poly(ethylene Glycol)
PFS	Progression-Free Survival
PIC	Polyion Complex
PK	Pharmacokinetic
PLAA	Poly(l-aspartamide)
PLGA	Poly(lactic-co-glycolic acid)
PMDETA	*N,N,N′,N″,N″*-Pentamethyldiethylenetriamine
PPI	Poly(Propylene Imine)
PPO	Poly(Propylene Oxide)
PSMA	Prostate-Specific Membrane Antigen
PVP	Poly(vinylpyrolidone)
RC	Regenerated Cellulose
RES	Reticuloendothelial System
RGD	Arginylglycylaspartic Acid
Rh	Hydrodynamic Radii
RNA	Ribonucleic Acid
ROS	Reactive Oxygen Species
rt	Room Temperature
SD	Standard Deviation
SEC	Size-Exclusion Chromatography
siRNA	Small Interfering RNA

SLS	Static Light Scattering Analysis
SSPS	Solid Phase Peptide Synthesis
TAM	Tumor Associated Macrophages
TAT	Trans Activating Regulatory Protein
TEM	Transmission Electron Microscopy
Tf	Transferrin
THF	Tetrahydrofuran
TNF-α	Tumor Necrosis Factor-α
Tyr	Tyrosine
Tyr-Glu	Tyrosyl-glutamic Acid
UV	Ultraviolet
VEGF	Vascular Endothelial Growth Factor
Vis	Visible

1. INTRODUCTION

1.1. Advantages of Nanomedicine

The employment of polymers or polymeric constructs in cancer therapeutics is an increasing trend for the past few decades [1, 2]. Especially their employment in various application areas as smart drug delivery, disease diagnosis as well as imaging systems and medical nanodevices draw attention to their vast potential [3-5]. Combining a drug to such a nanoconstruct increases the efficacy of the drug. Possibly this occurs without changing the molecular structure and the final cellular response to the drug [6]. During the distribution phase, these conjugated systems shield the drug from plasma proteins thereby increasing its stability, and its solubility eliminating the need for solubilizing excipients which cause various side effects [7-8]. Due to increased size of the final particle blood circulation half-lives, tumor accumulation and renal clearance rates of particles hence the carried drug cargo can be improved. As a result drug therapeutic indices of numerous drugs which are already in market can be enhanced notably by decreasing their final toxicities or increasing their overall efficacies [9]. Furthermore, adding specific targeting groups to these nano systems enables targeted delivery of cargo which can be drugs, imaging agents etc. to distinct cells or even organelles as needed [10].

Designed appropriately, release of cargo can be triggered via endogenous and/ or exogenous stimuli. Nanoparticles which are liable to endogenous triggers can dissociate due to differences in pH values, glucose and reactive oxygen species (ROS), hormone and enzyme concentrations at targeted tissues which arise owing to its pathological state [11]. Similarly generating systems for prolonged and sustained release of biomolecules is desired for coping with chronic diseases, hard to treat infections and cancer hence attaining platforms that are capable of continuous drug release for months instead of days [12].

Nanotherapeutics can provide also synergetic effects in co-delivery of conventional chemo- therapeutic drugs with agents targeting stem cells, small interfering RNA (siRNA),

antibodies or again with another drug for enhanced therapeutic efficacy, improved therapeutic index with reduced side effects[13]. Nanoparticles with suitable size and shell composition can benefit from transcytosis where they can pass through otherwise almost impassable epithelial and endothelial confines as of gastro-intestinal (GI) tract or blood-brain barrier[14]. Another compelling group of nanomedicine beside nanotherapeutics is nanoparticle-based theranostic agents serving both for diagnostics and treatment of relevant disease by enabling on site and real time imaging of delivered cargo hence instant monitoring of therapeutic response which will be crucial for the upcoming personalized medicine era [13].

1.2. Nanomedicine against Cancer

According to WHO reports cancer is still the second leading cause of death worldwide. The most recent global reports in 2012 stated occurrence of 14.1 million new cancer cases, 8.2 million cancer related deaths, and 32.6 million people living with cancer within 5 years of diagnosis. Furthermore based on GLOBOCAN estimations mortality will reach over 10 million in 2020. Nanomedicine on the other hand can help to decrease cancer related mortality owing to improved features of nanotherapeutic and nanotheranostic platforms designed to benefit from soft spots of tumor biology. Even though agents of nanomedicine are now on market the current treatment method for cancer therapy involves intervention by incision, radiation therapy and chemotherapeutic drugs. These methods aim to remove the tumor tissue by killing cancer cells however unspecificity of the process results in very harsh side effects on healthy cells thereby causing severe toxicity to the patient as well.

On the other hand nanotherapies employed for cancer treatment today benefit from various expedient features brought by design. For instance, nanoparticles can accumulate through passive targeting via enhanced permeability and retention effect (EPR) in tumor environment and when modified by receptor specific targeting group they can be uptaken by tumor cells via active targeting resulting in improved intercellular concentrations in tumor cells whereby evading most of healthy cell and resulting in considerable lower degrees of toxicities [15, 16]. Furthermore once internalized through receptor mediated

endocytosis they can escape triggering P-glycoprotein pathways which is one of the major mechanisms responsible for generation of multiple drug resistance in cancer cells [17]. Beside major problems as poor oral bioavailability, limited serum stabilities or unwanted bioaccumulation and toxicity at certain organs as kidneys, lung and/or spleen various nanotherapeutics are already marketed today and more are currently in development. Liposomes, PEGylated proteins, polypeptides or aptamers, protein-drug conjugates, polymeric nanoformulations surfactant or metallic nanoformulations are among frequently used marketed platforms for nanotherapeutics which are used in not only cancer therapy but for targeting mononuclear phagocytic system (MPS), drug solubilization, enzyme deficiencies, fighting viral or bacterial infections and more [18]. 33 commercialized nanotherapeutics were approved and in market worldwide as of January 2012 while 122 nanotherapeutics were in development and a total of 789 ongoing clinical trials with nanotherapeutics and nano devices were conducted still [19].

The first examples of nanotherapeutics research started at the end of 1970s by development of liposomes. To reduce cardiac toxicity of anthracycline drugs they were encapsulated into aqueous core of liposomes which are formed from phospholipid bilayers made of phospholipids and cholesterol. The size of liposome preparations ranging between 50 to 200 nm, so they are capable of carry high amounts of hydrophilic drugs in their aqueous core. Furthermore it is possible to encapsulate hydrophobic moieties as required in their hydrophobic bilayer membranes.

Doxil®, the first FDA-approved nano-drug (1995), provided the crucial polyethylene glycol PEG coating as a major feature to liposomal drug preparation of doxorubicin and its use as an approved treatment regimen for AIDS-related Kaposi sarcoma, multiple myeloma, ovarian cancer treatment (Figure 1.1). Due to its bilayer structure and protective PEG shell, the final liposome preparate with hydrodynamic size of 90 nm gained most wanted features such as high payloads of doxorubicin in liposome core, improved drug stability, prolonged drug circulation time in blood since liposome were able to escape from members of reticuloendothelial system (RES) which might result in organ toxicity and drop of plasma concentrations. Furthermore, the increased size of liposome nanoparticle enabled tissue accumulation via EPR based passive targeting and once internalized the

transmembrane ammonium sulfate driven drug encapsulation methodology made doxorubicin release at tumor tissue possible [20].

Even though doping high concentration of drugs into core or shell of liposomes improves biodistribution, pharmacokinetics (PK) and total tissue accumulation and release dynamics of chemotherapeutic drugs, the overall survival (OS) of patients treated with commercial liposomal formulations showed no significant increase in comparison to parent drug yet [21]. One possible exception to this is a liposome formulation of cytarabine and daunorubicin called Vyxeos that is still in clinical trials at phase III; compared to the classical treatment of parent drugs against acute myeloid leukemia with high-risk patients an OS increase of 9.56 months versus 5.95 months were reported for liposomal form [22].

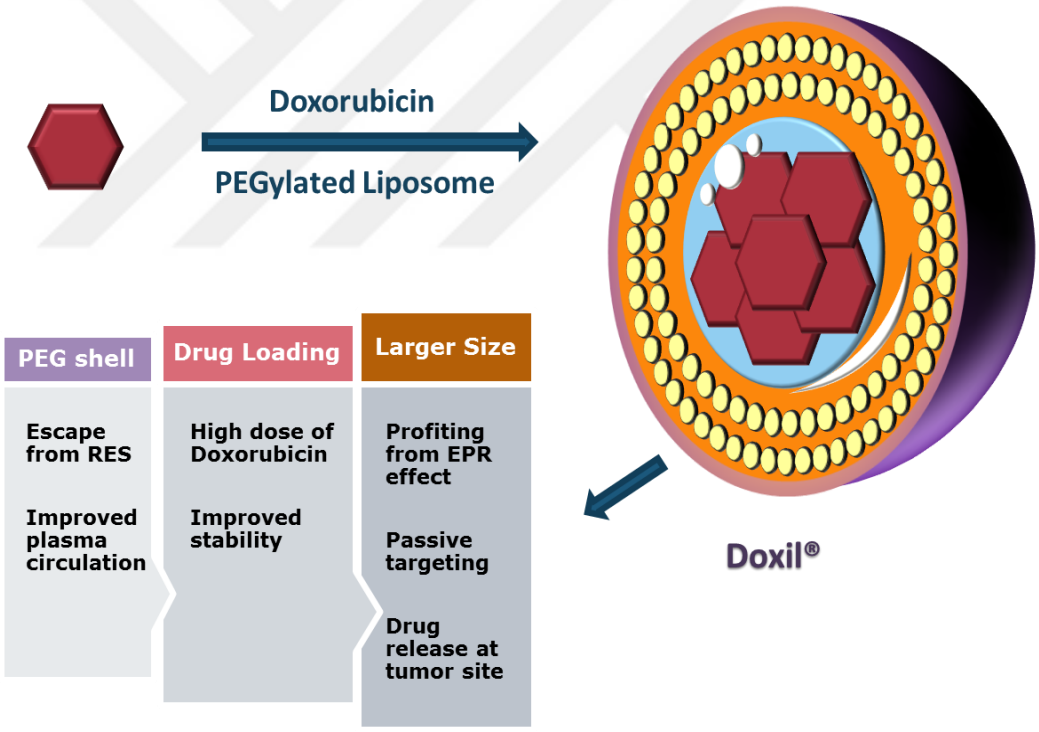

Figure 1.1. First approved liposomal drug, Doxil®.

Another critical type of nanotherapeutics is protein-drug conjugates. In recent years albumin gained importance as a drug carrier since conjugation of therapeutic agents to this naturally occurring protein results in enhanced pharmacokinetic properties to parent drug, likewise the simplicity of the final construct render this type of nanoconstruct rather

beneficial. In respect to these, the number of studies in clinical trials based on albumin conjugated drug conjugates is still increasing [23]. Abraxene® which's use against metastatic breast cancer was approved by FDA at 2005 and against non-small-cell lung cancer is at phase III was designed to overcome the issue of high hydrophobicity problem with paclitaxel.

Normally paclitaxel is administered with highly toxic excipients as Cremophor EL (polyoxyethylated castor oil); consequently administered drug dose was limited [24]. Thus employment of albumin-bound paclitaxel nanoparticle formulations with hydrodynamic size of 130 nm instead not only improved the maximum dose injected and tolerated but the span of dosing decreased significantly affecting PK and biodistribution of paclitaxel positively by improving achieved Cmax and area under the curve (AUC) values. Upon intravenous injection of Abraxane® nanoparticles, due to increase size of construct tumor accumulation via passive targeting occurs and due to dissociation of individual drug-albumin conjugates drugs are internalized by albumin dependent cell uptake mechanisms in high concentrations [25] (Figure 1.2).

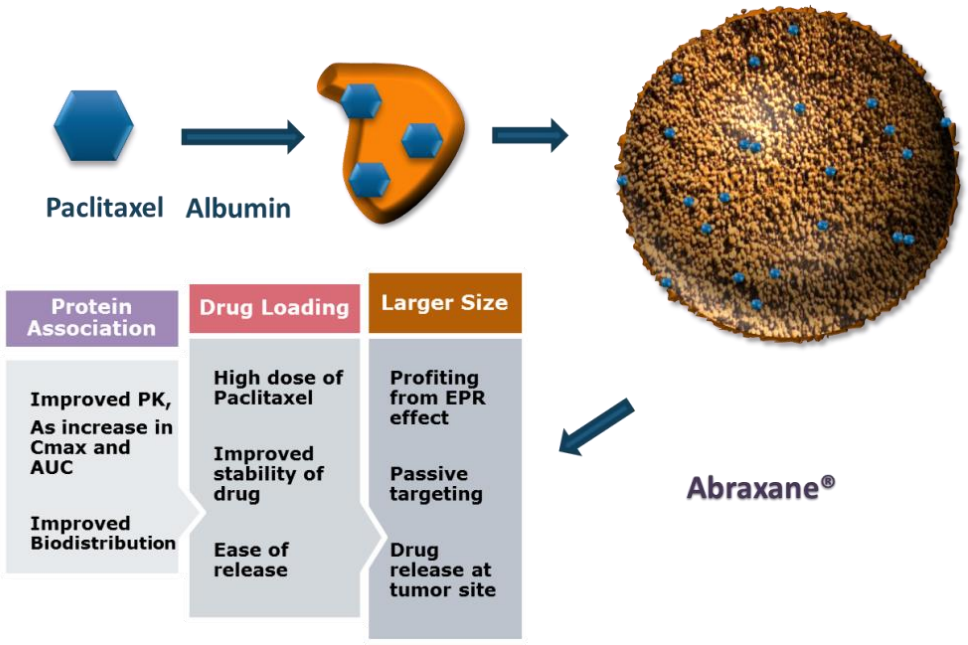

Figure 1.2. Albumin bound paclitaxel, Abraxane® as one of the first protein-drug conjugates.

Administrating Abraxane® every-3-week provided enhanced results in terms of OS and progression-free survival (PFS) in comparison of free paclitaxel for metastatic breast cancer patients however increasing the dosing frequency to once a week resulted in increased toxicity and indicated to the limit of this construct [26].

One of the vastest groups of cancer therapeutics is polymer-based nanoformulations as nanopharmaceuticals. This group containing very heterogeneous general design strategy has early examples as Copaxone®, that is a four amino acid polypeptide used against multiple sclerosis and FDA approved at 1996/2014 or Eligard® composed of leuprolide acetate in poly lactic-co-glycolic acid (PLGA) copolymer nanoparticles used against advanced prostate cancer as approved by FDA at 2002 [27]. However a more salient and advanced example of this category might be Genexol®, a polymeric micelle composed of composed of monomethoxy poly(ethylene glycol)-*block*-poly(D,L-lactide)(mPEG-b-PLA) copolymers (Figure 1.3).

Used for Cremophor EL-free delivery of paclitaxel, Genexol® treatment is employed as a regimen against metastatic breast cancer in South Korea since 2001 and several clinical trials at phase I–II and IV have been conducted for FDA approval for not only metastatic breast cancer but also non-small cell lung cancer (NSCLC) and pancreatic cancer. The results demonstrating significantly altered PK and overall response rates ranging between 40–68% are very promising in comparison to than solvent-based Taxol [28, 29].

The mPEG-b-PLA polymeric units of Genexol® are low molecular weight, even though it is not naturally occurring they are nontoxic as well as biodegradable. Furthermore the amphiphilic character of the polymeric units makes them not only water soluble which mitigates the use of excipients but also triggers formation of micelles acting as reservoir of hydrophobic paclitaxel. Owing to final micellar hydrodynamic diameter of 20-50 nm, the nanoparticles can benefit from EPR effect as in case with previous nanotherapeutics and *in vivo* stability [28].

1.3. Nanoparticle Design for Successful Systemic Drug Delivery to Tumors

In the previous section, multiple cancer therapeutics was listed approaching the same problem, cancer, from different angles. Even though some major issues with chemotherapy medications as solubility, poor biodistribution and PK factors were addressed and improved there is still room to progress since there are no perfect cure for this disease. At this junction, polymeric nanoparticles providing high level of resilience in design can serve to overcome many of the obstacles in order to optimize final efficacy of parent drug molecules. Furthermore, once chemically conjugated to the drug molecule final drug delivery system (DDS) gains novel PK profile due to which these platforms are considered as new chemical entities (NCE).

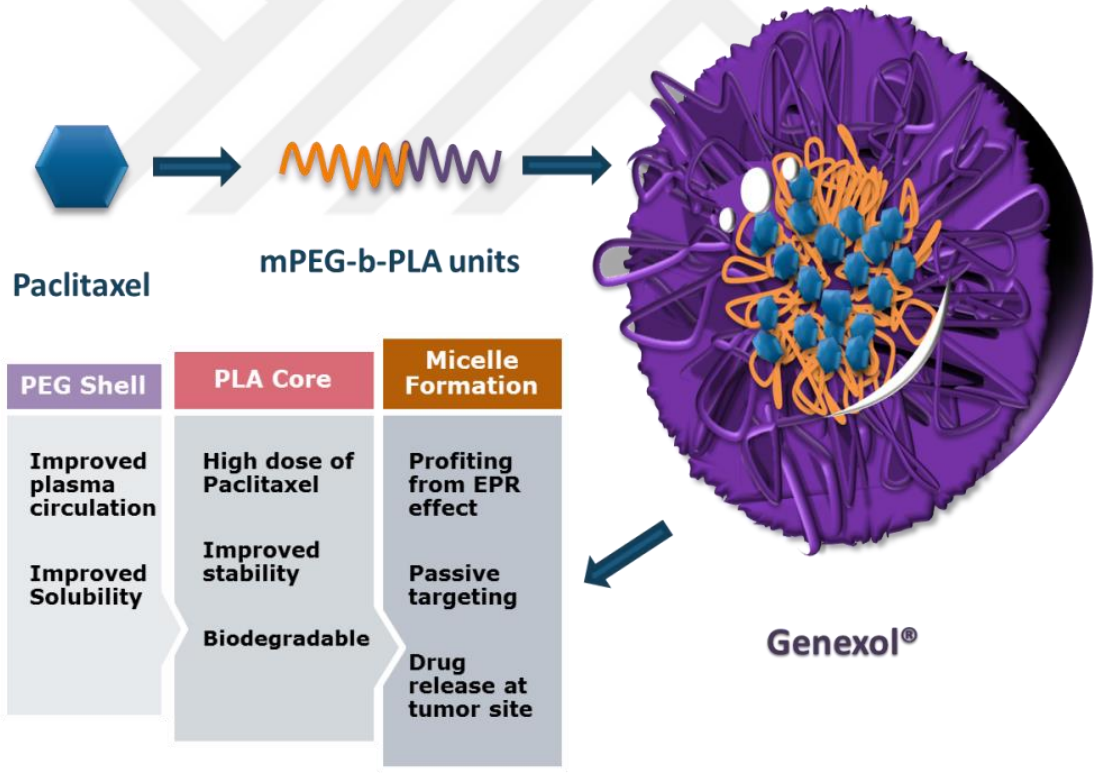

Figure 1.3. Polymeric micellar formulation of paclitaxel, Genexol®.

As nano-DDS platforms there are a few drugs as doxorubicin, camptothecin and paclitaxel, and again a handful types of polymers such as (N-(2-hydroxylpropyl)methacrylamide (HPMA) copolymer, poly-L- glutamic acid, PEG, PLA

and Dextran frequently selected due to their low cost, ease of synthesis but upmost for their non-toxic character hence biocompatibility [30]. However there are several more complex polymeric DDS with added multifunctionalities at various clinical trial phases [31, 32]. Still any novel construct should address one of the major concerns about polymeric nanomaterials that is the polydispersity index (PDI) which always higher than small molecules or naturally occurring macromolecules. High heterogeneity in size of polymers, where polymer fractions with different molecular weights varies too much, is problematic for characterization of final structure moreover it is harder to obtain reproducible PK data. That's why production of nanoparticles from polymeric units with homogeneous size distributions is favored. Dendrons and dendrimers were compelling options to achieve low PDI with their well-defined structures [33].

1.4. Effect of PEGylation

The nanostructure should not only provide sufficient solubilization of chemotherapeutic agent but it should also be able to stabilize the molecule prolonging its half-life. Furthermore the platform should show suitable physical, microbial and chemical stability starting with its time of manufacturing until it reaches its target tissue. One essential polymer that is frequently used for this purpose and more is PEG. This hydrophilic polymer is frequently favored and commonly employed in drug delivery systems due to its high solubility in water and its anti-biofouling effect. Covalent conjugation of synthetic PEG to DDS platforms provide not only improved solubility, stability and plasma residence, but also immunogenicity of the nanostructure is reduced significantly[34]. When covered with PEG nanoparticles are able to escape serum components and reach their destination fairly uninterrupted [35, 36].

Besides the PEGylated therapeutic proteins approved and commercialized in the early 90s, second generation PEGylated DDS with more sophisticated design are introduced to the market at present as pegaptanib marketed as Macugen or Macuverse that is a PEGylated RNA based aptamer targeting anti-vascular endothelial growth factor (VEGF) for the treatment of ocular vascular disease [37]. It is expected that more PEGylated product will be introduced in the future however it is interesting that among

other alternatives that can be used for modification of DDS PEG is the polymer to go. Naturally occurring polymers as polysaccharides as dextrans and hydroxyethyl starch or fatty acids and their derivatives seem as alternatives they might fail to fulfill one or more aspects of PEG, which is non-toxic, highly hydrophilic, uncharged, non-degradable but most importantly non-immunogenic or anti-biofouling. Likewise, its use has been approved and described as "generally recognized as safe" by FDA [38].

Synthesized ring opening polymerization of ethylene oxide, PEG polymer at various sizes can be manufactured with very narrow size distribution; approximately a PDI of 1.05 is achieved and accepted as standard for pharmaceutical applications. Even though linear PEG polymers of 5 or 10 kDa were commonly used, nowadays conjugated PEG polymer are chosen with more elaborate structures as branched, forked, multi-arm and in dendritic forms reaching sizes up to 40 kDa or even higher [39].

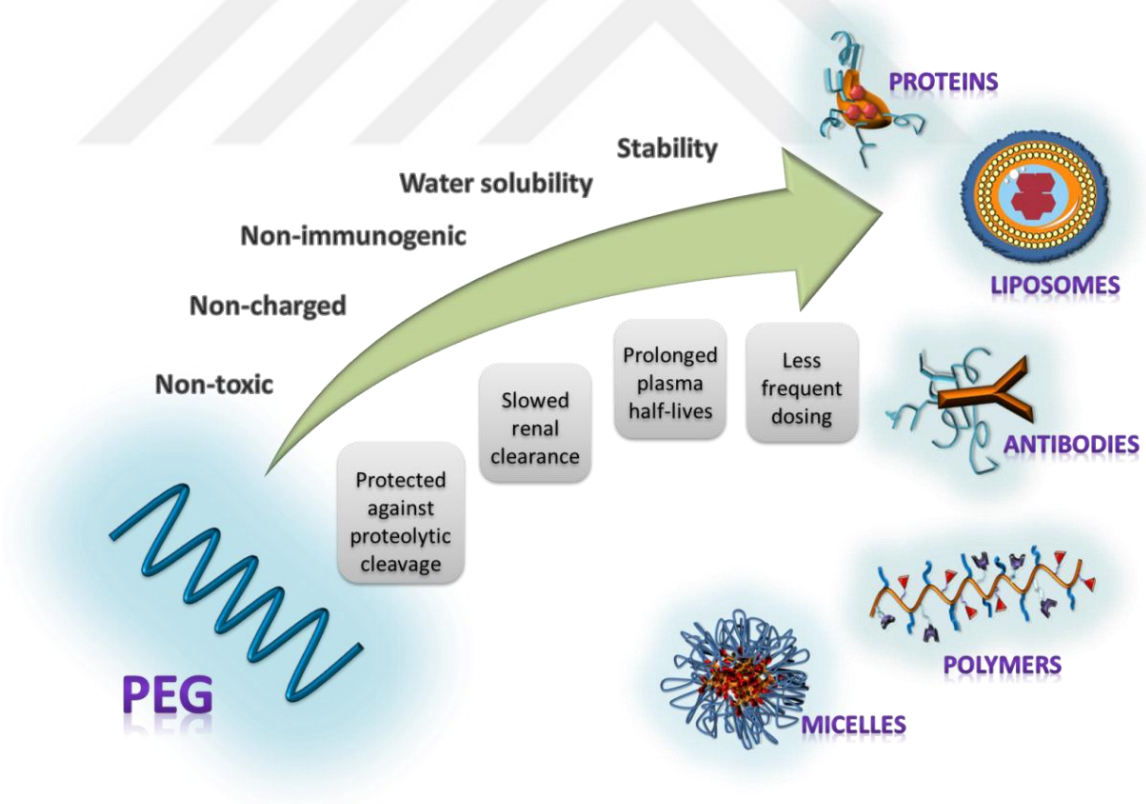

Figure 1.4. Advantages of PEG conjugation to biotherapeutics.

The ability of PEG to improve many therapeutic properties of conjugated constructs is due to its flexibility and capacity to coordinate with multiple water molecules. This in turn results in an extensive hydrodynamic radius that can be 5-10 times larger than that of the globular protein of the same molecular weight [40]. This increased hydration potential suggests the conjugated PEG chains provide a shield of water around the nano structure, protecting it from biologic environment. This in turn leads to prolonged plasma half-lives, hence less frequent administration of incorporated drug; escape from rapid renal clearance since PEG coat limits receptor-mediated protein uptake by cells of the reticuloendothelial (RES) system; protection from proteolytic cleavage by serum component on top of gained solubility and stability perks (Figure 1.4).

The shielding ability of PEG chains has also negative effects since it also affect the interaction capability of nanoconstruct with its target that can be a receptor, cell or tissue, which can be seen as inconsistency between *in vitro* and *in vivo* results from various therapeutics in development. Generally this causes poor *in vitro* activities in comparison with unmodified structure whereas due to prolonged plasma half-lives *in vivo* results are improved, as in the case of PEGylated interferon (IFN) formulation Pegasys with poor *in vitro* results but effective *in vivo* [41].

It is also important to point out that even though PEG is generally considered as non-biodegradable there are report indicating that it might be recognized and degraded by dehydrogenases as alcohol and aldehyde dehydrogenases and cytochrome P450-dependent oxidases [42, 43]. Similarly the non-immunogenic nature of PEG is under suspicion as stated by recent reports. For instance in clinical trials of PEGylated urate oxidase produced to adjust urate plasma concentration by gout patients, many participants developed antibodies resulting in rapid removal of construct hence poor results. Later it is found that the antibodies were specific not to urate oxidase enzyme but to PEG [44]. Then as well reports with liposomes indicated similar concerns where secondary dosing of same liposomal formulation fail to provide long plasma retention owing to generation of anti-PEG immunoglobulin M (IgM) antibodies [45]. Still, PEGylation is a mature technology with various examples of successful biopharmaceuticals in market for years.

1.5. Commonly used Polymer in DDS Platforms

PEGylation is a critical aspect of DDS design however to optimize the delivery platform additional polymers are required. The first examples of polymers used in clinic served most basic purposes. Poly(vinylpyrolidone) (PVP) and dextran were used as plasma expanders which have high molecular weight causing increased osmotic pressure hence increased plasma volume. Also polymers as Povidone that is an iodinated PVP polymer were used as antiseptics as well as wound dressings. However after 60s work on PEG-protein conjugates and during 70s after the pioneering research of multiple prominent groups as De Duve, Ringsdorf and Davis colleagues focused on lysosomotropic polymer–drug conjugates, amphiphilic block copolymer forming micelles, and again more PEG-protein conjugates, synthetic polymer–drug conjugates research accelerated quickly [46]. With the influence of biological developments as lysosomal uptake of biologically active agents and advances in defining the effect of structure and properties of pharmacologically active polymers rational design of a polymer applicable for anticancer polymer–drug conjugates was resulted in generation of N-(2-hydroxypropyl)methacrylamide (HPMA)-doxorubicin conjugates which is the first synthetic polymer based DDS that proceed to clinical trials phase I/II in 1994 [30]. Furthermore in 80s and 90s micellar DDS platforms entered phase I/II clinic trials by Kataoka and coworkers employing A-B type block copolymers of PEG and doxorubicin conjugated poly(aspartic acid) (Asp) and by Kabanov and coworkers employing A-B-A type Pluronic® block copolymers composed of PEG and poly(propylene oxide) encapsulating doxorubicin where the final particles indicated to be uptaken by Pgp-independent pathway resulting in significant decrease in multidrug-resistant (MDR) profile of tumors [47, 48].

Principles for water-soluble HPMA copolymer-based drug conjugates set based on suggestions of Ringsdorf were systematically tested and continuously proven useful led to overall model of four parts; a highly water soluble HPMA polymer that is modified by introduction of drugs and targeting agents incorporated to comonomer units which are conjugated to polymer backbone by biodegradable spacers [49]. Further studies highlighted the importance of molecular weight of non-biodegradable HPMA chosen as the delivery agent. To achieve optimal cellular uptake and biodistribution potential as well

as proper elimination of the residual backbone without causing any organ accumulation, 30kDa was the size selected for efficiency[50, 51].

A novel approach for drug delivery was introduction of a degradable peptidyl linker composed of four amino acids, Gly-Phe-Leu-Gly (GFLG), which stays uncleaved during circulating in blood but become a target for lysosomal proteases as cathepsin B once internalized by endosomal pathways [52].

Another factor affecting internalization is surface charge of nano constructs. Since the plasma membranes of cells are negatively charged and they are rich in hydrophobic components due to phospholipid bilayer structure, DDS platforms with hydrophobic regions or positive surface charges can interact and internalized though membranes more efficiently, this in turn gave rise to a range for drug loading weight percent that was optimized to around 10% endorsing non-specific membrane binding[53]. Also employing comonomers for receptor mediated targeting was achieved by addition of different types of ligands as sugars, peptides or antibodies providing better tumor accumulation profiles in comparison to parent drugs [54].

A HPMA-doxorubicin conjugate employing the GFLG linker showed promising result in Phase I/II clinical trials since the maximum tolerated dose (MTD) of doxorubicin was able to be increased to 320 mg per m2 which was almost 5 times of the regular dosing. Moreover the lack of cardiotoxicity even after high cumulative doses was encouraging. Prolonged plasma circulation times, absence of liver accumulation and effectivity at low doses in NSCLC, colorectal and chemo-resistant breast cancer patients were observed at Phase I trials but in Phase II only partial responses were observed. However this initial study showed that administering higher drug doses of doxorubicin without inducing immediate immune response or polymeric toxicity was possible [55].

A similar HPMA-doxorubicin conjugate used galactosamine molecules for targeting hepatocyte asialoglycoprotein receptor selective for hepatocellular carcinoma patients. 12 to 50-fold higher doxorubicin concentrations were achieved in liver in comparison to free drug and one third of patients showed tumor reduction highlighting the effect of additional targeting group [56]. Nonetheless when the GFLG spacer was replaced with an ester

linkage two HPMA-drug conjugates, HPMA- camptothecin and HPMA-paclitaxel exhibit poor results in corresponding clinical trials. HPMA- camptothecin failed to demonstrate any anti-tumor activity but caused severe cystitis and HPMA–paclitaxel construct displayed dose-limiting toxicity similar to free drug. It was suggested that conjugation of drugs through ester linkages resulted in preliminary drug release in the bloodstream instead before reaching tumor tissues and freed drug were quickly cleared via kidneys. These results emphasize the importance of design for DDS platforms [57, 58].

In contrast to non-biodegradable HPMA polymers suffering from size limitations, polymers of α-hydroxy acids, PGA and PLA, provide both biocompatibility and biodegradability to functionalizable DDSs. PGA, the first synthetic biodegradable polymer used in nanotherapeutics, is a bulk-eroding polymer with high level of crystallinity which can degrade rapidly through its ester backbone. On the other hand, there are to isomers of PLA, L-lactide and D-lactide and while pure polymers form L-form has semi-crystalline structure random PLA polymers of mixed isomers are amorphous. PLGA polymers are widely employed in DDS to obtained desirable size, stability and controlled release profiles to designed nano platforms which is approved by FDA for drug delivery purposes [59]. DDS produced from PLGA of chemotherapeutics can degrade into non-toxic, biodegradable monomers lactic acid and glycolic acid via either non-specific hydrolysis of ester backbone or get cleaved by lysosomal cathepsin B after endosomal uptake [30].

The degradation profile of generated polymeric systems can be modulated by changing the size, monomer content and arrangement (block vs. random), molecular weight, achieved crystallinity hence glass transition temperature of final polymers as well as introduction of additional polymeric components as PEG, manufacturing conditions and manner of administration [60]. These polymers can be used in combination with various anti-cancer agents as goserelin acetate encapsulated formulation Zoladex that is marketed in 1998 after FDA approval against breast and prostate cancers. Designed for subcutaneous injections to generate a slow releasing system, a constant concentration of goserelin acetate in blood was achieved [61]. Another example is Trelstar Depot that is a triptorelin pamoatea containing microparticle system used for treating prostate cancer which was commercialized after 2000 [62].

1.6. Effect of Nanoparticle Design on Pharmacokinetics and Biodistribution

After introduction of a nanoparticle into a biological environment as blood, interstitial fluid or extracellular matrix (ECM), the surface of particle interacts and adsorb macromolecules in plasma, generally proteins such as human serum albumin, lipoprotein, glycoprotein, and α, β, and γ globulins [63]. This resultant corona around the nanoparticle periphery might change the final efficiency of DDS since it affect the size, stability and surface charge of nanomaterials [64]. This in turn can affect various biological responses as biodistribution, toxicity, tumor extravasation and cellular internalization of NPs (Figure 1.5).

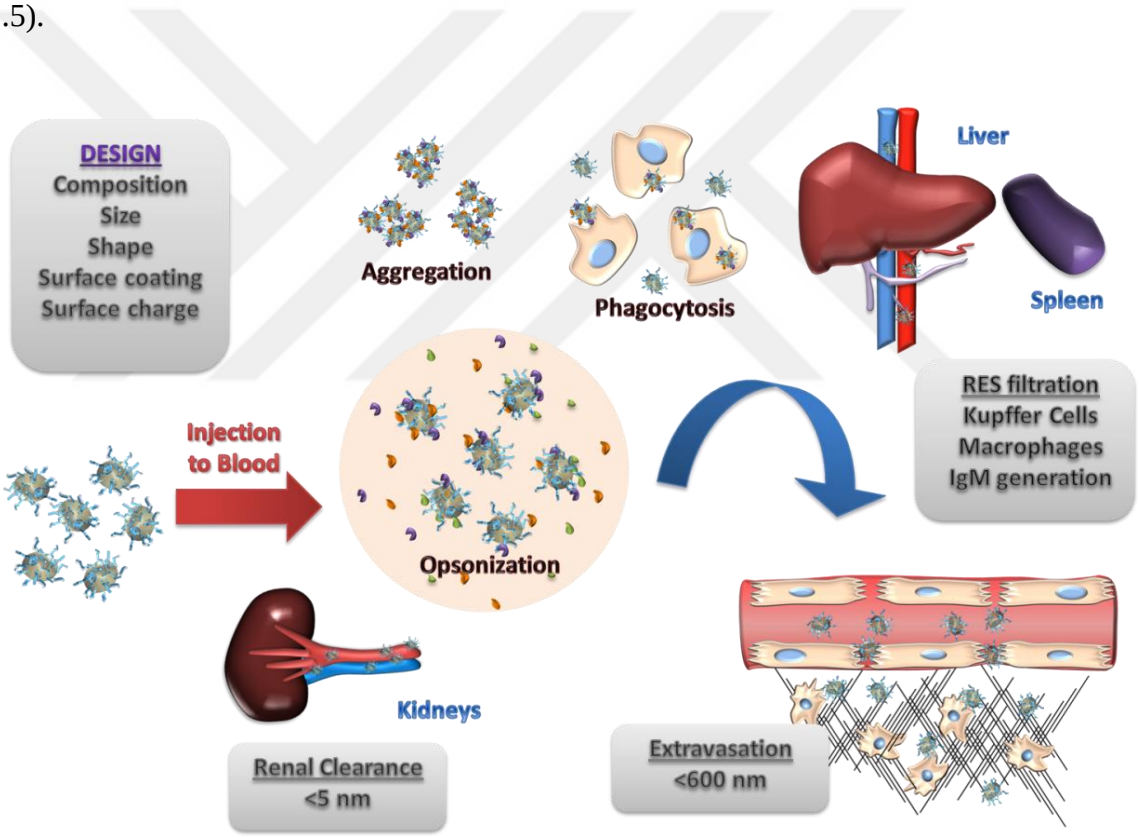

Figure 1.5. Factors affecting blood circulation and RES interaction

Nanotherapeutics, commonly with average size in the range of 10 to 200 nm, have the ability to escape renal clearance which have a cut off value of 5 nm hence circulating for longer periods of time through the blood stream. This extra period provides NPs with increased probability to reach the tumor environment and thus improved accumulation[65]. The final toxicity and efficacy of carried drug is significantly transformed since the

biological fate of drugs incorporated to NPs shows notable differences in terms of PK and biodistribution of parent drugs.

Nanotherapeutics can improve efficacy profiles of drug during three steps which are through interaction with RES interaction while in systemic circulation; extravasation from blood vessel and accumulation in tumor and finally uptake within the target cells and release of cargo. After injection of DDS into bloodstream the interaction of NPs with RES starts. RES is a system of macrophages located in various organs and locations as lymph nodes, adipose tissue, and bone marrow but the most important ones are those in spleen and liver since they can alter NPs clearance the most. The corona complex around NPs formed during circulation in serum media can trigger macrophage recognition and removal of those particles by phagocytosis, since macrophages are capable of detecting those serum proteins or opsonins on the corona [66]. Nagayama and coworkers verified this phenomena by showing a strong correlation between the amount of adsorbed complement protein C3 and immunoglobulin G (IgG) on 50-nm polystyrene NPs in serum and the rate of removal of those particles by Kupffer cells which are stellate macrophages located in the liver acting as a part of MPS [66]. Consequently any factor affecting the opsonization level of NPs determines level of interaction of NPs with component of RES which is the major element for obtaining desired blood circulation time and clearance rates. PEGylation of NPs, size, composition, surface charge measured by zeta potential, and shape of NPs are among those factors.

PEGylation of nanotherapeutics has not only positive effect on solubility and stability however PEG shell can also block association with serum proteins to some degree and protect NPs by steric hindrance. A study by Sadzuko and coworkers demonstrated that PEGylation of liposomal formulation of CPT-11 a 6 times greater serum AUC, a 3-fold decrease in removal by RES agents and a 6-fold increase in tumor drug concentration resulting in an almost 3-fold reduction in tumor weight [67]. Many aspects of PEG polymer forming the protective shell affect the level of protein adsorption, for instance confirmation of PEG chains, PEG densities and molecular weight of PEG can affect final performance. A study done by Fang et al. employed micelles with sizes ranging between100–200 nm, PEGylated with three different sized polymers, 2, 5, and 10 kDa and NPs with smallest size and its demonstrated that increased PEG length (10kDa) and PEG

density (increases for smaller NPs) decreased protein adsorption and improved tumor uptake [68]. Another study by Ernsting and coworkers used PEGylated NPs from acetylated carboxymethylcellulose with conjugated docetaxel and a 2kDa PEG corona found to be optimal for this DDS [69].

However even though PEGylation can significantly improve PK profiles and biodistribution clearance of NPs with RES cannot be eliminated completely, it has been shown that usually up to 50% of injected dose of drugs in nanotherapeutics get accumulated in liver and spleen in the first 48h after administration [70, 71]. So, more sophisticated surface modifications can further enhance NPs as in the case of conjugation of a so called “Self” peptide to the periphery of NPs which is a computationally designed peptide mimicking CD47 membrane protein of macrophages to inhibit phagocytosis of self. The incorporation of these “Self” peptides to the final structure in turn obstructed macrophage-mediated clearance of those NPs and resulted boosted plasma half-lives of drugs or dyes [72].

Size and morphology of NPs are other factor affecting circulation times. For escaping renal clearance a bigger size than 5 nm is sufficient whereas a secondary limit set by liver vascular fenestrations is also important since NPs smaller than 50 nm has the risk of uptake by liver’s hepatocytes. The optimum size of a DDS is limited by permeability of targeted tumor tissue since vascular fenestrations of tumors at different locations can vary 400 to 600 nm to microns [73]. A study investigating biodistribution of liposomes with sizes 30- 400 nm indicated that liposomes larger than 50 nm and smaller than 300 nm displayed 4 times more tumor uptake. Almost 25% of injected >50 nm and <300 nm particles were located in liver whereas this value was only 10% for 100 nm liposomes. Yet 40 to 50% of all injected <400 nm NPs were filtered by spleen probably due to size restrictions of intercellular slits of splenic sinus which is 500 nm at max [74, 75]. The study of Hrkach and coworkers investigated the optimal size docetaxel loaded NPS targeted to prostate solid tumors and among 63 candidates ranging between 28-224 nm, particles with a size of 100 nm provided best results in terms of tumor accumulation in contrast to liver and spleen [76].

Plasma half-lives and tumor extravasation is also affected by shape of NPs. After investigating interaction of ellipsoid or sphere shaped micro-sized polystyrene particles with macrophages, rate of internalization was found be increased with spherical forms [77]. Furthermore, phagocytosis rate was notably decreased with worm-like polystyrene particles in comparison to spherical ones [78]. Accordingly diverging from spherical shaped NPs led to improved blood circulation time and biodistribution. A filamentous formulation for PEG- poly(ε-caprolactone micelles exhibited significantly reduced macrophage interaction and plasma circulation times up to one week whereas the regular spherical shaped formulation was cleared after just 2 days. The extra flexibility provided by the filamentous shape led to alignment of those paclitaxel loaded filomicelles with blood flow and limited their interaction with surrounding macrophages [79].

Surface charge of nanotherapeutics represented as zeta potential values (ξ) is another determining factor for PK, biodistribution and cellular internalization. Typically, negative zeta potential values with ≤ 10 mV surface charges leads to clearance of NPs by RES members and positive values around > 10 mV show strong aggregation with opsonins, whereas optimum results in terms of minimum RES interaction and improved circulation times are observed with neutral NPs with zeta potentials in the limit of ± 10 mV [65]. It has been demonstrated that high positive as well as high negative surface charged PEG-oligocholic acid based micellar NPs were subjected to rapid opsonization and targeted by Kupffer cells to be cleared [80]. Similarly administration of a cationic liposome/DNA complex (lipoplex) resulted in aggregate formation in serum, which caused transient embolism in the lungs and clearance thorough river [81]. Additionally, charge shielding effect of PEGylation of NPs was also reported indicating that PEG can hinder serum protein association not only sterically but also minimizing extreme surface charges [81, 82].

1.7. Nanoparticle extravasation and retention in tumor environment

The transfer of NPs from blood to tumor vasculature is the second step of delivery. The presence of efflux transporters on endothelial barriers, epithelial barriers around organs and on blood-brain barrier is a major problem for permeability of small drugs [83,

84]. Still, specific enzymes residing on these barriers are able to detect and cleave various biologically active compounds as peptides or drug [85]. Also tight junctions are limiting the paracellular route between epithelial and endothelial barriers and they are especially impervious to the passage of hydrophilic moieties which might be problematic for small drug or NPs with unfit shell properties [86]. Similar to inflammatory mediators as histamine, positive charged particles were shown to be able to disrupt tight junctions by triggering endothelial contractions which results in increased leakiness and improved extravasation [87]. By employing vascular mediators such as nitric oxide and angiotensin II in combination with NP tumor extravasation and vascular permeability can be enhanced effectively [22].

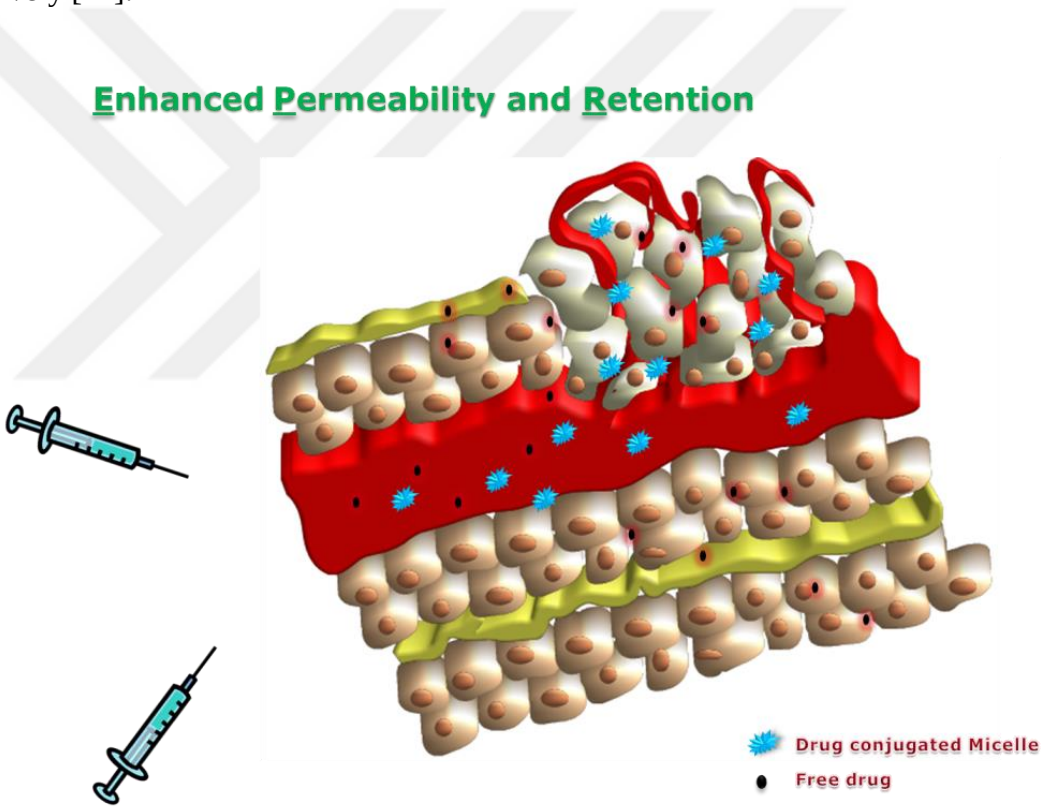

Figure 1.6. EPR effect for passive targeting of NPs

Dependent of tumor type, perivascular tumor space and NPs design this mechanism is very effective for permeable tumor types with poor lymphatic drainage. One of the most important advantages of conjugated polymer drug systems is that selective drug accumulation in tumor tissue is possible owing to the EPR effect [88]. This phenomenon arises from the specific characteristics of the abnormally active tumor cells (Figure 1.6). Due to their increased metabolic needs, tumor cells trigger angiogenesis resulting in a

hyper-vasculature around the tumor environment. For instance compared with normal vasculature of endothelial cells which have turnover of around 1000 days, the endothelial cells neovasculature can replenish in just 10 days [89]. The amplified growth rate and tumor vasculature result in a decrease in tissue organization as incomplete formation of distinct venules, arterioles or capillaries hence a novel permeability level for macromolecules arises. Once leaked into tumors, rate of NP propagation into tumor is also irregular due to the heterogeneous structure of tumor environment with divergent levels of vascular permeability and blood velocity.

Lack of sufficient lymphatic drainage bring about a selective increase in macromolecule accumulation in tumor tissue. On the contrast, free drug molecules can diffuse to any tissue and are filtered much easily due to their small size, whereas macromolecular drug conjugates are accumulated selectively in the tumor environment in an accumulative manner. This kind of passive targeting and long term retention aims to render these drug conjugates only locally toxic [90–92].

SMANCS, a therapeutic conjugate of neocarzinostatin and poly(styrene-comaleic acid) developed by Maeda and coworkers was the first construct employed to demonstrate the selective accumulation potentials of NPSs. Drug accumulation levels in various solid tumors including metastatic liver, lung, gallbladder, and pancreas cancer treated with a combination of Lipiodol and SMANCS were investigated and found to be 10 to 100-fold higher than healthy tissues by X-ray analysis [93]. A study employing 111In-DTPA-labeled PEGylated liposomes showed impact of long circulation times on body distribution where liposome accumulation was reported selectively in liver, spleen and squamous cell tumor as well as bowels and heart. When the DDS was changed to Doxil, the resulting body distribution profiles in Kaposi's sarcoma patients were in parallel with those of radiolabeled PEGylated liposomes [94].

Even though biodistribution profiles, plasma circulation times and related PK parameters are revised positively, typically overall survival of cancer patients can be increased less frequently in comparison to regular administration of parent drug [95]. For instance dosing docetaxel or liposomal Doxil to HIV-related Kaposi’s sarcoma as well as metastatic breast cancer patients did not exhibit significant overall survival differences in

clinical trials [96, 97]. Parallel results were reported from randomized phase III trials of routine doxorubicin regimen and liposomal DDS DaunoXome in advanced AIDS-related Kaposi's sarcoma patients with 28% and 25% overall survival rates respectively [98].

The irregularity of tumor vasculature resulting in heterogeneous perfusion hence variance in permeability levels for NPs furthermore it is much lower in the hypoxic center of tumor [99]. A study employing labeled liposomes showed that liposome accumulation was significantly higher in adenocarcinoma xenografts in contrast to normal tissue however the distribution of liposomes were tracked to be very homogenous throughout tumor tissue where perivascular clusters of liposomes were observed. Accumulation of NPs around tumor periphery is an indicator for poor perfusion instead of limited permeability [73]. One strategy to enhance blood perfusion profile is by targeting angiogenesis that is formation or modulation of blood vessels and controlled by growth factors released by both tumor and stromal cells.

VEGF is a widely expressed factor in tumors as a stimulator of angiogenesis and inhibition of VEGF was associated with decrease in tumor weight most possibly due to size and width decrease in vessels as well as increased tumor penetration of small drugs [100]. Even though this type of normalization of tumor vasculature can be effective for small molecule delivery of NPs can be problematic since normalization of blood vessels might lead to decreased permeability levels and cancel the improvement in perfusion. Still, vascular normalization was shown to be an effective method for enhanced tumor extravasation.

In a study by Tanaka and coworkers, Beroprost that is a prostaglandin I_2 analog was used to limit tumor blood flow in a rat tumor model. Administration of prostaglandin analog triggered vasodilation and diminishing effects of abnormal tumor vessels, eventually it caused decreased blood flow in tumor tissue up to 70%. However no significant change in normal organs as kidney and liver was observed. Besides the tumor accumulation of Evans blue–albumin complex increased 2-3 fold indicating that enhancing EPR is possible by modulating vascular blood flow and extravasation [101]. Another study was able to achieve analogous outcomes by applying small doses of nitroglycerin topically to enhance tumor-targeted delivery of PEG conjugated zinc protoporphyrin IX.

Nitroglycerin is converted to its active form nitric oxide (NO) under hypoxic and low pH conditions, which is typical for tumor tissue. NO as a vascular mediator promoted the permeability of tumor vasculature via vasodilation and reinforced macromolecule uptake by enhanced EPR [102].

Another strategy for modulating vasculature is through cytokines involved in systemic inflammation such as tumor necrosis factor-α (TNF-α) where it can induce vascular permeabilization. At effective doses TNF-α causes severe systemic toxicity due to body wide vascular leakage which limits its clinical utility. However low-dose TNF-α administration in combination with PEGylated liposomes was shown to be effective nonetheless. Homogeneous distribution of PEGylated long circulating liposomes was achieved in murine melanoma solid tumors. Accumulation levels improved 5- to 6-fold, intact liposomes were uptaken by tumor cells and resulting in enhanced tumor response [103].

Another group used intravenous TNF-α administration to improve oncolytic virotherapy which is a new approach for cancer therapy. Delivery of virus particles into tumors through endothelial cell layers was improved both *in vitro* and *in vivo* pinpointed to Rho A/Rho kinase dependent pathways [104]. Tumor irradiation is another method reported to enhance tumor specific distribution profiles of nanoconstructs. A PGA paclitaxel conjugate showed improved tumor accumulation in ovarian carcinoma xenografts after local tumor irradiation in 24h [105].

To improve tumor penetration of NPs the physiological features of tumor environment should be taken into account during designing particular DDS (Figure 1.7). After leaking into tumors, NPs must propagate through extracellular matrix with dense stromal tissue, endure and stay stable under high interstitial fluid pressures and face other cells as macrophages and fibroblasts before reaching tumor cells. Beside poor and heterogeneous blood perfusion in tumor environment there are irregularities in convective flow throughout tumor tissue.

To provide a direction for blood flow from vessels, through interstitial space and finally to lymphatic ducts there is a decrease in pressure in normal tissues. However due to

abnormal and heterogeneous vasculature permeability, poorly developed lymphatic drainage system, interstitial fibrosis and densification of surrounding stroma by matrix building activity mediated by fibroblasts occupying interstitial space, interstitial fluid pressure (IFP) around tumors are increased causing decreased transcapillary transport as well as less efficient drug delivery [106]. Reported with many types of cancer such as breast carcinoma, metastatic melanoma, head and neck carcinoma, and colorectal carcinoma reaching values as high as 60 mm Hg, IFP is uniform in tumor core but decrease significantly in its periphery obstructing tumor penetration further [107]. High IFP is suggested to effect response to treatment.

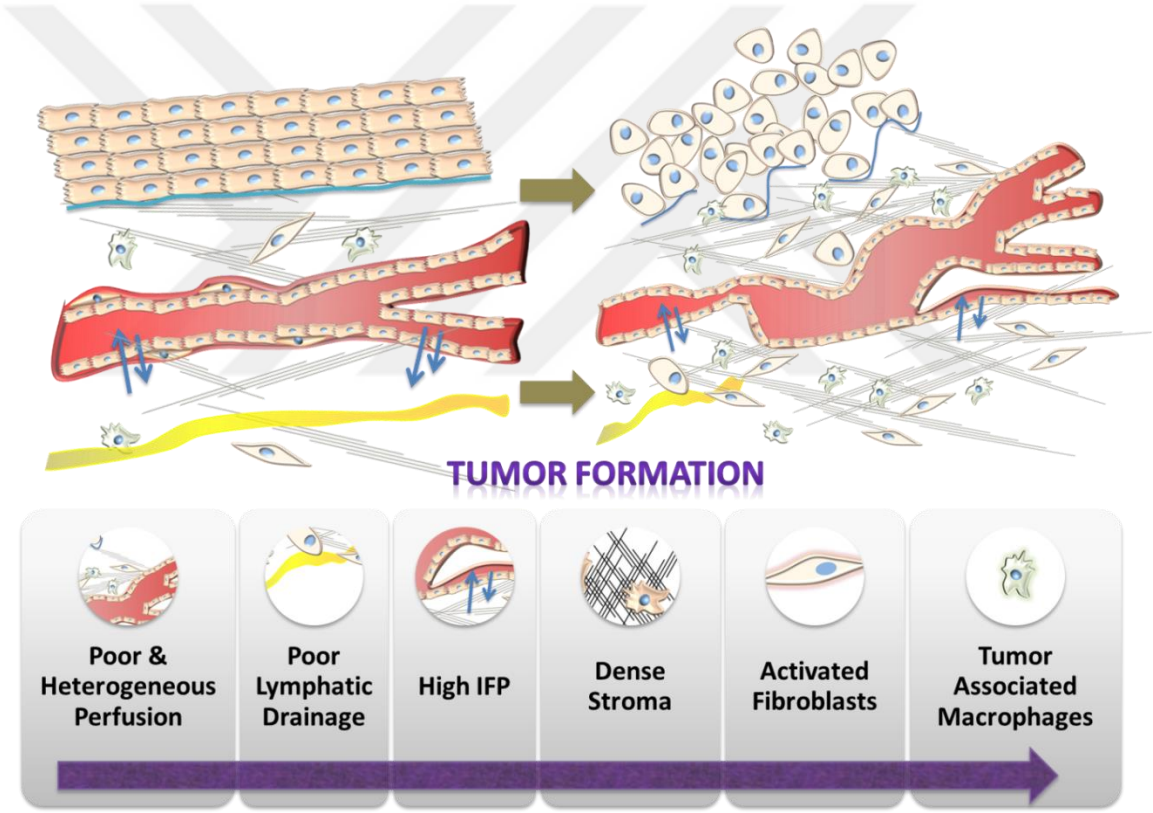

Figure 1. 7. Physiological factors affection NP extravasation and distribution in tumors.

Effect of high IFP was explored in a study where IFP was determined at the initial and final stages of radiotherapy on squamous cell carcinoma of the uterine cervix. Clinical response to radiotherapy was observed with patient showing a progressive decrease in IFP whereas and increased IFP was reported for non-responsive group or recurrence of cervical cancer [108]. So therapies aiming reduced IFPs in hope to increase the transvascular

transport in tumors are trending even though most of the data was generated using small molecules. Either decreasing IFP via triggering tumor vasculature by administrating anti-angiogenic drugs as bevacizumab, and cediranib or targeting stromal fibroblast to decrease contraction of interstitial matrix resulted in improved drug delivery to tumors [109, 110].

The bulk of tumor tissue is composed of high amounts of ECM, fibroblasts deploying ECM, immune cells as macrophages and basement membranes where the cancer cells themselves are only a smaller fraction of total tumor volume [111]. Similar to wound healing process increased rated of inflammatory and matrix building activity is characteristic for tumor tissue through its interaction with surrounding stromal cells, however unlike healthy tissue depending on stromal activation by cancer cells tumor tissue evolves into “a wound that never heals” as described by Hal Dvorak [112].

Cancer cells need their adjacent stroma to provide themselves with a continuous supply of nutrients and supportive environment. By triggering angiogenesis the reactive tumor stroma, desmoplasia, forms required blood and lymph vessels to meet the high turnover rate required for its rapid growth and spread [113]. By activating cell-surface and ECM-bound growth factors matrix metalloproteinases (MMPs) occupying ECM can relay information between cancer cells and its microenvironment. By degradation of ECM fibers as collagen, induction of growth factor by differentiated myofibroblasts and continued aggressive angiogenesis tumor vasculature forms and ultimately invasion of tumor cells through the degraded basement membrane occurs [114].

In this light cancer therapeutics targeting stromal elements are emerging for effective drug delivery. Polymeric conjugates of PEGylated acetylated carboxymethylcellulose and docetaxel (Cellax) were used against orthotopic breast tumor models with high numbers of activated cancer-associated fibroblasts (CAF) in their stroma [115]. Characterized by high α-smooth muscle actin (α-SMA) expression, these CAFs excrete cytokines inducing cell growth and progression of malignancy profile. Compared with regular docetaxel regimen, Cellax showed 70-fold improved tumor perfusion, almost complete removal of CAFs, 50% decrease in total ECM mass and IFP as well as more than 10-fold reduction in number of consecutive metastasis. These effects are suggested due to the high interaction of NPs with SPARC (secreted protein acidic and rich is cysteine) which expressed by stromal cell in

signifanctly high levels. Cellax that is shown to be adsorbed by serum albumin is recognized as a complex by SPARC+ stromal cells and internalized with α-SMA stromal cells (>85%). Another study demonstrated that tumors of fibroblast activation protein-vaccinated mice showed lower degrees of collagen expression resulting in less dense stroma thereby enabling improved doxorubicin, fluorescein and albumin uptake highlighting the potential of stromal targeting for both small molecular and macromolecular therapies [115].

Another essential stromal element is tumor associated macrophages (TAM), present in high number in tumor stroma they have crucial roles in tumor progression since they are essential in immune suppression, promotion proliferation, and metastases [116]. Interaction of macrophages in RES with NPs is well known and as expected, TAMs of stroma can affect NPs transport and drug release. For instance, a study of paclitaxel poliglumex (Opaxio) showed that concentration of drug and its metabolites were 100 to 1000 times higher in TAMs in comparison to tumor cells [117] and an MRI agent conjugated version of poliglumex conjugate indicated that NP carrying TAMs were especially crowded in necrotic areas suggesting that TAMs contributing to distribution of NPs within the tumor [118].

1.8. Active Targeting and Cellular Internalization of NPs

Cell membranes are generally impermeable for large particle, the size of a particle is limited upmost to 10 - 30 nm for uninterrupted passage through cell membranes [119]. Acting as a barrier thereby separating extracellular space, achieving concentration gradients inside cell membranes can orchestrate uptake of larger matter as proteins, nutrients or NPs through endocytotic pathways which is defined as “the de novo production of internal membranes from the plasma membrane lipid bilayer” [120].

Based on the macromolecule or particle to be internalized different types of endocytosis is used by cells. For clearing cellular debris and foreign cells from body by internalization and degradation, removal of opsonized particles, absorption of small solutes volumes the typical route for endocytosis is phagocytosis, that is employed for larger

micron sized particles and available only for professional phagocytic cells such as macrophages, neutrophils, or dendritic cells [121]. On the other hands uptake of nanoparticles occurs via pinocytosis which can be divided into two subgroups adsorptive pinocytosis and receptor-mediated endocytosis [122, 123]. Furthermore depending on type, size and surface properties of NPs to be internalized as well as size and involved proteins forming for pinocytosis process employs four mechanisms.

In macropinocytosis or adsorptive pinocytosis fluids are taken up in a non-specific manner where the vesicle size can vary between 100 nm to 5 μm [124]. In clathrin-mediated endocytosis that is a receptor-mediated endocytosis type, receptor recognition is required forming vesicles around 120 nm which are destined to lysosomal compartments. Similarly, in caveolae-mediated endocytosis that is also a receptor-mediated endocytosis pathway endocytotic vesicles forming around 80 nm do not fuse with lysosomes but just with early endosomes [124]. Finally in clathrin- and caveolin-independent endocytosis pathways vesicle size is much smaller, approximately 90 nm [121].

In case of internalization by clathrin-mediated endocytosis, endosomal escape of carried therapeutics must occur before fusing with lysosomes which are highly acidic. Size wise a maximum limit allowed for efficient internalization is suggested even the vesicle sizes may vary between species, type of cells and enveloped particle size [125]. The possibility and rate of internalization through endocytosis decreases rapidly for larger NPs with sizes above 200 nm [126]. However macropinocytosis triggering formation lamellipodia-like plasma membrane extensions around larger NPs rendering internalization of much larger PEGylated-poly-L-lysine NPs with sizes in the upper 200 nm range possible [127].

Another essential factor determining rate of internalization is shape. Internalization of protein-coated gold NPs was investigated on ovarian cancer cells, brain tumor cells and fibroblast cells that showed a spherical form was more efficient in comparison to rod-shaped NPs [128]. Similarly ellipsoid PLGA NPs were reported to be uptaken as slower rates than their spherical counterparts into endothelial cells [129].

The third factor affecting NP internalization is surface charge and modifications. Negatively charged NPs have disadvantage over positively charged and neutral ones since they are able to utilize clathrin-mediated endocytosis and the rate for other routes of endocytosis is significantly reduced. However clathrin-mediated endocytosis is favored for positively charged nanoconstructs besides upon inhibition of clathrin-mediated endocytosis high NP accumulation in HeLa cells were still achieved via activation of adsorptive endocytosis [130].

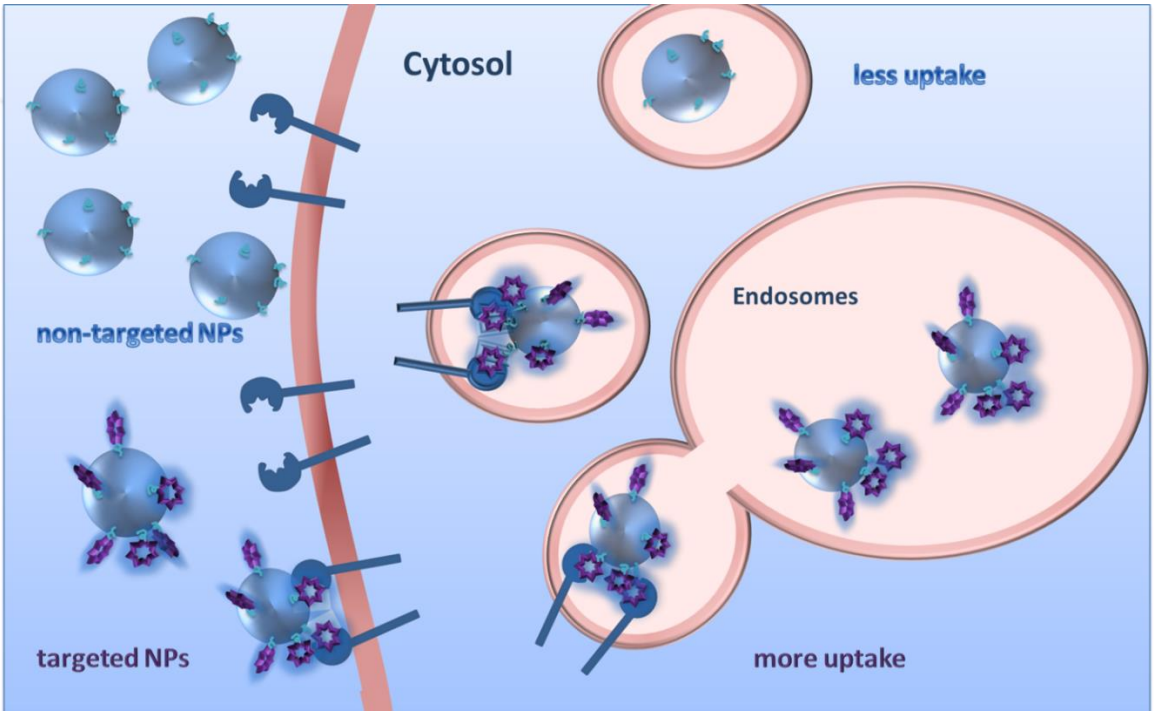

Figure 1.8. Effect of active targeting on NP internalization

Alternative delivery paths are reported for NPs modified with positively charged dendrimers such as poly(ethyleneimine) or poly(amidoamine) (PAMAM) where they can induce disruption of cell membranes and trigger formation of nanoholes providing improved permeability for NPs [131]. Similarly deployment of CdSe and CdSe/ZnS NPs in aggregates around the cell membrane can also result in permeabilization of membrane facilitating internalization [132]. Modifying the surface with proper ligands may control the particular route for endocytosis or lead to endosomal uptake alternatives. For instance conjugating cell-penetrating peptides onto NPs or encapsulating those gold NPs into liposomes can promote internalization through endosome independent pathways,

additionally efficacious nuclear targeting is displayed by an additional nuclear localization signaling peptide conjugation [133].

Target specificity is a limitation for NPs benefiting from passive targeting. An alternative approach addressing this specificity issue is active targeting or ligand-mediated targeting employing particular surface modifications of designed NPs with high affinity ligand moieties to targeted tumor cells (Figure 1.8). In order to benefit from active targeting ligands are chosen so that they can recognize and bind specifically to overexpressed receptors or biomolecules on tumor tissue element, cells or intercellular compartments [4, 134]. The overall efficiency *in vitro* and, most vitally *in vivo* of targeting groups can be affected by admiration route of NPs, opsonization level, ligand density on NP shell, size and shape of NPs as well as type of chosen ligand [135]. Ligands against electively expressed or produced proteins, sugars or lipids molecules presented on targeted tissues and cells can be determined including antibodies, proteins, small peptides, nucleic acids, sugars molecules and other small biomolecules as vitamins [136]. Multivalency arisen due to the increased surface area and incorporated modification of NPs systems augments the interaction between ligands and its target further, thereby increasing probability of recognition and internalization [137]. Even though active targeting can influence specific uptake of NPs general specificity of NP construct still depends on biodistribution of the ligand-functionalized NP and by the non-specific interactions of these targeted NPs with off target agents, highlighting the importance of NP design [134].

Improved cell internalization due to incorporated targeting groups provides improved efficacy for the therapeutic agents as exhibited by anti-HER2 monoclonal antibody fragments (Fab) conjugated PEGylated liposome constructs [138]. Anti-HER2 targeting showed no significant effect on biodistribution, tumor accumulation or long-circulating properties of liposomes yet selective cancer cell internalization was observed for anti-HER2 immunoliposomes in HER2-overexpressing breast cancer xenografts whereas non-targeting counterparts displayed mainly accumulation in stroma and surrounding macrophages [138]. In another study further enhancement of cell recognition was demonstrated by utilizing dual-ligand cancer targeting gold nanoparticles *in vitro*. Designed to explore the multivalent interaction potential of folate and glucose modified gold NPs on human epidermal cancer cells, cellular internalization of dual targeted NPs

was increased by 3.9 and 12.7 folds compared to folate targeted NPs or glucose targeted NPs due to multivalent interactions between both ligands with cancer cells [139].

The first targeted nanotherapeutics were generated employing antibodies due to their fine-tuned specificity and availability [16]. Antibodies are immunoglobulins (Ig) that can recognize specific antigens which are foreign structures. The hypervariable dimeric functional regions at the tip of antibodies are different for each antibody and specific for certain binding sites on antigens. The Fc fragment on the other hand serves for recognition by MPS and immune system. Monoclonal antibodies (Mab) harvested from a single hybridoma cell are widely investigated as targeting moieties since 80s and more than 30 Mabs are marketed as therapeutic agents for clinical use such as rituximab, trastuzumab, cetuximab and bevacizumab [134, 140].

The earliest example on targeted NPs were those in which liposomes were decorated with Mabs [140]. Since they are fairly large biomacromolecules with molecular weights around 150 kDa, the impact of Ab conjugation on NPs can cause significant increase in hydrodynamic size of final NPs and limit effective surface conjugation thus as an alternative conjugation strategies utilizing only the Fab instead of the complete Ab were generated [16]. Additionally available Fc fragments on Ab-NP conjugates can pose a problem since they can be recognized and rapidly cleared by MPS resulting in diminished plasma half-lives [141]. Finally Abs are relatively sensitive to environmental conditions as temperature, salt concentration and enzyme degradation which might create technical difficulties during their production and affect their stability on shelf. Nonetheless there are Ab targeted nanotherapeutics in clinical phases displaying promising results.

An doxorubicin loaded anti-EGFR immunoliposome construct was administrated to patients with EGFR overexpressing advanced tumors showing that this formulation was well tolerated up to 50 mg doxorubicin per m^2 resulting in 1 complete recovery (larynx), 1 partial recovery (mesothelioma) and 10 stable disease (2–12 months) among 26 patients [142]. Another clinical trial at stage I investigated the effect of doxorubicin encapsulated immunoliposome modified with Fab of GAH as targeting group against metastatic stomach cancers. These MCC-465 immunoliposomes showed improved cytotoxic activity against

several human stomach cancer cells in comparison to doxorubicin or non-targeted liposomes resulting in 10 stable disease cases for 6–20 weeks among 23 patients [143].

Other proteins can also be utilized as targeting groups due to their affinity for specific substrates. One such naturally occurring protein with endogenous target is transferrin (Tf) which is a glycoprotein of 80 kDa. Responsible for iron transport and regulation Tf can bind to transferrin-receptors with high affinity which are over expressed by various cancer cells [144]. Efficacy of paclitaxel loaded biodegradable NPs was explored in a murine model of prostate cancer. Animals treated with intratumoral Tf targeted paclitaxel loaded NPs displayed that received complete tumor regression and greater survival rate compared with those treated with non-targeted NPs or paclitaxel [145].

Peptides are favored type of targeting moieties due to their improved stability profiles, ease of synthesis and conjugation. Limited to amino acid sequences less with than 50 monomers they can be linear or cyclic depending on their final structure with improved target affinity. One significant targeting group is the RGD (arginine–glycine–aspartic acid) peptide family binding the $\alpha_v\beta_3$ integrin receptors overexpressed on particular cancer cells as well as angiogenic neovascular endothelial cells [146].

Commercialized as Cilengitide the cyclic RGD peptide cRGDfV is used as an antiangiogenic agent in brain cancer glioblastoma. This small drug candidate has been involved in over 30 clinical trials to date including many at Phase III stage yet even though it was reported to be well tolerated, due to poor efficacy further development was cancelled [147]. Yet employment of RGD peptide as conjugated targeting groups is a promising and popular strategy. For instance, doxorubicin encapsulated RGD targeted NPs were prepared with hydrodynamic diameter of 105 nm and almost neutral surface charges and they displayed regulating effect on the metastatic potential of pancreatic and renal cell cancer in mice. Doxorubicin efficacy was improved almost15 times and RGD targeted NPs showed clear reduction in angiogenesis at tumor environments [148].

In another preclinical study doxorubicin loaded RGD targeted sterically stabilized liposomes showed improved drug efficacies *in vitro* and *in vivo* against melanoma where

targeted NPs were internalized more efficiently, had augmented cytotoxicity on melanoma cells than non-targeted versions. Demonstrating prolonged circulation time and increased tumor accumulation as non-targeted NPs they showed improved tumor retention but higher splenic uptake as well [149]. Similar results were reported in another study with paclitaxel loaded PEG-PLA micelles with conjugated bicyclic RGD4C. Breast cancer cell line treatments *in vitro* and *in vivo* provided enhanced results for RGD conjugated constructs [150].

A more recent class of ligand are nucleic acid based aptamers composed of single stranded DNA, RNA or xenonucleic acids with very high affinity for their targets. Selected by generating large screening oligonucleotide libraries selected aptamers can bind to various targets of small molecules and proteins very strongly. Due to their negative charged phosphodiester backbone employing aptamers as targeting groups on the periphery of NPs can results in decreased blood circulation times due to net negative charge on NP surface. Moreover they can be targets for many nucleases as well rendering their stability as protruding targeting groups problematic [151]. Still an aptamer- drug conjugate showed improved tumor suppression and overall survival. Doxorubicin conjugated to the A10 RNA aptamer with very high affinity to prostate-specific membrane antigen (PSMA) resulted in approximately 2-folds growth in survival profiles in contrast to non-targeted versions [152].

Small molecular targeting ligands can be naturally occurring or synthetically produced; they are small in size, have low production cost and typically high stability profiles. A very commonly used small ligand is folic acid or folate which is a vitamin recognized by folate receptors with very high affinity. Overexpressed in many tumor types ovarian, brain, breast, colon, renal and lung cancers still their expression is patient dependent and treatments should be planned accordingly. Furthermore their use might be limited due to unspecificity since folate receptors are also expressed in healthy tissues and normal epithelia [134]. Still encouraging preclinical examples are present. For instance, folate targeted NPs carrying paclitaxel and yittrium-90 were able to exhibit improved survival in ovarian cancer [153].

Carbohydrates and their derivatives are also widely used small molecule ligands. Many targeting carbohydrate as mannose, glucose and galactose can be recognized by extracellular membrane proteins called lectins [154]. One of the first examples of targeted DDS was a galactosamine doxorubicin construct developed against primary and metastatic liver tumors which failed at phase II trials due to poor efficacy and unspecific liver targeting [56].

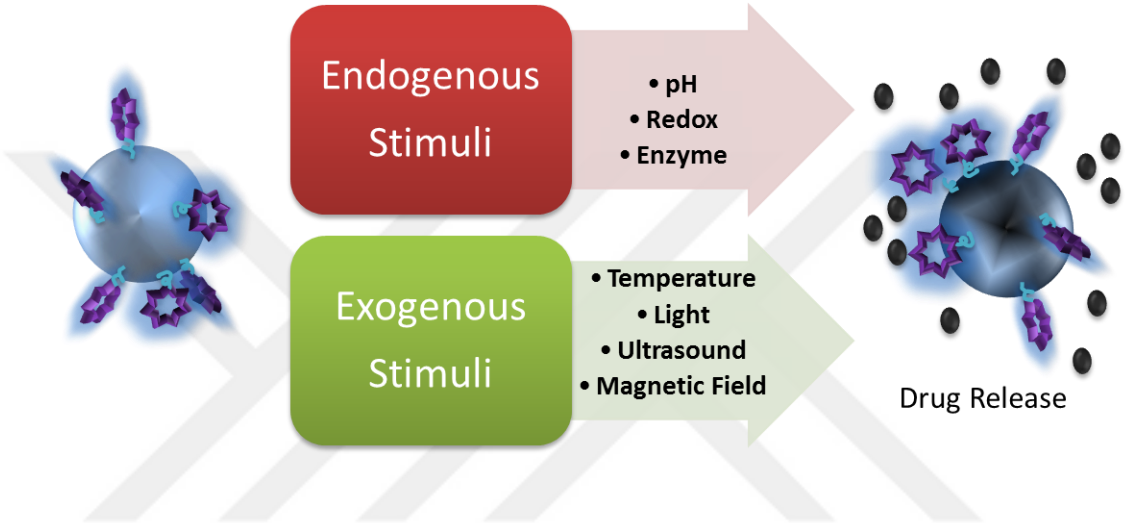

Figure 1.9. Blood Stimuli-responsive controlled drug release

Even though there are still no marketed nanotherapeutic utilizing targeting ligands for improved cell uptake there are multiple liposomal formulations and polymeric NP conjugates in clinical trials including HER2-targeted liposomes MM-302 utilizing a secondary HER2 targeting trastuzumab ligand in combination with HER2 targeted, doxorubicin encapsulating PEGylated liposomes for treatment of gastric and breast cancers [155], the first targeted and controlled-release polymeric NP, BIND-014 utilizing small synthetic ligands to target PSMA present on PLA-PEG micelle encapsulating docetaxel for solid tumor treatment [156] and the first targeted siRNA NP, CALAA-01 utilizing a linear cyclodextrin containing PEGylated polymer construct with transferrin targeting group containing siRNA for triggering RNA interference in production of M2 subunit of ribonucleotide reductase for solid tumor treatments [157].

1.9. Stimuli Responsive Controlled Drug Release

A critical aspect for therapeutic DDSs is controlled and in situ delivery of carried payloads at tumor environment. Gradually leaking NPs can lose their cargo through prolonged blood circulation and upon tumor accumulation only a small fraction of therapeutic can be delivered to tumors. After demonstrating the phase transition characteristics of polyacrylamide gels by Tanaka and studies reporting generation of thermal-sensitive liposome formulations in late 70s, research for similar controlled drug delivery platforms gained importance [158, 159].

Control mechanisms for triggering drug release within tumor environment can be incorporated into NP design based on subtle differences in tumor environment so on endogenous stimuli such as variations in pH, redox potential, concentrations of certain enzymes or specific analytes or alternatively NP degradation can be induced after tumor accumulation via various exogenous stimuli including temperature changes, magnetic fields, ultrasounds, light and electric fields (Figure 1.9) [22].

One of the most widely benefited endogenous stimuli is pH variations in tissues and in intracellular compartments as endosomes or lysosomes. Furthermore pathological conditions as cancer or inflammation can also generate pH gradients. Benefiting from pH differences between healthy tissue which is maintained generally at 7.4, the pH of tumor environment is typically lower than 7.0 due to high metabolic needs and increased glycolysis rates, NPs systems are generated to release their cargo at solid tumor [160]. Similarly upon internalization of NPs they are encapsulated by acidic endosomes (pH ~5–6) and after fusion with lysosomes (pH ~4–5) pH of media drops further which can be used for drug release as well [161]. There are two strategies generally followed for pH responsive DDS, using polymers with ionizable moieties with changeable confirmation in response to pH variations or using polymeric DDS with acid sensitive bonds which can be degraded to release attached therapeutics. For instance polyacetals can be rapidly hydrolyzed in acidic environments rendering them biodegradable and favored polymers for DDS [162].

A pH responsive DDS was generated by PEGylating commercially available aliphatic dendritic polyesters, Boltorn® H40, which form micelles in aqueous environment and encapsulating doxorubicin. Drug release was accelerated at low pH and after internalization by HeLa cells drug could be released in cytoplasm, exhibiting good cytotoxicity [163].

Glutathione (GSH) molecule with differential cytosolic (~2–10 mM) and extracellular concentrations (~2–10 μM) can trigger cleavage of disulphide bonds enabling production of redox-sensitive DDS design. Similar to intracellular concentration, tumor values of GSH is also elevated. Various NP systems as dendrimer–drug conjugates containing thiol-cleavable bonds, liposomes from quinone-lipid conjugates or nanogels with disulphide crosslinkers can benefit from GSH reduction for efficient drug delivery [164]. Likewise excessive accumulation of ROS in tumor tissue is providing an alternative stimuli for novel DDS [165]. One of the earliest redox responsive drug conjugates is Mylotarg where ozogamicin was conjugated to gemtuzumab through disulphide bonds. Approved by FDA in 2000, this conjugate was withdrawn from market since no significant clinical benefit over regular chemotherapy was observed for acute myeloid leukemia patients [166].

Enzymes can also be triggers for DDS providing high substrate specificity and selectivity even it is generally harder to control the primary induction instance. For instance, longer PEG chains providing long circulation times on NPs can be cleaved by matrix metalloproteinases through recognized linker regions resulting exposure of short peptides employed to accelerate cell internalization as in the case of trans activating regulatory protein (TAT) sequence decorated liposomes [167] and cell penetrating peptides CPP conjugated dextran-coated iron oxide NPs [168]. Using this PEG deshielding strategy, a study reported 70% increase in RNAi with their multifunctional envelope-type NP system designed for systemic delivery of siRNA in mice tumor models [169].

Drug release can be initiated by exogenous signals without depending on internal differences within biological system. Among external stimuli including magnetic fields, ultrasound irradiation and light illumination with ranging wavelengths, temperature responsive systems are among most investigated. Employing thermoresponsive drug

delivery platforms can result in improved delivery of therapeutic within tumor environment when the area is heated directly. NPs designed to retain their cargo at physiological temperature of 37°C can be triggered to release payloads immediately at temperatures higher than 40-45°C [170]. Among thermoresponsive systems as micelles, polyacrylamide NP, liposome formulations are well-studied with several types in clinical trials. One such example is ThermoDox from which rapid doxorubicin release can be induced by hyperthermia or radiofrequency ablation for treatment of breast and colorectal liver metastasis (phase II) and hepatocellular carcinoma (phase II) [171].

Light responsive systems are enabling generation of non-invasive drug release platforms which can be turn on and off on demand. By guiding triggering light beams once or multiple times as needed the location of drug release can be controlled. By employing high wavelength illumination such as near infra-red (NIR) radiation deeper tissues can be targeted but with restrains [165].

Ultrasound triggered DDS can also profit from spatiotemporal and on demand control similar to light responsive platforms however frequency tunable depth for tissue penetration is an outstanding advantage for future applications in drug delivery and cancer therapeutics. One study demonstrated that doxorubicin loaded into mesoporous silica NPs with “open state” conformations at low temperatures and at “close state” conformation at physiological temperatures can be released by ultrasound irradiation which triggers conformation change of NPs resulting in increased porosity hence drug release in proximity of targeted cells [172].

Magnetically responsive systems can also provide spatiotemporal release profiles for incorporated payloads furthermore NPs can be guided to the targeting tissues by external magnetic fields. It is also possible to induce temperature increase as well when an alternating magnetic field is applied. Besides, magnetic NPs can provide magnetic resonance imaging thus facilitating both diagnostic and therapeutic use of the DDS. A study designed multi-purpose folate receptor targeted thermosensitive magnetic liposomes which can be guided to targeted tumor cells via a permanent magnetic field. In combination with conjugated folate receptors magnetic liposomes demonstrated substantial increase in cellular uptake in comparison with folate targeted liposomes as well as Doxil.

A secondary magnetic field triggered hypothermia based release system drove rapid and controlled doxorubicin discharge from liposomes reflected by improved cytotoxicity profiles for folate receptor targeted thermosensitive magnetic liposomes *in vitro* [173].

1.10. Therapeutic Potential of Polymeric Micelles

Among the drug delivery systems micelles are one of the most promising systems due to their ease of preparation and ease of modification with various effective moieties such as drugs, targeting groups and labeling agents[174]–[177]. These attractive delivery agents serve as reservoirs for hydrophobic therapeutics as chemotherapy drugs and modified to release those slowly providing improved PK profiles. Micelles can be easily prepared simply from AB type diblock amphiphilic polymers when introduced into aqueous media they can self-assemble into NPs [178]. By controlling polymer composition and arrangement their size, shape, drug loading, release dynamics and targeting manner can be fine-tuned as required (Figure 1.10).

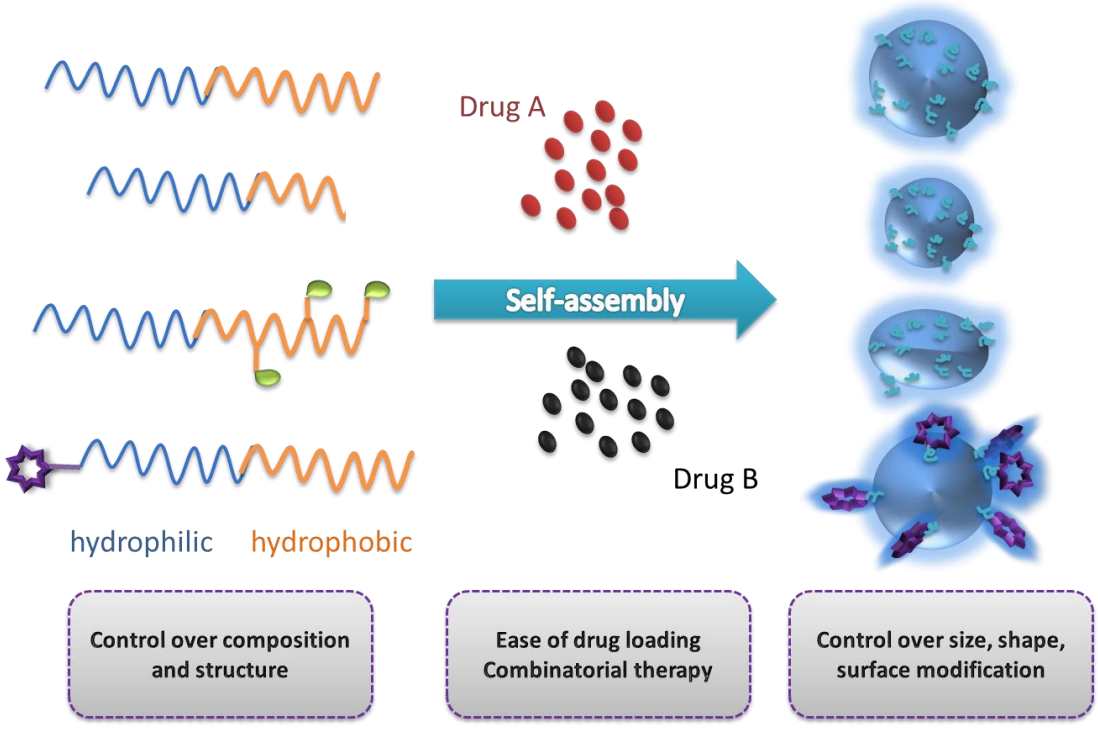

Figure 1.10. Micelle formation and design flexibility

The first micellar DDSs were generated via amphiphilic polymers in late 80s followed by extensive research in micelle based DDS studied to deliver a wide range of therapeutics as small molecular hydrophobic anti-cancer agents, small molecules for contrast/imaging, proteins and nucleic acids including plasmids and siRNA [179, 180]. There are multiple promising candidates to be marketed which are in clinical trials. Beside the pioneering paclitaxel loaded Genexol-PM at phase IV for treatment of head and neck or breast cancer there is pluronic SP1049C, which is assembled from block copolymers od PEG- poly(propylene oxide) (PPO) encapsulating doxorubicin at phase III for in advanced (inoperable or metastatic) adenocarcinoma of the esophagus cancer [181], PEG-PLA micelle, NK105 for paclitaxel delivery to breast cancer and previously treated advanced in phase I [182] or recurrent gastric cancer in phase II [183], and cisplatin doped PEG-PGA NC-6004 block copolymer micelles in patients with solid tumors at phase I stage clinical trials [184]. These studies demonstrated the benefits of polymeric micelles as injectable DDS with positive experimental and clinical results leading to development of similar or improved micellar delivery systems.

Polymeric micelle contains two distinct domains in their final structure, the hydrophobic core domain utilized as reservoir for hydrophobic molecules and the hydrophilic shell domain protecting the nano assembly from environmental agents. The formation of these domains is self-driven due to presence of hydrophilic and hydrophobic blocks of within block copolymers when introduced to aqueous media [180]. Core unit can encapsulate hydrophobic molecules through non-specific interactions or they can be conjugated to hydrophobic domains of block copolymers providing longer release profiles [185]. The hydrophilic shell, generally employing PEG polymers with varying size and confirmations, limits opsonization thereby improving serum stability, facilitating escape from RES agents including macrophages, decreasing filtration by kidneys and spleen thus contributing to prolonged blood circulation times.

There are extensively studied DDS platforms employing surfactant based micelles, soluble polymers, naturally occurring or synthesized insoluble polymers, lipoproteins and liposomes as alternative to polymeric micellar nanotherapeutics. There are both strong points and drawbacks to these delivery platforms [186]. For instance surfactant based micelles formed from low molecular weight charged molecules suffer from poor

thermodynamic and kinetic stability due to high critical micelle concentrations (CMC). Liposomes are also widely used delivery platforms with many samples in market and clinical trials however they show no significant advancement in efficacy of loaded therapeutics owing to shortcomings such as poor encapsulation efficiency, low shelf lives and fast leakage of drugs in aqueous core upon contact with plasma components leading to decreased their therapeutic potential [187]. On the other hand polymeric micelles can encapsulate high amounts of drugs exhibiting improved loading capacities, higher plasma stabilities and overall therapeutic potential. Benefiting from EPR driven passive targeting as other nano-DDS enhanced tumor accumulation is obtained. Using copolymers in block confirmation provides chemical flexibility where novel elements can be incorporated to core and shell enabling multifunctional nano therapeutic design with targeted and controlled drug delivery [188].

1.11. Modification Potential of Polymeric Micelles

Achieving therapeutically significant drug levels during systemic dosing of polymeric micelles is an essential issue for developing effective delivery platforms which can progress to clinical trials. An important factor to provide optimum drug loading efficiency depends on miscibility between incorporated drugs and polymeric units of micelles. Increased miscibility between drug and hydrophobic domains of exhibited by decreasing Floury–Huggins interaction parameter is representative for augmented drug incorporation into micelle core [189]. In addition to hydrophobic interactions, polar interactions and hydrogen bonds formed between polymers and drugs was shown to play a noteworthy part in drug solubilization potential as well. Increasing the hydrophobic domain of a block copolymer resulted in increased drug loading of two water insoluble Cucurbitacin anticancer drugs whereas the drug with higher hydrogen bond formation ability showed both increased encapsulation efficiency as well as decreased release rates in comparison to the lacking hydrogen bonding ability [190]. Further studies also indicated that the length, type and side chain substitutions on polymer chains can alter drug loading into core regions. For instance, drug loading content was increased from 3.1% to 4.4% when the poly(ε-caprolactone) (PCL) part of PEG-PCL block copolymers was increased 10-fold 2.5 to 25 kDa. Interestingly, hydrodynamic diameter of resultant micelles was also

affected where micelle size increased from 22.9 to 104.9 nm with the increasing PCL content [191]. A study achieved increased amphotericin B encapsulation by incorporating fatty acid to the side chains of side groups to hydrophobic poly(l-aspartic acid) part of PEG- poly(l-aspartic acid) polymeric micelles. Drug content of resulting micelles was increased 13-fold in comparison to micelles with benzyl core groups. Introducing pendent cholestryl, stearyl, palmitoyl and carboxyl substituent groups to micelle core resulted in improved drug loading of 1.8, 2.1, 2.3 and 2.7-fold respectively [192, 193].

Chemotherapy drugs are often administrated in combination to optimize treatment with minimum toxicity and overall survival [194]. Even though injection of multiple drugs with solubilizing agents there is the potential of aggregate formation and precipitation which may lead to embolisms or at least diminished of therapeutic activity of administered agents. To overcome precipitation drugs are typically injected successively and from separate preparations resulting in different PK profiles hence varied tumor accumulations. To achieve optimum efficacy from administered drugs DDS as polymeric micelles can be utilized providing delivery of multiple therapeutics simultaneously, with calculable dosing, parallel controlled release kinetics and optimized PK and biodistribution profiles [195].

A study developed a micellar delivery platform for multiple anti-cancer drugs form PEG-poly(aspartate hydrazide) block copolymers where doxorubicin and wortmannin were conjugated to separate polymers through acid-labile hydrazone bonds. Polymer–drug conjugates with distinct doxorubicin/ wortmannin content were assembled with sub-100 nm micelle size. Cytotoxicity experiments indicated that mixed micelles was able due achieve inhibitory effect with reduced doxorubicin due to synergetic activity of wortmannin on breast cancer cell lines highlighting the potential of utilizing polymeric micelles for combination therapy to reduce *in vivo* effective doses and toxicities of particular drugs [196]. It is also possible to incorporate drugs through conjugations to achieve predetermined drug loading as well as ease of incorporation for moderately hydrophobic drugs as demonstrated by a doxorubicin conjugated PEG–PLA polymer based micellar system where drug loading was improved 4-fold via conjugation [197].

One major obstacle for micellar DDS is retaining its stability upon administration into biological systems. Early elimination through RES recognition is typically avoided by PEG block forming a protective corona against harsh opsonization. However injecting micellar DDS to biological system with high volumes so under sink conditions can trigger immediate dissociation of aggregates which is an undeniable problem. When the concentration of the micelle forming units reaches a construct specific concentration, the units aggregate into micelles. This concentration, called critical micelle concentration, is very crucial for drug delivery systems as it indicates the thermodynamic stability of the particular micelle and it is generally depend on the hydrophobicity of block copolymer.

Upon dilution as in the case of injections to blood stream, micelle structure should not be disturbed which may result in burst release and premature delivery of cargo before reaching its target. So any micellar system designed to be a drug delivery system should have an approximate CMC value of 1 μM or lower [12, 198, 199]. Similarly micelles with low CMC values have higher possibilities to stay intact in blood circulation. However once under CMC micelles start to dissociate into polymeric units at different rates based on their kinetic stabilities which is largely determined by physical state of the core as crystallinity level. To improve thermodynamic and kinetic stability levels core modifications can be utilized such as adjusting hydrophobic block to achieve decreased CMC, stabilizing core by crosslinking or increasing intramicellar interactions.

The most common approach to decrease CMC is through increasing hydrophobic interactions in-between of block copolymers. It can be achieved by increasing the length of linear hydrophobic segment, introducing hydrophobic side chains as in the case of modification of core forming block-poly(l-aspartamide) (PLAA) block of PEG-PLAA micelles. Effect of changing PLAA length introducing spacer group or fatty acids at varied substitution levels were investigated and most prominent results were observed by changing length of the PLAA block and the level of fatty acids attached to the backbone. Attachment of multiple fatty acid chains resulted in an increase in micelle size and reduction of CMC whereas increased PLAA was reflected by increased micelle size and core viscosity [200].

To increase kinetic stability of polymeric micelles modifications to increase intramicellar interactions can be employed. In a study the rigidity of micelle core was increased by modifying PEO–PCL polymeric units with α-benzyl carboxylate groups thereby maximizing core stability through π–π stacking. The resulting micelles showed almost 100-fold decrease in their CMC values compared with PEO–PCL micelles with α-carboxyl on the PCL block [201].

Another strategy is to trigger micelle formation through oppositely charged block copolymers which can assemble into stable polyion complex (PIC) micelles. Due to ion-pairings between core forming polymer units as well as loaded charged bioactive molecules the resulting micelles are stable assemblies due to counter ion releasing polycations can decrease the dielectric constant of micelle core. Various biomolecules have been incorporated to PIC micelles including antisense oligonucleotides, plasmids, siRNAs as well as messenger RNAs (mRNA) and proteins [202]. Incorporation of hydrophobic agents as cholesterol to the core can further enhance core stability hence can improve *in vivo* effectivity of micelles [203].

Another advantage provided by use of PIC micelles for nucleic acid delivery with targets located in intracellular compartment is endosomal escape of nucleic acid based cargo which is typically prone to acid hydrolysis. Core-forming polycations can be altered to attain increased buffering capacity thereby resulting in disruption of endosomal membranes [204]. In a study PIC micelles were prepared via spontaneous self-assembly of anti-angiogenic siRNA fragments with block copolymers of PEG- poly(l-lysine). PEG block was further modified with an RGD peptide. Administration of stable RGD targeted PIC micelles were resulted in tumor growth inhibition of subcutaneous HeLa tumor models via gene silencing through encapsulated siRNA [205].

Core crosslinking strategy is another approach to obtain stable micelle core which show resistance to dissociation under harsh dilution condition subjected to after injections to blood stream. Hydrophobic block of block copolymers can be modified to have free thiol groups which can be later crosslinked with suitable linkers or with themselves via thermal or photo initiated polymerization or click chemistry [206]. However while crosslinking can improve core stability it can result in decreased excretion of NPs from

body. To overcome poor biodegradability reversible crosslinking was employed by advanced DDS platforms. For instance micelles composed of poly lysine and poly aspartate hydrophobic blocks as core forming units were core crosslinked by oxidizing thiol groups introduced to lysine block. Stable in blood circulation micelle dissociation was triggered after endocytosis in reducing environment of cell interior [207].

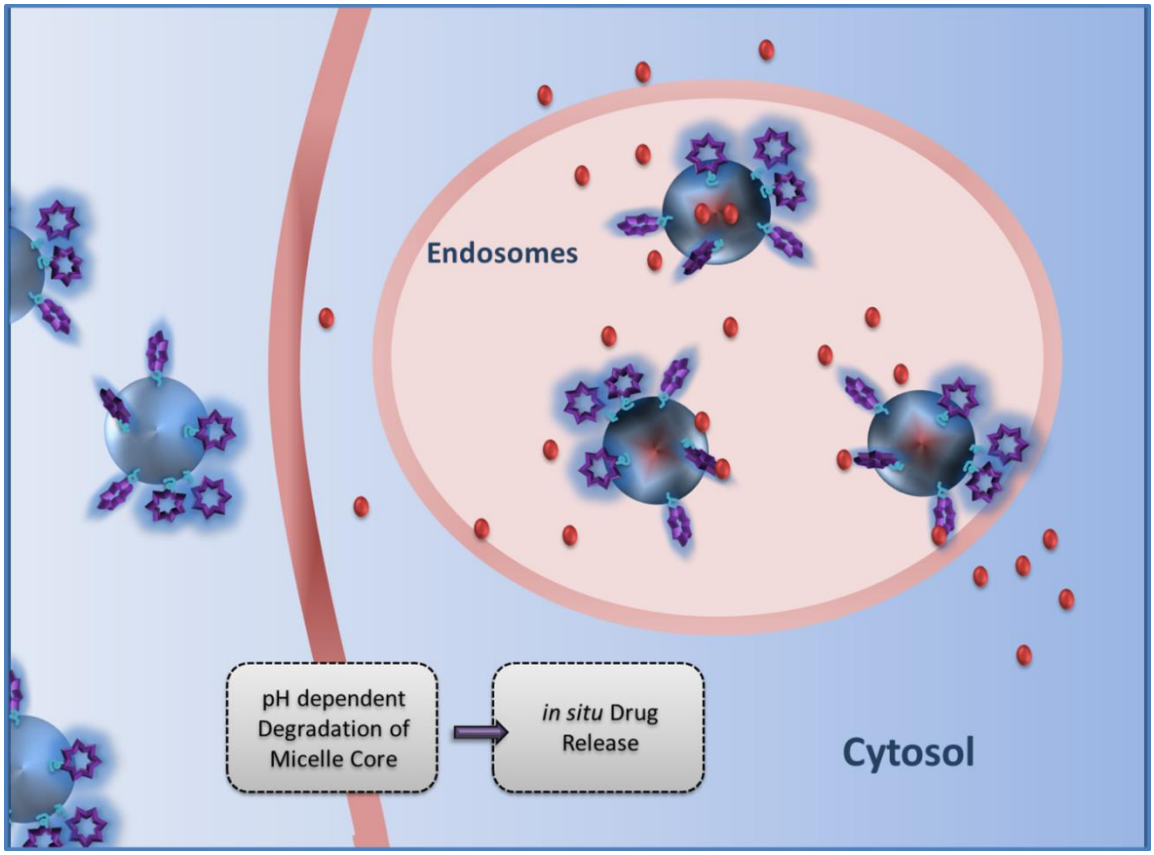

Figure 1.11. pH dependent micelle dissociation after cell uptake

Designing micelle core to achieve optimized drug release profiles is another concern for development of micellar DDS. Strong interaction between core forming units of block copolymers and encapsulated therapeutics is not only important to obtain high drug loading percentages but also it affects rate of drug delivery. Physically encapsulated drugs are typically released to environment through diffusion, while therapeutics trapped in the cores of polyion complexes are released via exchange reactions with free ions and proteins in the physiological media. To adjust the mode of delivery to achieve instant, sustained, pulsed

or delayed drug release profiles, rigidity and hydrophobicity of micellar core can be modified.

Many polymeric micellar DDS exhibits a sustained mode of release for incorporated therapeutics. For instance doxorubicin conjugated PEG- b-Asp provided a delayed profile for doxorubicin release which was not triggered until micelles were encapsulated into acidic endosomes (Figure 1.11). However amide linkages between drugs and aspartate monomers were found to be too stable for achieving sufficient drug release percentages *in vivo* [207]. Another group chemically conjugated doxorubicin to PEG-b- poly(D,L-lactic-co-glycolic acid) again via amide bond and they obtained a sustained release profile for resulting micelles which were incubated in phosphate buffered saline (PBS) and released only 50% of their cargo while complete drug release was observed in just 3 days for their physically doped counterparts. The same group improved *in vitro* cytotoxicity results by exchanging the amide linker with acid labile hydrazone linker between doxorubicin and PLA domain of PEG-b-PLA micelles. Release rates were increased 5-fold represented by improved toxicity levels obtained through in vitro studied done on human lymphoblast cells highlighting the role of pH dependent drug release triggered during endocytosis on drug efficacy [208].

In another approach for pH dependent drug release ester linkages were employed conjugating methotrexate to micelle forming PEG-b-poly(2-hydroxyethyl-L-aspartamide) block copolymers. By changing conjugation levels of drugs varied methotrexate release ranging between 5 to 20% was obtained within 21 day incubated in PBS. Conjugates with higher amounts of conjugated methotrexate showed not only improved CMC values but drug release was slower in comparison [209].

A study by Gillies and coworkers a pH responsive micellar delivery system was generated utilizing PEGylated hydrophobic dendrons of polylysine or polyester. Dendron periphery was further modified with highly acid-sensitive cyclic acetals containing hydrophobic groups. Introduction of rapidly cleavable acid hydrolysable linkers to the micelle core resulted in increased hydrophilicity of hydrophobic core which in turn lead to the destabilization of micelles enabling drug release near acidic environments but retaining stability at physiological pH values [210].

Physically encapsulated micellar formulations of chemotherapeutic drugs can provide significant improvements to *in vivo* antitumor activity by providing sustained release over shorter periods. For example NK105 which is now in clinical trials for treatment of various cancer types is micellar formulation of physically encapsulated paclitaxel in micelles composed of PEG-b-Asp block copolymers [211]. The hydrophobicity of aspartate block was increased via esterification reactions between its carboxylic acid groups and phenyl-1-butanol thereby improving both stability and drug loading as well as providing sustained drug release profiles from hydrophobic core. NK105 demonstrated much slower clearance rates in plasma than free drug, while NK105 was still detected in circulation up to 72 h after injection; paclitaxel was cleared after 24 h of injection. As a result paclitaxel encapsulated micelles achieved 25-fold higher AUC tumor values in comparison to free paclitaxel upon administration to human colonic cancer tumor bearing mice.

To shift the standard therapy employed in cancer treatments precise control over dosing of anti-cancer drug to tumor cells and stromal element is essential. The improved therapeutic indices of the administrated drugs can be obtained by controlling released drug concentrations, dosing duration and retention length of penetrated drugs in tumor environment. Exposing cancer cells to small doses of therapeutics over prolonged periods contributes to enhanced sensitivity to chemotherapy agents by those cells compared to higher doses over short intervals. In this context, polymeric micelles can provide the required controlled drug release dynamics granted by tunable and flexible design of their polymeric domains [212].

Polymeric micelle with already poor thermal stabilities may suffer from early release and to improve their kinetic stabilities determining dissociations rates under CMC values is crosslinking of micelle coronas thereby forming core-shell corona micelles using triblock copolymers [213]. However crosslinking of the micellar corona can affect core permeability so alter drug release rates. One study utilized triblock methacrylate copolymers with photo-cross-linkable moieties. Micellization was triggered under basic conditions and crosslinking was triggered via UV irradiation. Even though resulting

micelles were exhibited reversible pH-responsive behavior where cores displayed swelling at acidic drug release rates were not improved significantly.

Micelles typically employ PEG polymers as their hydrophilic block forming a protective shell around hydrophobic cores. Similar to other NPs utilization of PEG provides prolonged plasma circulation times by decreasing interactions with opsonins and RES recognition. However once in proximity of target tissue PEG shell might act as a shielding layer thereby impair diffusion rates and result in poor internalization profiles.

Micellar DDS can be designed to shed their PEG shell at the target site by differential pathological stimuli as change of pH or intracellular reducing environment resulting in improved dissociation of micelles and increased on target release rates. For instance PEG-b-poly(aspartamide) copolymer based micelle incorporated a biocleavable disulfide linkage between its Peg and polycations blocks so that detachment of PEG shell would be triggered under reducing environments and release of carried plasmid DNA would occur [214]. In accordance with design elements micelles displayed enhanced delivery of plasmid DNA inducing 1–3 fold higher gene transfection efficiency and faster onset of gene expression than PEG-b-poly(aspartamide) micelles lacking reducible disulfide linkages.

Approaches combining core-crosslinking and PEG shedding features can benefit from both improved serum stabilities and increased rates for cellular uptake and drug delivery. Polymeric micelles employing triblock copolymers of PEG-b-poly(L-lysine)-b-poly(rac-leucine) provided dual functions since shell forming PEG block was conjugated through disulfide bonds to poly(L-lysine) block and again poly(L-lysine) block was further crosslinked through its amines with disulfide-containing cross-linker. Introduction of redox sensitive disulfide linkages at multiple sites rendered PEG shell of micelles detachable and crosslinks at corona cleavable. Prepared crosslinked micelles demonstrated augmented camptothecin release rates at cytoplasmic GSH levels in comparison to PBS and GSH at physiological concentration. Similarly they exhibited improved *in vitro* cytotoxicity values and cell uptake by HeLa cell highlighting their potential use as DDS platforms [215].

The level of micelle complexity can be tuned by introducing hydrophobic polymer blocks to both sites of hydrophilic PEG block where the resulting micelles have PEG chains in a twisted and coiled confirmation thereby attaining “flower micelle” shapes due to the structure of their PEG shells (Figure 1.12). Hydrophobic molecules such as anticancer drugs can be covalently attached to the hydrophobic sides of these polymers or physically doped into the hydrophobic cores of micelles to further modify their release and stability profiles [216–218].

A study utilized ABC type triblock copolymers to form pH responsive flower micelles with poly(*N*ε-(3-diethylamino)propyl isothiocyanato-l-lysine)-b-PEG-b-PLA polymeric units. Polylysine block provided pH dependent hydrophobicity, hydrophobic at physiological pH and hydrophilic at acidic, PEG domain provided coiled PEG shell and finally PLA domain provided hydrophobic biodegradable core. Micelles with low CMC values and micelle size of 165 nm were obtained. Slightly acidic pH values as pH 6.8 demonstrated to trigger doxorubicin release and by increasing acidity to pH 6.0 release of encapsulated drug reached up to 90% over the course of 24h. On the other hand drug release was stabilized at 35% for micelles incubated at pH 7.4 [216].

A similar study constructed also generated a pH responsive flower micelle using PLA-b-PEG-b-poly(l-histidine) where core deformation was triggered even by small change in pH from 7.4 to 6.6 possibly driven by deprotonation of poly(l-histidine) block. Interestingly, it is demonstrated that after deformation of micelle core poly(l-histidine) block was located to the micelle periphery whereas micelle core was reformed by PLA block only which was traced by shift in emission spectra of encapsulated pyrene dye [219].

To investigate the surface charge on integrity micelle and effect on its PK profile, a an α-acetal-PEG-PLA polymer was synthesized which was later conjugated with small peptidyl ligands, tyrosine (Tyr) and tyrosyl-glutamic acid (Tyr-Glu) providing either neutral or negative surface charges at physiological pH values to prepared PEG-PLA micelles, respectively. Both micelle systems were demonstrated substantial circulation times in blood where 25% of administered dose was still detected after 24h. Additionally decreased spleen and liver accumulations of anionic micelles indicated the role of negative surface charge for avoiding non-specific organ accumulation [220]. However negative

surface charge of micelle may result in diminished cellular uptake rates and poor drug release profiles thereby limiting the potential of the system.

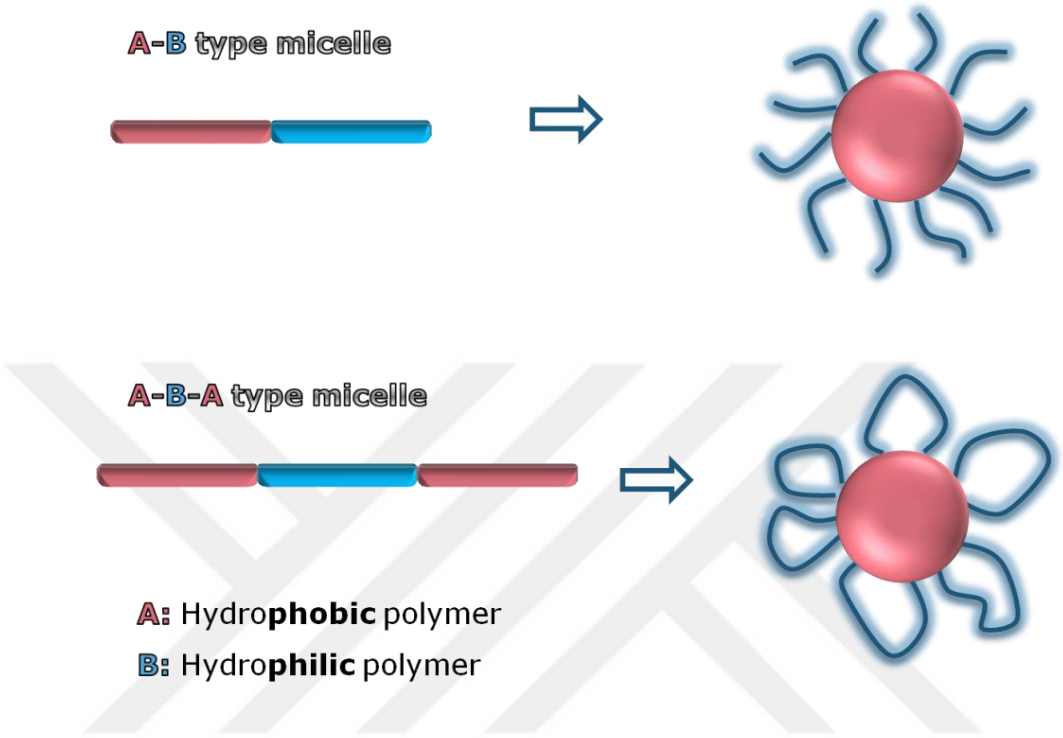

Figure 1.12. Flower micelle formation via triblock copolymers.

Another study utilized a pH dependent surface charge-switched polymeric micelle system consisting of PLA-b-PEG-b- Polylysine-2,3-dimethyl maleic acid (DMA) triblock copolymers. DMA providing anionic character at physiological pH dissociated from shell at slightly acidic media as tumor environment leading to a positive surface charge due to polylysine block at the shell. Furthermore poly histidine polymer encapsulated separately to the micelle core was able to induce drug release at acidic environments since its side chains became positively charged [221].

Another essential factor determining usefulness of PEG shell is its grafting density which can define the level of interaction of the micelle and other environmental elements affecting its final stability. Polymeric micelles composed of the graft copolymer, poly(d,l-lactide-*co*-2-methyl-2-carboxytrimethylenecarbonate)-*g*-PEG with varying PEG grafting densities (an average of 0.5–6 10 kDa PEG chains per backbone) were prepared thereby providing stable hydrophobic core composition while changing PEG amount incorporated.

Micelles with higher grafting density resisted dissociation in serum environment over the course of 72h incubation highlighting importance of PEG distribution for PK profiles of nanotherapeutics [222].

1.12. Dendrimers, Dendrons and Their Conjugates as Nanotherapeutics

Dendrimers or dendrons are polymers with well-defined structures due to their step-by-step preparation composed of AB_n type monomers (*n* usually 2 or 3) rather than the standard AB monomers which result in linear polymers. Secondly, they are synthesized in an iterative fashion which not only grants excellent unimolecular molecular weight distribution but also enables the required core and/or peripheral functionalization upon demand [174, 223, 224]. Furthermore their highly branched structures provide multiple modifiable surface groups and large interior volumes enabling host-guest chemistry [225]. Micelles prepared from dendritic domains have improved features as low PDI and low CMC values then linear polymeric micelles since their covalently bound stable internal cavities can limit dissociation significantly [226].

Newkome and coworkers introduced the concept of unimolecular micelles with providing a stable platform with lipophilic interior and a hydrophilic surface. Unlike micelle of linear polymers the unimolecular structure maximized thermodynamic and kinetic stability of resulting delivery platform. The internal hydrophobic regions were shown to serve as reservoir for hydrophobic small molecules, upon introduction of internal heterocyclic moieties association with specific binding of guest molecules was possible [227]. Additionally polytryptophane terminated dendrimers were prepared to highlight their potential for surface modifications [228]. These studies accelerated the employment of dendritic micelles in therapeutic systems for drug delivery, in gene therapy, and for carrying contrast agents in imaging.

Owing to their compact structure dendritic systems were shown to have enhanced rates for tissue extravasation and internalization in comparison to linear polymers with similar molecular weights. In a study by Ghandehari and coworkers utilized fluorescein isothiocyanate-labeled poly(amidoamine) PAMAM dendrimers with varying generations

hence size and molecular weight together with their linear counterparts PEG with similar molecular weights to inspect resulting differences with extravasation rates across microvascular endothelium [229]. By increasing PAMAM dendrimer generation an exponential increase in extravasation rates was reported. On the other hand the process of extravasation through endothelia pores was stalled more. For instance a generation 3 dendrimer was extravasated in 203.8 seconds whereas time required for the complementary 6 kDa linear PEG polymer to cross the epithelium was doubled to 453.9 seconds most probably due to the higher hydrodynamic volumes of PEG chains suggesting that on top of molecular weight of particles factors as molecular geometry may alter their microvascular extravasation.

Another study explored the effect of dendrimer surface charge on cell uptake as well as size and concentration on an everted rat intestinal sac system. Radio-iodinated cationic and anionic PAMAM dendrimers were incubated with everted sacs *in vitro* and by tracking the progress of radioactive agent with time demonstrating notable improved transfer rates for anionic dendrimers over serous membranes. Size wise the larger generation 5.5 anionic dendrimer displayed higher tissue accumulation then generations 2.5 or 3.5 dendrimers whereas cationic PAMAM dendrimers showed slightly slower serosal transfer rates however higher tissue accumulation rates [230].

One of the most widely investigated dendrimer family is PAMAM dendrimers which can have either amine groups or carboxylic acids for termini depending on step of synthesis to increase generation. The presence of these functional groups makes conjugation of various moieties possible. Furthermore encapsulation of hydrophobic guest molecules is possible by modifying dendritic cores with hydrophobic linkers and by noncovalent interactions through tertiary amines [231]. However the lack of biodegradability and impaired biocompatibility of PAMAM dendrimers are major factor restricting their use for biological applications.

A study used PAMAM dendrimers, poly(propylene imine), and PEG-grafted carbosilane dendrimers with different generations as well as surface functionalities to demonstrate their effect on biological properties *in vitro* [232]. In general dendrimers with amino termini exhibited concentration dependent hemolysis where deterioration of red cell

morphology was triggered even after 1 h incubation at low concentrations as 10 μg/mL. On the contrary, dendrimers with anionic surface charges exhibited diminished hemolytic behavior except high generation carboxylic acid terminated PAMAM dendrimers. Similarly enhancement of blood circulation times was observed generally for anionic dendrimers where intravenous administration of cationic PAMAM dendrimers showed rapid removal of in 1 h whereas anionic counterparts were still detected in blood stream (~20–40% recovered dose in blood). However introduction of PEG modification on potentially toxic cores improved resulting cytotoxicity profiles indicating the importance of PEG coating for biocompatibility. Modification of PAMAM surface with PEG to decrease its cytotoxic potential is encouraging however it has been suggested that incorporation of PEG chains can impair its encapsulation efficiency affected by length of attached polymers [233].

Surface modification potential of PAMAM dendrimers was displayed by another study where PAMAM dendrimers with generations three through six were mannose surface residues along with hydroxyl functional groups to improve biocompatibility. The degree of surface carbohydrate functionalization was stoichiometrically controllable furthermore effectivity of mannose sugars was demonstrated by quantitative precipitation assays employing mannose binding concanavalin A lectin [234].

Another group of dendrimer family with amine groups on the periphery is poly(propylene imine) (PPI) dendrimers commonly studied for biological applications. Suffering from similar problems as PAMAM due to their amine termini, PPI dendrimers were modified to obtain biocompatible surface groups or stimuli responsive controlled release platforms due to the presence of pH sensitive tertiary amines in their interior. The pH dependent pyrene release from unmodified PPI dendrimers highlighted their potential as controlled delivery systems however release can be triggered over a broad pH range. To fine-tune release dynamics amine groups on the surface was modified by of hydrophilic quaternary ammonium groups resulting in improved water solubility and release dynamics where pyrene release was limited to a more narrow range due to sealing effects of surface quaternary ammonium groups [235]. Also incorporation of PEG arms to the PPI dendrimer periphery resulted in augmented solubility, improved biocompatibility as well as increased plasma circulation times. Encapsulating betamethasone valerate and betamethasone

dipropionate as steroid drugs, drug release was induced at low pH values however incomplete. The staggered release was overcame by diluting the dendrimer-PEG conjugates thereby achieving complete release of cargo which might be impaired due to blocking effect of peripheral PEG chains [236].

In another study guanidinium groups were conjugated to PPI dendrimers together with PEG polymers to achieve both targeted and controlled drug delivery of betamethasone valerate. Loading capacity of dually modified dendrimers were increased to 11% in comparison to PEG modified dendrimers with 6% or unfunctionalized dendrimer 1.7%. Drug release was induced with NaCl addition suggested to an uncontrolled drug leakage which might be problematic for PEGylated PPI dendrimers as DDS [237].

Other types of dendrimers as benzyl ether and melamine-based were also used in combination with PEG modifications to generate soluble delivery systems. The periphery of benzyl ether dendrimers was modified via hydrolysable ester/carbonate/carbamate linkages to conjugate small molecules as cholesterol and amino acids and PEGylated to render the resulting dendrimers water soluble [238]. Even though the dendrimer backbones were non-biodegradable, high drug encapsulation percentages were achieved by benzyl ether dendrimers as in the case of indomethacin that was incorporated to the dendrimer interior with 11% weight percent and showed sustained drug release in vitro [239].

Due to the significant potential of dendrimers for biological applications various types of dendritic backbones were designed however to optimize their use in clinic the generated dendrimer should attain desired features including water solubility, biocompatibility and biodegradability. In this regard a group of biodegradable dendrimers composed of monomers occurring as intermediates or products in metabolic pathways or amino acids are synthesized [240]. Furthermore glycodendrimers utilizing carbohydrates in their core structures as well as at their branching points or at surface are promising constructs as antitumor and anti-infective compounds due to their provided multivalent binding potential [241].

Fréchet and coworkers introduced an ether based dendritic backbone similar to PEG granting biocompatibility to the dendrimer [242]. However the succeeding polyester based

dendrimers composed of 2,2-bis(hydroxymethyl)propionic acid (bis-MPA) monomer units and their conjugates with PEG provided not only biocompatibility and water solubility but also most requested biodegradability to the prepared DDS (Figure 1.13) [243]. The generation of polyester based dendrimers was followed by incorporation of various monomers including glycerol, succinic acid, phenylalanine and lactic acid to achieve production of bio-dendrimers for tissue engineering [244].

Aliphatic polyester dendritic systems based on 2,2-bis(hydroxymethyl)propionic acid show great potential not only due to their biocompatible structure but their provided biodegradable backbone enables pH sensitive drug delivery. Additionally their hydrophobicity can be fine-tuned by generation or peripheral functionalization. The multifunctionality of these dendrimers was demonstrated in a study by conjugating doxorubicin via a hydrazone linker to a high molecular weight (> 20 kDa) 3-arm PEG−dendrimer hybrid [245]. The drug release rates increased by increasing acidity whereas construct stayed stable at neutral pH. Due to gradual release of doxorubicin *in vitro* cytotoxicities on tested cell lines were lower than free drug but constructs exhibited effective toxicity with all cell lines tested. Cell uptake experiments on breast cancer cell lines indicated internalization of drug conjugates in cytosol whereas free drug was localized directly in cell nuclei. Furthermore upon intravenous administration of conjugates to CD1 mice after plasma circulation times for conjugates were significantly higher than free drug however due to their relatively small size as NPs conjugates were cleared in hours. Biodistribution of conjugates displayed minimal organ accumulations whereas doxorubicin showed unwanted accumulation at variety of organs such as the liver and heart. Thus this polyester dendron based system displayed promising features as a biodegradable controlled DDS after some modifications to improve its final pharmacokinetic behavior further.

Since plasma clearance can be regulated by increasing size of DDS thereby achieving high hydrodynamic volumes to escape renal clearance one approach to improve blood circulation times resides on increase dendrimer size. However to increase size of dendritic delivery system by increasing generation is unproductive since production of high generation dendrimers is rather time-consuming and it is possible to diverge from well-defined structure at higher generations. That lead to design of dendritic polymer

conjugate with amphiphilic characters giving rise to larger self-assembled NPs or micelles [240].

Linear-dendritic block copolymers utilizing PEG as hydrophilic block and either a polylysine or polyester dendron as hydrophobic dendron were synthesized where additional hydrophobic groups were attached to dendron peripheries via acid-labile cyclic acetal linkages [246]. Self-assembling to micelles in aqueous environment these dendritic conjugates were sensitive to pH resulting in micelle dissociation through hydrolysis of acetals under acidic condition such as tumor environment or endosomal compartments. Exhibiting fairly low CMC values in comparison to micelles formed from linear block copolymer, these micelles were stable at neutral pH. Providing a dendritic biodegradable core for encapsulating various hydrophobic drug these polyester dendron based micellar systems was able to adopt desired qualities of multiple DDS platforms.

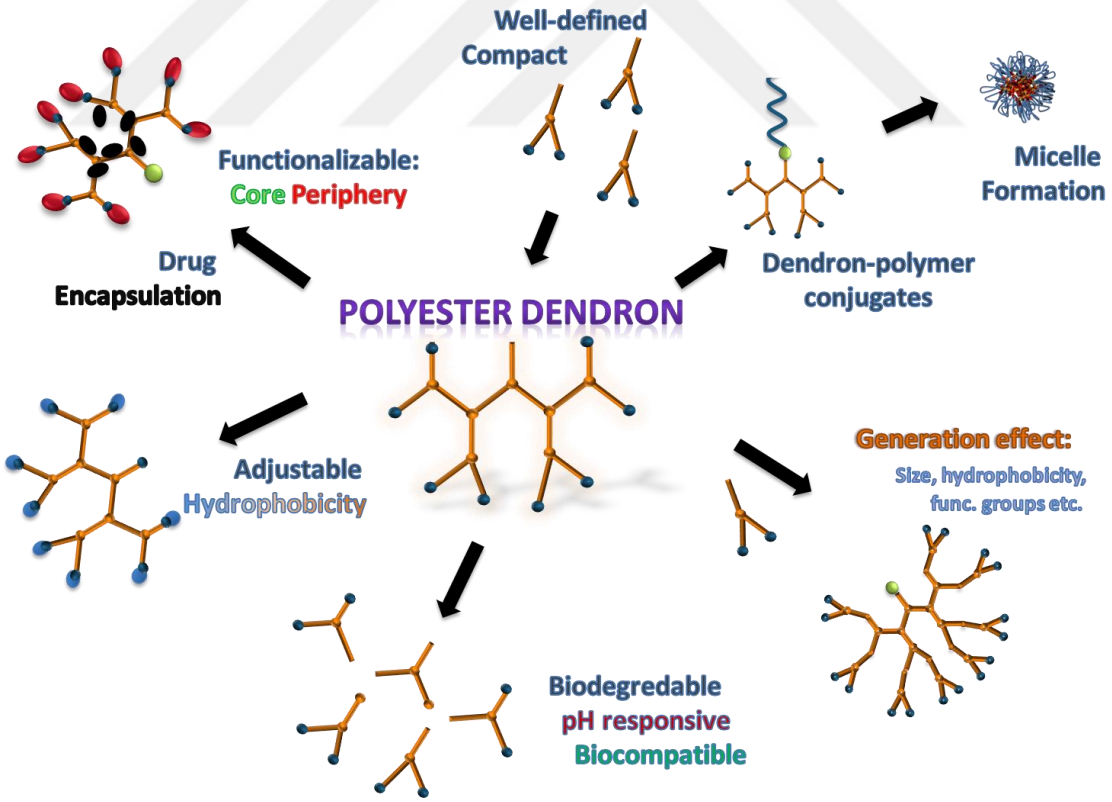

Figure 1.13. Advantages of polyester dendrons

Linear-dendritic block copolymers utilizing PEG as hydrophilic block and either a polylysine or polyester dendron as hydrophobic dendron were synthesized where additional hydrophobic groups were attached to dendron peripheries via acid-labile cyclic acetal linkages [246]. Self-assembling to micelles in aqueous environment these dendritic conjugates were sensitive to pH resulting in micelle dissociation through hydrolysis of acetals under acidic condition such as tumor environment or endosomal compartments. Exhibiting fairly low CMC values in comparison to micelles formed from linear block copolymer, these micelles were stable at neutral pH. Providing a dendritic biodegradable core for encapsulating various hydrophobic drug these polyester dendron based micellar systems was able to adopt desired qualities of multiple DDS platforms.

Similar strategies employing polymer dendron conjugates were developed including bow-tie type conjugates where two orthogonally protected dendrons were conjugated. By selective deprotection steps one dendron was coupled to PEG chains with varying sizes whereas the other dendron served for conjugation of other therapeutics [247]. Furthermore linear polymers containing dendrons at each unit were developed providing aliphatic polyester based highly functionalizable delivery systems with narrow-polydispersity, and biodegradability.

A dendronized ϵ-caprolactone-based polymer was synthesized with molecular weights as high as 80 k Da and with PDI values varying between 1.11 and 1.22 [248]. These dendron-polymer based systems demonstrated augmented PK profiles in contrast to those displayed by linear polymers with equivalent molecular weights and size thereby sustaining prolonged circulation half-lives and improved biodistribution profiles all in all standing out as effective nanotherapeutics [174].

Even though dendrimers and dendron-polymer conjugates present most appealing advantages in comparison there are still limited progress in commercialized product development. The only commercialized PAMAM based MRI imaging agent Gadomer-17 was discontinued whereas a polylysine dendrimer base virocide, Vivagel is in clinical trials as a HIV injection preventative topical gel [249].

1.13. Micelles with RGD and Trastuzumab Targeting Groups

Due to their high potential for flexible design micellar developed DDS can provide multiple functionalities synchronically such as increased circulation times, introduction of targeting groups for improved uptake profiles, stimuli responsive elements. An optimum micelle system can be developed to meet several requirements to achieve maximum drug efficacy. By increased size and shell properties prolonged circulation in blood stream is possible. By conjugating cancer cell specific targeting ligands to hydrophilic block selective uptake by pathological tissue is probable. Drug release can be regulated in a either endogenous and/ or exogenous stimuli responsive manner through alteration of core or shell structure providing. They can be equipped with signaling groups to further increase intracellular delivery of cargo as needed. In combination with therapeutics reporter dyes or contrast agents can be incorporated to their structure supplying real time monitoring of administered cargo. Also biocompatibility and biodegradability of constructs are critical factors for design so that after administration NPs do not lead to unwanted side effects as hemolysis or unspecific organ toxicity and after drug delivery depleted DDS system can be degraded to its building blocks and cleared from body completely and safely.

A multifunctional targeted micellar delivery system was developed exhibiting four-fold improvement in drug efficacy in comparison with non-targeted micelles and reduced toxicity to xenograft tumors then free paclitaxel injections [250]. A linear dendritic block copolymer (LDP) was synthesized employing two fully biodegradable blocks and short PEG chains in its structure. The hydrophobic block was composed of linear polypeptide block of poly(β-benzyl-l-aspartate), which can be degraded under acidic conditions or be cleaved by enzymes to amino acids and the hydrophilic block was engineered to contain generation 3 polyester dendron conjugated with 3 kDa PEG chains to its hydroxyl groups on the periphery which is also pH sensitive due to polyester linkages in its structure. A second LDP group containing folic acid moieties was prepared as well for ovarian cancer cell targeting. By mixing two types of LDPs ligand-clustered micelles encapsulating paclitaxel was generated. Targeted micelles displayed notable increased plasma eliminations half-lives of 15.6 h compared to that of free paclitaxel which was 4.3 h. Furthermore tumor accumulation of targeted micelles increased continuously over the course of 5 days. After administration of 2.5 mg/kg paclitaxel, free paclitaxel injected

group displayed body weight loss between 10% and 12% and hair loss whereas targeted or non-targeted micellar paclitaxel formulations did not resulted in any toxicity. Micelle uptake was clearly observed in 5 h and loaded cargo was located in cytosol in 10 h indicating micelle dissociation in acidic endosomal environment. Tumor efficacy after four doses of therapy over 22 days resulted in significant shrinkage of tumor size with folate-clustered LDP micelles at low paclitaxel doses (2.5 mg/kg) similar to non-targeted LDP micelles at high paclitaxel doses (10 mg/kg) whereas free paclitaxel dosing display almost no reduction in tumor weight.

Another study reported a polymeric micellar delivery system of paclitaxel composed of pH tunable polymeric block which are bearing folic acid molecules for targeting as well [251]. Encapsulated quantum dots acting as fluorescent imaging probe enabled visualization of administrated micelles *in vivo* real-time. Micelle forming polymers were engineered as a triblock copolymer of PEG, poly(N-(N′,N′-diisopropylaminoethyl) aspartamide) (PAsp(DIP)) and cholic acid. Also another set of folic acid conjugated triblock copolymer was prepared and mixed to render the resulting micelles targeting. (PAsp(DIP)) block formed a pH-sensitive core region which was hydrophobic at neutral pH but hydrophilic at acidic tumor environment or in endosomal compartments. Naturally occurring cholic acid on the other hand was utilized as a hydrophobic building block to improve drug encapsulation. Micelles were prepared at acidic pH where cholic acid helped to encapsulate paclitaxel whereas positively charged (PAsp(DIP)) interacted with negatively charged quantum dots. Upon changing pH to 7.4 drug and quantum dot doped micelles was obtained with folic acids at shell periphery. Quantum dot imaging of micelles in nude mice bearing Bel-7402 tumors demonstrated that tumor accumulation of targeted micelles peaked in 3 h whereas non-targeted micelles displayed weaker fluorescent signals. Growth inhibition of subcutaneous Bel-7402 tumors and survival rates of treated animals was notably better for targeted micelles in contrast to both non-targeted micelles and free paclitaxel injections. Moreover targeted-micelles inhibited tumor growth and they even resulted in decrease in tumor volumes. Similarly overall survival times of animals were increased significantly. Also induced apoptosis rates were detected to be increased for tumor cells of targeted-micelle treated mice monitored by elevated cleaved caspase-3 protein as well as DNA fragmentation.

RGD peptides are widely used targeting ligands binding preferably to $\alpha_v\beta_3$ integrins since this type of integrin is found to excessively upregulated on various tumor cells as well as on tumoral endothelial cells playing essential parts in induction of angiogenesis. When tumor volumes become approximately 2 mm^3 increased IFP inhibits diffusion of required metabolites for further tumor growth which leads to a hypoxic state in tumor environment. Development of hypoxia induce increased expression of proangiogenic elements including VEGF, platelet derived growth factor (PDGF), or TNF-α which in turn triggers formation of new blood vessels, disruption of basement membranes and ECM components [252]. These changes causes the transformation of tumor to from a nonangiogenic to an angiogenic phenotype thereby enabling rapid expansion of otherwise asymptomatic and nonmetastatic tumor mass and attaining a more metastatic character [253].

Integrins are among various protein families involved with progression of angiogenesis which are heterodimeric transmembrane glycoproteins. They can relay signals on their own as well as via interaction with growth factors receptors thereby they can play roles at multiple stages of cancer development as malignant transformation, tumor growth, progression, invasion, and metastasis [254]. Extensively expressed on blood vessels of human tumor biopsy samples $\alpha_v\beta_3$ integrins are associated with various types of cancers. For instance in breast cancer $\alpha_v\beta_3$ integrins are connected to bone metastasis, tumor growth, regulation of cellular response to chemotherapy hence increased chemosensitivity. Similarly they are upregulated in invasive regions displaying augmented cell motility in glioblastoma and they are correlated with activation of MMPs and induction of lymph node metastasis in pancreatic tumors [255]. Consequently RGD ligands are extensively used as targeting moieties for multifunctional micellar DDS.

A study utilized RGD targeted dendritic polymeric micelles with generation 3 PAMAM dendrimers forming at the core [256]. Poly(γ-benzyl-l-Glutamate) (PBLG) linear polymer block was conjugated to PAMAM periphery where benzyl group at the side chains served to improve docetaxel loading by noncovalent Pi-Pi stacking interactions. PEG chains were conjugated to PBLG block and finally PEG shell was decorated with cRGD to provide higher cellular uptake of docetaxel in to human liver cancer HepG2 cells. Micelles with average hydrodynamic diameter sizes around 80 nm were obtained with both

targeted and non-targeted micelles. Docetaxel loading was 16.4% and 17.3% for targeted and non-targeted dendritic micelles and the resulting micelles exhibited minimal release at physiological pH which was 21% over the course of 12 days. On the other hand at acidic media drug release approached 50% displaying improved release profiles altered by pH changes. HepG2 cells were incubated with coumarin 6-loaded targeted and non-targeted dendritic micelles and cellular uptake levels of coumarin 6 dye was doubled for targeted micelles after 12 h indicating effect of RGD conjugation on cell internalization. In parallel cytotoxicity experiments indicated that cell viabilities were inhibited most effectively via targeted micelles whereas free docetaxel resulted in similar or higher toxicity compared to non-targeted micelles due to sustained release dynamics.

Another study developed RGD targeted polymeric micellar delivery system of docetaxel for treatment of glioblastoma where poor penetration of the blood-brain-tumor barrier creates various problems for regular treatment regimens [257]. PLA-PEG block copolymers were utilized for micelle formulations and targeting groups were introduced by modifying PEG block with RGD and mixing two types of polymers to obtain targeted micelle encapsulating docetaxel physically. Non-targeted and targeted micelles displayed uniform size distribution with mean particle size ca. 90 nm and 120 nm respectively with high docetaxel loading capacities around 30%. Sustained drug release profiles were detected with 20% after 24 h and 60% by the end of seven days at physiological conditions. Cellular internalization experiments indicated maximum drug uptake was achieved in 1h followed by decreased rates of internalization after 4 h, where targeted micelles demonstrated significantly higher internalization. Furthermore spheroids prepared from U87MG and 9L cells responded to all docetaxel formulations however growth inhibitory effect was most prominent with targeted micelles where they caused almost 80% decrease in spheroid volumes. Additionally permeability of free docetaxel was detected to be rather poor and cytotoxic effect of free drug was observed only with cells located on the spheroid surface. Upon injection of blood stream all micellar formulations exhibited improved half-lives around 5 h, as compared with 1h of the free drug. Tumor xenografts with U87MG cells were used to display inhibitory potential of targeted micelles on glioblastoma tumors where they showed significant inhibition of tumor growth in contrast to controls and free drug treatments. Furthermore no loss of body weight was observed for micellar docetaxel formulations and accumulation of docetaxel was significantly lower in

heart, liver, spleen and lung and significantly higher in tumors for targeted formulations then free drug.

RGD functionalized polymeric micelles composed of doxorubicin conjugated PEG-PLA encapsulating combretastatin A4 (CA4) was developed to successively disrupt tumor vasculature and kill tumor cells exhibiting combinatorial effect [177]. Self-assembly of polymeric units resulted in formation of 30 nm sized micelles which demonstrated sequential and sustained release profiles for both drugs where a fast release of CA4 of 75.6% after 24 h, and a continuous release of DOX over a period of 20 days resulted by PLA hydrolysis. Targeted micelles were incubated with cocultured endothelial HUVECs and B16-F10 melanoma tumor cells which resulted in complete inhibition of endothelial cell growth in 24 h where tumors cells displayed high viability. After 36 h HUVECs were entirely destructed whereas significant tumor cell inhibition was reported which was expected due to differential incorporation types of drugs to the micelles. In B16-F10 tumor-bearing mice tumor accumulation was most prominent with targeted micelles and organ accumulations including in heart, liver, spleen, lung and kidney was lower than free drug treatment. Significant tumor inhibitory effect was observed with targeted micelle containing doxorubicin and CA4. Besides calculated tumor inhibition ratios indicated that combinatory treatment of drugs had improved effect on tumor volume control since inhibition ratio for targeted dual drug micelles was 90.3% whereas treatments with non-targeted micelles or targeted micelle containing drugs separately resulted in lower ratios 66.7% and 76.2% respectively.

Trastuzumab, a humanized monoclonal antibody marketed as Herceptin can be incorporated to DDS since its targeting receptor human epidermal growth factor receptor type 2 (HER2 also denoted as HER2/neu or ErbB-2) is found to be upregulated in 20 to 30% of invasive breast carcinomas. Typically, HER2 overexpression or presence of multiple copies of encoding gene is correlated with decrease OS and diminished chemosensitivity to anti-cancer drugs as well as therapeutic hormones [258].Trastuzumab can inhibit growth of HER2-dependent tumors by interacting with extracellular juxtamembrane domains of HER2 receptors thereby blocking down-stream signal transduction pathways which can trigger survival, proliferation and invasiveness of cancer cells. HER2 activation can be initiated by ligand binding via both homodimerization with

HER2 and heterodimerization with other transmembrane tyrosine kinase receptors HER1, HER3, and HER4 to regulate cell division, cell death, adhesion, migration and differentiation under normal conditions (Figure 1.14). First reported in rat neuroblastoma HER2-induced cell proliferation has been correlated with various malignant tumors however gene duplications are mostly described for breast cancer [259]. Furthermore HER2 shedding where extracellular domain of HER2 cleaved by stromal elements as MMPs can result in generation of constitutively active truncated receptor. Trastuzumab can recognize and bind to juxtamembrane portion of HER2 receptors which in turn results in blocking of HER2 shedding and receptor dimerization thereby preventing activation of intracellular tyrosine kinase domains.

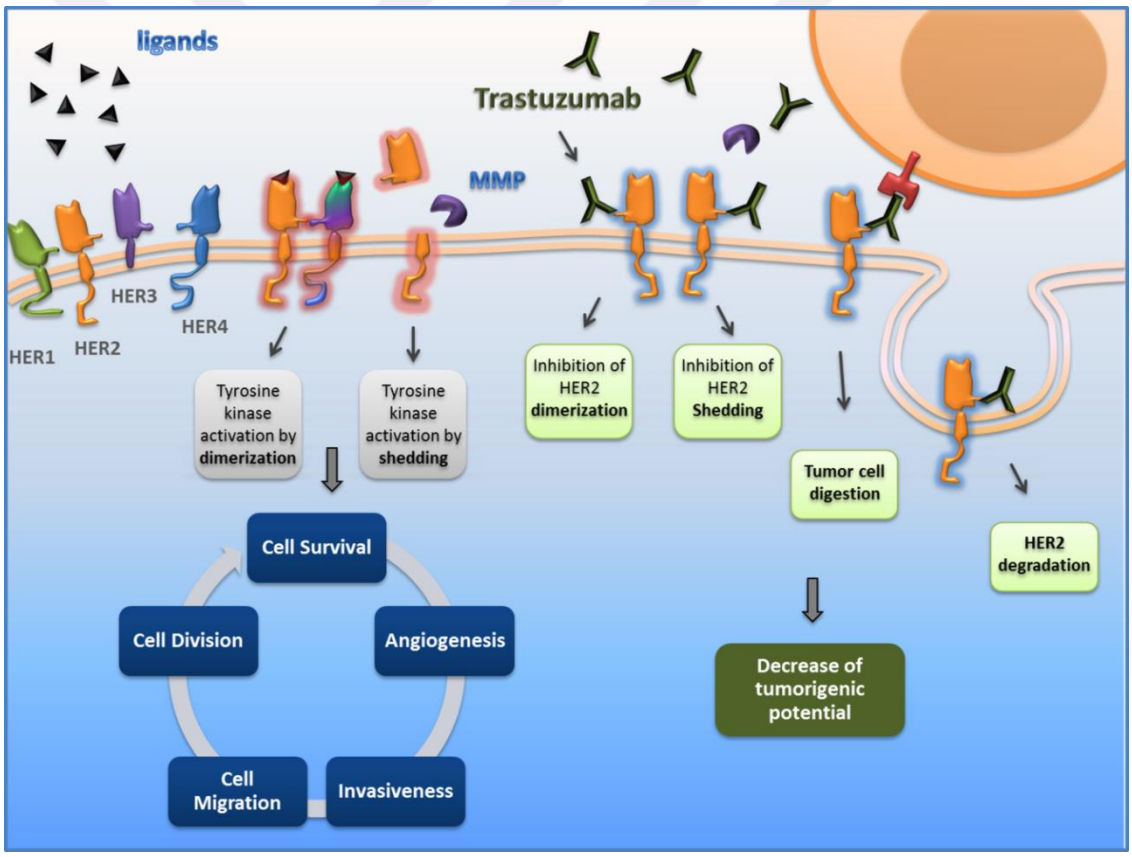

Figure 1.14. Mechanism of action for trastuzumab.

Another route for trastuzumab activity is increasing endocytotic destructions of HER2 receptors however the main mechanism for trastuzumab dependent toxicity may stem from immune activation. It has been suggested that Fc domains of trastuzumab IgG

can recruit immune effector cells as macrophages to HER2 overexpressing tumor cells and initiate cell lysis via phagocytosis which was supported by impaired trastuzumab activity observed in studies utilizing animals lacking Fc recognizing receptors on their effector cells [260]. Furthermore anti-angiogenic behavior of trastuzumab in an animal model of HER2 overexpressing breast cancer was reported where trastuzumab administrations led to normalization and regression of tumor vasculature [261]. As a result incorporation of targeting antibodies as trastuzumab to DDS is a promising approach for blocking HER2 signaling pathways and inhibiting the tumor growth in HER2 overexpressing breast cancer.

A cationic micellar nanoparticle system composed of biodegradable copolymers was employed to deliver paclitaxel with complexed trastuzumab antibodies for targeting HER2 targeting [262]. Prepared targeted micelles exhibited sizes over 200 nm and displayed 47.3% paclitaxel release over the first 59 h with 63.2% total release in 600 h. Cytotoxicity studies indicated that paclitaxel loaded trastuzumab targeted NPs notably decreased cell viability in comparison to trastuzumab alone. Furthermore effectivity of targeted NPs increased depending on HER2 expression levels of tested cell lines. Furthermore targeting ability of trastuzumab was demonstrated by cell internalization experiments using HER2 negative HEK293 cell line where limited NP uptake was reported even after 3h while time dependent NP uptake was clearly visible with HER2 expressing BT474 cell line.

A docetaxel delivery system composed of vitamin E TPGS which is used generally for bioavailability enhancer for drugs and a polo-like kinase 1 siRNA which is used for inhibiting of polo-like kinase 1 expression and thereby causing apoptosis via cell cycle arrest utilized trastuzumab conjugation for HER2 targeting [263]. Micelles were redox responsive due to disulfide linkages between vitamin E TPGS block and siRNAs. After trastuzumab conjugation, micelle size increased from 120 nm to 190 nm. Confocal microscopy experiments indicated after 2 h incubation HER2 overexpressing SK-BR-3 cells internalized targeted micelles successfully. Similarly *in vitro* quantitative experiments exhibited 53.4% and 38.6% higher cell uptake for targeted micelles then non-targeted counter parts after 0.5 h and 2 h of incubation respectively. Cytotoxicity experiments done with NIH3T3, MCF7, and SK-BR-3 cell lines with low, moderate and high HER2 expression levels respectively indicated significantly improved therapeutic efficacy for

docetaxel loaded micelles over free drug treatments no HER2 expression dependent difference in resulting cytotoxicity levels was reported.

Another study employed trastuzumab targeted polymeric micelles for delivery of a model drug, doxorubicin [264]. Micelles were composed of triblock copolymers of PLGA-b-polyhistidine-b-PEG providing pH sensitive sustained drug release. Trastuzumab was conjugated to micelles through copper-catalyzed click chemistry which resulted in micelle size increase from 100 nm to 130 nm. By increasing acidity of media, micelle size also increased up to 870 nm at pH 5.2 due to protonation of polyhistidine block. Likewise almost 80% release of encapsulated doxorubicin was reported at pH 5.2 in 8 h whereas it was around 40% at pH 7.4. Trastuzumab conjugation was shown to be effective in terms of internalization of micelles where targeted micelles displayed improved cell uptake for SK-BR-3 and MCF-7 cell lines. Also overall internalization was higher for SK-BR-3 cell line due to higher HER2 expression.

2. COMBRETASTATIN A-4 CONJUGATED ANTI-ANGIOGENIC MICELLAR DRUG DELIVERY SYSTEMS USING DENDRON-POLYMER CONJUGATES

The materials in this chapter have been adapted from the following article: Sumer Bolu, B., E. Manavoglu Gecici, and R. Sanyal, "Combretastatin A-4 Conjugated Antiangiogenic Micellar Drug Delivery Systems Using Dendron–Polymer Conjugates", *Molecular Pharmaceutics*, Vol. 13, No. 5, pp. 1482–1490, May 2016.

2.1. Introduction

Past decades have witnessed a significant interest towards utilization of polymeric constructs in cancer therapeutics [265–268]. Combination of a drug to polymeric carriers often increases the efficacy of the drug without changing its active molecular structure and mode of action. These carriers shield the drug from plasma proteins thereby increasing its stability, increases its solubility and thus eliminates the need of excipients that often causes additional diverse side effects [30, 202, 269]. Generally the conjugation of drugs to the polymeric construct renders them inactive and furthermore enables their transport to diseased tissues without premature distribution to various organs [14]. Increased size of the constructs hinders diffusion of drug molecules through cell membranes except through a more complex endocytosis mechanism [270, 271]. After endocytosis, the polymer based vehicles are fused with the lysosomes in which they are exposed to an acidic internal environment. This acidic environment often triggers the release of the drug from the construct once it is inside the cell [272, 273]. This system not only provides a more selective release mechanism but also helps to bypass multi drug resistance (MDR) as reported for certain cell types. The conjugated drug can survive the efflux mechanisms and this enables the treatment of otherwise chemoresistant cancer cells [274].

Another additional advantage of employing polymer-drug conjugates is associated with the enhanced permeability and retention (EPR) effect observed around the tumor environment [15, 275]. Due to increased cellular metabolism, angiogenesis i.e. growth of new blood vessels is triggered by tumor cells resulting in hypervasculature. The increased growth rate and tumor vasculature results in a disorganized tissue organization thus allowing permeability to macromolecules and their accumulation due to lack of sufficient lymphatic drainage. Hence in comparison to free drug, macromolecular drug conjugates are accumulated in the tumor environment selectively. This kind of passive targeting and long term retention renders these drug conjugates locally toxic. Finally the high molecular weight conjugates cannot easily escape renal clearance owing to their increased hydrodynamic volumes and hence possess longer plasma half-lives [276]. In summary, the micellization of drug conjugates with hydrodynamic sizes in the sub-200 nm range is crucial for tumor targeting and penetration, as well as conjugate stability [95, 277].

Over the past decades, polymeric micelles have emerged as an attractive drug delivery platform since they embody several of the above mentioned attributes for achieving passive targeting, along with possibility of also incorporating active targeting through appropriate surface functionalizations [278–280]. Traditionally, the polymeric building blocks utilized to obtain micelles consist of amphiphilic diblock copolymers composed of linear hydrophobic and hydrophilic blocks.

In recent years, advances in synthesis and functionalization of dendron-polymer conjugates have promoted their use as precursors for fabricating micelles [281, 282]. For example, their multivalency along with the well-defined disposition of peripheral functional groups of dendritic building blocks have been utilized to obtain micelles with dendritic outer shell [283]. In particular, dendron-polymer conjugates containing biodegradable dendritic systems based on polyesters have emerged as promising candidates for various biomedical applications including fabrication of drug delivery vehicles since they are biocompatible and biodegradable due to their hydrolytically cleavable ester backbone [284, 285]. The inherent hydrophobicity of polyester dendrons can be fine-tuned by functionalization, for example, they can be utilized to obtain amphiphilic constructs through their conjugation to hydrophilic polymers. This polarization of hydrophilic and hydrophobic regions in the macromolecule will lead to

micellar assemblies in aqueous media. The drug candidates can be incorporated into these carriers through non-covalent encapsulation or covalent conjugation. Conjugation of drugs through degradable linkers inside the micelle will ensure minimal drug release before accumulation into the tumor. In spite of this attractive attribute of the later approach, most of the studies reported to date uses drug encapsulation as a common approach due to less synthetic complexity [286]. Undoubtedly, design of dendron-polymer conjugates that can be readily functionalized with drug candidates will expand the utility of these delivery systems.

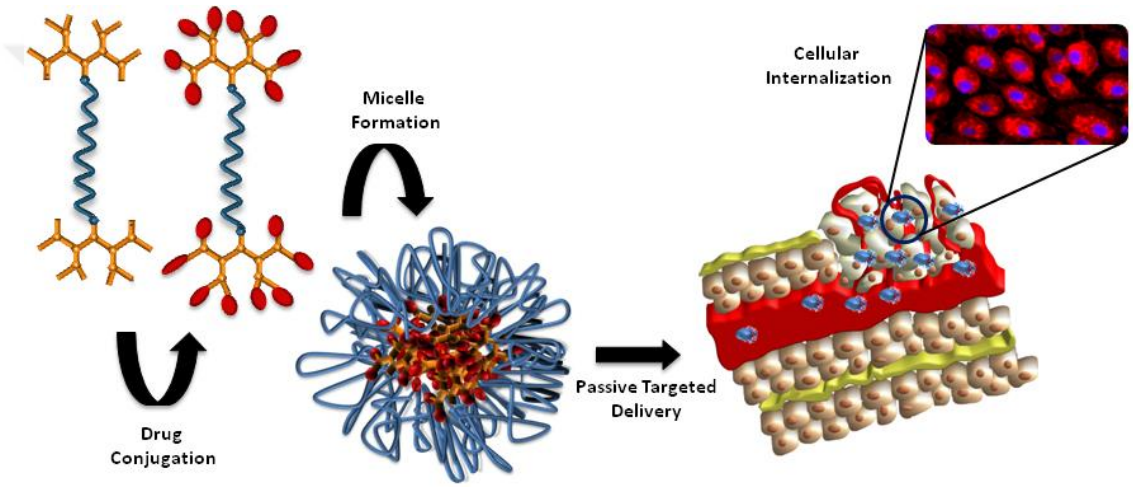

Figure 2.1. Schematic illustration of fabrication of drug loaded micellar constructs from dendron-polymer conjugates and their delivery to tumor vicinity.

In this study, a facile approach to obtain drug-conjugated polymeric micelles as a promising anti-angiogenic therapy platform using ‘clickable’ dendron-polymer conjugates is outlined (Figure 2.1). The drug-conjugated micellar precursors were obtained from conjugation of azide-containing drugs onto reactive alkyne group containing dendron-polymer conjugates. A series of triblock dendron-polymer-dendron (DPD) conjugates composed of a linear hydrophilic polyethylene glycol chain flanked by first through third generation of biodegradable polyester dendrons as hydrophobic outer blocks were used as polymeric scaffolds. Combretastatin A-4, an antiangiogenic agent [287] was coupled to these DPD conjugates through Huisgen type “click” chemistry. A variety of micellar assemblies were prepared from these conjugates and they were characterized to understand the impact of dendron generation. Thereafter, efficient internalization of these constructs

was demonstrated by doping with a hydrophobic dye, Nile Red, cytotoxicity of the drug conjugated constructs in contrast to those without the drug was investigated using cell viability assays, and the *in vitro* anti-angiogenic effects of these constructs were evaluated on human umbilical vein endothelial cells (HUVECs), which are capable of forming tubes on Matrigel thus mimicking angiogenesis.

2.2. Experimental Section

2.2.1. Materials

2,2-Bis(hydroxymethyl) propionic acid (BMPA), Dowex X50WX2, propargyl alcohol, 4-pentynoic acid and *N*, *N*'-dicyclohexylcarbodiimide (DCC) were purchased from Alfa Aesar. Polyethylene glycol was obtained from Fluka. All other reagents were purchased from Sigma Aldrich. All solvents were purchased from Merck and used as obtained without further purification unless otherwise noted. Ultra-pure water was obtained via Milli-Q Water Purification System (Milli-Q system, Millipore, Billerica, MA, USA). CA4 was synthesized according to literature procedure [288]. Azido functionalized 10 kDa PEG and compounds 1, 2 and 3 were synthesized and characterized according to previously described methods [289].

2.2.2. Instrumentation

The monomer and copolymer characterizations involved ^{1}H NMR spectroscopy (Varian 400 MHz NMR spectrometer) and Fourier transform infrared (ATR-FT-IR) spectroscopy (Nicolet 380, Thermo). Combretastatin-azide (4) was characterized by Liquid chromatography–mass spectrometry (LC-MS) analysis using a LCMS-2020-Mass Spectrometer System (Shimadzu) equipped with an C-18 5 μm 150 × 4.6 mm column. Mobile phase consisted of deionized water and HPLC grade acetonitrile (ACN) using the following gradient; LC: 0-3 min, 50% ACN; 3.01 min, 50% ACN; 8 min, 95% ACN; 8.01-11 min 50% ACN MS positive scan 100-600 m/z. Pyrene intensities for critical micelle

concentration (CMC) calculations were measured with a Varian Cary Eclipse Fluorescence spectrometer (Varian, Agilent).

The hydrodynamic radii (Rh) of micelles were determined via off-line dynamic light scattering analysis (DLS) and the molecular weight (MW) of micelles of G3-PEG was determined via off-line static light scattering analysis (SLS, Particle Size Analyzer 90Plus, Brookhaven). The anhydrous micelles of DPD constructs were visualized by a LVEM5 electron microscope system on transmission electron microscopy (TEM) mode (Delong Instruments, CZ).

2.2.3. Synthesis and Characterization of G1-PEG (1), G2-PEG (2) and G3-PEG (3)

Synthesis of ABA type dendritic linear triblock copolymers with dendron generations 1, 2 and 3 was done as previously reported in literature with minor modifications [289]. PEG 10K-diazides were used as linear polymer block.

2.2.4. Synthesis and Characterization of Combretastatin-azide (4)

CA4 (110 mg, 0.35 mmol), DCC (78.7 mg, 0.38 mmol) and 4-Dimethylaminopyridine (DMAP, 4.7 mg, 0.38 mmol) were dissolved in dichloromethane (CH_2Cl_2) (1.5 mL). 4-azidobutanoic acid (490 mg, 0.38 mmol) was added and the reaction was carried out under N_2 atmosphere at room temperature for 24 h. CH_2Cl_2 was evaporated and the crude product was dissolved in 1 mL of ethyl acetate then purified by filtration. Ethyl acetate was evaporated to give 108 mg of compound 4 as a yellowish solid (69 % yield). ^{1}H NMR ($CDCl_3$, δ, ppm) 7.80 (s, 2H), 7.10 (dd, 1H J = 8.4 Hz, J = 2.1 Hz), 6.98 (d, 1 H, J = 2.1 Hz), 6.83 (d, 1H, J = 8.4 Hz), 6.48 (s, 2H), 6.44 (s, 2H), 3.82 (s, 3 H), 3.78 (s, 3H), 3.69 (s, 6 H), 3.40 (t, 2 H, J = 7.1 Hz), 2.63 (t, 2 H, J = 7.1 Hz), 1.98 (m, 2 H). ^{13}C NMR ($CDCl_3$, δ, 400MHz) 24.5, 30.9, 50.6, 56.0, 61.1, 105.1, 112.1, 123.2, 123.3, 127.9, 129.0, 137.32, 139.4, 150.2, 153.1, 170.8. FT-IR (cm^{-1}); 2095, 1760. LC-MS; Expected [M+H] m/z= 428.5 and observed [M+H] m/z = 428.2.

2.2.5. Synthesis and Characterization of Comb-G1-PEG (5)

Compound 1 (20 mg, 0.002 mmol) and compound 4 (4 mg, 0.008 mmol) were dissolved in tetrahydrofuran (THF, 2 mL). In a separate flask, Cu(I)Br (0.005 mg, 0.001 mmol) and *N*, *N*,*N'*,*N'*,*N''*-Pentamethyldiethylenetriamine (PMDETA, 0.1 µL, 0.001 mmol) were dissolved in anhydrous THF (2 mL) and purged with N_2. The copper (Cu) containing mixture was then added onto the polymer-dendron conjugate containing solution and stirred at 40 °C for 7 d. The solution was filtered through aluminium oxide (Al_2O_3) column to remove copper salts. The solvent was concentrated under *vacuo* and the desired product was precipitated with diethyl ether, filtered and dried under *vacuo* yielding Comb-G1-PEG (15 mg, 75%) as a yellowish solid. ^{1}H NMR ($CDCl_3$, δ, ppm): 7.79 (s, 2H), 7.10 (dd, 4H, *J* = 8.5 Hz, *J* = 2.1 Hz), 6.97 (d, 4H, *J* = 2.0 Hz), 6.83 (d, 4H, *J* = 5.7 Hz), 6.47 (s, 8H), 6.43 (s, 8H), 5.22 (t, 4H, *J* = 8.0 Hz), 4.43 (m, 4H), 4.16-24 (m, 8H), 3.86 (m, 4H), 3.81 (s, 12H), 3.78 (s, 12H), 3.65-3.40 (bs, 900H), 3.44 (t, 8H, *J* = 4.8 Hz), 2.65 - 2.60 (m, 8H), 2.55 (t, 8H, J = 7.0 Hz), 2.42 (m, 8H), 1.99 (m, 8H), 1.19 (s, 6H).

2.2.6. Synthesis and Characterization of Comb-G2-PEG (6)

Compound 2 (60 mg, 0.005 mmol) and compound 4 (20 mg, 0.047 mmol) were dissolved in THF (3 mL). In a separate flask, Cu(I)Br (0.7 mg, 0.005 mmol) and PMDETA (1.2 µL, 0.005 mmol) was dissolved in anhydrous THF (3 mL) and purged with N_2. The Cu containing mixture was then added onto the polymer-dendron conjugate containing solution and stirred at 40 °C for 7 d. The solution was filtered through Al_2O_3 column to remove copper salts. The solvent was concentrated under *vacuo* and the desired product was precipitated with Et_2O, filtered and dried under *vacuo* yielding Comb-G2-PEG (40 mg, 50%) as a yellowish solid. ^{1}H NMR ($CDCl_3$, δ, ppm): 7.82 (s, 2H), 7.10 (m, 7H), 6.95 (bs, 7H), 6.80 (d, 7H, *J* = 8 Hz), 6.46 (s, 14H), 6.42 (s, 14H), 5.21 (bs, 4H), 4.41 (m, 4H), 4.08-4.25 (m, 24H), 3.87 (m, 4H), 3.83 (s, 21H), 3.79 (s, 21H), 3.65-3.40 (bs, 900H), 3.44 (m, 14H), 2.69 - 2.60 (m, 14H), 2.54 (m, 16H), 2.40 (m, 16H), 1.99 (m, 14H), 1.23 (s, 6H), 1.10 (s, 12H).

2.2.7. Synthesis and Characterization of Comb-G3-PEG (7)

Compound 3 (42 mg, 0.003 mmol) and compound 4 (25 mg, 0.059 mmol) were dissolved in anhydrous THF (3 mL). Cu(I)Br (0.9 mg, 0.006 mmol) and PMDETA (1.5 µL, 0.006 mmol) was dissolved in anhydrous THF (3 mL) and purged with N_2. The Cu containing mixture was then added onto the polymer-dendron conjugate containing solution and stirred at 40 °C for 7 d. Subsequently, solvent was evaporated and the crude product was dissolved in THF (50 mL). The solution was filtered through Al_2O_3 column to remove copper salts. The solvent was concentrated under *vacuo* and the desired product was precipitated with diethyl ether, filtered and dried under *vacuo* yielding Comb-G3-PEG (35 mg, 52%) as a yellowish viscous solid. ^{1}H NMR ($CDCl_3$, δ, ppm) 7.80 (s, 2H), 7.10 (d, 10H, J = 8.0 Hz), 6.96 (bs, 10H), 6.82 (m, 10H), 6.47 (s, 20H), 6.43 (s, 20H), 5.21 (bs, 4H), 4.42 (m, 4H), 4.03-4.25 (m, 56H), 3.86 (m, 4H), 3.80 (s, 30H), 3.75 (s, 30H), 3.65-3.40 (bs, 900H), 3.45 (m, 20H), 2.70 - 2.65 (m, 20H), 2.54 (m, 32H), 2.40 (m, 32H), 2.03 (m, 20H), 1.14 (s, 6H), 1.12 (s, 12H), 1.07 (s, 24H).

2.2.8. Micelle Preparation and Characterization

For preparation of micelles from ABA block copolymers with and without drug, copolymer stock solutions (1 mg/mL) in CH_2Cl_2 were prepared. Using a 100 µL syringe and making 1:10 serial dilutions with CH_2Cl_2 when necessary, exact amounts of dissolved polymer was added into glass vials for preparing dilutions ranging between 1×10^{-5} M to 5×10^{-9} M in 3 mL final volume. CH_2Cl_2 in the vials was then evaporated overnight. 10 µL from stock pyrene solution (1.8×10^{-4} M pyrene in acetone) was added into polymer containing vials and acetone was removed under *vacuo* for 2 h. Then, 3 mL of water was added onto each vial and the vials are sonicated at 70 °C for 1 h. Micelle solutions were then incubated 24 h under dark and fluorescence measurements were taken (Fluorescence spectroscopy, Cary Eclipse). Pyrene excitation spectra at emission wavelength 390 nm for the micelle samples were recorded and via the I_{338}/I_{334} ratio CMC values were calculated. Using the same micelle samples DLS measurement and TEM images were taken. For TEM images micelle solutions were dropped and air dried on copper grids, the mean size of the

micelle particles were determined by counting at least 100 particles via the Q-Capture Pro7 software. Additionally, the molecular weight of micelles prepared from G3-PEG was investigated by SLS analysis.

2.2.9. pH Dependent Release of CA4 from Micelles

The released drug content from synthesized DPD conjugates was determined by UV-Vis spectrometry. Briefly, 2 mg of Comb-G3-PEG was dissolved by 1 h sonication in 2 mL of pH 4.8 acetate buffer and in 2 mL of pH 7.4 phosphate-buffered saline (PBS) buffer separately. The resulting micelle solutions were then transferred into dialysis bags with MW cut-off 1000 Da. Dialysis bags were incubated in 30 mL of corresponding buffer solutions and incubated at 37 °C for 10 days. At predetermined time points, 50 μL samples were collected from inside of dialysis bags. UV absorbance at 254 and 327 nm was determined with a Nanodrop 1000 spectrophotometer (Thermo Scientific, USA).

As control free CA4 samples with the same initial concentrations dialysis experiments were done. In parallel to other experiments 50 μL samples were collected from inside of dialysis bags and quantified via UV spectroscopy. Significant portions of free drug, 68.5±0.4% and 86.3±0.3% were released in 1h and 2h respectively (Figure A.6). This data indicated, once released from drug conjugates, free drug can diffuse outside of dialysis bag in a short time span.

2.2.10. Serum Stability of Comb-G3-PEG micelles

4 mg/mL of Comb-G3-PEG micelle stock solution was prepared by 1 h sonication in water. Using the stock micelle solution, samples were prepared in 1XPBS and 50% Fetal Bovine Serum (FBS) with a final concentration of 2mg/mL. The resulting solutions were then incubated at 37 °C for 4 days. At predetermined time points, 75 μL samples were injected to PBS-GPC system. Area under the curve (AUC) values of micelle peaks with a retention time of 16.5 min were determined at 254 nm [290].

2.2.11. Cell Lines

Human umbilical vein endothelial cells (HUVEC) were obtained from Lonza. HUVECs were maintained according to the recommendations of Lonza (Lonza Inc., Allendale, NJ), using endothelial cell growth media-2 kit (EBM-2 supplemented with EGM-2 SingleQuot kit). Cells were incubated at 37 °C in a humidified atmosphere of 5% CO_2 and kept in logarithmic phase of growth throughout all experiments.

2.2.12. *In vitro* Cell Viability Assay

Cell viabilities were determined by Cell Counting Kit-8 (CCK-8, Fluka). Cells were seeded in 100 μL of culture medium at a density of 3000 cells/well into 96-well plates in quadruplicates for each drug concentration. After overnight incubation to let HUVECs to adhere, cell media was replaced with fresh medium containing various concentrations of conjugates, free drug, or controls. To increase the water solubility of Combretastatin A-4, stock solution was prepared in 20% dimethyl sulfoxide (DMSO) in growth medium (V/V) and subsequently diluted where the final dimethyl sulfoxide concentration was below 0.5% (V/V). DPD stock micelle solutions are prepared via sonication without DMSO addition. HUVECs were incubated continuously for 48h in the presence of the micellar conjugates. Following the treatment, cell media containing the conjugates was removed, wells were washed with 1X PBS. For 2 h+18 h pulse chase drug treatment, cells were incubated 2 h in drug containing solutions and incubated in fresh media for 18h before cell counting kit CCK-8 assay.

To determine the cell viability, 100 μL of culture medium together with 10 μL of CCK-8 solution was added into each well. After 4h of continious incubation the absorbance values at 450 nm was measured with a plate reader (Multiscan FC, Thermo Scientific, USA). Viability of treated cells was expressed as percentage of control cells (cell media only). Half maximal effective concentration (EC50) values were obtained from concentration response curves by nonlinear regression analysis.

2.2.13. Endothelial Cell Tube Formation Assay on HUVECs

Comb-G3-PEG micelle stock solution with concentration of 1µM of was prepared in complete EBM-2 cell media via sonication. Tube formation assay using Matrigel (BD Biosciences, USA) was done as previously reported with slight modifications [291].

Briefly, cold Matrigel samples were poured as triplicates for each concentration into 96 well plates. The gels were let to solidify at 37 °C for 30 min, 10^4 HUVECs were seeded per well. The micelle solutions were added immediately with final concentrations of 1 nM, 10 nM, 100 nM and 500 nM. The cells were incubated for 12 h at 37 °C and pictures of the formed tubes were collected via bright field microscopy. The collected images were processed using Angiogenesis Analyzer tool of Image J.

2.2.14. Nile Red Internalization in HUVECs

G3-PEG micelle stock solution with concentration of 1µM of was prepared in complete EBM-2 cell media in the presence of Nile Red (0.5 mg/mL) via sonication. The control sample was prepared simultaneously without G3-PEG addition. Additional control samples were prepared by adding G3-PEG and of Nile Red but without sonication. HUVECs were seeded as 3 x 10^4 cells per well into 24 well plates in triplicates for each time point and Nile Red doped micelles were added into the wells with a final DPD concentration of 100 nM and 1nM.

Cells were incubated for 1, 4 and 24 h at 37 °C and fixed using 4% formaldehyde after 4',6-diamidino-2-phenylindole (DAPI) staining. The images were collected via an inverted fluorescence microscope (Zeiss Observer A1 equipped with AxioCam MRc5) and processed with AxioVision software.

2.3. Results and Discussion

2.3.1. Synthesis and Characterization of Drug-conjugated Dendron-Polymer Conjugates

Drug conjugated dendron-polymer constructs were synthesized by attachment of CA4 to three DPD triblock copolymers, with increasing dendron generation using the azide-alkyne cycloaddition reactions (Figure 2.2). Aliphatic DPD triblock copolymers with alkyne groups at their dendritic periphery were synthesized using 2,2-bis(hydroxymethyl) propionic acid based dendron and linear PEG polymer, according to previously reported protocols [289].

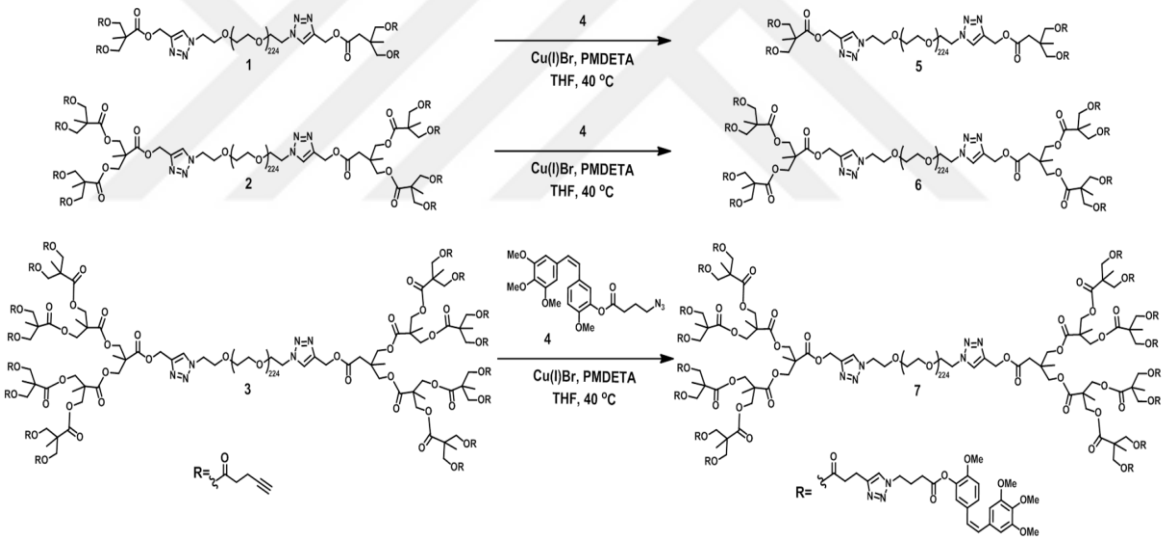

Figure 2.2. Synthesis of CA4 bearing dendron-polymer drug conjugates.

Three different generations of polyester dendrons were employed in this study in order to obtain increased drug attachment and variation in hydrophilic lipophilic balance (HLB) values for the conjugates, as well as increased drug attachment.

Azide-containing CA4 was synthesized and attached to alkyne-containing DPD conjugates in the presence of Cu(I)Br and PMDETA in THF at 40 ^{o}C. Drug-appended DPD conjugates devoid of free drugs were obtained in pure form using precipitation in

diethyl ether. Based on ^{1}H-NMR spectroscopy analysis it was deduced that the number of drugs conjugated per DPD conjugate increased with increasing dendron generation; 4, 7 and 10 drug molecules were conjugated to G1-PEG, G2-PEG and G3-PEG, respectively (Table 2.1).

Table 2. 1. Properties of DPD and DPD-Comb Conjugates and their resulting micelles.

Compound #	Name	Generation of Dendron	Drug per molecule	Drug Weight %	CMC, [M]	HLB
1	G1-PEG	1	-	-	$2.2\times10^{-6} \pm 6.2\times10^{-7}$	18.4
2	G2-PEG	2	-	-	$3.3\times10^{-7} \pm 2.8\times10^{-8}$	17.2
3	G3-PEG	3	-	-	$1.5\times10^{-7} \pm 3.4\times10^{-8}$	15.6
5	Comb-G1-PEG	1	4	7.9	$1.8\times10^{-6} \pm 4.8\times10^{-7}$	16.5
6	Comb-G2-PEG	2	7	15.0	$2.3\times10^{-7} \pm 5.3\times10^{-8}$	13.7
7	Comb-G3-PEG	3	10	18.4	$3.7\times10^{-8} \pm 2.2\times10^{-8}$	11.7

2.3.2. Critical Micelle Concentrations

CMC values for all DPD polymers were determined using the pyrene probe method [292]. Briefly, the otherwise water insoluble pyrene was encapsulated into the hydrophobic cores of the self-assembled micelles.

The increase in measured pyrene intensity and the shift of emission maxima towards 338 nm due to formation of pyrene excimers suggested micelle formation. By calculating the $I_{338}/_{334}$ ratio, CMC values for each dendron-polmer-dendron construct was inferred from the intersection of trend lines (Figure 2.3, Figure A.1).

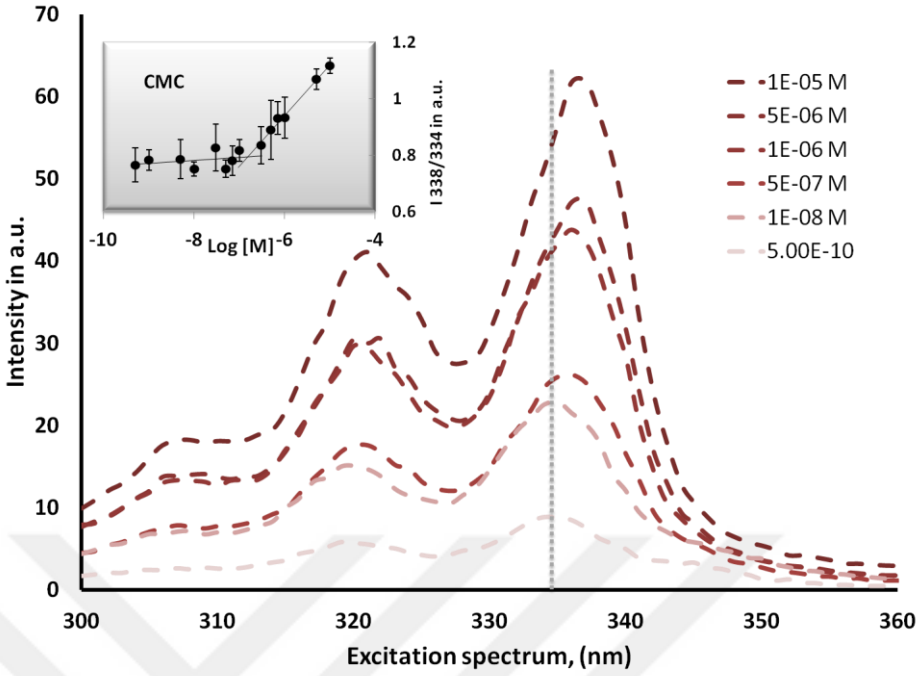

Figure 2.3. Pyrene excitation spectrum of G3-PEG micelles. Inset: $I_{338}/_{334}$ *vs.* log[Conc] graph to calculate CMC value.

CMC values for all dendron-polymer conjugates were in the nanomolar region which implies their stability at very low concentrations (Figure 2.4). This also suggested that these constructs may preserve their stability after harsh dilutions as in the case of drug injections hence they can be potentially viable candidates for *in vivo* applications. The HLB values of dendron-polymer conjugates were calculated according to reported methods[293] and sketched as two separate populations (Figure 2.4 (B)). The decrease in CMC values with decreasing dendron generation and increasing hydrophilicity beared a noticeably linear trend with the HLB value. This tendency suggested that CMC values of these micellar constructs are tunable depending on their HLB value and drug conjugation. The evolution of a secondary HLB correlation due to drug conjugation indicated a positive change in micellar stability and structure.

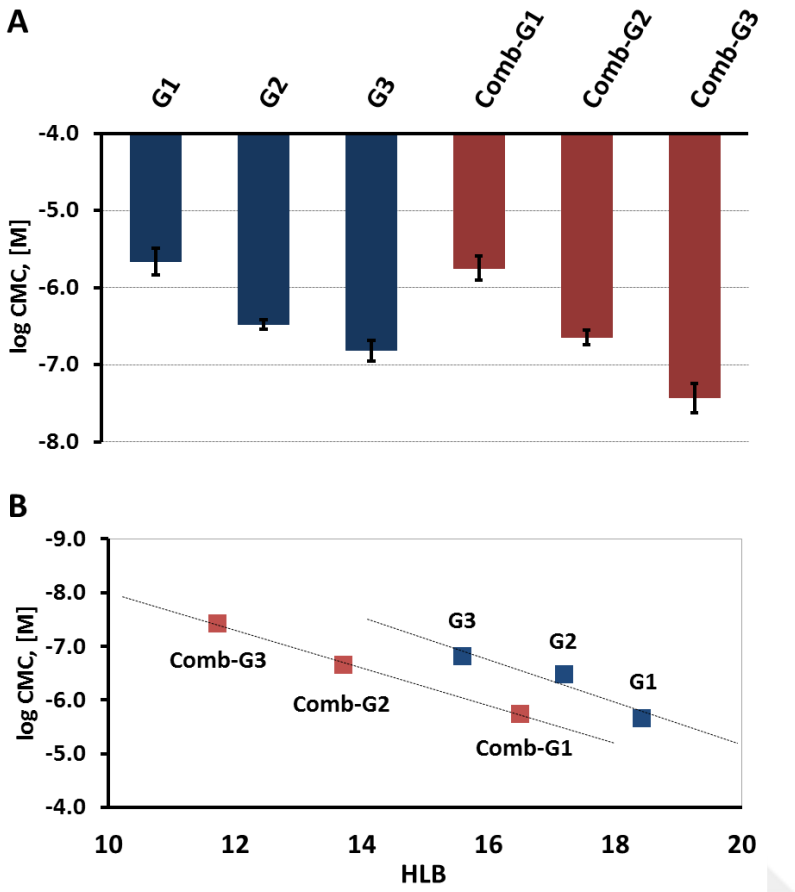

Figure 2.4. (A) CMC and (B) HLB graph of DPD and Comb-DPD series; HLB was calculated by HLB= $20M_P/(M_D+M_P)$ where M_P was mass of hydrophilic PEG block and M_D was hydrophobic block composed of dendron and drugs when present.

2.3.3. Size and Molecular Weight of Micelles

Determination of the CMC values was followed by investigation of the size of the obtained micelles based on the volume distribution obtained using batch mode DLS. Size measurements on micelles obtained using different DPD conjugates showed dependence on dendron generations and drug contents with a trend similar to that observed for variation in HLB values. The size of the micelles were within the sub-100 nm level as observed by batch mode DLS, varying between 37.7±2.4 nm and 81.3±3.1 nm (Figure 2.5). Additionally, static light scattering (SLS) analysis was carried out on the parent G3-PEG copolymer by preparing various micellar concentrations of G3-PEG and molecular weight of the resulting micelles were investigated. From SLS data it was derived that the

average molecular weight of the micelles was about 6.0×10^5 g/mol (Figure A.2). Considering the molecular weight of the dendron-polymer conjugate it can be deduced that G3-PEG micelles were composed of about 42 of these units.

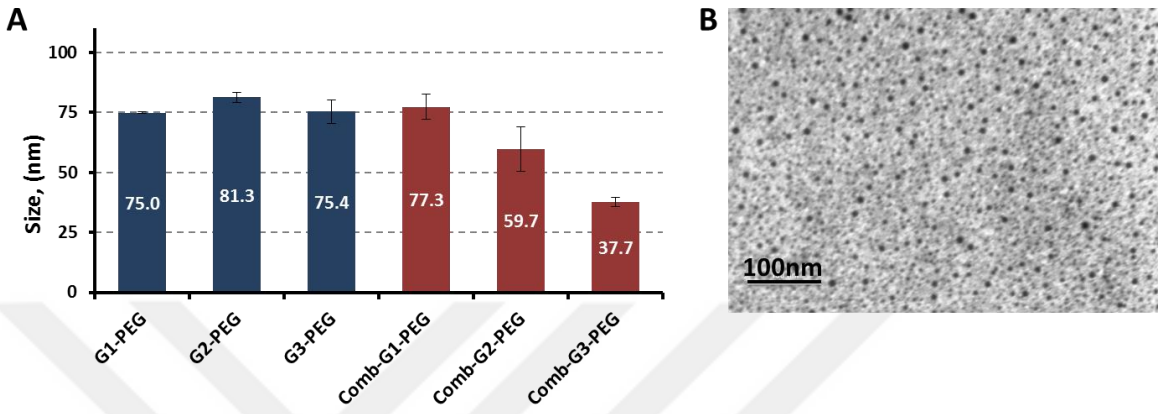

Figure 2.5. (A) Size of micelles from volume distribution by batch mode DLS analysis. (B) TEM image of Comb-G3-PEG micelles.

TEM analysis of the drug conjugated Comb-G3-PEG micelles indicated a uniform size distribution where the mean diameter was observed to be 7.7 nm ± 1.3 nm (Figure 2.5 (B)). A comparatively lower size observed via TEM analysis, when compared to the solution state DLS analysis was not surprising considering the non-solvated dry state of the micellar assemblies. The size range of these micelles in solution was encouraging since it suggested that once introduced to blood stream, these micelles might be able to surpass the renal clearance. Furthermore, due to the small size of the Comb-G3-PEG micelles they have the potential to penetrate into solid tumors, since it has been demonstrated that smaller micelles have higher tumor penetration [294].

2.3.4. pH Dependent Drug Release from Micelles

A controversial feature of micellar drug delivery is the “burst effect”. Especially when the cargo is physically doped i.e. non-covalently encapsulated into the micelle, an immediate release of drug is observed leading to a sharp increase in drug concentration at

microenvironment within hours. While the cargo may reach the target tissue, premature release due to change in micellar stability is possible. However, in systems where drug molecules are covalently conjugated the effects of burst release may be significantly reduced [295]. A pH dependent gradual CA4 release was observable through 10 days with overall drug release of 94.4±2.6% and 68.1±8.8% at pH 4.8 and pH 7.4, respectively (Figure 4). This difference in profiles may provide an increased drug release at acidic environments such as in the lysosome. Moreover, micelle stability in serum containing environment was investigated and it is shown that Comb-G3-PEG micelles have similar stability levels in PBS and in FBS (Figure A.5). The slower release, as observed for our system is important due to the fact that accumulation in tumor via EPR effect takes place over several hours depending on tumor location and type. Furthermore, such slow release profiles providing a steady level of drug might minimize the dose as well as frequency of drug administrations [269, 296].

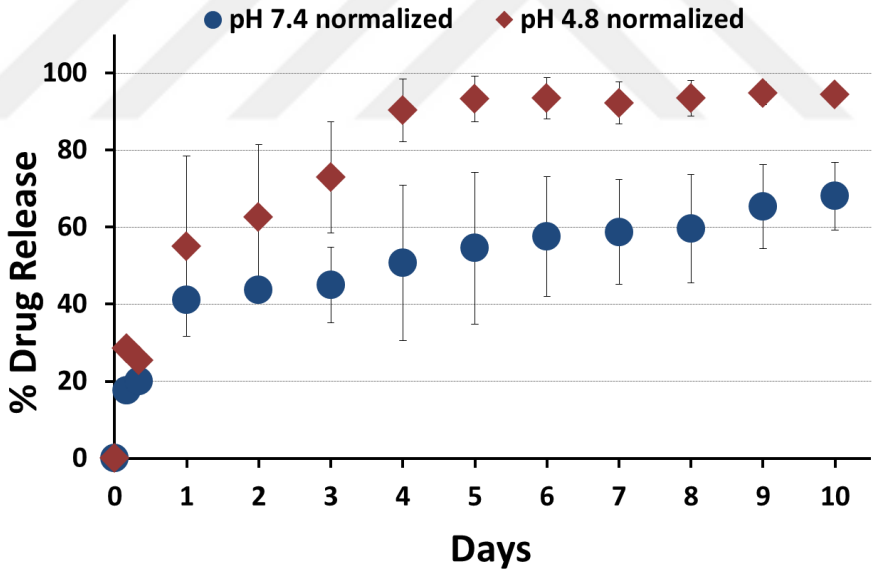

Figure 2.6. CA4 release profiles from Comb-G3-PEG micelles.

2.3.5. Determination of *in vitro* Cytotoxicity of Drug Conjugates on HUVECs

Effect of the anti-angiogenic drug CA-4 containing micelles was investigated on HUVECs, to analyze their inhibitory effect on vessel formation. Drug alone was highly cytotoxic towards HUVECs in 48 h as well as at 2 h+18 h pulse chase treatment,

demonstrating the potential toxicity of free drug as a therapeutic agent. However, in case of drug conjugated DPD counterparts due to gradual release dynamics, much higher EC50 values were obtained (Figure 2.7). Notably, all three drug conjugated constructs were able to achieve significant decrease in cell viabilities in 48 h (Figure 2.7). As expected, due to the biocompatible nature of the building blocks, the parent DPDs devoid of any drug exhibited very limited cytotoxicity on HUVECs (Figure A.3). Hence to overcome the potential toxicity of free drug *in vivo*, CA4 conjugated DPD micelles are excellent candidates.

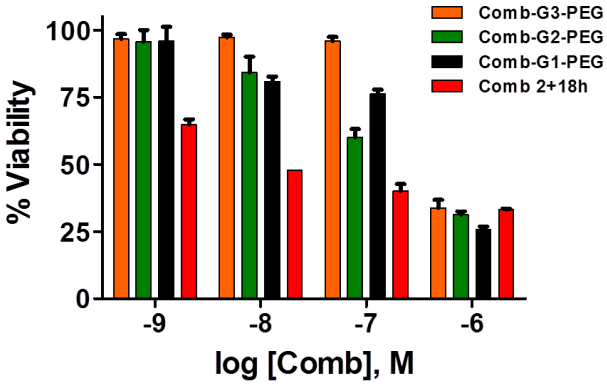

Sample	EC50, [M]
Comb, 2+18h	$4.28\times10^{-10}\pm2.6\times10^{-10}$
Comb, 48h	$2.59\times10^{-13}\pm3.4\times10^{-13}$
Comb-G3-PEG	$4.6\times10^{-7}\pm 1.2\times10^{-7}$
Comb-G2-PEG	$1.09\times10^{-7}\pm3.4\times10^{-8}$
Comb-G1-PEG	$2.01\times10^{-7}\pm7.0\times10^{-8}$
G3-PEG	$>1\times10^{-4}$
G2-PEG	$>1\times10^{-4}$
G1-PEG	$>1\times10^{-4}$

Figure 2.7. Viabilities of HUVECs treated with drug containing DPD micelles and free drug and EC50 values of individual samples.

2.3.6. Micelle Internalization by HUVECs

The hydrophobic Nile Red dye was doped to the polyester core of G3-PEG micelles to show the internalization of DPD micelles into HUVECs. In HUVECs treated with Nile Red doped G3 micelles red fluorescence increased dramatically over time where as in HUVECs treated with hydrophobic dye alone, barely noticeable internalization was observed even after 24 h (Figure 2.8). In control experiments, this kind of time dependent increase in dye intensity was not observed where Nile Red was added to G3-PEG polymer without initiation of micelle formation (Figure A.4). It can be deduced that Nile Red internalization was clearly due to incorporation of the dye into the hydrophobic core of G3-

PEG micelles. It was also evident that the HUVECs cell growth and viability were not significantly affected by G3-PEG treatment.

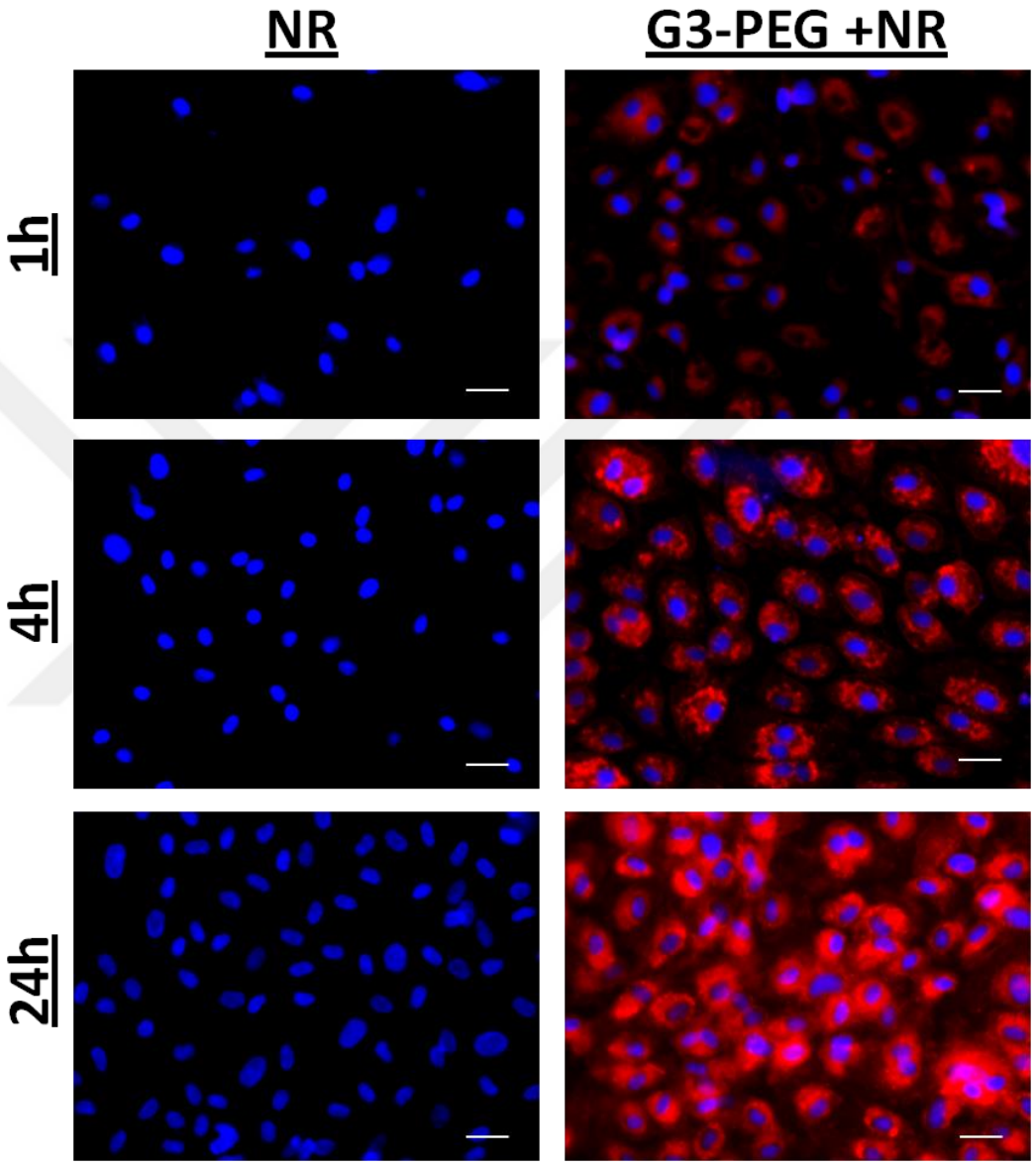

Figure 2.8. Nile Red internalization by HUVECs. Scale bar 100 µm.

2.3.7. Endothelial Cell Tube Formation Assay on HUVECs

The *in vitro* cellular internalization and toxicity studies were followed by tube formation assay, a technique widely used to probe the anti-angiogenic efficacy [297, 298].

In this assay, HUVECs form three dimensional capillary like vasculature on the solid Matrigel which is a growth factor reduced basement membrane hence providing a suitable milieu for investigation of anti-angiogenic agents. Matrigel data indicated an inhibition of junction formation as well as a noticeable decrease in total tube length when exposed to 500 nM CA4 containing Comb-G3-PEG based micelle solution (Figure 2.9). Compared to the control and 1 nM samples with 73±14 and 69±20 junctions, respectively, the number of junctions for the 500 nM sample decreased, over four fold, to 16±7. Similarly, a threefold decrease in total tube length values is apparent upon comparison of 1 nM and 500 nM samples 16040±1336 vs. 6287±1604 respectively. It is observed that the gradual increase of CA4 in micelle solutions effectively impairs the tube formation capability of HUVECs, thus highlighting the anti-angiogenic potential of CA4 conjugated micelles.

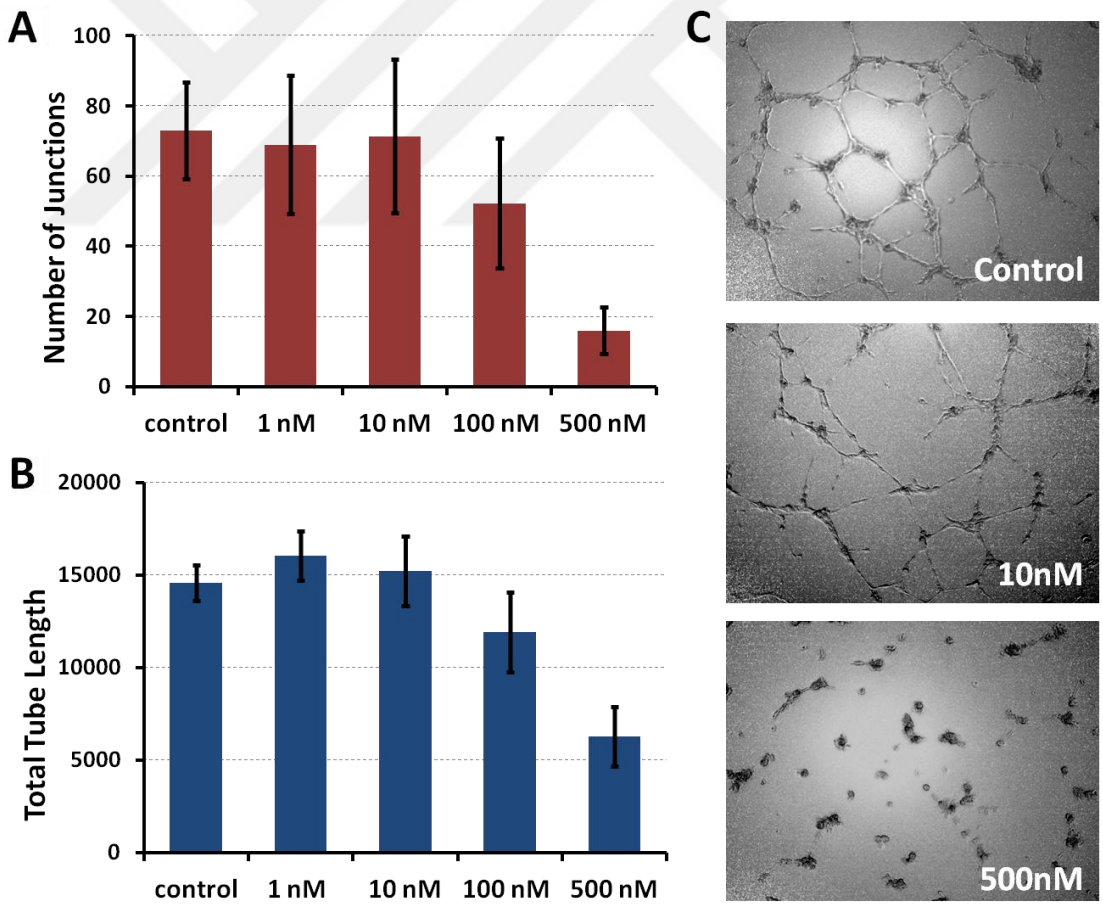

Figure 2.9. Anti-angiogenic assay using HUVECs on Matrigel. (A) Number of junctions and (B) total tube lengths between HUVECs C) Representative Matrigel images.

2.4. Conclusions

Dendron-polymer conjugates with well-defined structures were synthesized and conjugated with an anti-angiogenic drug CA4. The CMC values were in the sub nanomolar range for drug conjugated DPD micelles and it was observed that the stability of micelles could be increased by decreasing the HLB through an increase in dendron generation and drug content. The DLS measurements showed that the sizes of the formulated micelles were below 100 nm, suggesting that while escaping renal clearance, this system may benefit from EPR effect. Drug release was pH dependent and increased at acidic pH which is a desirable release profile since this implies that drug release will be improved once the cargo reaches acidic tumor site or it is internalized. The constructs without drug conjugation showed minimal cytotoxicity on HUVECs, whereas drug conjugated micelles showed significant decrease in cell viability. Cell internalization study of dye doped micellar constructs indicated their facile uptake in spite of the PEG based corona. Also, endothelial cell tube formation assay confirmed the activity of CA4 conjugated constructs against angiogenesis. The delivery vehicle described here can be also loaded with other anti-cancer drugs that inhibit the tumor with other modes of action, thus offering possibility of combination therapy. Overall, the dendron-polymer conjugate based stable and tunable drug delivery system outlined here provides an attractive and tunable platform for combating cancer via efficient inhibition of angiogenesis.

3. DESIGNING DENDRON-POLYMER CONJUGATE BASED TARGETED DRUG DELIVERY PLATFORMS WITH A 'MIX-AND-MATCH' MODULARITY

3.1. Introduction

Polymeric micelles are emerging as a promising class of drug delivery system to address various challenges in the area of cancer therapeutics since they can be loaded with various drugs thereby increasing their bioavailability, and improving the pharmacokinetics and overall efficacy [18, 177, 299]. In general, the low molecular weight of many of the chemotherapy agents results in their fast clearance, thus decreasing the residence time in the body. Oftentimes, the hydrophobic character of these drugs makes the addition of excipients like Cremophore®EL a necessity. While the excipient increases the solubility of the hydrophobic drug through its emulsification, a variety of toxic side effects have been noted which warrants search for safer alternatives [300]. Combined with the narrow therapeutic indices and added systemic toxicities of such formulations at effective doses leading to increased mortality rates, conventional chemotherapy is far from perfect.

To overcome some of these challenges, utilization of nano-sized carriers of chemotherapy agents are on the rise because to their potential to eliminate several of these disadvantages. For instance, to improve efficacy and decrease prominent cardiotoxicity of anthracyclines, liposomal formulations such as Doxil are widely used in the clinic. In recent years, polymeric micelles have been employed in the clinic as another class of nano-sized delivery agent [4]. These are expected to be efficient carriers due to their ability to deliver encapsulated drugs in high concentrations at tumor sites, as well as to provide sustained release profiles thereby significantly improving the pharmacokinetics of the drug [65, 182].

Assembled from macromolecules with distinct hydrophobic and hydrophilic regions, polymeric micelles are supramolecular assemblies possessing the ability to load various

hydrophobic drugs solo [301, 302] or in combination [303, 304]. PEG based polymers are widely used as the hydrophilic micelle exterior rendering the nanoparticles water soluble and enabling them to avoid or minimize interaction with plasma proteins due to their lack of surface charge [305]. Linear or hyperbranched hydrophobic polymeric domains encapsulating the drugs are shielded by this protective layer from opsonization and unwanted interaction by reticuloendothelial system (RES). The hydrophobic domains in these carriers also improve the stability of drugs by preventing their degradation under prolonged exposure to physiological conditions [306, 307]. Using highly branched, symmetrical and well-defined polyester dendrons as the hydrophobic component of micelles improves their critical micelle concentration (CMC) values, and their biodegradability through hydrolytic or enzyme dependent degradation results in gradual drug release [282, 308].

It is known that pegylated micelles can circulate in plasma for prolonged periods of time in stealth state escaping capture by mononuclear phagocyte system (MPS) [11, 309]. Circulating nano-therapeutic agents can accumulate in tumor tissue by Enhanced Permeation and Retention (EPR) effect. Due to lack of a well-organized vasculature network and impaired lymphatic drainage, tumor environment has rather heterogeneous and leaky morphology enabling accumulation of drug loaded nanoparticles in tumor tissue in a size and shape dependent manner [15]. Consequently, macromolecules with hydrodynamic sizes larger than 7 nm escaping renal filtration or RES can diffuse through tumor vessel and accumulate there by EPR [70, 310]. This type of passive targeting achieves retention of loaded cargo around tumor environment, however, to trigger cellular uptake despite the anti-biofouling PEG based exterior employment of ligands targeting over expressed receptors on tumor cells and triggering endocytosis or phagocytosis mechanisms is crucial [299]. In particular, Arg-Gly-Asp (RGD) sequence containing peptides are widely used since they are known to target αυβ3/ αυβ5 integrin receptors that are over-expressed in various tumor cells and tumor angiogenic vessels [311–313].

In this study a “mix and match” micellar drug delivery system was designed by employing dendron-polymer conjugates. As primary constructs, to constitute the bulk of the micelle, two different types of conjugates, first one based on an AB diblock type, and the second one using an ABA triblock type dendron-polymer conjugates were synthesized.

The first block (A) was composed of a hydrophobic biodegradable polyester dendron, while the other block was linear PEG polymer. Although the building blocks are quite similar, subtle differences in the micellar aggregates formed using these building blocks can be expected. While for the first construct it can be anticipated that the AB-type dendron polymer conjugates are incorporated into the construct from one end i.e. from the dendron unit, whereas for the ABA type construct, the polymeric components are incorporated into the construct from both of the dendron units flanking the hydrophilic PEG chain. Furthermore, this would also lead to differences in the display of the PEG chains on the surface. These differences can be expected to manifest themselves as differences in size and stability of the micellar constructs, as well as their drug loading capacities and may be even their interaction with cells.

To render these constructs suitable for active-targeting, a cyclic peptide based targeting ligand containing dendron-polymer conjugate was utilized as a secondary construct. For dendritic part of all constructs forming hydrophobic core of micellar constructs, an acetal protected generation-4 polyester dendron (G4OX) was used to obtain low CMC values, act as efficient hydrophobic drug reservoirs, as well as be acid labile so that hydrolysis under acidic conditions lead to enhanced drug release. For the hydrophilic part linear PEG polymers were used; 2kDa for AB type primary construct, 6kDa for ABA type primary construct and 3.5kDa for secondary construct bestowing excellent solubility along with size commensuration of the hydrophilic block in all constructs. By mixing primary and secondary constructs in different feed ratios, micelles with varying amounts of targeting groups were obtained, and the effect of introducing the cyclic RGD peptide-based construct on properties from size and stability, to drug release and cellular internalization was investigated. A widely used anti-cancer drug Docetaxel was encapsulated into the micelles and the change in drug efficacy modulated by the micellar carrier was probed *in vitro* on two RGD-sequence recognizing cancer cell lines, namely the MDA-MB-231, human breast cancer and A549, lung cancer. At the onset of the study, it is anticipated that an in depth understanding of the subtle differences in the macromolecular building blocks composing these micellar constructs, would allow for optimization towards an ideal construct. Moreover, the ‘mix and match’ nature of the optimal construct would allow one to rapidly obtain a drug loaded suitably targeted nano-therapeutic system for various types of cancers (Figure 3.1).

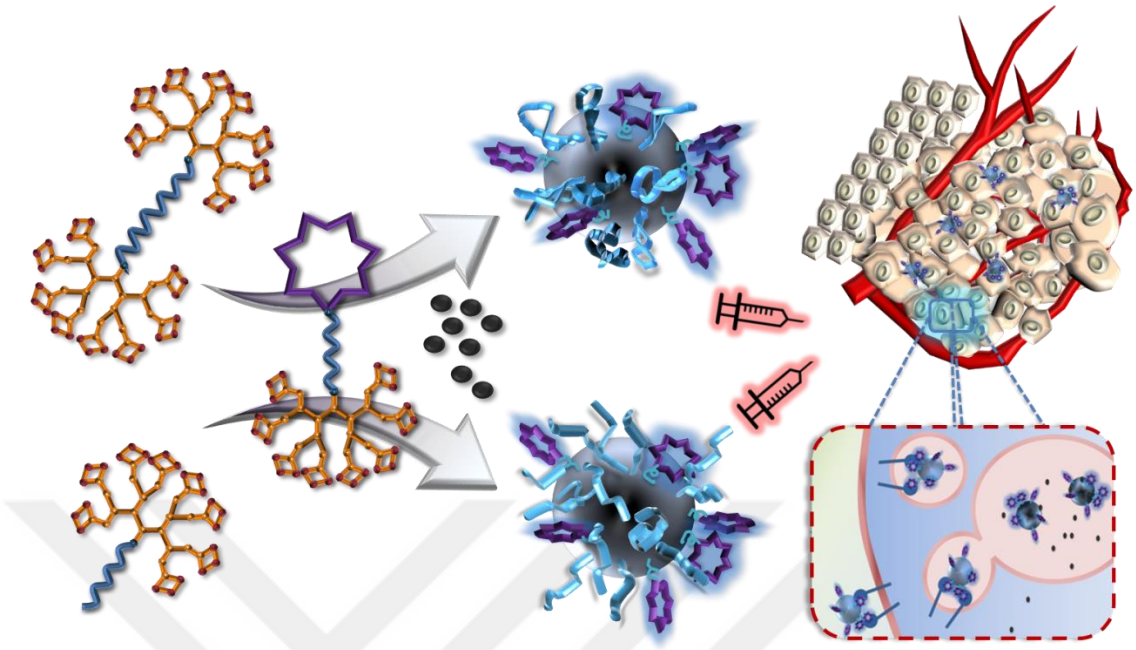

Figure 3.1. Schematic illustration of AB type 2K and ABA type 6K micelles with RGD containing secondary construct for improved docetaxel delivery into tumor cells.

3.2. Experimental Section

3.2.1. Materials

Bis-MPA, Dowex X50WX2, propargyl alcohol, 4-pentynoic acid were purchased from Alfa Aesar. All PEGs were obtained from Fluka. Azide PEG succinimidyl carboxymethyl ester (N3-PEG3.5kDa-NHS) was purchased from JenKem Technology (USA). All amino acids required for cRGDfK synthesis was purchased from Protein Technologies Inc. (USA). All solvents were purchased from Merck, all dyes including Nile red (NR), 1,1′-dioctadecyl-3,3,3′,3′-tetramethylindocarbocyanine perchlorate (DiI) and 3,3′-dioctadecyloxacarbocyanine perchlorate (DiO) were purchased from Sigma Aldrich and they were used as obtained without further purification unless otherwise noted. Bis-azido functionalized 6kDa PEG, azido functionalized 2kDa methoxyl PEG (m-PEG-OH) and generation 4 bis-MPA polyester dendron (G4OX) , cRGDfK were synthesized and characterized according to previously described methods[289, 314, 315].

3.2.2. Instrumentation

The monomer and copolymer characterizations involved ^{1}HNMR spectroscopy (Avanche III HD, Bruker, USA) and ATR-FT-IR spectroscopy (Nicolet 380, Thermo Scientific, USA). Synthesized dendrons, polymers and conjugates were further analyzed on Matrix-assisted laser desorption/ionization/time of flight (MALDI-TOF) spectrometer (Axima Performance, Shimadzu Biotech, Japan). cRGDfK production was achieved through solid phase peptide synthesis (SSPS, PS3 Peptide Synthesizer, Protein Technologies Inc., USA). Nile Red (NR) intensities for critical micelle concentration (CMC) determinations are measured with a Varian Cary Eclipse Fluorescence spectrometer (Varian, Agilent, USA). Wet size of the micelles was monitored with dynamic light scattering (DLS, Zetasizer ZS, Malvern, USA) and their dry form was measured on transition electron microscopy (TEM) mode of LVEM5 Electron Microscope (Delong Instruments, USA). Docetaxel was quantified by Liquid chromatography–mass spectrometry (LC-MS) analysis using a LCMS-2020-Mass Spectrometer System (Shimadzu, Japan) equipped with an C-18 5 μm 150 × 4.6 mm column. Mobile phase consisted of deionized water and HPLC grade acetonitrile (ACN) using the following gradient; LC: 0-3 min, 50% ACN; 3.01 min, 50% ACN; 8 min, 95% ACN; 8.01-11 min 50% ACN MS single ion mode (SIM) 807.9 m/z. Ultra-pure water was obtained via MilliQ Water Purification System (Merck Millipore, USA). UV/vis spectroscopy experiments were done on Nanodrop 2000 (Thermo Scientific, USA). Time dependent dye internalization experiments were done with an inverted fluorescent microscope (Zeiss Observer A1 equipped with AxioCam MRc5) and images were processed with AxioVision software. Both dye internalization and competitive binding was studied by flow cytometry (Guava EasyCyte, Merck Millipore, USA).

3.2.3. Synthesis and Characterization of G4OX

Fourth generation polyester dendron with an alkyne group at the focal point was synthesized as previously reported in literature [315].

3.2.4. Synthesis of Primary Constructs mPEG2K-G4OX (2K) and G4OX-PEG6K-G4OX (6K)

Synthesis of AB and ABA type dendritic linear diblock and triblock copolymers with G4OX dendron was adapted from literature with minor modifications[185]. Following the synthesis of linear polymer blocks mPEG2K-N_3 and N_3-PEG6K-N_3, synthesis of primary constructs providing the main participant of micelle achieved via Huisgen type "click" reaction. Alkyne core of the G4 dendron (200 mg, 0.0946 mmol) was reacted with azide functional groups on mPEG2K-N_3 (126.08 mg, 0.0630 mmol) and N_3-PEG6K-N_3 (189.13 mg, 0.0315 mmol) in the presence of Cu(I)Br (189.13 mg, 0.0315 mmol) and PMDETA (19.97 µL, 0.0946 mmol) in 3 mL THF resulting in176.29 mg mPEG2K-G4OX (2) with 68% and 209.6 mg of G4OX-PEG6K-G4OX (3) with 65% yield (Figure 3.2). ^{1}H NMR of mPEG2K-G4OX (CD3OD, δ, ppm): 7.86 (s, 1H), 5.23 (s, 2H), 4.54 (t, *J*=10 Hz, 2H), 4.28-4.19 (m, 60 H), 3.80-3.40 (s, 172 H), 3.37 (s, 3H), 1.41 (s, 24H); 1.35 (s, 24H); 1.30 (s, 6H), 1.28 (s, 12H), 1.14 (s, 24H) (Figure A.7). ^{1}H NMR of G4OX-PEG6K-G4OX (CD3OD, δ, ppm): 7.86 (s, 2H), 5.23 (s, 4H), 4.54 (t, *J*=10 Hz, 4H), 4.28-4.19 (m, 120 H), 3.80-3.40 (s, 756 H), 1.41 (s, 48H); 1.35 (s, 48H); 1.30 (s, 12H), 1.28 (s, 24H), 1.14 (s, 48H) (Figure A.7).

3.2.5. Synthesis of cRGDfK by SSPS

cRGDfK synthesis was achieved using solid phase peptide synthesis methodology based on literature[314]. The peptide was characterized in LC-MS through its retention time and expected and observed [MH^+] value of 604.

3.2.6. Synthesis of NHS-PEG3.5K-G4OX

Synthesis of AB type dendritic linear diblock copolymers with G4OX dendron was adopted from literature with modifications[185]. Alkyne core of the G4 dendron (200mg, 0.0946mmol) was reacted to azide functional groups on N_3-PEG2K-NHS (208.04mg, 0.0630mmol) in presence of Cu(I)Br (9.17mg, 0.0630mmol) and PMDETA (13.31µL,

0.0630mmol) in 3mL THF resulting in 232.13mg product with 68% yield (Figure 3.3). ^{1}H NMR of NHS-PEG3.5K-G4OX (CD3OD, δ, ppm): 7.86 (s, 1H), 5.23 (s, 2H), 4.54 (t, *J*=10 Hz, 2H), 4.28-4.19 (m, 60 H), 3.80-3.40 (s, 300 H), 2.84 (s, 4H), 1.41 (s, 24H); 1.35 (s, 24H); 1.30 (s, 6H), 1.28 (s, 12H), 1.14 (s, 24H).

3.2.7. Synthesis of cRGDfK-PEG3.5K-G4OX

Conjugation of cRGDfK to NHS-PEG3.5K-G4OX was adopted from literature with modifications[185]. *N*-Hydroxysuccinimide activated NHS-PEG3.5K-G4OX (200mg, 0.0333mmol) was conjugated to cRGDfK (200 mg, 0.0333 mmol) from its lysine residue in presence of *N*,*N*-diisopropylethylamine (DIPEA) (31.82 mL, 0.3333 mmol) in 2.5mL dimethylformamide (DMF) at room temperature in 48h. Resulting conjugate was purified by dialysis in water for 1 day. cRGDfK-PEG3.5K-G4OX was obtained as a yellowish powder. (Figure 3.3). ^{1}H NMR of cRGDfK-PEG3.5K-G4OX (DMSO, δ, ppm): 7.73 (s, 1H), 7.48-7.00 (m, 5H), 5.17 (s, 2H), 4.50 (t, *J*=5 Hz, 2H), 4.30-3.6 (m, 60 H), 3.60-3.40 (s, 300 H) , 1.34 (s, 24H); 1.22-1.13 (m, 45H); 1.01 (s, 24H) (Figure 3.3).

3.2.8. Micelle Preparation

Four types of mix and match micelles were prepared using different weight ratios of primary constructs mPEG2K-G4OX (2K) or G4OX-PEG6K-G4OX (6K) and cRGDfK-PEG3.5K-G4OX (RGD). For preparation of micelles with and without drug, solvent evaporation method was employed; briefly copolymer stock solutions (10 mg/mL) in methanol were prepared. By combining required volumes from primary and secondary polymer stock solutions exact amounts of dissolved polymers with certain weight ratios were distributed into glass vials. After addition of water, methanol in vials was evaporated.

3.2.9. Loading of Docetaxel into Micelles

For drug loading, docetaxel stock solutions in methanol were prepared (10 mg/mL) and exact volumes of drug stock solution were added onto polymer solution, vortexed

briefly and methanol in vials were evaporated before addition of water to obtain micelles. To remove excess drug molecules, prepared micelles were dialyzed in water for 2 days. Removal of free drug and drug precipitates were tracked by LC-MS and DLS respectively.

3.2.10. Determination of Docetaxel Content

Drug loaded micelles were lyophilized to determine their dry weight. Subsequently, they were dissolved in ACN and their docetaxel content was quantified via LC-MS.

3.2.11. Determination of Critical Micelle Concentration (CMC)

Four set of NR doped micelles were prepared by solvent evaporation method; 2K 100-0, 2K 60-40, 6K 100-0 and 6K 60-40. Polymer stock solutions containing primary and secondary constructs with desired weight ratios were prepared. Using these stocks, serial dilutions were made in methanol and solutions containing polymers with final concentrations ranging between 1 mg/mL to $3x10^{-5}$ mg/mL were obtained. Nile Red solution in methanol (50 µL, 0.1mg/mL) was added into each vial and after addition of deionized water (3 mL), methanol was evaporated.

Fluorescence measurements were taken with excitation wavelength of 550 nm and emission spectra between 575 and 700nm were recorded for NR doped micelle samples. By measuring the blue shifted peak at 636nm (660nm in aqueous environment) CMC values were calculated [316, 317].

3.2.12. Determination of Micelle Size and Dilution Stability by DLS

Eight set of micelles at different concentrations (higher than CMC) with or without drug were prepared by solvent evaporation method; 2K 100-0, 2K 90-10, 2K 80-20, 2K 60-40, 6K 100-0, 6K 90-10, 6K 80-20, and 6K 60-40. Their effective size (diameters) were

determined at 37°C. To monitor effect of dilution on micelle stability, prepared micelles were diluted up to 0.005µg/mL (lower than CMC) and DLS measurements were repeated.

3.2.13. Determination of Micelle Size by TEM

Four set of drug loaded micelles were prepared by solvent evaporation method; 2K 100-0 D, 2K 60-40 D, 6K 100-0 D and 6K 60-40 D. Micelle solutions were dropped onto copper grids and air dried before image acquisition. Mean size of micelle were found by counting at least 100 particles via the Q-Capture Pro7 software.

3.2.14. pH Dependent Docetaxel Release from Micelles

Four set of drug loaded micelles (10mg/mL) were prepared by solvent evaporation method; 2K 100-0, 2K 60-40, 6K 100-0 and 6K 60-40. Stock micelle solutions were diluted with acetate buffer at pH 4.8 and PBS buffer at pH 7.4 separately with 5mg/mL final concentrations. Resulting micelle solutions were transferred into dialysis bags with MW cut-off 1 kDa. Dialysis bags were immersed in 1L of corresponding buffer solutions and incubated at 37 °C for 10 days. At predetermined time points, 1mL aliquots were collected and released Docetaxel was quantified by LC-MS analysis.

3.2.15. Investigation of Serum Stability of Micelles using FRET

Four set of micelles were prepared by solvent evaporation method; 2K 100-0 F, 2K 60-40 F, 6K 100-0 F and 6K 60-40 F containing 1 weight percent Förster resonance energy transfer (FRET) dye pair DiI and DiO. As previously reported in literature[318], serum stability profiles of micelles were determined by the decrease in FRET signal. Micelle solutions diluted 1:1 with FBS were incubated at 37 °C for 2 days and excited at 484nm their emission intensities were recorded at 501 (I501) and 565 (I565) for DiO and DiI respectively at predetermined time points. The change in FRET ratio, I565/(I565 + I501), was calculated and normalized to time zero.

3.2.16. Cell Lines

A549 and MDA-MB-231 cell lines purchased from ATCC (LGC Standards, Germany) and grown according to manufacturer's culture methods requirements. Cells were incubated at 37 °C in a humidified atmosphere of 5% CO_2 and kept in logarithmic phase of growth throughout all experiments.

3.2.17. *In vitro* Cell Viability Assay

Cell number and cell viability were determined by Cell Counting Kit-8 (CCK-8, Fluka). Cells were seeded in 100 µL of culture medium at a density of 3000 cells/well for A549 and MDA-MB-231 cells into 96-well plates in quadruplicates for each drug concentration. After overnight incubation cell media was replaced with fresh medium containing various concentrations of conjugates, free drug, or polymer only controls. For free drug treatments docetaxel stock solution was prepared in 20% DMSO in growth medium (V/V) and subsequently diluted where the final DMSO concentration was below 0.5% (V/V). All cells were incubated continuously for 48h in the presence of the micellar conjugates. For 2h+22h pulse chase drug treatment, cells were incubated 2h in drug containing solutions and incubated in fresh media for 22h before CCK-8 assay. To determine the cell viability, 100 µL of culture medium together with 10 µL of CCK-8 solution was added into each well. After 4h incubation the absorbance values at 450nm was measured with a plate reader (Multiscan FC, Thermo Scientific, USA). Viability of treated cells was expressed as percentage of control cells (cell media only). EC50 values were obtained from concentration response curves by nonlinear regression analysis.

3.2.18. Cellular Internalization of NR doped Micelles

Four set of NR doped micelles were prepared by solvent evaporation method; 2K 100-0 NR, 2K 60-40 NR, 6K 100-0 NR and 6K 60-40 NR. MDA-MB-231 cells seeded onto 24 well plates were treated with 1 wt% NR containing micelle solutions with 0.1mg/mL final concentration. As control samples, same amount of NR was added into

wells. Cells were then incubated for 1, 3 and 24 hours at 37°C. They were fixed using 4% formaldehyde after DAPI staining and fluorescence images were collected via inverted fluorescent microscope (Zeiss Observer A1 equipped with AxioCam MRc5) and processed with AxioVision software.

3.2.19. cRGDfK Dependent Cell Binding Assay

Four set of NR doped micelles were prepared by solvent evaporation method; 2K 100-0, 2K 60-40, 6K 100-0 and 6K 60-40. MDA-MB-231 cells seeded onto 24 well plates were treated with 2.5 wt% NR containing micelle solutions with 0.1mg/mL final concentration. As control samples, same amount of NR was added into wells. Also free cRGDfV, a cyclic integrin-binding peptide possessing higher binding affinity to RGD specific integrins compared to RGD[319] was added as an inhibitor into another set of wells. Cells were then incubated for 1 and 3 hours at 37°C. After each treatment cells were trypsinized and NR intensities were determined by flow cytometry (Guava easyCyte) and results were processed on guavaSoft software.

3.3. Results and Discussion

3.3.1. Synthesis and Characterization of Dendron-Polymer Conjugates

To construct micelles in a modular fashion with varying amounts of surface ligands, three different dendron-polymer conjugates were synthesized. As primary constructs an AB type dendron-PEG conjugate mPEG2K-G4OX (2K) and an ABA type dendron-PEG-dendron conjugate G4OX-PEG6K-G4OX (6K) were synthesized to constitute the major component of assembled micelles. The fourth generation hydrophobic dendron unit provides the driving force for assembly of these conjugates when exposed to aqueous environments. As the secondary construct, an AB type dendron-polymer conjugate, cRGDfK-PEG3.5K-G4OX (RGD), bearing the integrin targeting cRGDfK group at the PEG chain-end was synthesized. The targeting peptide was conjugated at the chain end of the hydrophilic PEG chain so that it is displayed on the surface of the micelle. To obtain

the AB and ABA type primary constructs, a hydrophobic fourth generation polyester dendron (G4OX) containing an alkyne group at its core was conjugated with azide functionalized linear PEG polymers (2kDa, 6kDa) via the copper catalyzed azide-alkyne "Huisgen Click" reaction (Figure 3.2).

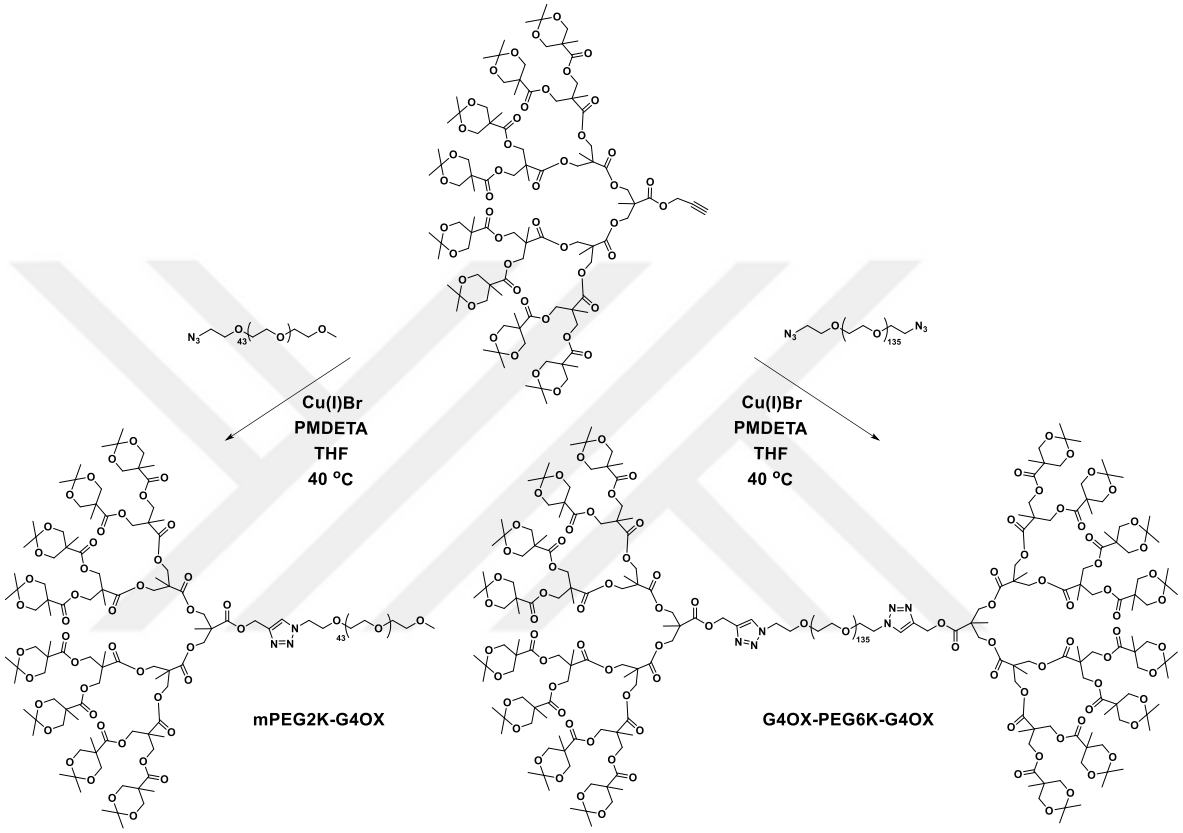

Figure 3.2. Synthesis of primary constructs mPEG2K-G4OX (2K) and G4OX-PEG6K-G4OX (6K).

The chemical composition of the dendron-polymer conjugates was verified using ^{1}H-NMR analysis (Figure A.7), where apart from the expected proton resonances belonging to the PEG and dendron components, the presence of the signal belonging to the proton on the triazole ring (around 7.86 ppm) confirms their conjugation though the triazole moiety. To obtain the dendron-polymer conjugate containing the targeting group at the end of the hydrophilic PEG chain, a hetero-bifunctional PEG (3.5 kDa) containing a NHS ester and an azide unit was utilized (Figure 3.3). First, the fourth generation polyester dendron was attached using the azide-alkyne click reaction, followed by the conjugation of the amine group containing cyclic RGD peptide to the NHS-activated carboxylic acid group. After

purification, the ^{1}H-NMR spectrum of the targeting ligand-containing dendron-polymer conjugate revealed the expected proton resonances at 7.86 ppm arising from the triazole ring, and also displayed signals between 7.00-7.48 ppm belonging to various protons on the cRGDfK fragment (Figure A.8).

3.3.2. Generation and Characterization of Micelles Formed from Primary and Secondary Constructs

With the polymeric building blocks for fabricating the micelles at hand, two sets of micelles (with and without the drug) were obtained using one of the primary constructs, 2K or 6K PEG-based, along with the targeting ligand containing secondary construct at various weight percentages (wt%) (Table 3.1).

Table 3.1. Micelle Compositions and Drug Contents.

Item	Micelle	mPEG2K-G4OX	G4OX-PEG6K-G4OX	cRGDfK-PEG3.5K-G4OX	Drug Content wt%
1	2K 100-0	100	0	0	0
2	2K 60-40	60	0	40	0
3	2K 100-0 D	100	0	0	9.86±0.25
4	2K 60-40 D	60	0	40	10.13±0.36
5	6K 100-0	0	100	0	0
6	6K 60-40	0	60	40	0
7	6K 100-0 D	0	100	0	10.21±0.21
8	6K 60-40 D	0	60	40	9.93±0.43
9	2K 90-10	90	0	10	0
10	2K 80-20	80	0	20	0
11	6K 90-10	0	90	10	0
12	6K 80-20	0	80	20	0

Micelles were formed via solvent evaporation method followed by dialysis. Drug loading ranged between 9.86±0.25% and 10.21±0.21% and it was observed that the type of primary construct or the weight percent of secondary construct did not affect final encapsulation efficiency. Since same G4OX polyester dendrons constitute the core of all these micellar constructs, this result is in parallel with expectations.

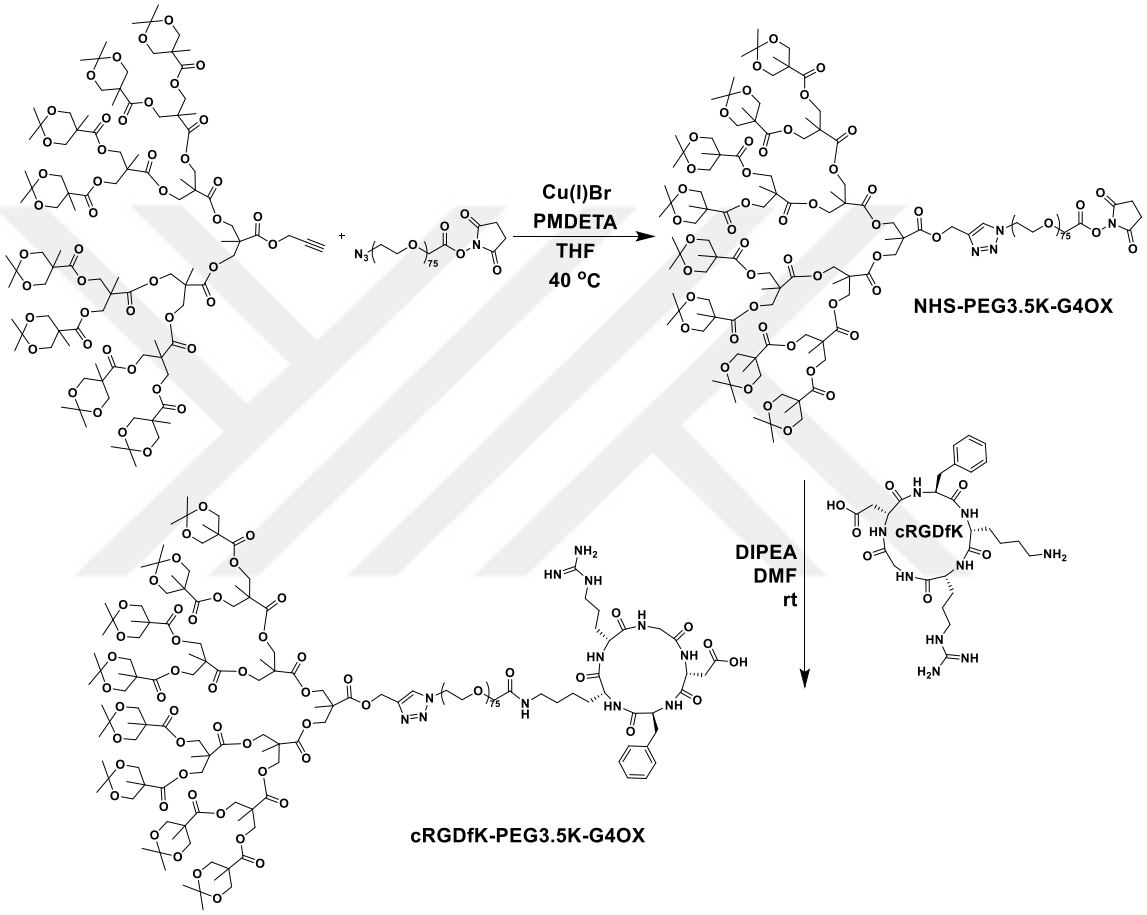

Figure 3.3. Synthesis of secondary construct cRGDfK-PEG3.5K-G4OX.

3.3.3. Critical Micelle Concentrations

The CMC of these micelles were determined using a fluorescent probe, namely, Nile red (NR). When in aqueous media, NR molecules form excimers, quenching their signal, however once introduced into the hydrophobic core of micelles, the dyes solubilize and an increase in peak intensity with a hypsochromic shift is observed in their emission spectrum. The CMC values of NR doped 2K and 6K micelle sets prepared with varying

weight ratios were investigated by tracking the blue-shifted NR peak emission intensity at 636nm (λ_{ex}=550nm) and determining the intersection of resulting trendlines (Figure 3.4).

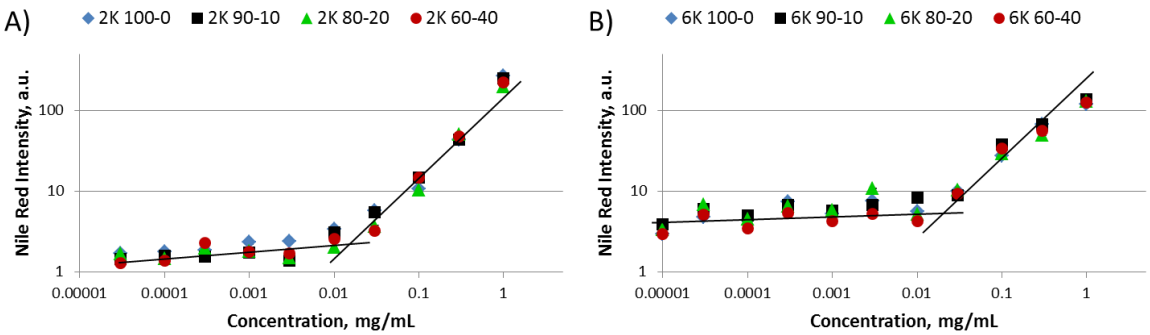

Figure 3.4. Nile Red emission spectra of 2K (A) and 6K (B) micelles.

It was observed that the CMC values of 2K micelles were around 0.012 mg/mL, whereas the CMC of ABA type 6K micelles were almost three times higher (0.033 mg/mL). But once these values are converted to molar scale by converting mg values of contributing primary and/or secondary constructs while preparing individual micelles to moles, CMC of both micelles types are quite similar (around 2.5x10^{-6}M) (Figure 3.5).

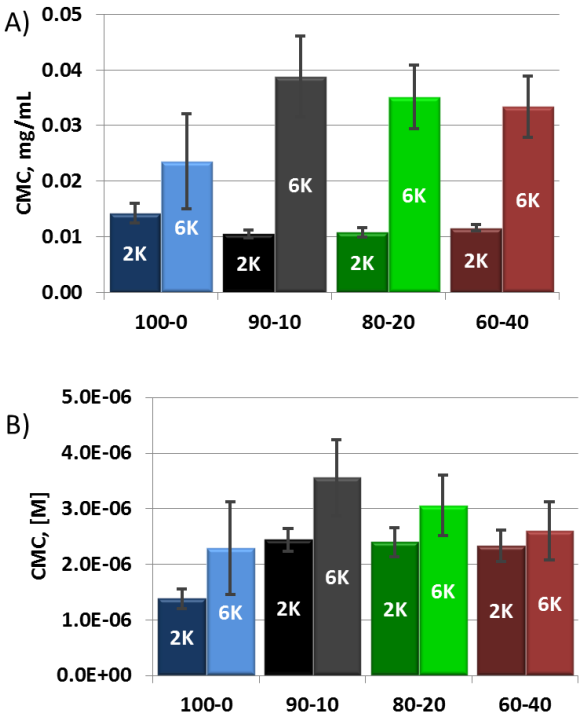

C)

Construct	CMC, mg/mL	CMC, [M]
2K 100-0	0.014 ±0.002	1.4E-06 ±8.3E-07
2K 90-10	0.011 ±0.001	2.4E-06 ±6.8E-07
2K 80-20	0.011 ±0.001	2.4E-06 ±5.4E-07
2K 60-40	0.012 ±0.001	2.3E-06 ±5.2E-07
6K 100-0	0.024 ±0.009	2.3E-06 ±1.7E-07
6K 90-10	0.039 ±0.007	3.6E-06 ±2.1E-07
6K 80-20	0.035 ±0.006	3.1E-06 ±2.6E-07
6K 60-40	0.033 ±0.006	2.6E-06 ±2.8E-07

Figure 3.5. CMC values of 2K and 6K micelles by mg/mL (A), molarity (B) in graphical and in tabular (C) representation.

As seen in Figure 3.5(B), introduction of RGD bearing secondary construct had a slightly negative effect on both 2K and 6K micelles. This might indicate that introduction of a new component to a micellar system can affect its overall stability but that can also be overcome by increasing feed ratio of secondary component by equilibrating different components. Yet since CMC values were too close to each other and standard deviations were notably high, this trend should be further supported by similar data from other micellar systems.

3.3.4. Micelle Size and Stability towards Dilution

To study the effective size of the micellar constructs in aqueous environment, DLS measurements of micelles prepared at different feed ratios and with or without drug encapsulation were undertaken (Figure 3.6).

A)

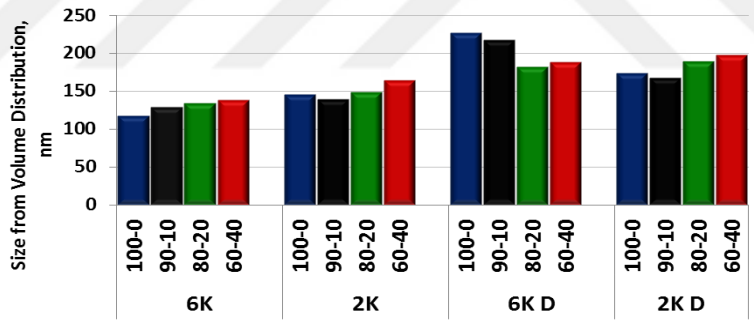

B)

	Size[a, b]	Std [b]	PDI		Size[a, b]	Std [b]	PDI
2K 100-0	145.3	±63.9	0.100	**2K 100-0 D**	173.1	±88.2	0.212
2K 90-10	138.7	±63.6	0.112	**2K 90-10 D**	167.5	±78.0	0.168
2K 80-20	148.5	±71.4	0.136	**2K 80-20 D**	188.8	±92.0	0.198
2K 60-40	163.9	±72.6	0.104	**2K 60-40 D**	197.8	±107.2	0.180
6K 100-0	117.5	±51.37	0.120	**6K 100-0 D**	226.2	±113.7	0.232
6K 90-10	128.3	±56.35	0.109	**6K 90-10 D**	217.7	±108.8	0.210
6K 80-20	133.4	±58.64	0.097	**6K 80-20 D**	182.2	±82.3	0.137
6K 60-40	138.5	±102.4	0.201	**6K 60-40 D**	188.0	±94.2	0.182

[a] size from volume distribution, [b] nm

Figure 3.6. Effective size diameters from volume distributionin nm of 2K and 6K micelle sets with or without drug (D) encapsulation A) graphical and B) tabular representation.

Interestingly, it was observed that on an average, the 6K micelles (118-139 nm) were slightly smaller than 2K micelles (145-164 nm) without drug encapsulation. After docetaxel loading, the 2K micelles (168-198 nm) were smaller when compared to their 6K feed ratio counterparts (182 nm-226 nm). As expected, a slight increase in the micellar size was observed in all cases upon loading the hydrophobic drug. Introduction of the targeting peptide bearing secondary component to both 2K and 6K micelle systems resulted in a slight increase in their size. A similar trend was observed for drug loaded 2K micelles. However introduction of the secondary construct in increasing feed ratios resulted in a decrease in micelle sizes as well as PDI values for 6K micelles. For drug loaded 2K and 6K micelles, incorporation of secondary construct to the resulting assemblies lead to a slight decrease in PDI values which might indicate improved size distribution.

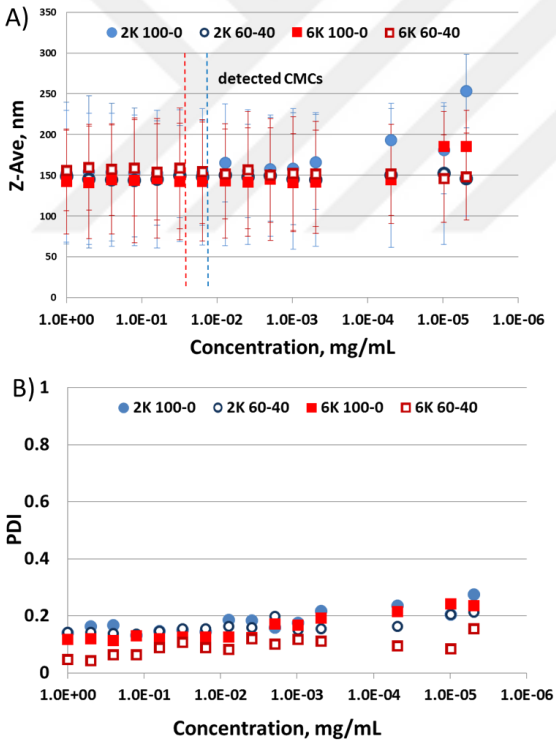

C)

	Final Conc., µg/mL	CMC, mg/mL	Dilution factor
2K 100-0	0.005	0.014	2867
2K 60-40	0.005	0.012	2458
6K 100-0	0.005	0.024	4915
6K 60-40	0.005	0.033	6758

Figure 3.7. Micelle (A) Z-average size (B) PDI values obtained after serial dilutions and (C) corresponding dilution factors.

Micelle integrity below CMC values was also investigated by diluting four types of micelles to 0.005µg/mL concentration which coincides to over thousand fold dilutions beyond CMC values (Figure 3.7C). Notably, the integrity of micelles was retained even

under such harsh dilutions and PDI values remained near 0.2 (Figure 3.7B). Only notable size change was observed for 2K 100-0 micelles at very high dilutions. The 6K 100-0 micelle set also displayed minor increase in size, yet neither of the targeting group containing micelles (2K 60-40 nor 6K 60-40) exhibited any noticeable change in their size (Figure 3.7A). Importantly, all micelles demonstrated prominent resistance against harsh dilutions which makes these assemblies promising candidates for various applications.

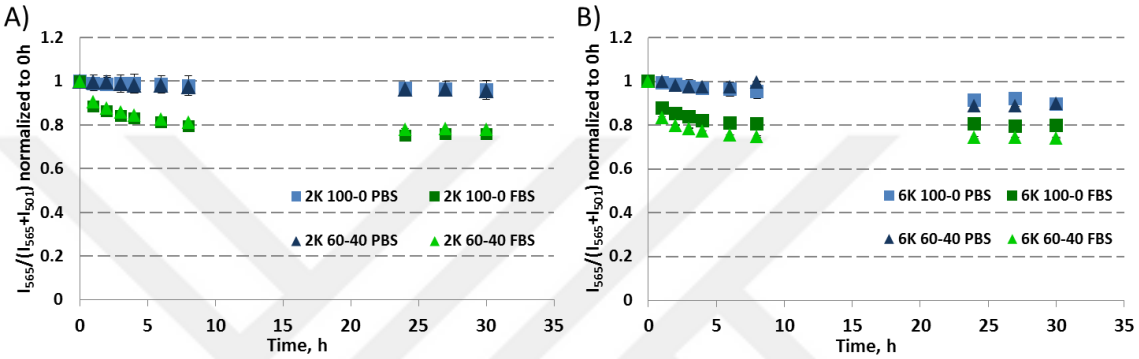

C)

Micelle	Ratio in 1xPBS	Ratio in FBS
2K 100-0 F	0.96	0.76
2K 60-40 F	0.96	0.78
6K 100-0 F	0.90	0.80
6K 60-40 F	0.90	0.74

Figure 3.8. Normalized FRET ratios of 2K (A) and 6K (B) micelles in graphical representation. Final FRET ratios at 30 hours are given in table (C).

Serum stability of the same set of micelles was investigated by FRET analysis using previously established protocols [318]. Effect of serum proteins triggering release from micelles was monitored by the change of fluorescence signal intensities of FRET pair DiO and DiI at 501 and 565nm. During serum incubation, release of encapsulated dyes would eliminate energy transfer between donor DiO and acceptor DiI dye resulting in a decrease in FRET intensity at 565nm and an increase in DiO signal at 501nm. Hence micelle instability was recorded as a decrease the FRET normalized ratio I565/(I565 + I501) (Figure 3.8). Micelle solutions were incubated in FBS or in 1x PBS for 30 h. Calculated FRET ratios suggested that both 2K and 6K micelles were stable in 1xPBS for 30 h, whereas incubation in FBS resulted in a small decrease in FRET ratio from 1 to 0.80-0.74

(Figure 3.8C). Also increasing the amount of the targeting group containing secondary construct in the micelles did not affect their stabilities in FBS notably.

The two types of drug loaded 2K and 6K micelles were also investigated using TEM to determine their size in dry form. Even though the sizes of drug loaded 2K and 6K micelle determined via DLS varied by 60nm (Figure 3.6B), once dried their size difference decreased dramatically. In dry form it is highly possible that PEG component of both 2K and 6K micelles shrinks considerably. Consequently, measured micelle mean diameters were considerably smaller and ranged between 23 to 26 nm (Figure 3.9). This decrease is important because it indicates that even the micellar sizes in their solvated state are around 200 nm, the micelle cores are much smaller, which should enable them to pass through much smaller barriers.

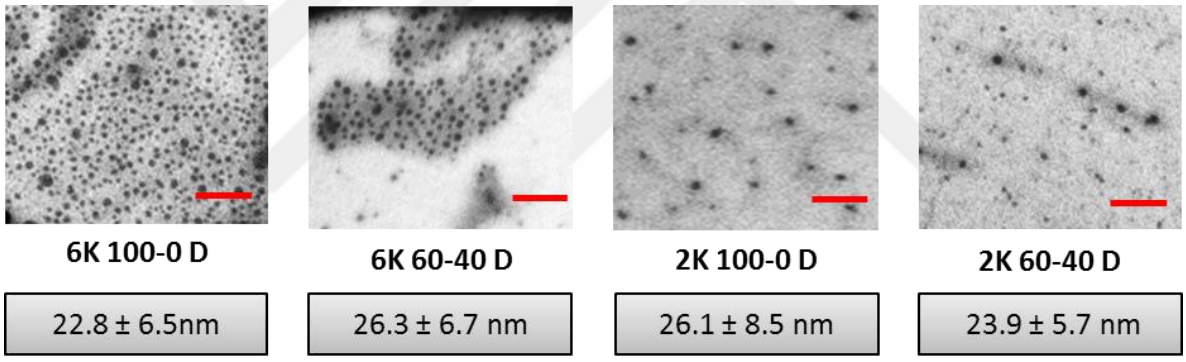

Figure 3.9. Dry micelles and measured mean micelle diameter values from TEM. Scale bar 200 nm.

3.3.5. pH Dependent Docetaxel Release from Micelles

Release profile of encapsulated drug is especially important for micellar systems since they are generally prone to early release due to lack of more durable covalent bonds stabilizing the assembly. To determine drug release profiles, docetaxel release at pH 7.4 and pH 4.8 was monitored using LC-MS. Since the core of 2K and 6K micelles were composed of biodegradable polyester G4 dendrons, release in acidic environment was expected to be higher than those at physiological buffer system. Furthermore, to check the

effect of secondary construct on drug release, a set of 2K and 6K micelle (100-0 and 60-40) with and without the targeting ligand component were compared.

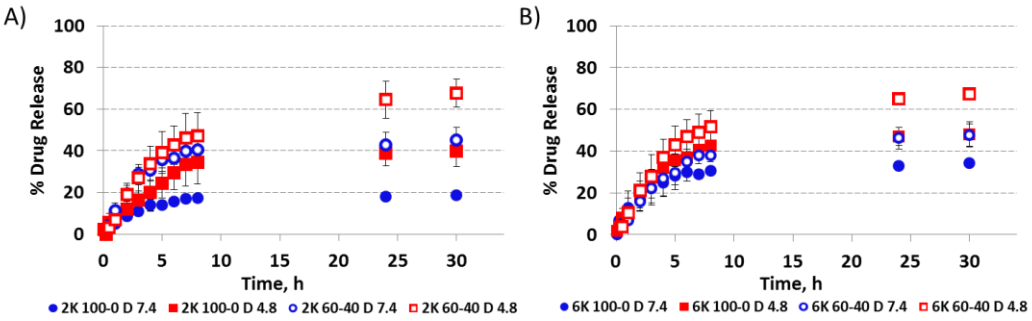

C)

Micelle	% D release at pH 7.4	% D release at pH 4.8
2K 100-0 X	18.6±1.7	39.8±7.4
2K 60-40 X	45.3±5.8	67.7±6.7
6K 100-0 X	34.1±0.5	48.1±6.0
6K 60-40 X	47.8±5.3	67.5±2.9

Figure 3.10. Percent docetaxel release profiles from 2K (A) and 6K (B) micelles in graphical representation. Final release percentages at 30 h are given in table (C).

After 30 hours of incubation at 37°C, it was observed that 2K micelles were more stable in terms of drug release at 7.4. In the absence of secondary construct, docetaxel release percent reached to only 18.6±1.7% for 2K 100-0 D micelles, whereas it was almost double for the 6K 100-0 D micelles with 34.1±0.5% (Figure 3.10). Introduction of the RGD bearing secondary construct increased docetaxel release for both 2K and 6K at pH 7.4. On the other hand, drug release was notably increased for all micelle types at pH 4.8 as expected and reached to a maxima of 68% for both 2K and 6K 60-40 D micelle sets in 30 hours.

The increase in percent drug release indicates that employing a secondary construct, even with the same core structure, can alter release profiles of micelle systems formed from AB and ABA type polymers. However, the increased release at acidic pH combined with the targeting effect of RGD group at their periphery suggests the suitability of these micellar constructs for delivery applications.

3.3.6. *In vitro* Cellular Internalization of Targeted and Non-targeted Micellar Constructs

To assess cellular internalization, the 2K and 6K micelles with and without targeting group were incubated with MDA-MB-231 human breast cancer cells. In order to visualize internalization of the cargo, micelles were doped with a hydrophobic dye, namely, Nile Red. In comparison to the control well, where NR was added to cell containing media in the absence of any micelles, there was a visible increase in the NR intensity in the cells treated with all micelle types after 1 h of incubation (Figure 3.11).

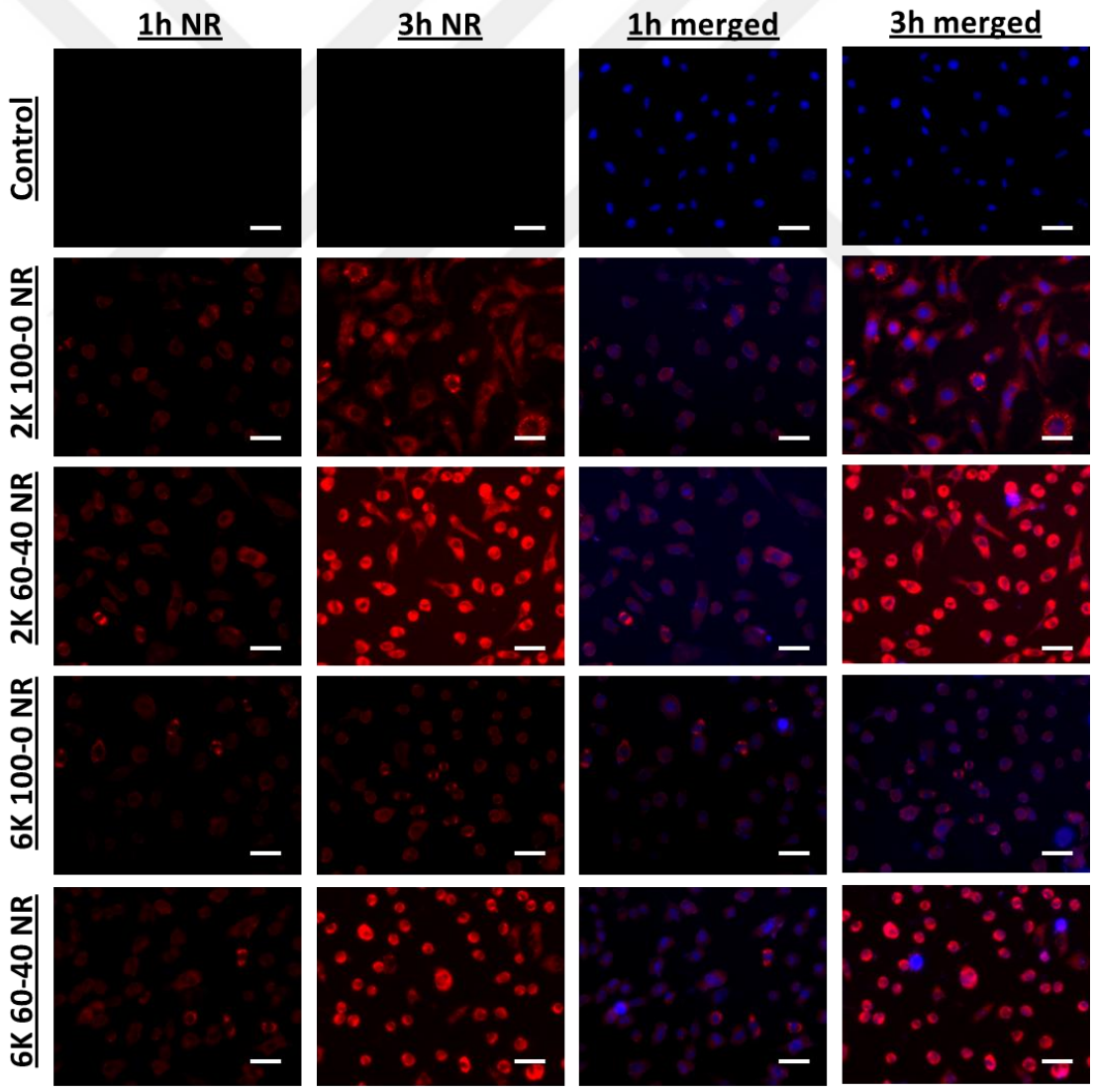

Figure 3.11. Nile Red internalization experiments of NR doped 2K and 6K micelles. Scale bar 50μm.

There was a minute difference between 100-0 and 60-40 micelles, the latter showing more internalization in comparison. After 3 hours, NR signal considerably increased in all wells except the control, indicating cell internalization of NR was improved dramatically once encapsulated into micelles and the uptake increased over time. Here it is important to note that NR signal at both 60-40 micelles rose dramatically highlighting the significance of the RGD targeting group for internalization through active targeting. A change in cell shape histology was also notable at 3 h for 60-40 micelles; possibly due to interaction of RGD on micelles with integrin receptors on the cell surfaces the shape of MDA-MB-231 cells become rounder instead of their more spread counterparts. Also a slightly increased NR intensity was observed for 2K micelles in contrast to 6K micelles, thus hinting higher internalization efficiency with the AB type dendron-polymer conjugates.

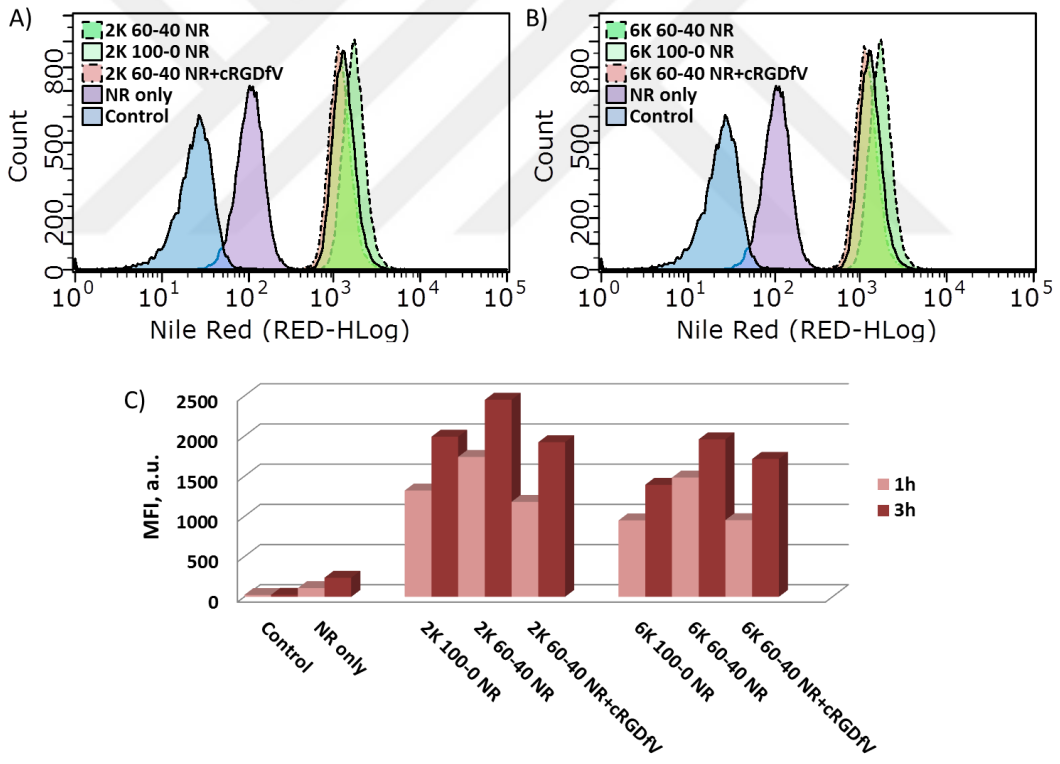

Figure 3.12. Nile Red cell internalization histograms by flow cytometry of doped 2K (A) and 6K (B) micelles and Nile Red dye only at 1 hour. MFI values were presented in (C).

The cellular internalization of the NR doped targeted and non-targeted micelles were also investigated using flow cytometry. To further emphasize the RGD dependent internalization, cRGDfV was employed acting as a competitive inhibitor of conjugated

cRGDfK for integrin binding. It is known that cRGDfV has higher binding affinity towards the integrin domains on cell surfaces [319, 320]. After 1 hour, a significant increase in NR internalization was observed for all micelles, however 2K micelles showed higher mean fluorescence intensity (MFI) values compared to 6K counterparts (Figure 3.12). Besides NR internalization was higher for both the 60-40 micelles compared to 100-0 micelles, where the later ones were devoid of RGD moieties on micelle surface. Furthermore, addition of cRGDfV to cell media in combination with 60-40 NR micelles resulted in a decrease in NR intensity, with values comparable to the 100-0 NR counterparts, indicating that the increased internalization was due to interaction of RGD on secondary construct with the integrins on MDA-MB-231 cell surfaces. After 3 hours the NR MFI values increased further (Figure 3.12C) thus highlighting the time dependent, gradual manner of internalization.

3.3.7. *In vitro* Cellular Viability Assays

Cellular toxicity levels of 2K and 6K micelles were investigated on two cell lines expressing one or more of RGD recognizing integrins [255, 321]. After 48h continuous incubation of blank micelles with cells cell viabilities were determined via CCK-8 assay (Figure 3.13). MDA-MB-231 breast cancer cell line showed minimal growth inhibition even at 1 mg/mL polymer concentration.

Micelle cytotoxicity was also well compensated by A549 lung carcinoma cell line; varying between 62 to 100% at 1 mg/mL polymer concentration, cell viability was unhindered at concentrations of 0.5mg/mL and lower. There were no trending differences between 2K and 6K micelles or at different feed ratios of secondary construct, valid for both cell lines. For instance, 2K micelles showed improved viability in comparison to 6K set for MDA-MB-231. On the other hand viability profiles of 6K were slightly better for A549 cells at certain concentrations. Similarly, addition of RGD containing secondary construct did not result in a distinct cytotoxicity increase at the tested cell lines. Despite the 48 h long incubation time with blank micelle solutions, all tested cell lines exhibited significant cell viability, demonstrating their potentials as drug delivery platforms.

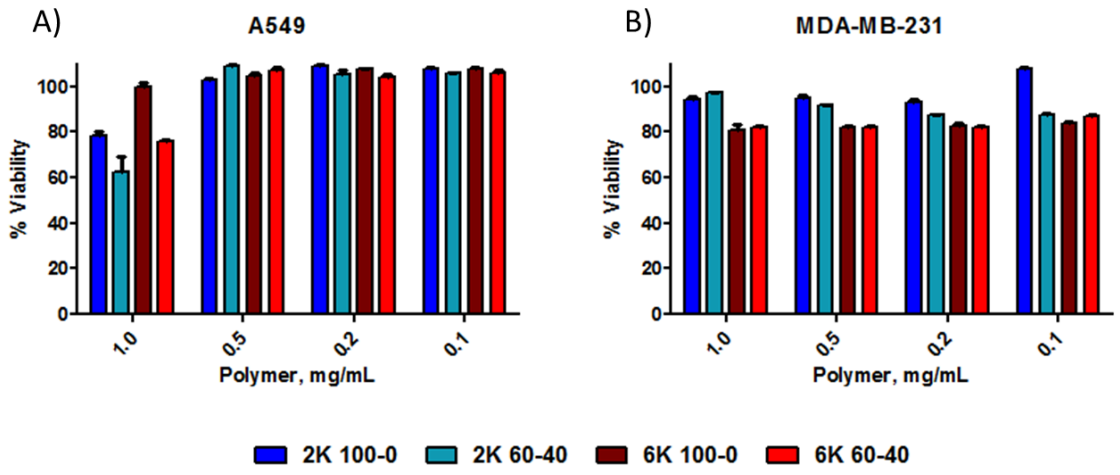

Figure 3.13. Cell Viabilities of empty 2K and 6K micelles on A549 (A), and MDA-MB-231 (B) cell lines after 48 hours of continuous incubation.

3.3.8. *In vitro* Cell Viability Assay with Docetaxel Loaded Micelles

Four types of docetaxel encapsulated micelles were incubated with A549 and MDA-MB-231 cell lines for 48 hours continuously, resulting cell viabilities were compared to controls and percent viabilities were calculated (Figure 3.14). For all cell lines cellular toxicities of 2K and 6K 100-0 D micelles were similar at almost all concentrations. Furthermore, introduction of RGD to 2K and 6K systems improved cytotoxicity for all cell lines and at almost all concentrations. The decrease in cell viabilities was more prominent with MDA-MB-231 cells. For MDA-MB-231 at 10^{-6}M, cell viability of 2K 60-40 D micelles decreased to 48% whereas 2K 100-0 D micelles resulted in 67% viability similarly only 41% of 6K 60-40 D treated cells were alive where this ratio was around 63% for 6K 100-0 D micelles. For A549, 2K 60-40 D showed a notable decrease in cell viability at most concentrations (max 14.4% at 10^{-7}M) compared to non-targeted 2K 100-0 D micelles but change with 6K 60-40 D micelles were not too distinct. Still, docetaxel showed best overall cytotoxicity on A549 cell line and construct itself induced minimal cytotoxicity to A549 cells (Figure 3.13A).

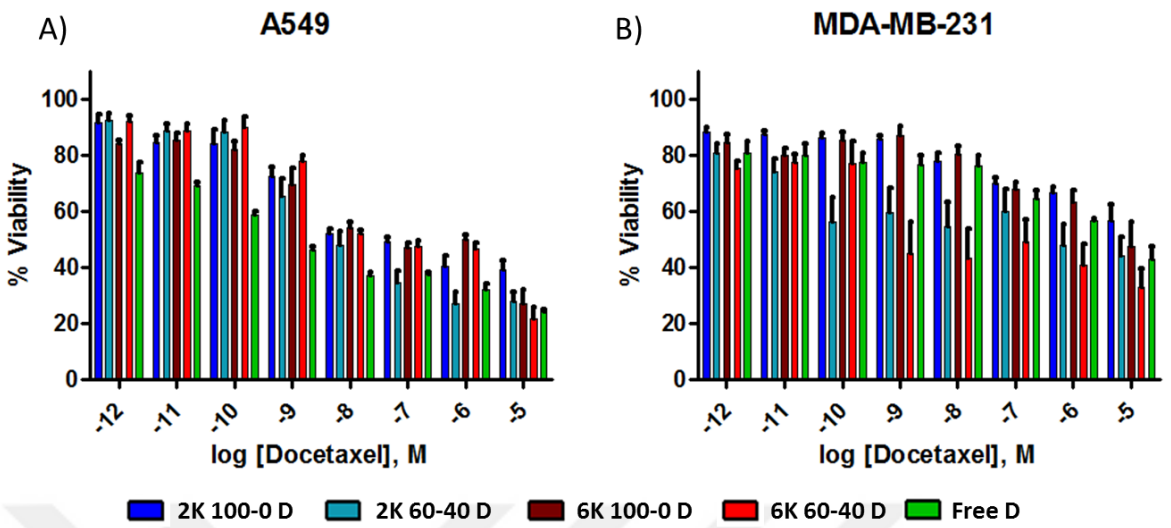

Figure 3.14. Cell Viabilities of Docetaxel loaded 2K and 6K micelles on A549 (A), and MDA-MB-231 (B) cell lines after 48 hours of continuous incubation.

Compared to free drug values, EC_{50} values showed an increase for all micelle types with A549 cell lines (Table 3.2). This type of increase can be expected owing to the gradual release dynamics of drug molecules from micelles. On the other hand, MDA-MB-231 cell line showed almost no change in EC_{50} values for 100-0 feed ratio whereas a dramatic decrease occurred with 60-40 micelles, indicating a positive effect of RGD targeting on cellular toxicity.

Table 3.2. EC_{50} values of micellar or free docetaxel for A549 and MDA-MB-231 lines.

Constructs	**EC_{50} on A549, [M]**	**EC_{50} on MDA-MB-231, [M]**
2K 100-0 X	2.29×10^{-9}	2.63×10^{-8}
2K 60-40 X	2.05×10^{-9}	2.18×10^{-11}
6K 100-0 X	3.31×10^{-9}	1.27×10^{-7}
6K 60-40 X	3.83×10^{-9}	3.41×10^{-10}
Docetaxel	2.44×10^{-10}	9.89×10^{-8}

To emphasize the impact of RGD on cellular internalization, a pulse chase experiment was done with MDA-MB-231 cell line; in this case incubation time of drug and drug doped micelles were shortened to 2 hours followed by 22 hours incubation in fresh media. If secondary construct containing micelles had any positive effect on cell binding and hence internalization of encapsulated drugs, a notable change in cell viabilities of 60-40 micelle set was expected. Indeed, a prominent decrease in cell number with respect to free docetaxel was observed with 60-40 micelles with pulse chase treatment (Figure 3.15B). At 10^{-6} M, cell viability was 54.3% for 2K 60-40 and 57.8% for 6K 60-40 micelles. The difference between 100-0 counterpart was 32.9% for 2K 60-40 and 28.1% for 6K 60-40 micelles. Free drug on the other hand showed almost no growth inhibition and 100-0 micelles achieved slight cytotoxicities even at highest concentration.

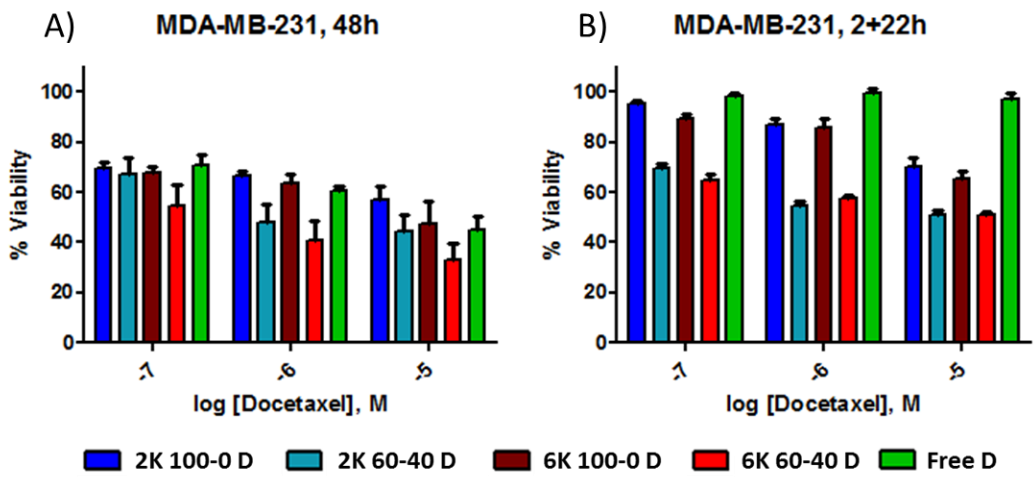

Figure 3.15. Cell viabilities of docetaxel loaded 2K and 6K micelles on MDA-MB-231 cell line after 48 hours of continuous incubation (A) and 2+22 (B) hours of pulse chase incubation.

3.4. Conclusion

Two types of micellar systems were generated using polymer-dendron conjugates: an AB type diblock construct using a 2K PEG and an ABA type triblock construct using a 6K PEG as the middle block. Both primary constructs contained a fourth generation polyester dendron as the hydrophobic component. The micellar system was designed such that

varying amount of targeting ligands could be introduced on their surface. This was accomplished by introduction of a secondary dendron-polymer construct bearing a cyclic RGD targeting group. Micelles fabricated possessed very low CMC values (ca. 10^{-6}M), and they preserved their stability on further dilutions. Likewise, serum stability experiments indicated that they were stable in FBS and able to escape burst release which is a pronounced problem for most micelle system. Importantly, the drug loaded micelles exhibited pH related docetaxel release emphasizing the enhanced delivery of their cargo near acidic tumor environment or once internalized into targeted cells. Their hydrodynamic sizes were ranging around 200 nm which is suitable for benefiting from EPR effect except maybe for dense tumor types. However TEM images indicated their dry size was much smaller, around 25nm, suggesting that the bulk of micelle size is stemmed from their flexible PEG shell. Docetaxel cytotoxicities were especially improved with RGD containing 60-40 micelle sets. Pulse-chase experiments highlighted the importance of micellar drug delivery; particularly 60-40 micelles showed improved cytotoxicity where free drug itself failed to act at these conditions. Cell internalization studies by microscopy and flow cytometry showed NR incorporation to cells increased dramatically by micelle encapsulation. Additionally RGD containing 60-40 micelles displayed improved results in parallel to cytotoxicity data.

In general, the 2K micelles showed slightly better results and can be chosen as a preferred candidate for applications, due to their facile synthesis, when compared with the ABA type conjugates. It is also important to note that this modular micellar drug delivery construct can be used with different types of cancer by simply changing the targeting group on secondary construct and the encapsulated drug. This ‘mix and match’ palate for optimizing effective drug delivery to various types of cancers would make then attractive candidates in the field.

4. TRASTUZUMAB TARGETED MICELLAR DELIVERY OF DOCETAXEL USING DENDRON-POLYMER CONJUGATES

4.1. Introduction

Utilization of nano particles (NP) as nanotherapeutics is favored owing to introduction of multiple advantages in comparison to regular chemotherapy. Combining a drug to such a nanoconstruct increases the efficacy of the drug. Possibly this occurs without changing the molecular structure and the final cellular response to the drug [6]. During the distribution phase, these conjugated systems shield the drug from plasma proteins thereby increasing its stability, and its solubility eliminating the need for solubilizing excipients which cause various side effects [7, 8]. Due to increased final size blood circulation half-lives, tumor accumulation and renal clearance rates of particles hence the carried drug cargo can be improved. As a result drug therapeutic indices of numerous drugs which are already in market can be enhanced notably by decreasing their final toxicities or increasing their overall efficacies [9]. Furthermore, adding specific targeting groups to these nano systems enables targeted delivery of cargo which can be drugs, imaging agents etc. to distinct cells or even organelles as needed [10].

Among the drug delivery systems micelles are one of the most promising systems due to their ease of preparation and ease of modification with various effective moieties such as drugs, targeting groups and labeling agents [174–177]. These attractive delivery agents serve as reservoirs for hydrophobic therapeutics such as chemotherapy drugs and they are modified to release those slowly providing improved PK profiles. Micelles can be easily prepared simply from AB type diblock amphiphilic copolymers when introduced into aqueous media they can self-assemble into NPs [178]. By controlling polymer composition and arrangement their size, shape, drug loading, release dynamics and targeting manner can be fine-tuned as required. Micelles prepared from dendritic domains have improved features as low PDI and low critical micelle concentration (CMC) values than linear polymeric micelles since their covalently bound stable internal cavities can

limit dissociation significantly [226]. Aliphatic polyester dendritic systems based on 2,2-bis(hydroxymethyl)propionic acid show great potential not only due to their biocompatible structure but also due to their provided biodegradable backbone enabling pH sensitive drug delivery [246].

Target specificity is a limitation for NPs benefiting from passive targeting. An alternative approach addressing this specificity issue is active targeting or ligand-mediated targeting employing particular surface modifications of designed NPs with high affinity ligand moieties to targeted tumor cells. In order to benefit from active targeting, ligands are chosen so that they can recognize and bind specifically to overexpressed receptors or biomolecules on tumor tissue element, cells or intercellular compartments [4, 134]. Ligands against electively expressed or produced proteins, sugars or lipids molecules presented on targeted tissues and cells can be determined including antibodies, proteins, small peptides, nucleic acids, sugars molecules and other small biomolecules as vitamins [136]. Multivalency arisen due to the increased surface area and incorporated modification of NPs systems augments the interaction between ligands and its target further, thereby increasing probability of recognition and internalization [137].

The first targeted nanotherapeutics were generated employing antibodies due to their fine-tuned specificity and availability [16]. Trastuzumab, a humanized monoclonal antibody marketed as Herceptin can be incorporated to DDS since its targeting receptor human epidermal growth factor receptor type 2 (HER2 also denoted as HER2/neu or ErbB-2) is found to be upregulated in 20 to 30% of invasive breast carcinomas. Typically, HER2 overexpression or presence of multiple copies of encoding gene is correlated with decreased OS and diminished chemosensitivity to anti-cancer drugs as well as therapeutic hormones [258]. Trastuzumab can inhibit growth of HER2-dependent tumors by interacting with extracellular juxtamembrane domains of HER2 receptors thereby blocking down-stream signal transduction pathways which can trigger survival, proliferation and invasiveness of cancer cells. Another route for trastuzumab activity is increasing endocytotic destructions of HER2 receptors however the main mechanism for trastuzumab dependent toxicity may stem from immune activation. It has been suggested that Fc domains of trastuzumab IgG can recruit immune effector cells as macrophages to HER2 overexpressing tumor cells and initiate cell lysis via phagocytosis which was supported by

impaired trastuzumab activity observed in studies utilizing animals lacking Fc recognizing receptors on their effector cells [260]. Furthermore anti-angiogenic behavior of trastuzumab in an animal model of HER2 overexpressing breast cancer was reported where trastuzumab administrations led to normalization and regression of tumor vasculature [261]. As a result incorporation of targeting antibodies as trastuzumab to DDS is a promising approach for blocking HER2 signaling pathways and inhibiting the tumor growth in HER2 overexpressing breast cancer.

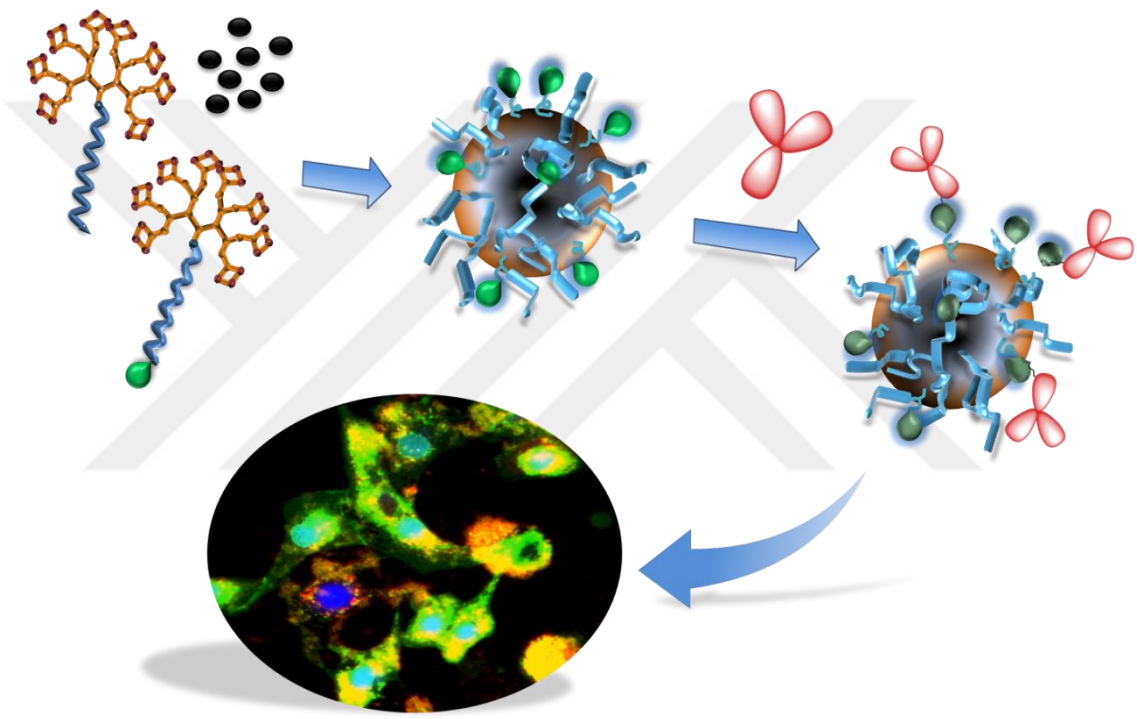

Figure 4.1. Trastuzumab targeted delivery of docetaxel via micelles formed from two constructs.

In this study a dendritic micellar platform for docetaxel delivery was created utilizing two different block copolymers (Figure 4.1). As primary constructs, providing the bulk of the micelle, a dendritic block copolymers composed of generation 4 polyester dendrons, G4OX conjugated to monofunctional 2 kDa PEG linear hydrophilic block was chosen. As secondary construct, G4OX dendron was clicked to biheterofunctional 3.5 kDa PEG units with N-hydroxysuccinimide (NHS) activated carboxylic acid which will enable surface modification of formed dendron-polymer micelles (DP) with trastuzumab antibodies through their free amine groups. Core forming G4OX dendrons was used for achieving low CMC values, and pH dependent controlled release of loaded docetaxel triggered around

acidic tumor environment or upon cellular uptake. Linear PEG blocks of constructs provide water solubility, protection from plasma proteins and surface functionalization. The resulting dendritic DDS is biodegradable, nontoxic and stimuli responsive that offers targeted delivery of docetaxel to HER2 overexpressing cancer cells.

4.2. Experimental Section

4.2.1. Materials

Bis-MPA, Dowex X50WX2, propargyl alcohol, 4-pentynoic acid were purchased from Alfa Aesar. All PEGs were obtained from Fluka. Azide PEG succinimidyl carboxymethyl ester (N3-PEG3.5kDa-NHS) was purchased from JenKem Technology (USA). Trastuzumab was purified from purchased Herceptin flacon from Roche. Pierce™ BCA protein assay kit and pHrodo™ Red, succinimidyl ester were purchased from Thermo Fisher Scientific. All solvents were purchased from Merck and used as obtained without further purification unless otherwise noted. Azido functionalized 2 kDa methoxyl PEG (m-PEG-OH) and generation 4 bis-MPA polyester dendron (G4OX) were synthesized and characterized according to previously described methods [289, 315].

4.2.2. Instrumentation

The monomer and copolymer characterizations involved ^{1}H NMR spectroscopy (Avanche III HD, Bruker, USA) and ATR-FT-IR spectroscopy (Nicolet 380, Thermo Scientific, USA). Synthesized dendrons, polymers and conjugates were further analyzed on MALDI-TOF spectrometer (Axima Performance, Shimadzu Biotech, Japan). 3,3'-Dioctadecyloxacarbocyanine perchlorate (DiO) intensities for dye loading calculations were measured with a Varian Cary Eclipse Fluorescence spectrometer (Varian, Agilent, USA). Wet size and zeta potential of the micelles was monitored with dynamic light scattering (DLS, Zetasizer ZS, Malvern, USA). Docetaxel was quantified by Liquid chromatography–mass spectrometry (LC-MS) analysis using a LCMS-2020-Mass Spectrometer System (Shimadzu, Japan) equipped with an C-18 5 μm 150 × 4.6 mm

column. Mobile phase consisted of deionized water and HPLC grade acetonitrile (ACN) using the following gradient; LC: 0-3 min, 50% ACN; 3.01 min, 50% ACN; 8 min, 95% ACN; 8.01-11 min 50% ACN MS single ion mode (SIM) 807.9 m/z. Ultra-pure water was obtained via MilliQ Water Purification System (Merck Millipore, USA). UV/vis spectroscopy experiments for BCA assay and pHrodo Red were done on Nanodrop 2000 (Thermo Scientific, USA). Time dependent dye internalization experiments were done with an inverted fluorescent microscope (Zeiss Observer A1 equipped with AxioCam MRc5) and images were processed with AxioVision software. Both dye internalization and competitive binding was studied by flow cytometry (Guava EasyCyte, Merck Millipore, USA).

4.2.3. Synthesis and Characterization of G4OX(1)

Frechet type polyester generation 4 dendron with alkyne focal groups was synthesized as previously reported in literature[315]. Propargyl alcohol providing the alkyne core to the final dendron was reacted with anhydride of bis-MPA in presence of DMAP and pyridine to give G1 polyester dendron. Through successive deprotection of acetonide protecting groups and acylation with anhydride of generation 1 dendron G4 polyester dendron was synthesized G4OX was obtained as a colorless gel. ^{1}H NMR (CD3OD, δ, ppm) 4.72 (d, *J*=12 Hz, 2H), 4.27 (m, 28H), 4.14 (d, *J*= 17.28 Hz, 16H), 3.61 (d, *J*= 40 Hz, 16H), 2.57 (t, *J*= 3.4, 1H), 1.40 (s, 24H), 1.34 (s, 24H), 1.31 (s, 3H), 1.27 (s, 12H), 1.26 (s, 6H), 1.14 (s, 24H).FT-IR (cm-1): 3260. MALDI-TOF Expected [MH^+] 2217, observed [MH^+] 2218.

4.2.4. Synthesis of Primary Constructs mPEG2K-G4OX (2)

Synthesis of AB type dendritic linear diblock copolymers with G4OX dendron was adopted from literature with minor modifications[185]. Following the synthesis of linear polymer blocks mPEG2K-N_3, synthesis of primary construct providing the main participant of micelle achieved via Huisgen type “click” reaction (Figure 4.2). Alkyne core of the G4 dendron (200mg, 0.0946mmol) was reacted to azide functional groups on mPEG2K-N_3

(126.08mg, 0.0630mmol) in the presence of Cu(I)Br (189.13mg, 0.0315mmol) and PMDETA (19.97µL, 0.0946mmol) in THF resulting in176.29mg mPEG2K-G4OX (2) with 68% yield. ^{1}H NMR of mPEG2K-G4OX (CD3OD, δ, ppm): 7.86 (s, 1H), 5.23 (s, 2H), 4.54 (t, *J*=10 Hz, 2H), 4.28-4.19 (m, 60 H), 3.80-3.40 (s, 172 H), 3.37 (s, 3H), 1.41 (s, 24H); 1.35 (s, 24H); 1.30 (s, 6H), 1.28 (s, 12H), 1.14 (s, 24H).

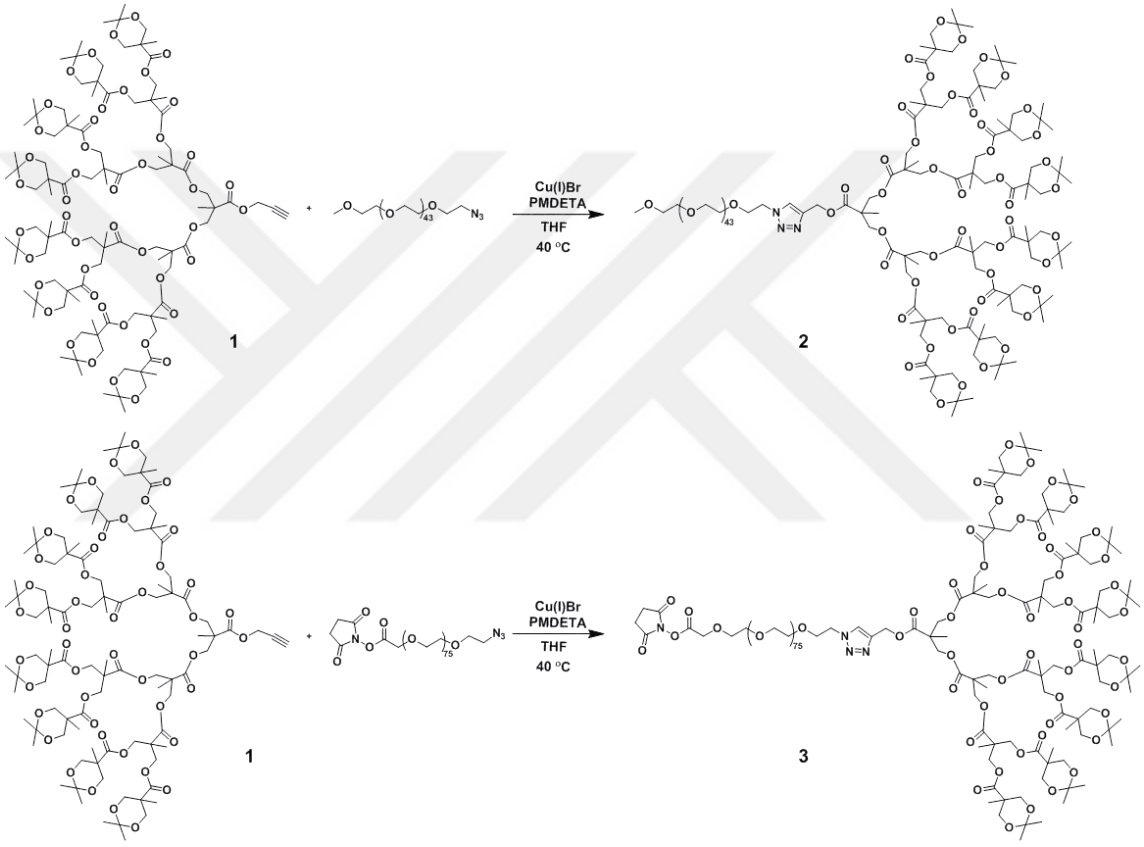

Figure 4.2. Synthesis of primary and secondary constructs.

4.2.5. Synthesis of NHS-PEG3.5K-G4OX (3)

Synthesis of AB type dendritic linear diblock copolymers with G4OX dendron was adopted from literature with modifications[185]. Alkyne core of the G4 dendron (200mg, 0.0946mmol) was reacted to azide functional groups on N_3-PEG2K-NHS (208.04mg, 0.0630mmol) in presence of Cu(I)Br (9.17mg, 0.0630mmol) and PMDETA (13.31µL, 0.0630mmol) in 3mL THF resulting in 232.13mg product with 68%. 1H NMR of NHS-

PEG3.5K-G4OX (CD3OD, δ, ppm): 7.86 (s, 1H), 5.23 (s, 2H), 4.54 (t, *J*=10 Hz, 2H), 4.28-4.19 (m, 60 H), 3.80-3.40 (s, 300 H), 2.84 (s, 4H), 1.41 (s, 24H); 1.35 (s, 24H); 1.30 (s, 6H), 1.28 (s, 12H), 1.14 (s, 24H).

4.2.6. Preparation of pHrodo Red conjugated Trastuzumab (4)

pHrodo Red dye was conjugated to trastuzumab as previously reported in literature [322]. Briefly, succinimidyl ester of pHrodo™ Red (0.395 nmol) and trastuzumab (0.044 nmol) was incubated in 0.1 M Na_2HPO_4 buffer at pH 8.5 for 30 min at room temperature (Figure 4.3). The reaction mixture was then dialyzed with 1 kDa molecular weight cut-off (MWCO) regenerated cellulose (RC) in water for 1 day. The average number of conjugated dyes per antibody was determined by sketching pHrodo Red calibration curve via UV/vis spectroscopy. Resulting trastuzumab- pHrodo Red conjugate (mabR) contained 2-3 dyes per molecule.

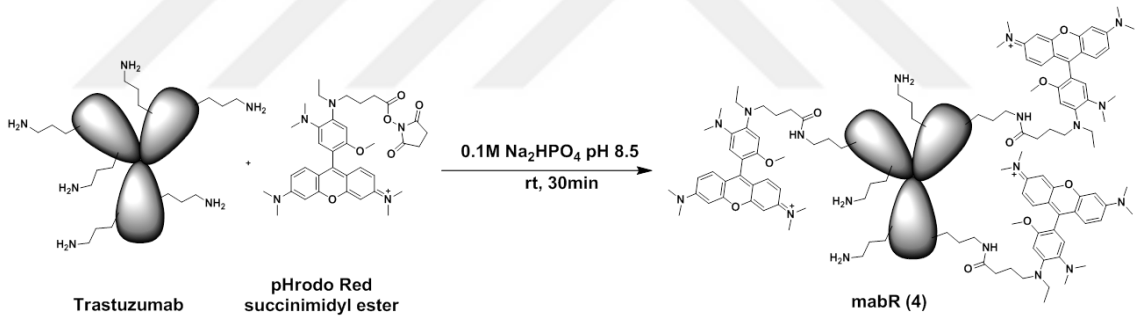

Figure 4.3. Synthesis of pHrodo Red dye conjugated trastuzumab

4.2.7. Preparation of non-targeted (DP) and trastuzumab targeted micelles (DPT)

For preparation of DP micelles with and without drug, solvent evaporation method was employed. Briefly copolymer stock solutions (10 mg/mL) in methanol were prepared. By combining required volumes from primary and secondary polymer stock solutions exact amounts of dissolved polymers with 3:2 weight ratios were distributed into glass vials. After addition of water, methanol in vials was evaporated. For trastuzumab targeted micelles (DPT), micelle solutions were incubated with mabR (1:100, or 1:50 mabR to

polymeric NHS mole ratios) in 0.1M Na_2HPO_4 at pH 8.5 for 1h, micelles were then dialyzed over 8 hours in water while changing water per 2h. To remove unbound mabR, micelles were centrifuged for 2x 10 min at 17000 g and supernatants were removed after each step. For non-targeted micelles (DP) micelles were incubated in parallel with 1-aminopropanol instead of trastuzumab under same conditions (Figure 4.4).

4.2.8. Loading of Docetaxel into Micelles

For drug loading, docetaxel stock solutions in methanol were prepared (10 mg/mL). Exact volumes of drug stock solution were added onto polymer solution and they were vortexed briefly. Methanol in vials was evaporated subsequently. To remove excess drug molecules, prepared micelles were dialyzed with 1 kDa MWCO RC membranes over 2 days in water at sink conditions. Removal of free drug and drug precipitates were tracked by LC-MS and DLS respectively. Surface modifications with mabR or 1-aminopropanol were done afterwards.

4.2.9. Determination of Docetaxel Content

Docetaxel loaded micelles DP and DPT were lyophilized to determine their dry weight. Subsequently, they were dissolved in ACN and their docetaxel content was quantified via LC-MS.

4.2.10. Determination of mabR Content on DPT micelles

Trastuzumab content on DPT micelles were quantified via BCA protein assay by following manufacturer's instructions. Enhanced protocol was employed where supplied albumin standard were used as calibration curve samples. DP micelles and polymers with same amount were used as negative controls whereas mabR with known concentration were used as positive control. Final weight percent (wt%) was determined to be 9.7% for DPT micelles prepared by 1:100 mabR to polymeric NHS ratios. To demonstrate

conjugation of mabR with succinimidyl esters on micelles, trastuzumab was conjugated to NHS-PEG3.5K-G4OX and molecular weights of resulting conjugates were determined by MALDI-TOF.

4.2.11. Determination of Micelle Size and Zeta Potential by DLS

Docetaxel loaded micelles DP and DPT were prepared at 0.01mg/mL polymer concentration. Their effective size diameters were determined at 37°C in water. Additionally their zeta potentials were also measured at 37°C in water and in 1X phosphate buffered saline (PBS) at pH 7.4.

4.2.12. pH Dependent Docetaxel Release from Micelles

Docetaxel loaded micelles DP and DPT were prepared at 5 mg/mL polymer concentration containing 9.7 % and 9.9 % docetaxel by weight. Stock micelle solutions were diluted with acetate buffer at pH 4.8 and PBS buffer at pH 7.4 separately with 2.5 mg/mL final polymer concentrations. Resulting micelle solutions were transferred into dialysis bags with MW cut-off 1kDa. Dialysis bags were immersed in 1L of corresponding buffer solutions and incubated at 37 °C for 10 days. At predetermined time points 1mL samples were collected and released docetaxel was quantified by LC-MS analysis.

4.2.13. Cell Lines.

MCF-7 and SK-OV-3 cell lines purchased from ATCC (LGC Standards, Germany) and grown according to manufacturer's culture methods requirements. Cells were incubated at 37 °C in a humidified atmosphere of 5% CO_2 and kept in logarithmic phase of growth throughout all experiments.

4.2.14. *In vitro* Cell Viability Assay

Cell number and cell viability were determined by Cell Counting Kit-8 (CCK-8, Fluka). Cells were seeded in 100 μL of culture medium at a density of 5000 cells/well for MCF-7 and SK-OV-3 into 96-well plates in quadruplicates for each drug concentration. After overnight incubation cell media was replaced with fresh medium containing various concentrations of conjugates, free drug, or polymer only controls. For free drug treatments docetaxel stock solution was prepared in 20% DMSO in growth medium (V/V) and subsequently diluted where the final DMSO concentration was below 0.5% (V/V). All cells were incubated continuously for 48h in the presence of the micellar conjugates. Cytotoxicities of trastuzumab only, DP and DPT micelles without encapsulated drugs were also determined in parallel with same concentrations in parent experiments conducted with trastuzumab conjugated and drug doped micelles. For 2h+22h pulse chase drug treatment, cells were incubated 2h in drug containing solutions and incubated in fresh media for 22h before CCK-8 assay. To determine the cell viability, 100 μL of culture medium together with 10 μL of CCK-8 solution was added into each well. After 4h incubation the absorbance values at 450nm was measured with a plate reader (Multiscan FC, Thermo Scientific, USA). Viability of treated cells was expressed as percentage of control cells (cell media only). EC50 values were obtained from concentration response curves by nonlinear regression analysis through Graphpad Prism software.

4.2.15. Micelle Internalization via Fluorescence Microscopy

DP and DPT micelles were prepared at 5 mg/mL polymer concentration encapsulating 1 wt % DiO dye. MCF-7 and SK-OV-3 cells seeded onto 24 well plates and DiO doped DP and DPT micelle solutions were added into wells with 0.1 mg/mL final polymer concentrations. Cells were then incubated for 2, 4 and 24 hours at 37°C. Trastuzumab was added in excess to another set of micelle containing wells to investigate their hindering effect on internalization of targeted micelles. After incubation cell nuclei were stained with DAPI and cells were fixed using 4% formaldehyde. Fluorescence images were collected via inverted fluorescent microscope (Zeiss Observer A1 equipped with AxioCam MRc5) and processed with AxioVision software.

4.2.16. Trastuzumab Dependent Cell Binding Assay

DP and DPT micelles were prepared at 5 mg/mL polymer concentration encapsulating 1 wt % DiO dye. MCF-7 and SK-OV-3 cells seeded onto 24 well plates and DiO doped DP and DPT micelle solutions were added into wells with 0.1 mg/mL final polymer concentrations. Cells were then incubated for 2 and 4 h at 37°C. Trastuzumab was added in excess to another set of micelle containing wells to investigate their hindering effect on internalization of targeted micelles. After each treatment cells were trypsinized. DiO intensities were determined by flow cytometry (Guava easyCyte) and results were processed on guavaSoft software.

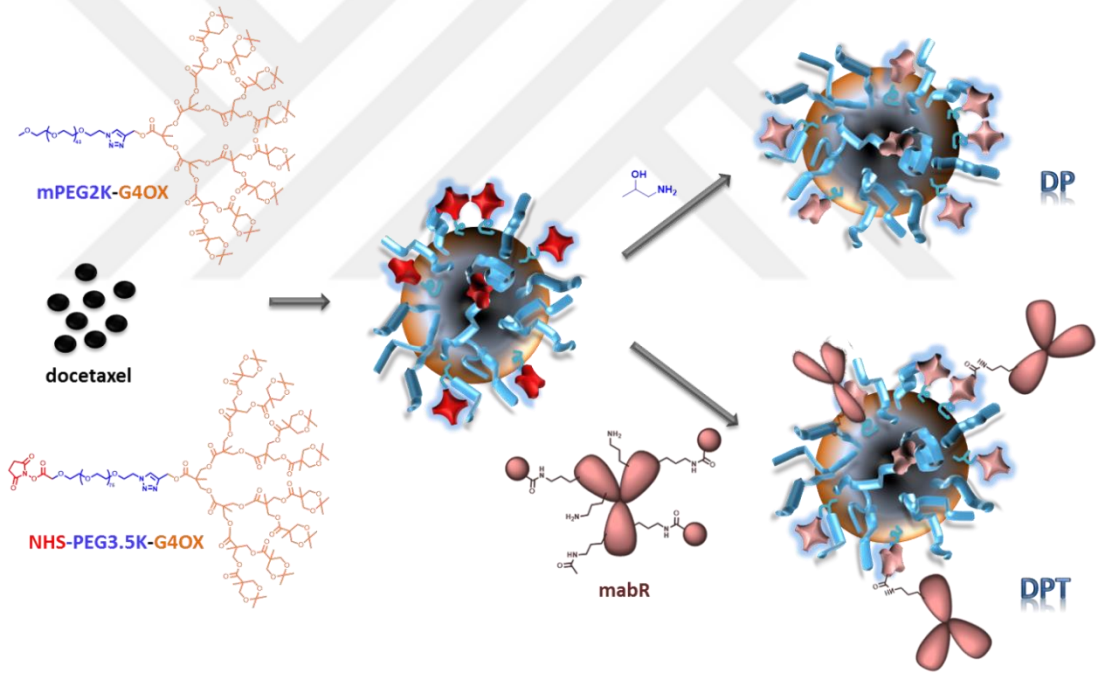

Figure 4. 4. Preparation of DP and DPT micelles.

4.3. Results and Discussion

4.3.1. Synthesis and Characterization of Dendron-Polymer Conjugates

Two different dendron-polymer conjugates were synthesized; mPEG2K-G4OX forming the bulk of micelle and NHS-PEG3.5K-G4OX for decorating micelle shell

periphery with trastuzumab. G4OX polyester dendrons with alkyne groups at focal points clicked with azide functionalized linear PEG polymers, 2 kDa, and 3.5k Da. Trastuzumab was conjugated successfully to micelle surface with 9.7 wt % when added with 1:100 mab to polymeric NHS ratio (Figure 4.4). To demonstrate the effectivity of conjugation between succinimidyl ester on secondary construct and trastuzumab was investigated by MALDI analysis (Figure A.14). The shift observed in m/z values of trastuzumab in comparison to trastuzumab polymer conjugate indicates to effective conjugation of antibody to secondary construct. However presence of multiple peaks suggest that conjugation might occur multiple times resulting in unwanted crosslink formation between micelles.

4.3.2. Generation and Characterization of DP and DPT Micelles

Docetaxel encapsulated trastuzumab targeted DPT and non-targeted DP micelles were prepared using 3:2 wt% ratios of primary and secondary constructs. Drug content of DP and DPT micelles were found to be 9.7 % and 9.9 % by weight respectively.

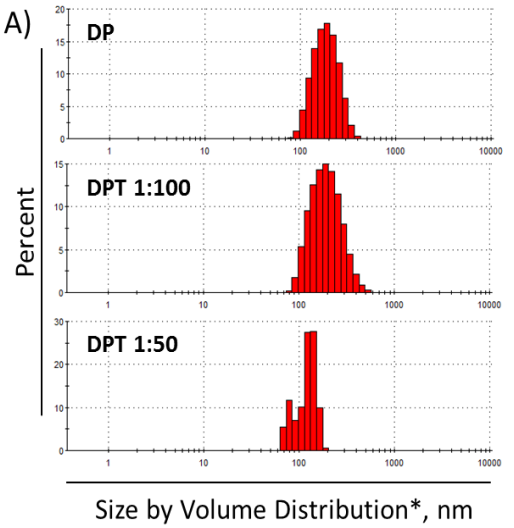

B)

	Z-Ave	Size*	PDI
DP	176.9 ±1.9	190.6 ±57.41	0.057
DPT 1:100	185.2 ±4.7	202.1 ±75.38	0.135
DPT 1:50	1815 ±710	129.7 ±72.6	0.905

Figure 4.5. Effective size diameters of DP and DPT micelles A) as histograms, B) in tabular form.

Hydrodynamic volumes of drug loaded DP and DPT micelles were measured via DLS analysis (Figure 4.5). DP micelles without conjugated mabR displays narrow PDI

values and Z-average size around 177 nm. Conjugation of mabR with 1:100 mab to polymeric NHS ratio, resulted in minor increase in both size and PDI values of targeted DPT micelles. However upon doubling the amount of mabR during conjugation prepared DPT micelles started to precipitate which is reflected by high Z-average values and very poor PDI values close to 0.9. Hence 1:100 conjugation ratio was chosen for the rest of the study.

Surface charge is very important for final effectivity of DDS since it can affect various biological properties such as opsonization, tissue extravasation and cell internalization. Typically, negative zeta potential values with ≤ 10 mV surface charges leads to clearance of NPs by RES members and positive values around > 10 mV show strong aggregation with opsonins, whereas optimum results in terms of minimum RES interaction and improved circulation times are observed with neutral NPs with zeta potentials in the limit of ± 10 mV [65].

Table 4. 1. Zeta potential of DP and DPT micelles.

Micelle	**Media**	**ZP**
DP	H_2O	-25.3 ±1.25
DPT 1:100	H_2O	-14.2 ±1.97
DPT 1:50	H_2O	-9.13 ±2.53
DP	PBS	-5.3 ±1.79
DPT 1:100	PBS	-2.6 ±1.17
DPT 1:50	PBS	-5.8 ±1.29

In this aspect zeta potential of micelles were determined in water and in 1X PBS (Table 4.1). In water all micelles demonstrated negative zeta potentials in the ≤ 10 mV range however in PBS zeta potential values closer to neutral as -5.3 mV for DP and -2.6 mV for DPT. Addition of trastuzumab resulted in a slight shift of zeta potential towards neutral which is favored as well.

4.3.3. pH Dependent Docetaxel Release from Micelles

One of the most widely benefited endogenous stimuli is pH variations in tissues and in intracellular compartments as endosomes or lysosomes. Furthermore pathological conditions as cancer or inflammation can also generate pH gradients. Benefiting from pH differences between healthy tissue which is maintained generally at 7.4, the pH of tumor environment is typically lower than 7.0 due to high metabolic needs and increased glycolysis rates, NPs systems are generated to release their cargo at solid tumor [160]. Similarly upon internalization of NPs they are encapsulated by acidic endosomes (pH ~5–6) and after fusion with lysosomes (pH ~4–5) pH of media drops further which can be used for drug release as well [161].

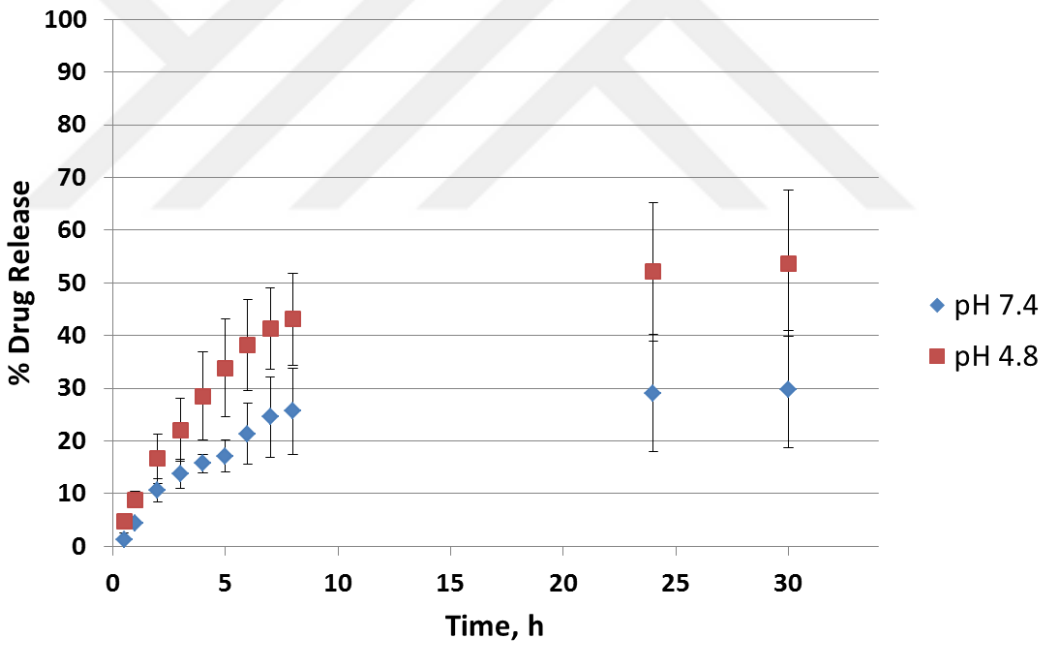

Figure 4.6. pH dependent docetaxel release.

Employing polyester based dendron core is crucial since drug release can be triggered in acidic environments due to hydrolysis of acetals at the dendron periphery as well as ester groups at dendritic branches. To determine docetaxel release from DPT micelle they were incubated in buffer solution at pH 7.4 and pH 4.8 and release drug was monitored via LC-MS analysis. As expected release profile of encapsulated drug was higher in acidic media owing to biodegradable character of G4OX polyester dendron

(Figure 4.6). Over the course of 30 h DPT micelles released 29.8±11.1 % of its cargo at pH 7.4 whereas drug release reached to 53.7±13.9 % at pH 4.8. Overall this system displayed pH dependent controlled release profile for docetaxel highlighting its potential as a DDS further.

4.3.4. *In vitro* Cell Viability Assay with Docetaxel loaded Micelles

Cytotoxicity profiles of micellar formulation of docetaxel were investigated on HER 2 overexpressing SK-OV-3 ovarian cancer cell line and moderately HER2 expressing MCF-7 breast cancer cell lines [323]–[326]. DP and DPT micelles as well as free docetaxel was incubated with SK-OV-3 and MCF-7 cells for 48 h continuously or in pulse-chase manner where after 2 h incubation cells were grown 22 h in fresh cell media. EC50 values were higher for non-targeted DP micelles for both cell lines as expected due to slow release mechanism of encapsulated drug (Table 4.2). However upon introduction of targeting trastuzumab group through DPT micelles EC50 values approached to those of free drug for cell lines.

Table 4.2. EC50 values after 48 h incubations.

Constructs	**EC50 on MCF-7, [M]**	**EC50 on SK-OV-3, [M]**
DP	$2.76x10^{-5}$	$5.22x10^{-5}$
DPT	$2.91x10^{-9}$	$1.78x10^{-9}$
Docetaxel	$1.83x10^{-11}$	$7.80x10^{-9}$

For MCF-7 cells treated continuously, cell viabilities decreased as low as 46 % for free drug at high drug concentrations (10^{-5}M), whereas DP micelles displayed 68% viability. DPT micelles on the other hand resulted in a slight increase in cell viability to 44 % in contrast to free drug; however at lower concentrations free drug cytotoxicities were slightly higher (Figure 4.7). For SK-OV-3 cell line cytotoxic effect of docetaxel was greater at 10^{-5}M, where cell viabilities dropped to 37 %, similarly DPT micelles resulted in

reduced viability (28 %) at this concentration however at higher concentrations free drug displayed minor increase in cell viability. A pulse-chase treatment set-up was explored to highlight the effectiveness of targeting trastuzumab antibody. Cells were incubated in presence of docetaxel loaded micelle or free docetaxel for 2 h enabling them to interact with cells. Subsequently cell media was removed and after an additional 22 h incubation to allow cellular response to uptaken materials cell viabilities were determined. Shortening of initial incubation should result in decreased uptake of free drug however since micellar docetaxel can be internalized through more complex routes as pinocytosis or receptor mediated endocytosis higher amounts of drug can be incorporated in to the cells in shorter intervals.

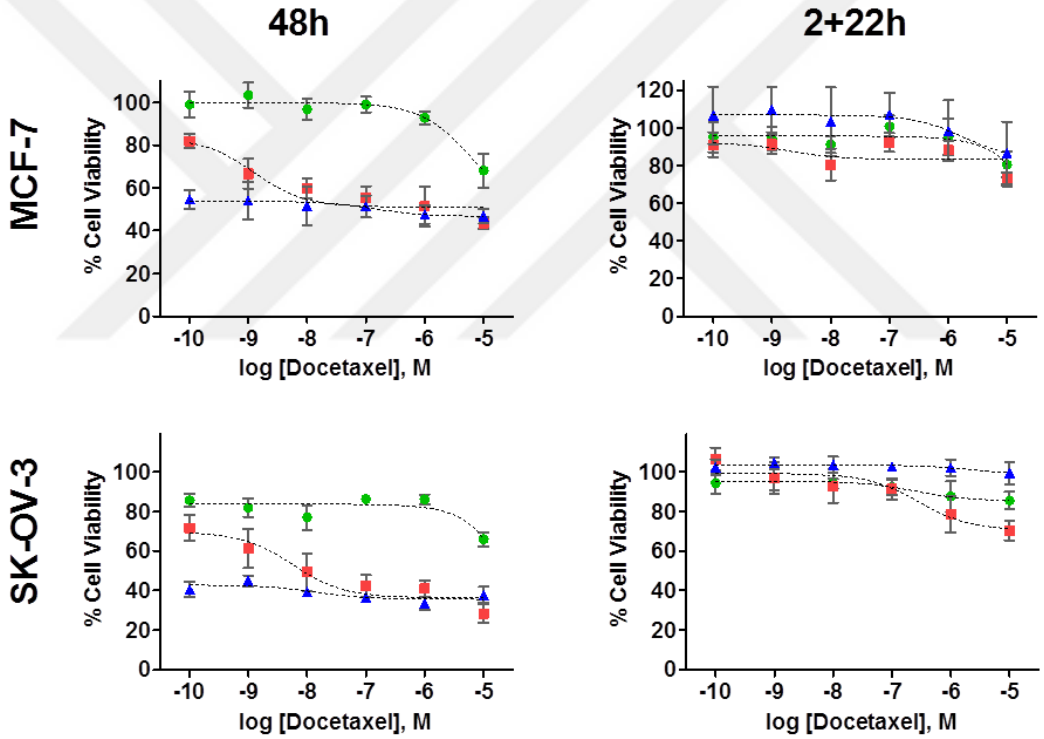

Figure 4. 7. Resulting cell viabilities after 48 h and 2+22 h incubation with micellar and free formulations of docetaxel.

In general, both MCF-7 and SK-OV-3 cell lines displayed increased cell viabilities overall however it is expected due to shortened incubation periods. Free docetaxel was unable to cause prominent cytotoxicity on MCF-7 cells which was 87 % at 10^{-5} M drug concentration. Yet docetaxel encapsulated in DP micelles exhibited increased toxicity at all concentrations, for instance at 10^{-5} M cell viability declined to 81 %. DPT micelles showed

further decrease and at 10^{-5} M calculated viability was 73 %. Similar results were obtained for SK-OV-3 cell line. Free docetaxel failed to demonstrate significant cell toxicity where at 10^{-5} M cell viability was around 99 %, however DPT micelles were able to decrease this value up to 70 % whereas DP micelles resulted in viability of 85 %. The change between DP and DPT micelles were more notable at higher concentrations. These results indicate that delivery of docetaxel in compact micelle cores enabled faster internalization of drug and trastuzumab conjugation on micelles increased drug toxicities slightly more.

4.3.5. *In vitro* Cell Viability Assay with Empty Micelles

To investigate effect of DP and DPT micelles as well as trastuzumab acting as targeting group on cell viability, MCF-7 and SK-OV-3 cells were treated with constructs at same amount of corresponding to particular drug concentrations. After 48 h incubation with constructs without drugs both cell lines displayed minimal decrease in cell viabilities (Figure 4.8).

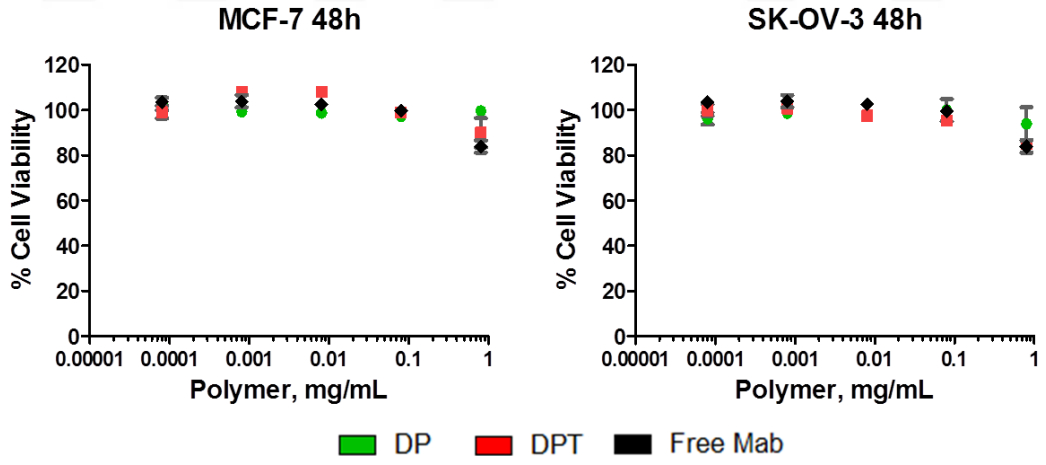

Figure 4.8. Cytotoxicity of blank DP and DPT micelles as well as free trastuzumab *in vitro*.

Even at high concentrations corresponding to 10^{-4} M docetaxel DP treatment resulted in 99 % cell viability whereas this value dropped a bit with antibody and antibody containing DPT micelles to 84 % and 90 % respectively in MCF-7 cell line. Similarly in SK-OV-3 cell line at 10^{-4} M, incubation with DP micelles led to 94 % viability and for

trastuzumab containing samples it decreased to 84 % for DPT and 85 % for trastuzumab only. This suggests that micelles or antibody only exhibits minimal effect on MCF-7 and SK-OV-3 cells *in vitro* and cytotoxicity is due to encapsulated docetaxel.

4.3.6. Internalization of DiO loaded DP and DPT micelles

To determine cellular internalization of hydrophobic DiO dye which is generally used in combination with organic solvents to stain cellular membranes, DiO encapsulated DP and DPT micelles were prepared and added on to MCF-7 and SK-OV-3 cells. Trastuzumab on DPT micelles was pre-labeled with pHrodo Red, which is a dye demonstrating increased red fluorescence at acidic pH so an increase in red fluorescence is expected upon incorporation into acidic endosomal compartments. Trastuzumab was added in excess onto another group of cells in combination with DPT to exhibit any inhibitory effect.

In general micellar encapsulation of DiO provided effective internalization of dye by both cell lines (Figure 4.9). Also a time dependent increase in fluorescence intensity was visible indicating continuous uptake of micelle encapsulated cargo. Similarly addition of a targeting group on to micelle surface increased DiO internalization notably, for both cell lines and micelle types DiO intensities increased gradually. Furthermore the number of dye incorporated cells increased over time as indicated by overlay images of DAPI stained nuclei and DiO dye as well as pHrodo Red that contributed by mabR on micelle periphery. Comparable to DiO incorporation pHrodo Red signal from micellar mabR increased by time however the difference between 4 h and 24 h was less obvious for pHrodo Red. Furthermore at 4 h especially more notable with SK-OV-3 cells, pHrodo Red signal localized more toward cell periphery however at 24 h it was more wide spread, which might be due to maximized internalization and merging with more acidic compartments as lysosomes. Addition of excess trastuzumab together with DPT micelles resulted in suppression of DiO fluorescence for both cell lines however more apparent with SK-OV-3 cell line most possibly by impaired receptor dependent uptake of DPT micelles. Internalization of DP and DPT micelles exhibited comparable trends for MCF-7 and SK-OV-3 cell lines with minor differences such as increased DiO intensity for DPT micelles at

24 h and decreased signal upon addition of excess trastuzumab for SK-OV-3 cells. This can be due to differential HER2 expression levels between tested cell lines. Since SK-OV-3 cells overexpressed HER2 receptors uptake of trastuzumab targeted DPT micelles occurred more commendably.

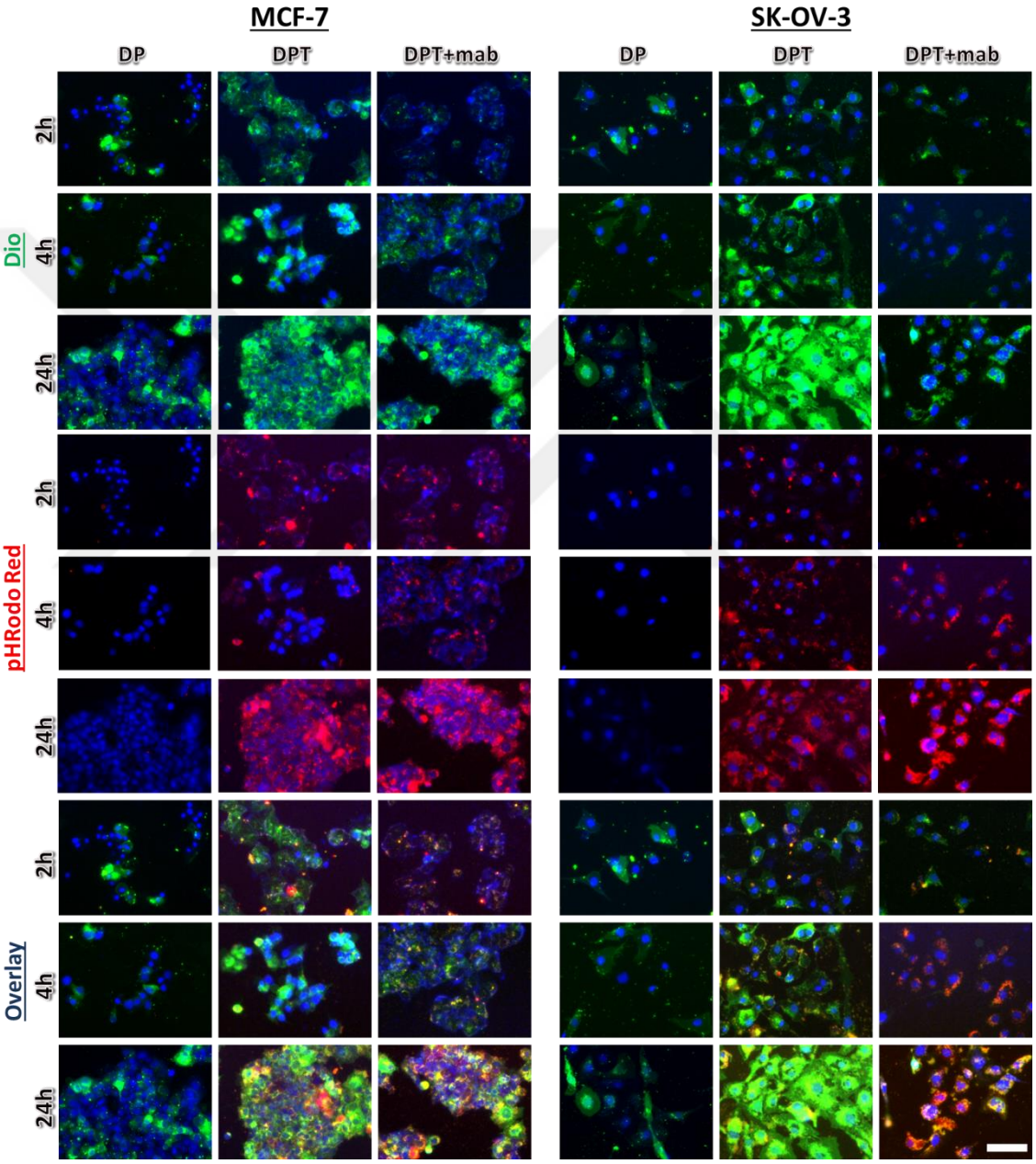

Figure 4.9. Internalization of DiO doped DP and DPT micelles by MCF-7 and SK-OV-3 cell lines. Scale bar 25 µm.

Flow cytometry experiments were done to efficiently quantify incorporation of DiO to MCF-7 and SK-OV-3 cell lines (Figure 4.10). DP micelles achieved green fluorescence levels around 80 for SK-OV-3 cells and 35 for MCF-7 cells after 4 h. However these values increased notably once treated with DPT micelles for both cell lines. With SK-OV-3 cells DiO florescence intensity was measured as 3526 at 2 h increasing slightly at 4 h. The change in DiO intensity at 2 h and 4 h were more notable for DPT treated MCF-7 cells where dye signal increased from 2281 to 4257. Besides, addition of excess trastuzumab resulted in reduced DiO intensity for both cell lines. For instance it decreased from 3526 to 1667 with SK-OV-3 cell lines and from 2281 to 1544 with MCF-7 cells at 2 h incubation. The shift in cell population is more evident from histograms (Figure 4.10 B)), especially for SK-OV-3 cells.

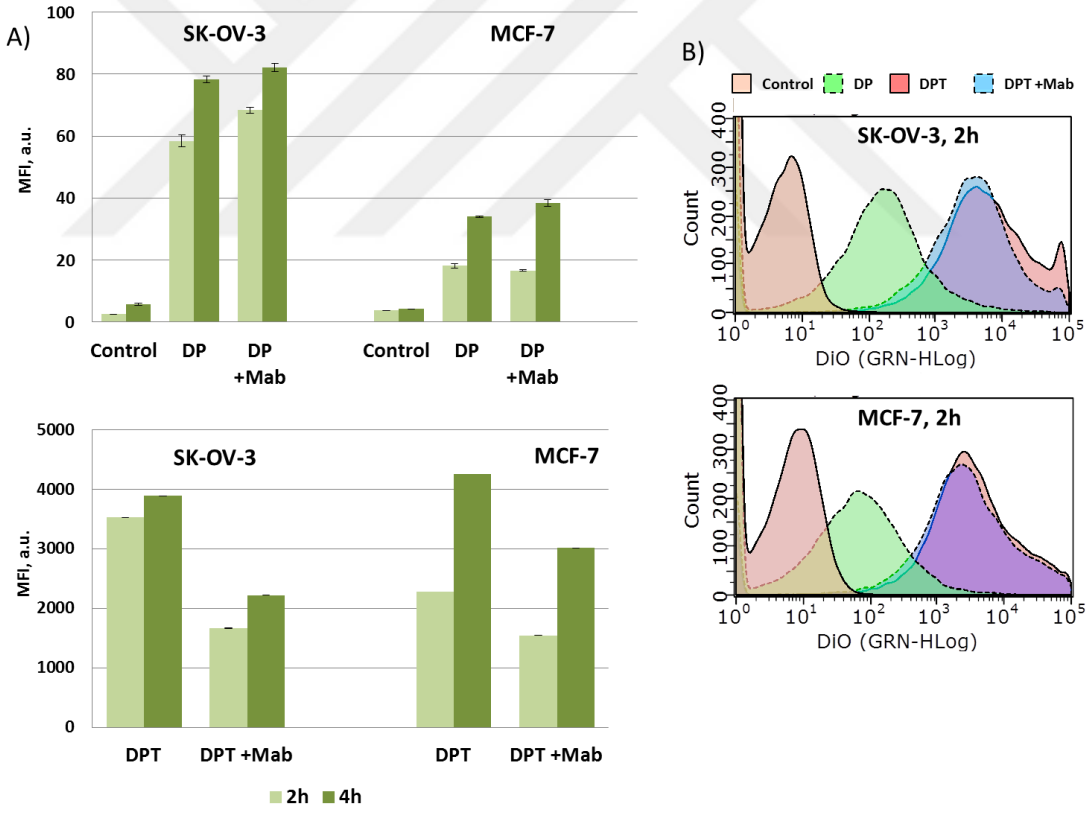

Figure 4.10. Flow cytometry data of MCF-7 and SK-OV-3 cell lines treated with DiO encapsulated DP and DPT micelles A) in graphical representation and B) in histograms.

4.4. Conclusion

A micellar delivery platform employing biodegradable G4OX polyester dendrons at the core and linear PEG polymers at the shell was generated. Owing to utilizing a secondary construct with biheterofunctional PEG block trastuzumab antibodies could be introduced as targeting groups to the micelle periphery. Docetaxel was loaded to micelles and pH dependent drug release was demonstrated. Targeted DPT micelles were shown to display similar cytotoxicity level as free drug *in vitro* while constructs themselves showed minimal toxicity. Internalization experiments via fluorescence microscopy and flow cytometry indicated increased uptake for DPT micelles which can be impaired by addition of excess trastuzumab, suggesting receptor mediated uptake. Hence this trastuzumab targeted docetaxel loaded micelle system is a great candidate as a nano drug delivery platform since it can benefit from many features of nano particles as improved biodistribution and pharmacokinetics, it is stimuli responsive, biodegradable and it can provide specific cell targeting after tumor accumulation due to employment of a therapeutic antibody as targeting group.

5. CONCLUSIONS

Dendron-polymer conjugates with well defined structures were synthesized and conjugated with an anti-angiogenic drug CA-4. The CMC values were in the sub nanomolar range for drug conjugated DPD micelles and it was observed that the stability of micelles could be increased by decreasing the HLB through an increase in dendron generation and drug content. The DLS measurements showed that the hydrodynamic sizes of the formulated micelles were below the critical 100nm, suggesting that this system may benefit from EPR effect, as well as escape renal clearance. The drug release was pH dependent and was favored by acidic pH which is suitable for release after reaching acidic tumor site or cellular internalization. The constructs without drug conjugation showed minimal cytotoxicity on HUVECs, whereas drug conjugated micelles showed significant decrease in cell viability. Cell internalization study of dye doped micellar constructs indicated their facile uptake in spite of the PEG based corona. Also, endothelial cell tube formation assay confirmed the activity of the CA4 conjugated constructs against angiogenesis. The delivery vehicle described here can be also loaded with other anti-cancer drugs that inhibit the tumor with other modes of action, thus offering possibility of combination therapy. Overall, the dendron-polymer conjugate based stable and tunable drug delivery system outlined here provides an attractive and tunable platform for combating cancer via efficient inhibition of angiogenesis. However eventhough this sytem has the potential as a sustained release nanotherapeutic it lacks targeting groups to improve cell internalization.

To create a modular micellar system with easily changeable targeting groups and encapsulated drug the second drug delivery platform was engineered. Two types of micellar systems were generated using polymer-dendron conjugates: an AB type diblock construct using a 2K PEG and an ABA type triblock construct using a 6K PEG as the middle block. Both primary constructs contained a fourth generation polyester dendron as the hydrophobic component. The micellar system was designed such that varying amount of targeting ligands could be introduced on their surface. This was accomplished by introduction of a secondary dendron-polymer construct bearing a cyclic RGD targeting

group. Micelles fabricated possessed very low CMC values (ca. 10^{-6}M), and they preserved their stability on further dilutions. Likewise, serum stability experiments indicated that they were stable in FBS and able to escape burst release which is a pronounced problem for most micelle system. Importantly, the drug loaded micelles exhibited pH related docetaxel release emphasizing the enhanced delivery of their cargo near acidic tumor environment or once internalized into targeted cells. Their hydrodynamic sizes were ranging around 200 nm which is suitable for benefiting from EPR effect except maybe for dense tumor types. However TEM images indicated their dry size was much smaller, around 25nm, suggesting that the bulk of micelle size is stemmed from their flexible PEG shell. Docetaxel cytotoxicities were especially improved with RGD containing 60-40 micelle sets. Pulse-chase experiments highlighted the importance of micellar drug delivery; particularly 60-40 micelles showed improved cytotoxicity where free drug itself failed to act at these conditions. Cell internalization studies by microscopy and flow cytometry showed NR incorporation to cells increased dramatically by micelle encapsulation. Additionally RGD containing 60-40 micelles displayed improved results in parallel to cytotoxicity data. In general, the 2K micelles showed slightly better results and can be chosen as a preferred candidate for applications, due to their facile synthesis, when compared with the ABA type conjugates. It is also important to note that this modular micellar drug delivery construct can be used with different types of cancer by simply changing the targeting group on secondary construct and the encapsulated drug. This ‘mix and match’ palate for optimizing effective drug delivery to various types of cancers would make then attractive candidates in the field.

To further emphazise the potential of previous micellar DDS, the targeting group was changed with a more complex monoclonal antibody for the final delivery platform. A micellar delivery platform employing biodegradable G4OX polyester dendrons at the core and linear PEG polymers at the shell was generated. Owing to utilizing a secondary construct with biheterofunctional PEG block trastuzumab antibodies could be introduced as targeting groups to the micelle periphery. Docetaxel was loaded to micelles and pH dependent drug release was demonstrated. Targeted DPT micelles were shown to display similar cytotoxicity level as free drug *in vitro* while constructs themselves showed minimal toxicity. Internalization experiments via fluorescence microscopy and flow cytometry indicated increased uptake for DPT micelles which can be impaired by addition of excess

trastuzumab, suggesting receptor mediated uptake. Hence this trastuzumab targeted docetaxel loaded micelle system is a great candidate as a nano drug delivery platform since it can benefit from many features of nano particles as improved biodistribution and pharmacokinetics, it is stimuli responsive, biodegradable and it can provide specific cell targeting after tumor accumulation due to employment of a therapeutic antibody as targeting group.

All three DDS generated in this thesis were biocompatible, biodegradable. Additionally the drug release profiles were pH dependent highlighting their potential as controlled delivery agents. It has been shown that the crucial physical micellar properties as size and CMC were adjustable with employment of polyester dendrons furthermore by changing the drug loading type from chemical to physical different types of drug release profiles were achieved. All of the studied micellar systems displayed improved dye uptake profiles even without incorporation of targeting groups as RGD and trastuzumab all in all highlighting their potential as suitable DDS and they are ready for *in vivo* stage.

REFERENCES

1. Parveen, S., R. Misra, and S. K. Sahoo, "Nanoparticles: a boon to drug delivery, therapeutics, diagnostics and imaging", *Nanomedicine Nanotechnology Biology Medicine*, Vol. 8, No. 2, pp. 147–166, 2012.
2. Sirova, M., T. Mrkvan, T. Etrych, P. Chytil, P. Rossmann, M. Ibrahimova, L. Kovar, K. Ulbrich, and B. Rihova, "Preclinical evaluation of linear HPMA-doxorubicin conjugates with pH-sensitive drug release: efficacy, safety, and immunomodulating activity in murine model.", *Pharmaceutical Research*, Vol. 27, No. 1, pp. 200–208, 2010.
3. Murray, J. C., L. M. Weiner, and C. W. Shuptrine, "Antibody-Based Immunotherapy of Cancer", *Cell*, Vol. 148. pp. 1081–1084, 2012.
4. Peer, D., J. M. Karp, S. Hong, O. C. Farokhzad, R. Margalit, and R. Langer, "Nanocarriers as an emerging platform for cancer therapy", *Nature Nanotechnology*, Vol. 2, No. 12, pp. 751–760, 2007.
5. Ferrari, M., "Cancer nanotechnology: opportunities and challenges", *Nature Reviews Cancer*, Vol. 5, No. 3, pp. 161–171, 2005.
6. Xiao, H., H. Song, Q. Yang, H. Cai, R. Qi, L. Yan, S. Liu, Y. Zheng, Y. Huang, T. Liu, and X. Jing, "A prodrug strategy to deliver cisplatin(IV) and paclitaxel in nanomicelles to improve efficacy and tolerance.", *Biomaterials*, Vol. 33, No. 27, pp. 6507–19, September 2012.
7. Duncan, R., "Development of HPMA copolymer-anticancer conjugates: clinical experience and lessons learnt.", *Advanced Drug Delivery Reviews*, Vol. 61, No. 13, pp. 1131–48, November 2009.
8. Kopecek, J. and P. Kopecková, "HPMA copolymers: origins, early developments, present, and future.", *Advanced Drug Delivery Reviews*, Vol. 62, No. 2, pp. 122–49, February 2010.
9. Yang, D., S. Van, Y. Shu, X. Liu, Y. Ge, X. Jiang, Y. Jin, and L. Yu, "Synthesis, characterization, and in vivo efficacy evaluation of PGG-docetaxel conjugate for potential cancer chemotherapy.", *International Journal of Nanomedicine*, Vol. 7, pp.

581–9, January 2012.

10. Biswas, S. and V. P. Torchilin, "Nanopreparations for organelle-specific delivery in cancer", *Advanced Drug Delivery Reviews*, Vol. 66. pp. 26–41, 2014.
11. Liu, D., F. Yang, F. Xiong, and N. Gu, "The smart drug delivery system and its clinical potential", *Theranostics*, Vol. 6, No. 9, pp. 1306–1323, 2016.
12. Trivedi, R. and U. B. Kompella, "Nanomicellar formulations for sustained drug delivery: strategies and underlying principles.", *Nanomedicine (Lond).*, Vol. 5, No. 3, pp. 485–505, April 2010.
13. Chidambaram, M., R. Manavalan, and K. Kathiresan, "Nanotherapeutics to Overcome Conventional Cancer Chemotherapy Limitations", *Journal of Pharmacy & Pharmaceutical Sciences*, Vol. 14, No. 1, p. 67, February 2011.
14. Kratz, F., "Albumin as a drug carrier: design of prodrugs, drug conjugates and nanoparticles.", *Journal of Controlled Release*, Vol. 132, No. 3, pp. 171–83, December 2008.
15. Maeda, H., J. Wu, T. Sawa, Y. Matsumura, and K. Hori, "Tumor vascular permeability and the EPR effect in macromolecular therapeutics: a review", *Journal of Controlled Release*, Vol. 65, No. 1–2, pp. 271–284, March 2000.
16. Allen, T. M., "Ligand-targeted therapeutics in anticancer therapy.", *Nature Reviews Cancer*, Vol. 2, No. 10, pp. 750–763, October 2002.
17. Larsen, a K., a E. Escargueil, and a Skladanowski, "Resistance mechanisms associated with altered intracellular distribution of anticancer agents", *Pharmacology Therapy*, Vol. 85, No. 3, pp. 217–229, 2000.
18. Weissig, V., T. Pettinger, and N. Murdock, "Nanopharmaceuticals (part 1): products on the market", *International Journal of Nanomedicine*, Vol. 9, No. 1, p. 4357, September 2014.
19. Etheridge, M. L., S. A. Campbell, A. G. Erdman, C. L. Haynes, S. M. Wolf, and J. McCullough, "The big picture on nanomedicine: The state of investigational and approved nanomedicine products", *Nanomedicine: Nanotechnology, Biology, and Medicine*, Vol. 9, No. 1. pp. 1–14, 2013.
20. Barenholz, Y. (Chezy), "Doxil® — The first FDA-approved nano-drug: Lessons

learned", *Journal of Controlled Release*, Vol. 160, No. 2, pp. 117–134, 2012.

21. Petersen, G. H., S. K. Alzghari, W. Chee, S. S. Sankari, and N. M. La-Beck, "Meta-analysis of clinical and preclinical studies comparing the anticancer efficacy of liposomal versus conventional non-liposomal doxorubicin", *Journal of Controlled Release*, Vol. 232, pp. 255–264, June 2016.

22. Shi, J., P. W. Kantoff, R. Wooster, and O. C. Farokhzad, "Cancer nanomedicine: progress, challenges and opportunities", *Nature Reviews Cancer*, Vol. 17, No. 1, pp. 20–37, November 2016.

23. Elsadek, B. and F. Kratz, "Impact of albumin on drug delivery — New applications on the horizon", *Journal of Controlled Release*, Vol. 157, No. 1, pp. 4–28, January 2012.

24. Damascelli, B., G. Cant, F. Mattavelli, P. Tamplenizza, P. Bidoli, E. Leo, F. Dosio, A. M. Cerrotta, G. Di Tolla, L. F. Frigerio, F. Garbagnati, R. Lanocita, A. Marchian, G. Patelli, C. Spreafico, V. Tich, V. Vespro, and F. Zunino, "Intraarterial chemotherapy with polyoxyethylated castor oil free paclitaxel, incorporated in albumin nanoparticles (ABI-007)", *Cancer*, Vol. 92, No. 10, pp. 2592–2602, November 2001.

25. Desai, N., V. Trieu, Z. Yao, L. Louie, S. Ci, A. Yang, C. Tao, T. De, B. Beals, D. Dykes, P. Noker, R. Yao, E. Labao, M. Hawkins, and P. Soon-Shiong, "Increased antitumor activity, intratumor paclitaxel concentrations, and endothelial cell transport of cremophor-free, albumin-bound paclitaxel, ABI-007, compared with cremophor-based paclitaxel.", *Clinical Cancer Research*, Vol. 12, No. 4, pp. 1317–24, February 2006.

26. Rugo, H. S., W. T. Barry, A. Moreno-Aspitia, A. P. Lyss, C. Cirrincione, E. Leung, E. L. Mayer, M. Naughton, D. Toppmeyer, L. A. Carey, E. A. Perez, C. Hudis, and E. P. Winer, "Randomized Phase III Trial of Paclitaxel Once Per Week Compared With Nanoparticle Albumin-Bound Nab-Paclitaxel Once Per Week or Ixabepilone With Bevacizumab As First-Line Chemotherapy for Locally Recurrent or Metastatic Breast Cancer: CALGB 40502/NCCTG N0", *Journal of Clinical Oncology*, Vol. 33, No. 21, pp. 2361–2369, July 2015.

27. Sartor, O., M. Jayson, M. . Dineen, and et al., "Eligard: leuprolide acetate in a novel

sustained-release delivery system", *Urology*, Vol. 61, No. 2, pp. 25–31, February 2003.

28. Lee, K. S., H. C. Chung, S. A. Im, Y. H. Park, C. S. Kim, S.-B. Kim, S. Y. Rha, M. Y. Lee, and J. Ro, "Multicenter phase II trial of Genexol-PM, a Cremophor-free, polymeric micelle formulation of paclitaxel, in patients with metastatic breast cancer", *Breast Cancer Research Treatment*, Vol. 108, No. 2, pp. 241–250, March 2008.

29. Caster, J. M., A. N. Patel, T. Zhang, and A. Wang, "Investigational nanomedicines in 2016: a review of nanotherapeutics currently undergoing clinical trials", *Wiley Interdisciplinar Reviews Nanomedicine & Nanobiotechnology*, Vol. 9, No. 1, p. 1416, January 2017.

30. Duncan, R., "Polymer conjugates as anticancer nanomedicines", *Nature Reviews Cancer*, Vol. 6, No. 9, pp. 688–701, September 2006.

31. Moses, M. A., H. Brem, and R. Langer, "Advancing the field of drug delivery", *Cancer Cell*, Vol. 4, No. 5, pp. 337–341, November 2003.

32. Farokhzad, O. and R. Langer, "Nanomedicine: Developing smarter therapeutic and diagnostic modalities", *Advanced Drug Delivery Reviews*, Vol. 58, No. 14, pp. 1456–1459, December 2006.

33. Gillies, E. R. and J. M. J. Frechet, "Dendrimers and dendritic polymers in drug delivery", *Drug Discovery Today*, Vol. 10, No. 1, pp. 35–43, January 2005.

34. Harris, J. M. and R. B. Chess, "Effect of pegylation on pharmaceuticals", *Nature Reviews Drug Discovery*, Vol. 2, No. 3, pp. 214–221, March 2003.

35. Veronese, F. M. and G. Pasut, "PEGylation, successful approach to drug delivery", *Drug Discovery Today*, Vol. 10, No. 21, pp. 1451–1458, Nov. 2005.

36. Sousa-Herves, A., R. Riguera, and E. Fernandez-Megia, "PEG-dendritic block copolymers for biomedical applications", *New Journal of Chemistry*, Vol. 36, No. 2, p. 205, 2012.

37. Ng, E. W. M., D. T. Shima, P. Calias, E. T. Cunningham, D. R. Guyer, and A. P. Adamis, "Pegaptanib, a targeted anti-VEGF aptamer for ocular vascular disease", *Nature Reviews Drug Discovery*, Vol. 5, No. 2, pp. 123–132, February 2006.

38. Pasut, G. and F. M. Veronese, "Polymer–drug conjugation, recent achievements and general strategies", *Progressive Polymers Science*, Vol. 32, No. 8–9, pp. 933–961, August 2007.

39. Gaberc-Porekar, V., I. Zore, B. Podobnik, and V. Menart, "Obstacles and pitfalls in the PEGylation of therapeutic proteins.", *Current Opinions Drug Discovery Devel.*, Vol. 11, No. 2, pp. 242–250, 2008.

40. Basu, A., K. Yang, M. Wang, S. Liu, R. Chintala, T. Palm, H. Zhao, P. Peng, D. Wu, Z. Zhang, J. Hua, M.-C. Hsieh, J. Zhou, G. Petti, X. Li, A. Janjua, M. Mendez, J. Liu, C. Longley, Z. Zhang, M. Mehlig, V. Borowski, M. Viswanathan, and D. Filpula, "Structure−Function Engineering of Interferon-β-1b for Improving Stability, Solubility, Potency, Immunogenicity, and Pharmacokinetic Properties by Site-Selective Mono-PEGylation", *Bioconjugate Chemistry*, Vol. 17, No. 3, pp. 618–630, May 2006.

41. Bailon, P., A. Palleroni, C. A. Schaffer, C. L. Spence, W.-J. Fung, J. E. Porter, G. K. Ehrlich, W. Pan, Z.-X. Xu, M. W. Modi, A. Farid, W. Berthold, and M. Graves, "Rational Design of a Potent, Long-Lasting Form of Interferon: A 40 kDa Branched Polyethylene Glycol-Conjugated Interferon α-2a for the Treatment of Hepatitis C", *Bioconjugate Chemistry*, Vol. 12, No. 2, pp. 195–202, March 2001.

42. Beranová, M., R. Wasserbauer, D. Vanćurová, M. Štifter, J. Očenášková, and M. Mára, "Effect of cytochrome P-450 inhibition and stimulation on intensity of polyethylene degradation in microsomal fraction of mouse and rat livers", *Biomaterials*, Vol. 11, No. 7, pp. 521–524, September 1990.

43. Kawai, F., "Microbial degradation of polyethers", *Applied Microbiology and Biotechnology*, Vol. 58, No. 1, pp. 30–38, January 2002.

44. Ganson, N. J., S. J. Kelly, E. Scarlett, J. S. Sundy, and M. S. Hershfield, "Control of hyperuricemia in subjects with refractory gout, and induction of antibody against poly(ethylene glycol) (PEG), in a phase I trial of subcutaneous PEGylated urate oxidase", *Arthritis Research Therapy*, Vol. 8, No. 1, p. R12, 2006.

45. Wang, X., T. Ishida, and H. Kiwada, "Anti-PEG IgM elicited by injection of liposomes is involved in the enhanced blood clearance of a subsequent dose of PEGylated liposomes", *Journal of Controlled Release*, Vol. 119, No. 2, pp. 236–

244, June 2007.

46. De Duve, C., T. De Barsy, B. Poole, A. Trouet, P. Tulkens, and F. Van Hoof, "Lysosomotropic agents", *Biochemical Pharmacology*, Vol. 23, No. 18, pp. 2495–2531, September 1974.

47. Kabanov, A. V, E. V Batrakova, and V. Y. Alakhov, "Pluronic® block copolymers for overcoming drug resistance in cancer", *Advanced Drug Delivery Reviews*, Vol. 54, No. 5, pp. 759–779, September 2002.

48. Nakanishi, T., S. Fukushima, K. Okamoto, M. Suzuki, Y. Matsumura, M. Yokoyama, T. Okano, Y. Sakurai, and K. Kataoka, "Development of the polymer micelle carrier system for doxorubicin", *Journal of Controlled Release*, Vol. 74, No. 1–3, pp. 295–302, July 2001.

49. Ulbrich, K. and V. Subr, "Structural and chemical aspects of HPMA copolymers as drug carriers.", *Advanced Drug Delivery Reviews*, Vol. 62, No. 2, pp. 150–66, February 2010.

50. Seymour, L. W., R. Duncan, J. Strohalm, and J. Kopeček, "Effect of molecular weight (Mw) of N-(2-hydroxypropyl)methacrylamide copolymers on body distribution and rate of excretion after subcutaneous, intraperitoneal, and intravenous administration to rats", *Journal of Biomedical Materials Research*, Vol. 21, No. 11, pp. 1341–1358, November 1987.

51. Seymour, L. W., Y. Miyamoto, H. Maeda, M. Brereton, J. Strohalm, K. Ulbrich, and R. Duncan, "Influence of molecular weight on passive tumour accumulation of a soluble macromolecular drug carrier", *European Journal of Cancer*, Vol. 31, No. 5, pp. 766–770, January 1995.

52. Duncan, R., H. C. Cable, J. B. Lloyd, P. Rejmanová, and J. Kopeček, "Polymers containing enzymatically degradable bonds, 7. Design of oligopeptide side chains in poly[N-(2-hydroxypropyl)methacrylamide] copolymers to promote efficient degradation by lysosomal enzymes", *Die Makromolecular Chemie*, Vol. 184, No. 10, pp. 1997–2008, October 1983.

53. Mccormick, L. A., L. C. W. Seymour, R. Duncan, and J. Kopecek, "Interaction of a Cationic N-(2-hydroxypropyl)methacrylamide Copolymer with Rat Visceral Yolk Sacs Cultured in vitro and Rat Liver in vivo", *Journal of Bioactive Compatitive*

Polymers, Vol. 1, No. 1, pp. 4–19, January 1986.

54. Seymour, L. W., K. Ulbrich, P. S. Steyger, M. Brereton, V. Subr, J. Strohalm, and R. Duncan, "Tumour tropism and anti-cancer efficacy of polymer-based doxorubicin prodrugs in the treatment of subcutaneous murine B16F10 melanoma.", *British Journal of Cancer*, Vol. 70, No. 4, pp. 636–41, October 1994.

55. Vasey, P. A., D. Bissett, M. Strolin-Benedetti, I. Poggesi, M. Breda, L. Adams, P. Wilson, M. A. Pacciarini, S. B. Kaye, J. Cassidy, S. Burtles, D. Fraier, E. Frigerio, and J. Cassidy, "Phase I clinical and pharmacokinetic study of 3'-deamino-3'-(2-methoxy-4-morpholinyl)doxorubicin (FCE 23762).", *Cancer Research*, Vol. 55, No. 10, pp. 2090–6, May 1995.

56. Seymour, L. W., D. R. Ferry, D. Anderson, S. Hesslewood, P. J. Julyan, R. Poyner, J. Doran, A. M. Young, S. Burtles, and D. J. Kerr, "Hepatic Drug Targeting: Phase I Evaluation of Polymer-Bound Doxorubicin", *Journal of Clinical Oncology*, Vol. 20, No. 6, pp. 1668–1676, March 2002.

57. Meerum Terwogt, J. M., W. W. ten Bokkel Huinink, J. H. Schellens, M. Schot, I. a Mandjes, M. G. Zurlo, M. Rocchetti, H. Rosing, F. J. Koopman, and J. H. Beijnen, "Phase I clinical and pharmacokinetic study of PNU166945, a novel water-soluble polymer-conjugated prodrug of paclitaxel.", *Anticancer Drugs*, Vol. 12, No. 4, pp. 315–323, 2001.

58. Schoemaker, N. E., C. van Kesteren, H. Rosing, S. Jansen, M. Swart, J. Lieverst, D. Fraier, M. Breda, C. Pellizzoni, R. Spinelli, M. G. Porro, J. H. Beijnen, J. H. M. Schellens, and W. ten Bokkel Huinink, "A phase I and pharmacokinetic study of MAG-CPT, a water-soluble polymer conjugate of camptothecin", *British Journal of Cancer*, Vol. 87, No. 41, pp. 608–614, September 2002.

59. Jain, J. P., W. Yenet Ayen, A. J. Domb, and N. Kumar, "Biodegradable Polymers in Drug Delivery", *Biodegradable Polymers in Clinical Use and Clinical Development*, Hoboken, NJ, USA: John Wiley & Sons Inc., pp. 1–58, 2011.

60. Anderson, J. M. and M. S. Shive, "Biodegradation and biocompatibility of PLA and PLGA microspheres", *Advanced Drug Delivery Reviews*, Vol. 28, No. 1, pp. 5–24, October 1997.

61. West, C. P., M. A. Lumsden, S. Lawson, J. Williamson, and D. T. Baird, "Shrinkage

of uterine fibroids during therapy with goserelin (Zoladex): a luteinizing hormone-releasing hormone agonist administered as a monthly subcutaneous depot", *Fertility and Sterility*, Vol. 48, No. 1, pp. 45–51, July 1987.

62. Crawford, E. D. and J. M. Phillips, "Six-month gonadotropin releasing hormone (GnRH) agonist depots provide efficacy, safety, convenience, and comfort", *Cancer Management and Research*, Vol. Volume 3, p. 201, July 2011.

63. Nel, A. E., L. Mädler, D. Velegol, T. Xia, E. M. V. Hoek, P. Somasundaran, F. Klaessig, V. Castranova, and M. Thompson, "Understanding biophysicochemical interactions at the nano–bio interface", *Nature Materials*, Vol. 8, No. 7, pp. 543–557, July 2009.

64. Monopoli, M. P., C. Åberg, A. Salvati, and K. A. Dawson, "Biomolecular coronas provide the biological identity of nanosized materials", *Nature Nanotechnology*, Vol. 7, No. 12, pp. 779–786, December 2012.

65. Li, S.-D. and L. Huang, "Pharmacokinetics and Biodistribution of Nanoparticles", *Molecular Pharmaceutics*, Vol. 5, No. 4, pp. 496–504, August 2008.

66. Moghimi, S. M. and C. Hunter, "Capture of Stealth Nanoparticles by the Body's Defences", *Critical Reviews Therapy Drug Carrier Systems*, Vol. 18, No. 6, p. 24, 2001.

67. Sadzuka, Y., S. Hirotsu, and S. Hirota, "Effect of liposomalization on the antitumor activity, side-effects and tissue distribution of CPT-11", *Cancer Letters*, Vol. 127, No. 1–2, pp. 99–106, May 1998.

68. Fang, C., B. Shi, Y.-Y. Pei, M.-H. Hong, J. Wu, and H.-Z. Chen, "In vivo tumor targeting of tumor necrosis factor-α-loaded stealth nanoparticles: Effect of MePEG molecular weight and particle size", *European Journal of Pharmaceutical Sciences*, Vol. 27, No. 1, pp. 27–36, January 2006.

69. Ernsting, M. J., W.-L. Tang, N. W. MacCallum, and S.-D. Li, "Preclinical pharmacokinetic, biodistribution, and anti-cancer efficacy studies of a docetaxel-carboxymethylcellulose nanoparticle in mouse models", *Biomaterials*, Vol. 33, No. 5, pp. 1445–1454, February 2012.

70. Alexis, F., E. Pridgen, L. K. Molnar, and O. C. Farokhzad, "Factors Affecting the Clearance and Biodistribution of Polymeric Nanoparticles", *Molecular*

Pharmaceutics, Vol. 5, No. 4, pp. 505–515, August 2008.

71. Choi, C. H. J., C. A. Alabi, P. Webster, and M. E. Davis, "Mechanism of active targeting in solid tumors with transferrin-containing gold nanoparticles", *Proceedings of the National Academy of Sciences*, Vol. 107, No. 3, pp. 1235–1240, January 2010.

72. Tomayko, M. M., C. P. Reynolds, D. G. Mackensen, R. K. Jain, J. A. McCammon, and D. E. Discher, "Determination of subcutaneous tumor size in athymic (nude) mice.", *Cancer Chemotherapy & Pharmacology*, Vol. 24, No. 3, pp. 148–54, 1989.

73. Yuan, F., M. Dellian, D. Fukumura, M. Leunig, D. A. Berk, V. P. Torchilin, and R. K. Jain, "Vascular permeability in a human tumor xenograft: molecular size dependence and cutoff size.", *Cancer Research*, Vol. 55, No. 17, pp. 3752–6, September 1995.

74. Liu, D., A. Mori, and L. Huang, "Role of liposome size and RES blockade in controlling biodistribution and tumor uptake of GM1-containing liposomes", *Biochimica et Biophysica Acta (BBA) - Biomembranes*, Vol. 1104, No. 1, pp. 95–101, February 1992.

75. Chen, L.-T. and L. Weiss, "The Role of the Sinus Wall in the Passage of Erythrocytes Through the Spleen", *Blood*, Vol. 41, No. 4, 1973.

76. Jain, K. K., J. C. Leroux, C. Khemtong, S. G. Yang, D. G. Anderson, …, "Advances in the field of nanooncology.", *BMC Medicine*, Vol. 8, No. 12, p. 83, December 2010.

77. Champion, J. A. and S. Mitragotri, "Role of target geometry in phagocytosis.", *Proceedings of the National Academy of Sciences U. S. A.*, Vol. 103, No. 13, pp. 4930–4, March 2006.

78. Champion, J. A. and S. Mitragotri, "Shape Induced Inhibition of Phagocytosis of Polymer Particles", *Pharmaceutical Research*, Vol. 26, No. 1, pp. 244–249, January 2009.

79. Geng, Y., P. Dalhaimer, S. Cai, R. Tsai, M. Tewari, T. Minko, and D. E. Discher, "Shape effects of filaments versus spherical particles in flow and drug delivery", *Nature Nanotechnology*, Vol. 2, No. 4, pp. 249–255, April 2007.

80. Xiao, K., Y. Li, J. Luo, J. S. Lee, W. Xiao, A. M. Gonik, R. G. Agarwal, and K. S.

Lam, "The effect of surface charge on in vivo biodistribution of PEG-oligocholic acid based micellar nanoparticles", *Biomaterials*, Vol. 32, No. 13, pp. 3435–3446, May 2011.

81. Zhang, J., F. Liu, and L. Huang, "Implications of pharmacokinetic behavior of lipoplex for its inflammatory toxicity", *Advanced Drug Delivery Reviews*, Vol. 57, No. 5, pp. 689–698, April 2005.

82. Levchenko, T. S., R. Rammohan, A. N. Lukyanov, K. R. Whiteman, and V. P. Torchilin, "Liposome clearance in mice: the effect of a separate and combined presence of surface charge and polymer coating", *International Journal of Pharmaceutics*, Vol. 240, No. 1–2, pp. 95–102, June 2002.

83. Abbott, N. J., L. Rönnbäck, and E. Hansson, "Astrocyte–endothelial interactions at the blood–brain barrier", *Nature Reviews Neuroscience*, Vol. 7, No. 1, pp. 41–53, January 2006.

84. Takano, M., R. Yumoto, and T. Murakami, "Expression and function of efflux drug transporters in the intestine", *Pharmacology Therapy*, Vol. 109, No. 1–2, pp. 137–161, January 2006.

85. El-Bacha, R. S. and A. Minn, "Drug metabolizing enzymes in cerebrovascular endothelial cells afford a metabolic protection to the brain.", *Cellular Molecular Biology (Noisy-le-grand).*, Vol. 45, No. 1, pp. 15–23, February 1999.

86. Ward, P. D., T. K. Tippin, and D. R. Thakker, "Enhancing paracellular permeability by modulating epithelial tight junctions", *Pharmaceutical Science & Technology Today*, Vol. 3, No. 10, pp. 346–358, October 2000.

87. Deli, M. A., "Potential use of tight junction modulators to reversibly open membranous barriers and improve drug delivery", *Biochimica et Biophysica Acta (BBA) - Biomembranes*, Vol. 1788, No. 4, pp. 892–910, April 2009.

88. Duncan, R., "Polymer conjugates for tumour targeting and intracytoplasmic delivery. The EPR effect as a common gateway?", *Pharmaceutical Science & Technology Today*, Vol. 2, No. 11, pp. 441–449, November 1999.

89. Hobson, B. and J. Denekamp, "Endothelial proliferation in tumours and normal tissues: Continuous labelling studies", *British Journal of Cancer*, Vol. 49, No. 4, pp. 405–413, April 1984.

90. Muggia, F. M., "Doxorubicin-Polymer Conjugates : Further Demonstration of the Concept of Enhanced Permeability and Retention Doxorubicin-Polymer Conjugates : Further Demonstration of the Concept of Enhanced Permeability and Retention", *Clinical Cancer Research*, Vol. 5, pp. 7–8, 1999.

91. Koo, A. N., K. H. Min, H. J. Lee, S.-U. Lee, K. Kim, I. C. Kwon, S. H. Cho, S. Y. Jeong, and S. C. Lee, "Tumor accumulation and antitumor efficacy of docetaxel-loaded core-shell-corona micelles with shell-specific redox-responsive cross-links.", *Biomaterials*, Vol. 33, No. 5, pp. 1489–99, February 2012.

92. Eckman, A. M., E. Tsakalozou, N. Y. Kang, A. Ponta, and Y. Bae, "Drug release patterns and cytotoxicity of PEG-poly(aspartate) block copolymer micelles in cancer cells.", *Pharmaceutical Research*, Vol. 29, No. 7, pp. 1755–67, July 2012.

93. Konno, T., H. Maeda, K. Iwai, S. Maki, S. Tashiro, M. Uchida, and Y. Miyauchi, "Selective targeting of anti-cancer drug and simultaneous image enhancement in solid tumors by arterially administered lipid contrast medium", *Cancer*, Vol. 54, No. 11, pp. 2367–2374, 1984.

94. Harrington, K. J., G. Rowlinson-Busza, K. N. Syrigos, P. S. Uster, R. M. Abra, and J. S. W. Stewart, "Biodistribution and pharmacokinetics of 111In-DTPA-labelled pegylated liposomes in a human tumour xenograft model: implications for novel targeting strategies", *British Journal of Cancer*, Vol. 83, No. 2, pp. 232–238, June 2000.

95. Jain, R. K. and T. Stylianopoulos, "Delivering nanomedicine to solid tumors", *Nature Reviews Clinical Oncology*, Vol. 7, No. 11, pp. 653–664, November 2010.

96. Northfelt, D. W., B. J. Dezube, J. A. Thommes, B. J. Miller, M. A. Fischl, A. Friedman-Kien, L. D. Kaplan, C. Du Mond, R. D. Mamelok, and D. H. Henry, "Pegylated-liposomal doxorubicin versus doxorubicin, bleomycin, and vincristine in the treatment of AIDS-related Kaposi's sarcoma: results of a randomized phase III clinical trial.", *Journal of Clinical Oncology*, Vol. 16, No. 7, pp. 2445–51, July 1998.

97. O'Brien, M. E. R., N. Wigler, M. Inbar, R. Rosso, E. Grischke, A. Santoro, R. Catane, D. G. Kieback, P. Tomczak, S. P. Ackland, F. Orlandi, L. Mellars, L. Alland, and C. Tendler, "Reduced cardiotoxicity and comparable efficacy in a phase

III trial of pegylated liposomal doxorubicin HCl (CAELYXTM/Doxil") versus conventional doxorubicin for first-line treatment of metastatic breast cancer", *Annual Oncology*, Vol. 15, No. 3, pp. 440–449, March 2004.

98. Gill, P. S., J. Wernz, D. T. Scadden, P. Cohen, G. M. Mukwaya, J. H. von Roenn, M. Jacobs, S. Kempin, I. Silverberg, G. Gonzales, M. U. Rarick, A. M. Myers, F. Shepherd, C. Sawka, M. C. Pike, and M. E. Ross, "Randomized phase III trial of liposomal daunorubicin versus doxorubicin, bleomycin, and vincristine in AIDS-related Kaposi's sarcoma.", *Journal of Clinical Oncology*, Vol. 14, No. 8, pp. 2353–64, August 1996.

99. Choi, M., K. Choi, S.-W. Ryu, J. Lee, and C. Choi, "Dynamic fluorescence imaging for multiparametric measurement of tumor vasculature", *Journal of Biomedical Optics*, Vol. 16, No. 4, p. 46008, 2011.

100. Baker, C. H., C. C. Solorzano, I. J. Fidler, F. Winkler, D. J. Hicklin, and R. K. Jain, "Blockade of vascular endothelial growth factor receptor and epidermal growth factor receptor signaling for therapy of metastatic human pancreatic cancer.", *Cancer Research*, Vol. 62, No. 7, pp. 1996–2003, April 2002.

101. Tanaka, S., T. Akaike, J. Wu, J. Fang, T. Sawa, M. Ogawa, T. Beppu, and H. Maeda, "Modulation of Tumor-selective Vascular Blood Flow and Extravasation by the Stable Prostaglandin I_2 Analogue Beraprost Sodium", *Journal of Drug Targeting*, Vol. 11, No. 1, pp. 45–52, January 2003.

102. Seki, T., J. Fang, and H. Maeda, "Enhanced delivery of macromolecular antitumor drugs to tumors by nitroglycerin application", *Cancer Science*, Vol. 100, No. 12, pp. 2426–2430, December 2009.

103. Seynhaeve, A. L. B., C. E. Vermeulen, A. M. M. Eggermont, T. L. M. ten Hagen, G. aan de Wiel-Ambagtsheer, S. T. van Tiel, A. M. M. Eggermont, and T. L. M. ten Hagen, "Cytokines and vascular permeability: an in vitro study on human endothelial cells in relation to tumor necrosis factor-alpha-primed peripheral blood mononuclear cells.", *Cell Biochemistry and Biophysics*, Vol. 44, No. 1, pp. 157–69, 2006.

104. Seki, T., F. Carroll, S. Illingworth, N. Green, R. Cawood, H. Bachtarzi, V. Šubr, K. D. Fisher, and L. W. Seymour, "Tumour necrosis factor-alpha increases

extravasation of virus particles into tumour tissue by activating the Rho A/Rho kinase pathway", *Journal of Controlled Release*, Vol. 156, No. 3, pp. 381–389, December 2011.

105. Gorski, D. H., M. A. Beckett, N. T. Jaskowiak, D. P. Calvin, H. J. Mauceri, R. M. Salloum, S. Seetharam, A. Koons, D. M. Hari, D. W. Kufe, and R. R. Weichselbaum, "Blockage of the vascular endothelial growth factor stress response increases the antitumor effects of ionizing radiation.", *Cancer Research*, Vol. 59, No. 14, pp. 3374–8, July 1999.

106. Heldin, C.-H., K. Rubin, K. Pietras, and A. Östman, "High interstitial fluid pressure -an obstacle in cancer therapy", *Nature Reviews Cancer*, Vol. 4, No. 10, pp. 806–813, October 2004.

107. Boucher, Y., L. T. Baxter, and R. K. Jain, "Interstitial pressure gradients in tissue-isolated and subcutaneous tumors: implications for therapy.", *Cancer Research*, Vol. 50, No. 15, pp. 4478–84, August 1990.

108. Roh, H. D., Y. Boucher, S. Kalnicki, R. Buchsbaum, W. D. Bloomer, and R. K. Jain, "Interstitial hypertension in carcinoma of uterine cervix in patients: possible correlation with tumor oxygenation and radiation response.", *Cancer Research*, Vol. 51, No. 24, pp. 6695–8, December 1991.

109. Jain, R. K., "Normalizing tumor vasculature with anti-angiogenic therapy: A new paradigm for combination therapy", *Nature Medicine*, Vol. 7, No. 9, pp. 987–989, September 2001.

110. Pietras, K., "Increasing tumor uptake of anticancer drugs with imatinib", *Seminars in Oncology*, Vol. 31, pp. 18–23, April 2004.

111. Rønnov-Jessen, L., O. W. Petersen, and M. J. Bissell, "Cellular changes involved in conversion of normal to malignant breast: importance of the stromal reaction.", *Physiological Reviews*, Vol. 76, No. 1, pp. 69–125, January 1996.

112. Flier, J. S., L. H. Underhill, and H. F. Dvorak, "Tumors: Wounds That Do Not Heal", *New England Journal of Medicine*, Vol. 315, No. 26, pp. 1650–1659, December 1986.

113. Mueller, M. M. and N. E. Fusenig, "Friends or foes — bipolar effects of the tumour stroma in cancer", *Nature Reviews Cancer*, Vol. 4, No. 11, pp. 839–849, November

2004.

114. Kalluri, R., "Angiogenesis: Basement membranes: structure, assembly and role in tumour angiogenesis", *Nature Reviews Cancer*, Vol. 3, No. 6, pp. 422–433, June 2003.

115. Murakami, M., M. J. Ernsting, E. Undzys, N. Holwell, W. D. Foltz, and S.-D. Li, "Docetaxel Conjugate Nanoparticles That Target -Smooth Muscle Actin-Expressing Stromal Cells Suppress Breast Cancer Metastasis", *Cancer Research*, Vol. 73, No. 15, pp. 4862–4871, August 2013.

116. Allavena, P., A. Sica, G. Solinas, C. Porta, and A. Mantovani, "The inflammatory micro-environment in tumor progression: The role of tumor-associated macrophages", *Critical Reviews in Oncology & Hematology*, Vol. 66, No. 1, pp. 1–9, April 2008.

117. Shaffer, S. A., C. Baker-Lee, J. Kennedy, M. S. Lai, P. de Vries, K. Buhler, and J. W. Singer, "In vitro and in vivo metabolism of paclitaxel poliglumex: identification of metabolites and active proteases", *Cancer Chemotherapy Pharmacology*, Vol. 59, No. 4, pp. 537–548, March 2007.

118. Jackson, E. F., E. Esparza-Coss, X. Wen, C. S. Ng, S. L. Daniel, R. E. Price, B. Rivera, C. Charnsangavej, J. G. Gelovani, and C. Li, "Magnetic Resonance Imaging of Therapy-Induced Necrosis Using Gadolinium-Chelated Polyglutamic Acids", *International Journal of Radiation Oncology*, Vol. 68, No. 3, pp. 830–838, July 2007.

119. Smith, A. E., "How Viruses Enter Animal Cells", *Science*, Vol. 304, No. 5668, pp. 237–242, April 2004.

120. Doherty, G. J. and H. T. McMahon, "Mechanisms of Endocytosis", *Annual Review of Biochemistry*, Vol. 78, No. 1, pp. 857–902, June 2009.

121. Zhao, F., Y. Zhao, Y. Liu, X. Chang, C. Chen, and Y. Zhao, "Cellular Uptake, Intracellular Trafficking, and Cytotoxicity of Nanomaterials", *Small*, Vol. 7, No. 10, pp. 1322–1337, May 2011.

122. Kannan, S., P. Kolhe, V. Raykova, M. Glibatec, R. M. Kannan, M. Lieh-Lai, and D. Bassett, "Dynamics of cellular entry and drug delivery by dendritic polymers into human lung epithelial carcinoma cells", *Journal of Biomaterials Science, Polymer*

Edition, Vol. 15, No. 3, pp. 311–330, January 2004.

123. Rejman, J., V. Oberle, I. S. Zuhorn, and D. Hoekstra, "Size-dependent internalization of particles via the pathways of clathrin- and caveolae-mediated endocytosis.", *Biochemistry Journal*, Vol. 377, No. Pt 1, pp. 159–69, January 2004.

124. Kettler, K., K. Veltman, D. van de Meent, A. van Wezel, and A. J. Hendriks, "Cellular uptake of nanoparticles as determined by particle properties, experimental conditions, and cell type", *Environmental Toxicology and Chemistry*, Vol. 33, No. 3, pp. 481–492, March 2014.

125. Patel, L. N., J. L. Zaro, and W.-C. Shen, "Cell Penetrating Peptides: Intracellular Pathways and Pharmaceutical Perspectives", *Pharmaceutical Research*, Vol. 24, No. 11, pp. 1977–1992, September 2007.

126. McMahon, H. T. and E. Boucrot, "Molecular mechanism and physiological functions of clathrin-mediated endocytosis", *Nature Reviews Molecular Cell Biology*, Vol. 12, No. 8, pp. 517–533, July 2011.

127. Walsh, M., M. Tangney, M. J. O'Neill, J. O. Larkin, D. M. Soden, S. L. McKenna, R. Darcy, G. C. O'Sullivan, and C. M. O'Driscoll, "Evaluation of Cellular Uptake and Gene Transfer Efficiency of Pegylated Poly- <scp>l</scp> -lysine Compacted DNA: Implications for Cancer Gene Therapy", *Molecular Pharmaceutics*, Vol. 3, No. 6, pp. 644–653, Dec. 2006.

128. B. Devika Chithrani and W. C. W. Chan, "Elucidating the Mechanism of Cellular Uptake and Removal of Protein-Coated Gold Nanoparticles of Different Sizes and Shapes", *Nano Letters*, Vol. 7, No. 6, pp. 1542–1550, Jun. 2007.

129. Yoo, J.-W., N. Doshi, and S. Mitragotri, "Endocytosis and Intracellular Distribution of PLGA Particles in Endothelial Cells: Effect of Particle Geometry", *Macromolecules Rapid Communications*, Vol. 31, No. 2, December 2009.

130. Harush-Frenkel, O., N. Debotton, S. Benita, and Y. Altschuler, "Targeting of nanoparticles to the clathrin-mediated endocytic pathway", *Biochemical and Biophysical Research Communications*, Vol. 353, No. 1, pp. 26–32, February 2007.

131. Hong, S., A. U. Bielinska, A. Mecke, B. Keszler, J. L. Beals, X. Shi, L. Balogh, B. G. Orr, J. R. Baker, and M. M. Banaszak Holl, "Interaction of Poly(amidoamine) Dendrimers with Supported Lipid Bilayers and Cells: Hole Formation and the

Relation to Transport", *Bioconjugate Chemistry*, Vol. 15, No. 4, pp. 774–782, July 2004.

132. Kirchner, C., T. Liedl, S. Kudera, T. Pellegrino, A. M. Javier, H. E. Gaub, S. Stölzle, N. Fertig, and W. J. Parak, "Cytotoxicity of Colloidal CdSe and CdSe/ZnS Nanoparticles", *Nano Letters*, Vol. 5, No. 2, pp. 331–338, Feb. 2005.

133. Nativo, P., I. A. Prior, and M. Brust, "Uptake and Intracellular Fate of Surface-Modified Gold Nanoparticles", *ACS Nano*, Vol. 2, No. 8, pp. 1639–1644, August 2008.

134. Kamaly, N., Z. Xiao, P. M. Valencia, A. F. Radovic-Moreno, and O. C. Farokhzad, "Targeted polymeric therapeutic nanoparticles: design, development and clinical translation", *Chemical Society Reviews*, Vol. 41, No. 7, p. 2971, 2012.

135. Valencia, P. M., M. H. Hanewich-Hollatz, W. Gao, F. Karim, R. Langer, R. Karnik, and O. C. Farokhzad, "Effects of ligands with different water solubilities on self-assembly and properties of targeted nanoparticles", *Biomaterials*, Vol. 32, No. 26, pp. 6226–6233, September 2011.

136. Saha, R. N., S. Vasanthakumar, G. Bende, and M. Snehalatha, "Nanoparticulate drug delivery systems for cancer chemotherapy", *Molecular Membrane Biology*, Vol. 27, No. 7, pp. 215–231, October 2010.

137. Wang, J., S. Tian, R. A. Petros, M. E. Napier, and J. M. DeSimone, "The Complex Role of Multivalency in Nanoparticles Targeting the Transferrin Receptor for Cancer Therapies", *Journal of the American Chemical Society*, Vol. 132, No. 32, pp. 11306–11313, August 2010.

138. Kirpotin, D. B., "Antibody Targeting of Long-Circulating Lipidic Nanoparticles Does Not Increase Tumor Localization but Does Increase Internalization in Animal Models", *Cancer Research*, Vol. 66, No. 13, pp. 6732–6740, July 2006.

139. Li, X., H. Zhou, L. Yang, G. Du, A. S. Pai-Panandiker, X. Huang, and B. Yan, "Enhancement of cell recognition in vitro by dual-ligand cancer targeting gold nanoparticles", *Biomaterials*, Vol. 32, No. 10, pp. 2540–2545, April 2011.

140. Leserman, L. D., J. Barbet, F. Kourilsky, and J. N. Weinstein, "Targeting to cells of fluorescent liposomes covalently coupled with monoclonal antibody or protein A", *Nature*, Vol. 288, No. 5791, pp. 602–604, December 1980.

141. Weinberg, W. C., M. R. Frazier-Jessen, W. J. Wu, A. Weir, M. Hartsough, P. Keegan, and C. Fuchs, "Development and regulation of monoclonal antibody products: Challenges and opportunities", *Cancer Metastasis Reviews*, Vol. 24, No. 4, pp. 569–584, December 2005.

142. Mamot, C., R. Ritschard, A. Wicki, G. Stehle, T. Dieterle, L. Bubendorf, C. Hilker, S. Deuster, R. Herrmann, and C. Rochlitz, "Tolerability, safety, pharmacokinetics, and efficacy of doxorubicin-loaded anti-EGFR immunoliposomes in advanced solid tumours: a phase 1 dose-escalation study", *The Lancet Oncology*, Vol. 13, No. 12, pp. 1234–1241, December 2012.

143. Matsumura, Y., "Phase I and pharmacokinetic study of MCC-465, a doxorubicin (DXR) encapsulated in PEG immunoliposome, in patients with metastatic stomach cancer", *Annual Oncology*, Vol. 15, No. 3, pp. 517–525, March 2004.

144. Choi, C. H. J., C. A. Alabi, P. Webster, and M. E. Davis, "Mechanism of active targeting in solid tumors with transferrin-containing gold nanoparticles", *Proceedings of the National Academy of Sciences*, Vol. 107, No. 3, pp. 1235–1240, January 2010.

145. Sahoo, S. K., W. Ma, and V. Labhasetwar, "Efficacy of transferrin-conjugated paclitaxel-loaded nanoparticles in a murine model of prostate cancer", *International Journal of Cancer*, Vol. 112, No. 2, pp. 335–340, November 2004.

146. Shi, J., Z. Xiao, N. Kamaly, and O. C. Farokhzad, "Self-Assembled Targeted Nanoparticles: Evolution of Technologies and Bench to Bedside Translation", *Accounts of Chemical Research*, Vol. 44, No. 10, pp. 1123–1134, October 2011.

147. Stupp, R., M. E. Hegi, T. Gorlia, S. C. Erridge, M. Weller,…, "Cilengitide combined with standard treatment for patients with newly diagnosed glioblastoma with methylated MGMT promoter (CENTRIC EORTC 26071-22072 study): a multicentre, randomised, open-label, phase 3 trial", *The Lancet Oncology*, Vol. 15, No. 10, pp. 1100–1108, September 2014.

148. Murphy, E. A., B. K. Majeti, L. A. Barnes, M. Makale, S. M. Weis, K. Lutu-Fuga, W. Wrasidlo, and D. A. Cheresh, "Nanoparticle-mediated drug delivery to tumor vasculature suppresses metastasis", *Proceedings of the National Academy of Sciences*, Vol. 105, No. 27, pp. 9343–9348, July 2008.

149. Xiong, X.-B., Y. Huang, W.-L. LU, X. Zhang, H. Zhang, T. Nagai, and Q. Zhang, "Intracellular delivery of doxorubicin with RGD-modified sterically stabilized liposomes for an improved antitumor efficacy: In vitro and in vivo", *Journal of Pharmaceutical Sciences*, Vol. 94, No. 8, pp. 1782–1793, August 2005.

150. Hu, Z., F. Luo, Y. Pan, C. Hou, L. Ren, J. Chen, J. Wang, and Y. Zhang, "Arg-Gly-Asp (RGD) peptide conjugated poly(lactic acid)-poly(ethylene oxide) micelle for targeted drug delivery", *Journal of Biomedical Materials Research Part A*, Vol. 85A, No. 3, pp. 797–807, June 2008.

151. Xiao, Z. and O. C. Farokhzad, "Aptamer-Functionalized Nanoparticles for Medical Applications: Challenges and Opportunities", *ACS Nano*, Vol. 6, No. 5, pp. 3670–3676, May 2012.

152. Bagalkot, V., O. C. Farokhzad, R. Langer, and S. Jon, "An Aptamer–Doxorubicin Physical Conjugate as a Novel Targeted Drug-Delivery Platform", *Angewante Chemie International Edition*, Vol. 45, No. 48, pp. 8149–8152, December 2006.

153. Werner, M. E., S. Karve, R. Sukumar, N. D. Cummings, J. A. Copp, R. C. Chen, T. Zhang, and A. Z. Wang, "Folate-targeted nanoparticle delivery of chemo- and radiotherapeutics for the treatment of ovarian cancer peritoneal metastasis", *Biomaterials*, Vol. 32, No. 33, pp. 8548–8554, 2011.

154. Zhang, H., Y. Ma, and X.-L. Sun, "Recent developments in carbohydrate-decorated targeted drug/gene delivery", *Medicine Research Reviews*, 2009.

155. Espelin, C. W., S. C. Leonard, E. Geretti, T. J. Wickham, and B. S. Hendriks, "Dual HER2 Targeting with Trastuzumab and Liposomal-Encapsulated Doxorubicin (MM-302) Demonstrates Synergistic Antitumor Activity in Breast and Gastric Cancer", *Cancer Research*, Vol. 76, No. 6, pp. 1517–1527, March 2016.

156. Hrkach, J., D. Von Hoff, M. M. Ali, E. Andrianova, S. Zale, …, "Preclinical Development and Clinical Translation of a PSMA-Targeted Docetaxel Nanoparticle with a Differentiated Pharmacological Profile", *Science Transl. Medicine*, Vol. 4, No. 128, p. 128ra39-128ra39, April 2012.

157. Davis, M. E., J. E. Zuckerman, C. H. J. Choi, D. Seligson, A. Tolcher, C. A. Alabi, Y. Yen, J. D. Heidel, and A. Ribas, "Evidence of RNAi in humans from systemically administered siRNA via targeted nanoparticles", *Nature*, Vol. 464, No.

7291, pp. 1067–1070, April 2010.

158. Yatvin, M. B., J. N. Weinstein, W. H. Dennis, and R. Blumenthal, "Design of liposomes for enhanced local release of drugs by hyperthermia", *Science (80-.).*, Vol. 202, No. 4374, pp. 1290–1293, 1978.

159. Tanaka, T., "Collapse of gels and the critical endpoint", *Phys. Reviews Letters*, Vol. 40, No. 12, pp. 820–823, 1978.

160. Neri, D. and C. T. Supuran, "Interfering with pH regulation in tumours as a therapeutic strategy.", *Nature Reviews Drug Discovery*, Vol. 10, No. 10, pp. 767–77, 2011.

161. Liu, J., Y. Huang, A. Kumar, A. Tan, S. Jin, A. Mozhi, and X.-J. Liang, "pH-sensitive nano-systems for drug delivery in cancer therapy.", *Biotechnology Advanced*, Vol. 32, No. 4, pp. 693–710, 2013.

162. Gillies, E. R., J. M. J. Fréchet, S. D. Fowler, Y. Sakurai, T. Seto, K. Kataoka, and J. R. Geffner, "A new approach towards acid sensitive copolymer micelles for drug delivery", *Chemical Communications*, Vol. 103, No. 14, pp. 1640–1641, 2003.

163. Tu, C., L. Zhu, F. Qiu, D. Wang, Y. Su, X. Zhu, and D. Yan, "Facile PEGylation of Boltorn® H40 for pH-responsive drug carriers", *Polymer (Guildf).*, Vol. 54, No. 8, pp. 2020–2027, April 2013.

164. Saito, G., J. A. Swanson, and K. D. Lee, "Drug delivery strategy utilizing conjugation via reversible disulfide linkages: Role and site of cellular reducing activities", *Advanced Drug Delivery Reviews*, Vol. 55, No. 2. pp. 199–215, 2003.

165. Mura, S., J. Nicolas, and P. Couvreur, "Stimuli-responsive nanocarriers for drug delivery", *Nature Mater.*, Vol. 12, No. 11, pp. 991–1003, October 2013.

166. Chudasama, V., A. Maruani, and S. Caddick, "Recent advances in the construction of antibody–drug conjugates", *Nature Chemistry*, Vol. 8, No. 2, p. 114, January 2016.

167. Zhu, L., P. Kate, and V. P. Torchilin, "Matrix Metalloprotease 2-Responsive Multifunctional Liposomal Nanocarrier for Enhanced Tumor Targeting", *ACS Nano*, Vol. 6, No. 4, pp. 3491–3498, April 2012.

168. Harris, T. J., G. von Maltzahn, M. E. Lord, J.-H. Park, A. Agrawal, D.-H. Min, M. J.

Sailor, and S. N. Bhatia, "Protease-Triggered Unveiling of Bioactive Nanoparticles", *Small*, Vol. 4, No. 9, pp. 1307–1312, September 2008.

169. Hatakeyama, H., H. Akita, E. Ito, Y. Hayashi, M. Oishi, Y. Nagasaki, R. Danev, K. Nagayama, N. Kaji, H. Kikuchi, Y. Baba, and H. Harashima, "Systemic delivery of siRNA to tumors using a lipid nanoparticle containing a tumor-specific cleavable PEG-lipid", *Biomaterials*, Vol. 32, No. 18, pp. 4306–4316, June 2011.

170. Torchilin, V. P., "Multifunctional, stimuli-sensitive nanoparticulate systems for drug delivery", *Nature Reviews Drug Discovery*, Vol. 13, No. 11, pp. 813–827, October 2014.

171. Tagami, T., W. D. Foltz, M. J. Ernsting, C. M. Lee, I. F. Tannock, J. P. May, and S.-D. Li, "MRI monitoring of intratumoral drug delivery and prediction of the therapeutic effect with a multifunctional thermosensitive liposome", *Biomaterials*, Vol. 32, No. 27, pp. 6570–6578, September 2011.

172. Paris, J. L., M. V. Cabañas, M. Manzano, and M. Vallet-Regí, "Polymer-Grafted Mesoporous Silica Nanoparticles as Ultrasound-Responsive Drug Carriers", *ACS Nano*, Vol. 9, No. 11, pp. 11023–11033, November 2015.

173. Pradhan, P., J. Giri, F. Rieken, C. Koch, O. Mykhaylyk, M. Döblinger, R. Banerjee, D. Bahadur, and C. Plank, "Targeted temperature sensitive magnetic liposomes for thermo-chemotherapy", *Journal of Controlled Release*, Vol. 142, No. 1, pp. 108–121, February 2010.

174. Ambade, A. V., E. N. Savariar, and S. Thayumanavan, "Dendrimeric Micelles for Controlled Drug Release and Targeted Delivery", *Molecular Pharmaceutics*, Vol. 2, No. 4, pp. 264–272, August 2005.

175. Wang, Y., T. Yang, X. Wang, J. Wang, X. Zhang, and Q. Zhang, "Targeted polymeric micelle system for delivery of combretastatin A4 to tumor vasculature in vitro.", *Pharmaceutical Research*, Vol. 27, No. 9, pp. 1861–1868, September 2010.

176. Nasongkla, N., E. Bey, J. Ren, H. Ai, C. Khemtong, J. S. Guthi, S.-F. Chin, A. D. Sherry, D. A. Boothman, and J. Gao, "Multifunctional polymeric micelles as cancer-targeted, MRI-ultrasensitive drug delivery systems.", *Nano Letters*, Vol. 6, pp. 2427–2430, 2006.

177. Wang, Y., T. Yang, X. Wang, W. Dai, J. Wang, X. Zhang, Z. Li, and Q. Zhang,

"Materializing sequential killing of tumor vasculature and tumor cells via targeted polymeric micelle system", *Journal of Controlled Release*, Vol. 149, No. 3, pp. 299–306, February 2011.

178. Kataoka, K., A. Harada, and Y. Nagasaki, "Block copolymer micelles for drug delivery: design, characterization and biological significance.", *Advanced Drug Delivery Reviews*, Vol. 47, pp. 113–131, 2001.

179. Cho, K., X. Wang, S. Nie, Z. Chen, and D. M. Shin, "Therapeutic Nanoparticles for Drug Delivery in Cancer", *Clinical Cancer Research*, Vol. 14, No. 5, pp. 1310–1316, March 2008.

180. Kataoka, K., A. Harada, and Y. Nagasaki, "Block copolymer micelles for drug delivery: design, characterization and biological significance", *Advanced Drug Delivery Reviews*, Vol. 47, No. 1, pp. 113–131, March 2001.

181. Armstrong, A. and et al., "SP1049C as first-line therapy in advanced (inoperable or metastatic) adenocarcinoma of the oesophagus: A phase II window study", *Journal of Clinical Oncology*, Vol. 24, No. 18s, p. Abstract 4080, 2006.

182. Mukai, H., K. Kato, T. Esaki, S. Ohsumi, Y. Hozomi, N. Matsubara, T. Hamaguchi, Y. Matsumura, R. Goda, T. Hirai, and Y. Nambu, "Phase I study of NK105, a nanomicellar paclitaxel formulation, administered on a weekly schedule in patients with solid tumors", *Invest. New Drugs*, Vol. 34, No. 6, pp. 750–759, December 2016.

183. Kato, K., K. Chin, T. Yoshikawa, K. Yamaguchi, Y. Tsuji, T. Esaki, K. Sakai, M. Kimura, T. Hamaguchi, Y. Shimada, Y. Matsumura, and R. Ikeda, "Phase II study of NK105, a paclitaxel-incorporating micellar nanoparticle, for previously treated advanced or recurrent gastric cancer", *Invest. New Drugs*, Vol. 30, No. 4, pp. 1621–1627, August 2012.

184. Plummer, R., R. H. Wilson, H. Calvert, A. V Boddy, M. Griffin, J. Sludden, M. J. Tilby, M. Eatock, D. G. Pearson, C. J. Ottley, Y. Matsumura, K. Kataoka, and T. Nishiya, "A Phase I clinical study of cisplatin-incorporated polymeric micelles (NC-6004) in patients with solid tumours", *British Journal of Cancer*, Vol. 104, No. 4, pp. 593–598, February 2011.

185. Sumer Bolu, B., E. Manavoglu Gecici, and R. Sanyal, "Combretastatin A-4

Conjugated Antiangiogenic Micellar Drug Delivery Systems Using Dendron–Polymer Conjugates", *Molecular Pharmaceutics*, Vol. 13, No. 5, pp. 1482–1490, May 2016.

186. Lu, Y. and K. Park, "Polymeric micelles and alternative nanonized delivery vehicles for poorly soluble drugs", *International Journal of Pharmaceutics*, Vol. 453, No. 1, pp. 198–214, August 2013.

187. Ahmad, Z., A. Shah, M. Siddiq, and H.-B. Kraatz, "Polymeric micelles as drug delivery vehicles", *RSC Advanced*, Vol. 4, No. 33, p. 17028, 2014.

188. Xiong, X.-B., A. Falamarzian, S. M. Garg, and A. Lavasanifar, "Engineering of amphiphilic block copolymers for polymeric micellar drug and gene delivery", *Journal of Controlled Release*, Vol. 155, No. 2, pp. 248–261, October 2011.

189. Nagarajan, R., M. Barry, and E. Ruckenstein, "Unusual selectivity in solubilization by block copolymer micelles", *Langmuir*, Vol. 2, No. 2, pp. 210–215, March 1986.

190. Patel, S. K., A. Lavasanifar, and P. Choi, "Roles of Nonpolar and Polar Intermolecular Interactions in the Improvement of the Drug Loading Capacity of PEO-b -PCL with Increasing PCL Content for Two Hydrophobic Cucurbitacin Drugs", *Biomacromolecules*, Vol. 10, No. 9, pp. 2584–2591, September 2009.

191. Shuai, X., H. Ai, N. Nasongkla, S. Kim, and J. Gao, "Micellar carriers based on block copolymers of poly(ε-caprolactone) and poly(ethylene glycol) for doxorubicin delivery", *Journal of Controlled Release*, Vol. 98, No. 3, pp. 415–426, August 2004.

192. Falamarzian, A. and A. Lavasanifar, "Optimization of the hydrophobic domain in poly(ethylene oxide)-poly(ε-caprolactone) based nano-carriers for the solubilization and delivery of Amphotericin B", *Colloids Surfaces B Biointerfaces*, Vol. 81, No. 1, pp. 313–320, November 2010.

193. Lavasanifar, A., J. Samuel, S. Sattari, and G. S. Kwon, "Block Copolymer Micelles for the Encapsulation and Delivery of Amphotericin B", *Pharmaceutical Research*, Vol. 19, No. 4, pp. 418–422, 2002.

194. Scripture, C. D. and W. D. Figg, "Drug interactions in cancer therapy", *Nature Reviews Cancer*, Vol. 6, No. 7, pp. 546–558, July 2006.

195. Vicent, M. J., F. Greco, R. I. Nicholson, A. Paul, P. C. Griffiths, and R. Duncan, "Polymer Therapeutics Designed for a Combination Therapy of Hormone-

Dependent Cancer", *Angewante Chemie*, Vol. 117, No. 26, pp. 4129–4134, June 2005.

196. Bae, Y., T. A. Diezi, A. Zhao, and G. S. Kwon, "Mixed polymeric micelles for combination cancer chemotherapy through the concurrent delivery of multiple chemotherapeutic agents", *Journal of Controlled Release*, Vol. 122, No. 3, pp. 324–330, October 2007.

197. Yoo, H. S. and T. G. Park, "Biodegradable polymeric micelles composed of doxorubicin conjugated PLGA–PEG block copolymer", *Journal of Controlled Release*, Vol. 70, No. 1–2, pp. 63–70, January 2001.

198. Yamamoto, Y., K. Yasugi, A. Harada, Y. Nagasaki, and K. Kataoka, "Temperature-related change in the properties relevant to drug delivery of poly(ethylene glycol)-poly(D,L-lactide) block copolymer micelles in aqueous milieu.", *Journal of Controlled Release*, Vol. 82, No. 2–3, pp. 359–71, August 2002.

199. La, S. B., T. Okano, and K. Kataoka, "Preparation and characterization of the micelle-forming polymeric drug indomethacin-incorporated poly(ethylene oxide)-poly(beta-benzyl L-aspartate) block copolymer micelles.", *Journal of Pharmaceutical Sciences*, Vol. 85, No. 1, pp. 85–90, January 1996.

200. Lavasanifar, A., J. Samuel, and G. S. Kwon, "The effect of alkyl core structure on micellar properties of poly(ethylene oxide)-block-poly(l-aspartamide) derivatives", *Colloids Surfaces B Biointerfaces*, Vol. 22, No. 2, pp. 115–126, October 2001.

201. Mahmud, A., X.-B. Xiong, and A. Lavasanifar, "Novel Self-Associating Poly(ethylene oxide)- b lock -poly(ε-caprolactone) Block Copolymers with Functional Side Groups on the Polyester Block for Drug Delivery", *Macromolecules*, Vol. 39, No. 26, pp. 9419–9428, December 2006.

202. Cabral, H. and K. Kataoka, "Progress of drug-loaded polymeric micelles into clinical studies", *Journal of Controlled Release*, Vol. 190, pp. 465–476, September 2014.

203. Oba, M., K. Miyata, K. Osada, R. J. Christie, M. Sanjoh, W. Li, S. Fukushima, T. Ishii, M. R. Kano, N. Nishiyama, H. Koyama, and K. Kataoka, "Polyplex micelles prepared from ω-cholesteryl PEG-polycation block copolymers for systemic gene delivery", *Biomaterials*, Vol. 32, No. 2, pp. 652–663, 2011.

204. Kanayama, N., S. Fukushima, N. Nishiyama, K. Itaka, W.-D. Jang, K. Miyata, Y. Yamasaki, U. Chung, and K. Kataoka, "A PEG-Based Biocompatible Block Catiomer with High Buffering Capacity for the Construction of Polyplex Micelles Showing Efficient Gene Transfer toward Primary Cells", *ChemMedChem*, Vol. 1, No. 4, pp. 439–444, April 2006.

205. Christie, R. J., Y. Matsumoto, K. Miyata, T. Nomoto, S. Fukushima, K. Osada, J. Halnaut, F. Pittella, H. J. Kim, N. Nishiyama, and K. Kataoka, "Targeted Polymeric Micelles for siRNA Treatment of Experimental Cancer by Intravenous Injection", *ACS Nano*, Vol. 6, No. 6, pp. 5174–5189, June 2012.

206. Jiang Hi, B. Qi, M. Lepage, and Y. Zhao, "Polymer Micelles Stabilization on Demand through Reversible Photo-Cross-Linking", *Macromolecules*, Vol. 40, No. 4, pp. 790–792, February 2007.

207. Meng, F., W. E. Hennink, and Z. Zhong, "Reduction-sensitive polymers and bioconjugates for biomedical applications", *Biomaterials*, Vol. 30, No. 12. pp. 2180–2198, 2009.

208. Yoo, H. S., E. A. Lee, and T. G. Park, "Doxorubicin-conjugated biodegradable polymeric micelles having acid-cleavable linkages", *Journal of Controlled Release*, Vol. 82, No. 1, pp. 17–27, July 2002.

209. Li, Y. and G. S. Kwon, "Methotrexate Esters of Poly(Ethylene Oxide)-Block-Poly(2-Hydroxyethyl-L-Aspartamide). Part I: Effects of the Level of Methotrexate Conjugation on the Stability of Micelles and on Drug Release", *Pharmaceutical Research*, Vol. 17, No. 5, pp. 607–611, 2000.

210. Elizabeth R. Gillies, and Thomas B. Jonsson, and J. M. J. Fréchet, "Stimuli-Responsive Supramolecular Assemblies of Linear-Dendritic Copolymers", 2004.

211. Hamaguchi, T., Y. Matsumura, M. Suzuki, K. Shimizu, R. Goda, I. Nakamura, I. Nakatomi, M. Yokoyama, K. Kataoka, and T. Kakizoe, "NK105, a paclitaxel-incorporating micellar nanoparticle formulation, can extend in vivo antitumour activity and reduce the neurotoxicity of paclitaxel", *British Journal of Cancer*, Vol. 92, No. 7, pp. 1240–1246, April 2005.

212. Allen, T. M., "Drug Delivery Systems: Entering the Mainstream", *Science* ., Vol. 303, No. 5665, pp. 1818–1822, March 2004.

213. Bütün, V., X.-S. Wang, M. V. de Paz Báñez, K. L. Robinson, N. C. Billingham, S. P. Armes, and Z. Tuzar, "Synthesis of Shell Cross-Linked Micelles at High Solids in Aqueous Media", *Macromolecules*, Vol. 33, No. 1, pp. 1–3, January 2000.

214. Takae, S., K. Miyata, M. Oba, T. Ishii, N. Nishiyama, K. Itaka, Y. Yamasaki, H. Koyama, and K. Kataoka, "PEG-Detachable Polyplex Micelles Based on Disulfide-Linked Block Catiomers as Bioresponsive Nonviral Gene Vectors", *Journal of the American Chemical Society*, Vol. 130, No. 18, pp. 6001–6009, May 2008.

215. Wang, K., Y. Liu, W.-J. Yi, C. Li, Y.-Y. Li, R.-X. Zhuo, and X.-Z. Zhang, "Novel shell-cross-linked micelles with detachable PEG corona for glutathione-mediated intracellular drug delivery", *Soft Matter*, Vol. 9, No. 3, pp. 692–699, 2013.

216. Oh, K. T., Y. T. Oh, N.-M. Oh, K. Kim, D. H. Lee, and E. S. Lee, "A smart flower-like polymeric micelle for pH-triggered anticancer drug release", *International Journal of Pharmaceutics*, Vol. 375, No. 1–2, pp. 163–169, Jun. 2009.

217. Tominaga, Y., M. Mizuse, A. Hashidzume, Y. Morishima, and T. Sato, "Flower micelle of amphiphilic random copolymers in aqueous media.", *The Journal of Physical Chemistry B*, Vol. 114, pp. 11403–11408, 2010.

218. Van Butsele, K., S. Cajot, S. Van Vlierberghe, P. Dubruel, C. Passirani, J.-P. Benoit, R. Jérôme, and C. Jérôme, "pH-Responsive Flower-Type Micelles Formed by a Biotinylated Poly(2-vinylpyridine)- block -poly(ethylene oxide)- block -poly(ε -caprolactone) Triblock Copolymer", *Advanced Functional Materials*, Vol. 19, pp. 1416–1425, 2009.

219. Lee, E. S., K. T. Oh, D. Kim, Y. S. Youn, and Y. H. Bae, "Tumor pH-responsive flower-like micelles of poly(l-lactic acid)-b-poly(ethylene glycol)-b-poly(l-histidine)", *Journal of Controlled Release*, Vol. 123, No. 1, pp. 19–26, October 2007.

220. Yamamoto, Y., Y. Nagasaki, Y. Kato, Y. Sugiyama, and K. Kataoka, "Long-circulating poly(ethylene glycol)–poly(d,l-lactide) block copolymer micelles with modulated surface charge", *Journal of Controlled Release*, Vol. 77, No. 1–2, pp. 27–38, November 2001.

221. Oh, K. T., D. Kim, H. H. You, Y. S. Ahn, and E. S. Lee, "pH-sensitive properties of surface charge-switched multifunctional polymeric micelle", *International Journal*

of Pharmacology, Vol. 376, No. 1–2, pp. 134–140, July 2009.

222. Logie, J., S. C. Owen, C. K. McLaughlin, and M. S. Shoichet, "PEG-Graft Density Controls Polymeric Nanoparticle Micelle Stability", *Chemistry of Materials*, Vol. 26, No. 9, pp. 2847–2855, May 2014.

223. Gillies, E. and J. Frechet, "Dendrimers and dendritic polymers in drug delivery", *Drug Discovery Today*, Vol. 10, No. 1, pp. 35–43, January 2005.

224. Medina, S. H. and M. E. H. El-Sayed, "Dendrimers as carriers for delivery of chemotherapeutic agents.", *Chemical Reviews*, Vol. 109, No. 7, pp. 3141–57, July 2009.

225. Zeng, F. and S. C. Zimmerman, "Dendrimers in Supramolecular Chemistry: From Molecular Recognition to Self-Assembly", *Chemical Reviews*, Vol. 97, No. 5, pp. 1681–1712, Augugust 1997.

226. Patri, A. K., I. J. Majoros, and J. R. Baker, "Dendritic polymer macromolecular carriers for drug delivery", *Current Opinions in Chemistry & Biology*, Vol. 6, No. 4, pp. 466–471, August 2002.

227. Newkome, G. R., C. N. Moorefield, G. R. Baker, M. J. Saunders, and S. H. Grossman, "Unimolecular Micelles", *Angewante Chemie International Ed. English*, Vol. 30, No. 9, pp. 1178–1180, September 1991.

228. Newkome, G. R., X. Lin, and C. D. Weis, "Polytryptophane terminated dendritic macromolecules", *Tetrahedron: Asymmetry*, Vol. 2, No. 10, pp. 957–960, January 1991.

229. El Sayed, M., M. F. Kiani, M. D. Naimark, A. H. Hikal, and H. Ghandehari, "Extravasation of Poly(amidoamine) (pamam) Dendrimers Across Microvascular Network Endothelium", *Pharmaceutical Research*, Vol. 18, No. 1, pp. 23–28, 2001.

230. Wiwattanapatapee, R., B. Carreño-Gómez, N. Malik, and R. Duncan, "Anionic PAMAM Dendrimers Rapidly Cross Adult Rat Intestine In Vitro: A Potential Oral Delivery System?", *Pharmaceutical Research*, Vol. 17, No. 8, pp. 991–998, 2000.

231. Watkins, D. M., Y.Sayed-Sweet, J. W. Klimash, N. J. Turro, and D. A. Tomalia, "Dendrimers with Hydrophobic Cores and the Formation of Supramolecular Dendrimer−Surfactant Assemblies", *Langmuir*, Vol. 13, No. 12, pp. 3136–3141, June 1997.

232. Malik, N., R. Wiwattanapatapee, R. Klopsch, K. Lorenz, H. Frey, J. Weener, E. Meijer, W. Paulus, and R. Duncan, "Dendrimers: Relationship between structure and biocompatibility in vitro, and preliminary studies on the biodistribution of 125I-labelled polyamidoamine dendrimers in vivo", *Journal of Controlled Release*, Vol. 65, No. 1–2, pp. 133–148, March 2000.

233. Yang, H., J. J. Morris, and S. T. Lopina, "Polyethylene glycol–polyamidoamine dendritic micelle as solubility enhancer and the effect of the length of polyethylene glycol arms on the solubility of pyrene in water", *Journal of Colloid Interface Science*, Vol. 273, No. 1, pp. 148–154, May 2004.

234. Woller, E. K., E. D. Walter, J. R. Morgan, D. J. Singel, and M. J. Cloninger, "Altering the Strength of Lectin Binding Interactions and Controlling the Amount of Lectin Clustering Using Mannose/Hydroxyl-Functionalized Dendrimers", *Journal of the American Chemical Society*, Vol. 125, No. 29, pp. 8820–8826, Jul. 2003.

235. Sideratou, Z., D. Tsiourvas, and C. M. Paleos, "Quaternized Poly(propylene imine) Dendrimers as Novel pH-Sensitive Controlled-Release Systems", *Langmuir*, Vol. 16, No. 4, pp. 1766–1769, Feb. 2000.

236. Sideratou, Z., D. Tsiourvas, and C. M. Paleos, "Solubilization and Release Properties of PEGylated Diaminobutane Poly(propylene imine) Dendrimers", *Journal of Colloid Interface Science*, Vol. 242, No. 1, pp. 272–276, October 2001.

237. Paleos, C. M., D. Tsiourvas, Z. Sideratou, and L. Tziveleka, "Acid- and Salt-Triggered Multifunctional Poly(propylene imine) Dendrimer as a Prospective Drug Delivery System", *Biomacromolecules*, Vol. 5, No. 2, pp. 524–529, Mar. 2004.

238. Liu, M., K. Kono, and J. M. J. Frechet, "Water-soluble dendrimer-poly(ethylene glycol) starlike conjugates as potential drug carriers", *Journal of Polymers Science Part A Polymer Chemistry*, Vol. 37, No. 17, pp. 3492–3503, September 1999.

239. Liu, M., K. Kono, and J. M. . Fréchet, "Water-soluble dendritic unimolecular micelles", *Journal of Controlled Release*, Vol. 65, No. 1–2, pp. 121–131, March 2000.

240. Gillies, E. R. and J. M. . Fréchet, "Dendrimers and dendritic polymers in drug delivery", *Drug Discovery Today*, Vol. 10, No. 1, pp. 35–43, January 2005.

241. Bezouška, K., "Design, functional evaluation and biomedical applications of

carbohydrate dendrimers (glycodendrimers)", *Reviews Molecular Biotechnology*, Vol. 90, No. 3–4, pp. 269–290, May 2002.

242. Grayson, S. M., M. Jayaraman, J. M. J. Fréchet, J. G. Verkade, E. Gianasi, J. Strohalm, and R. Duncan, "Convergent synthesis and 'surface' functionalization of a dendritic analog of poly(ethylene glycol)", *Chemical Communications*, Vol. 112, No. 14, pp. 1329–1330, 1999.

243. Henrik R. Ihre, Omayra L. Padilla De Jesús, J., and Francis C. Szoka, and Jean M. J. Fréchet, "Polyester Dendritic Systems for Drug Delivery Applications: Design, Synthesis, and Characterization", 2002.

244. Grinstaff, M. W., "Biodendrimers: New Polymeric Biomaterials for Tissue Engineering", *Chemistry - A European Journal*, Vol. 8, No. 13, p. 2838, July 2002.

245. Padilla De Jesús, O. L., H. R. Ihre, L. Gagne, J. M. J. Fréchet, and F. C. Szoka, "Polyester Dendritic Systems for Drug Delivery Applications: In Vitro and In Vivo Evaluation", *Bioconjugate Chemistry*, Vol. 13, No. 3, pp. 453–461, May 2002.

246. Elizabeth R. Gillies, and Thomas B. Jonsson, and J. M. J. Fréchet, "Stimuli-Responsive Supramolecular Assemblies of Linear-Dendritic Copolymers", 2004.

247. Gillies, E. R. and J. M. J. Fréchet, "Designing Macromolecules for Therapeutic Applications: Polyester DendrimerPoly(ethylene oxide) "Bow-Tie" Hybrids with Tunable Molecular Weight and Architecture", *Journal of the American Chemical Society*, Vol. 124, No. 47, pp. 14137–14146, November 2002.

248. Lee, C. C., S. M. Grayson, and J. M. J. Fréchet, "Synthesis of narrow-polydispersity degradable dendronized aliphatic polyesters", *Journal of Polymers Science Part A Polymer Chemistry*, Vol. 42, No. 14, pp. 3563–3578, July 2004.

249. Svenson, S. and D. A. Tomalia, "Dendrimers in biomedical applications—reflections on the field", *Advanced Drug Delivery Reviews*, Vol. 64, pp. 102–115, December 2012.

250. Poon, Z., J. A. Lee, S. Huang, R. J. Prevost, and P. T. Hammond, "Highly stable, ligand-clustered "patchy" micelle nanocarriers for systemic tumor targeting", *Nanomedicine Nanotechnology, Biology Medicine*, Vol. 7, No. 2, pp. 201–209, April 2011.

251. Wang, W., D. Cheng, F. Gong, X. Miao, and X. Shuai, "Design of Multifunctional

Micelle for Tumor-Targeted Intracellular Drug Release and Fluorescent Imaging", *Advanced Materials*, Vol. 24, No. 1, pp. 115–120, January 2012.

252. Carmeliet, P., "Mechanisms of angiogenesis and arteriogenesis", *Nature Medicine*, Vol. 6, No. 4, pp. 389–395, April 2000.

253. Naumov, G. N., L. A. Akslen, and J. Folkman, "Role of Angiogenesis in Human Tumor Dormancy: Animal Models of the Angiogenic Switch", *Cell Cycle*, Vol. 5, No. 16, pp. 1779–1787, August 2006.

254. Switala-Jelen, K., K. Dabrowska, A. Opolski, L. Lipinska, M. Nowaczyk, and A. Gorski, "The Biological Functions of β3 Integrins", *Folia Biology (Praha).*, Vol. 50, No. 5, pp. 143–52, 2004.

255. Danhier, F., A. Le Breton, and V. Préat, "RGD-Based Strategies To Target Alpha(v) Beta(3) Integrin in Cancer Therapy and Diagnosis", *Molecular Pharmaceutics*, Vol. 9, No. 11, pp. 2961–2973, November 2012.

256. Tang, X., S. Zhou, X. Tao, J. Wang, F. Wang, and Y. Liang, "Targeted delivery of docetaxel via Pi-Pi stacking stabilized dendritic polymeric micelles for enhanced therapy of liver cancer", *Materials Science and Engineering C*, Vol. 75, pp. 1042–1048, June 2017.

257. Li, A., Y. Zheng, G. Liu, W. Liu, P. Cao, and Z. Bu, "Efficient delivery of docetaxel for the treatment of brain tumors by cyclic RGD-tagged polymeric micelles", *Molecular Medicine Reports*, Vol. 11, No. 4, pp. 3078–3086, November 2014.

258. Yarden, Y., "Biology of HER2 and its importance in breast cancer.", *Oncology*, Vol. 61 Suppl 2, No. suppl 2, pp. 1–13, 2001.

259. Tai, W., R. Mahato, and K. Cheng, "The role of HER2 in cancer therapy and targeted drug delivery", *Journal of Controlled Release*, Vol. 146, No. 3, pp. 264–275, September 2010.

260. Ravetch, J. V., R. A. Clynes, T. L. Towers, and L. G. Presta, "Inhibitory Fc receptors modulate in vivo cytoxicity against tumortargets", *Nature Medicine*, Vol. 6, No. 4, pp. 443–446, April 2000.

261. Hudis, C. A., "Trastuzumab — Mechanism of Action and Use in Clinical Practice", *New England Journal of Medicine*, Vol. 357, No. 1, pp. 39–51, 2007.

262. Lee, A. L. Z., Y. Wang, H. Y. Cheng, S. Pervaiz, and Y. Y. Yang, "The co-delivery of paclitaxel and Herceptin using cationic micellar nanoparticles", *Biomaterials*, Vol. 30, No. 5, pp. 919–927, February 2009.

263. Zhao, J., Y. Mi, and S.-S. Feng, "Targeted co-delivery of docetaxel and siPlk1 by herceptin-conjugated vitamin E TPGS based immunomicelles", *Biomaterials*, Vol. 34, No. 13, pp. 3411–3421, April 2013.

264. Zhou, Z., A. Badkas, M. Stevenson, J.-Y. Lee, and Y.-K. Leung, "Herceptin conjugated PLGA-PHis-PEG pH sensitive nanoparticles for targeted and controlled drug delivery", *International Journal of Pharmaceutics*, Vol. 487, No. 1–2, pp. 81–90, June 2015.

265. Duncan, R. and R. Gaspar, "Nanomedicine(s) under the microscope.", *Molecular Pharmaceutics*, Vol. 8, No. 6, pp. 2101–41, December 2011.

266. Kopeček, J., "Biomaterials and Drug Delivery: Past, Present, and Future", *Molecular Pharmaceutics*, Vol. 7, No. 4, pp. 922–925, August 2010.

267. Iyer, A. K., Z. Duan, and M. M. Amiji, "Nanodelivery systems for nucleic acid therapeutics in drug resistant tumors.", *Molecular Pharmaceutics*, Vol. 11, No. 8, pp. 2511–26, August 2014.

268. Larson, N. and H. Ghandehari, "Polymeric conjugates for drug delivery", *Chemistry of Materials*, Vol. 24, No. 5, pp. 840–853, March 2012.

269. Brannon-Peppas, L. and J. O. Blanchette, "Nanoparticle and targeted systems for cancer therapy", *Advanced Drug Delivery Reviews*, Vol. 64, pp. 206–212, December 2012.

270. Duncan, R. and S. C. W. Richardson, "Endocytosis and Intracellular Trafficking as Gateways for Nanomedicine Delivery: Opportunities and Challenges", *Molecular Pharmaceutics*, Vol. 9, No. 9, pp. 2380–2402, September 2012.

271. Kitchens, K. M., R. B. Kolhatkar, P. W. Swaan, and H. Ghandehari, "Endocytosis inhibitors prevent poly(amidoamine) dendrimer internalization and permeability across Caco-2 cells.", *Molecular Pharmaceutics*, Vol. 5, No. 2, pp. 364–9, January 2008.

272. Ganta, S., H. Devalapally, A. Shahiwala, and M. Amiji, "A review of stimuli-responsive nanocarriers for drug and gene delivery.", *Journal of Controlled Release*,

Vol. 126, No. 3, pp. 187–204, March 2008.

273. Iversen, T.-G., T. Skotland, and K. Sandvig, "Endocytosis and intracellular transport of nanoparticles: Present knowledge and need for future studies", *Nano Today*, Vol. 6, No. 2, pp. 176–185, April 2011.

274. Brigger, I., C. Dubernet, and P. Couvreur, "Nanoparticles in cancer therapy and diagnosis", *Advanced Drug Delivery Reviews*, Vol. 54, No. 5, pp. 631–651, September 2002.

275. Matsumura, Y. and H. Maeda, "A New Concept for Macromolecular Therapeutics in Cancer Chemotherapy: Mechanism of Tumoritropic Accumulation of Proteins and the Antitumor Agent Smancs", *Cancer Research*, Vol. 46, No. 12_Part_1, pp. 6387–6392, December 1986.

276. Choi, H. S., W. Liu, P. Misra, E. Tanaka, J. P. Zimmer, B. Itty Ipe, M. G. Bawendi, and J. V Frangioni, "Renal clearance of quantum dots.", *Nature Biotechnology*, Vol. 25, No. 10, pp. 1165–70, October 2007.

277. Allen, T. M. and P. R. Cullis, "Drug delivery systems: entering the mainstream.", *Science*, Vol. 303, No. 5665, pp. 1818–22, March 2004.

278. Binauld, S. and M. H. Stenzel, "Acid-degradable polymers for drug delivery: a decade of innovation.", *Chemical Communications (Cambrigde).*, Vol. 49, No. 21, pp. 2082–102, March 2013.

279. Miyata, K., R. J. Christie, and K. Kataoka, "Polymeric micelles for nano-scale drug delivery", *Reatcive Functional Polymers*, Vol. 71, No. 3, pp. 227–234, March 2011.

280. Xiong, X.-B., Z. Binkhathlan, O. Molavi, and A. Lavasanifar, "Amphiphilic block co-polymers: Preparation and application in nanodrug and gene delivery", *Acta Biomaterials*, Vol. 8, No. 6, pp. 2017–2033, 2012.

281. Gheybi, H. and M. Adeli, "Supramolecular anticancer drug delivery systems based on linear–dendritic copolymers", *Polymer Chemistry*, Vol. 6, No. 14, pp. 2580–2615, March 2015.

282. Gillies, E. R., T. B. Jonsson, and J. M. J. Fréchet, "Stimuli-Responsive Supramolecular Assemblies of Linear-Dendritic Copolymers", *Journal of the American Chemical Society*, Vol. 126, No. 38, pp. 11936–11943, September 2004.

283. Tyagi, R., S. Malhotra, A. F. Thünemann, A. Sedighi, M. Weber, A. Schäfer, and R. Haag, "Investigations of Host–Guest Interactions with Shape-Persistent Nonionic Dendritic Micelles", *The Journal of Physical Chemistry C*, Vol. 117, No. 23, pp. 12307–12317, June 2013.

284. Oelker, A. M., J. A. Berlin, M. Wathier, and M. W. Grinstaff, "Synthesis and characterization of dendron cross-linked PEG hydrogels as corneal adhesives.", *Biomacromolecules*, Vol. 12, No. 5, pp. 1658–65, May 2011.

285. Lundberg, P., M. V. Walter, M. I. Montañez, D. Hult, A. Hult, A. Nyström, and M. Malkoch, "Linear dendritic polymeric amphiphiles with intrinsic biocompatibility: synthesis and characterization to fabrication of micelles and honeycomb membranes", *Polymer Chemistry*, Vol. 2, No. 2, pp. 394–402, January 2011.

286. Gong, J., M. Chen, Y. Zheng, S. Wang, and Y. Wang, "Polymeric micelles drug delivery system in oncology.", *Journal of Controlled Release*, Vol. 159, No. 3, pp. 312–23, May 2012.

287. Griggs, J., J. C. Metcalfe, and R. Hesketh, "Targeting tumour vasculature: the development of combretastatin A4.", *The Lancet Oncology*, Vol. 2, No. 2, pp. 82–7, February 2001.

288. Gaukroger, K., J. Hadfield, L. Hepworth, N. J. Lawrence, and A. T. McGown, "Novel syntheses of cis and trans isomers of combretastatin A-4", *Journal of Organic Chemistry*, Vol. 66, No. 24, pp. 8135–8138, 2001.

289. Altin, H., I. Kosif, and R. Sanyal, "Fabrication of “Clickable” Hydrogels via Dendron Polymer Conjugates", *Macromolecules*, pp. 3801–3808, 2010.

290. Cammas, S., T. Matsumoto, T. Okano, Y. Sakurai, and K. Kataoka, "Design of functional polymeric micelles as site-specific drug vehicles based on poly (a-hydroxy ethylene oxide-co-p-benzyl L-aspartate) block copolymers", *Materials Science and Engineering C*, Vol. 4, No. 97, pp. 241–247, 1997.

291. Arnaoutova, I. and H. K. Kleinman, "In vitro angiogenesis: endothelial cell tube formation on gelled basement membrane extract.", *Nature Protocols*, Vol. 5, No. 4, pp. 628–635, 2010.

292. Turro, N. J. and P. Kuo, "Pyrene Excimer Formation in Micelles of Nonionic Detergents and of Water-Soluble Polymers", *Langmuir*, No. 6, pp. 438–442, 1986.

293. Bae, J. W., R. M. Pearson, N. Patra, S. Sunoqrot, L. Vuković, P. Král, and S. Hong, "Dendron-mediated self-assembly of highly PEGylated block copolymers: a modular nanocarrier platform.", *Chemical Communications*, Vol. 47, No. 37, pp. 10302–10304, October 2011.

294. Cabral, H., Y. Matsumoto, K. Mizuno, Q. Chen, M. Murakami, M. Kimura, Y. Terada, M. R. Kano, K. Miyazono, M. Uesaka, N. Nishiyama, and K. Kataoka, "Accumulation of sub-100 nm polymeric micelles in poorly permeable tumours depends on size", *Nature Nanotechnology*, Vol. 6, No. 12, pp. 1–9, December 2011.

295. Yoo, H. S., K. H. Lee, J. E. Oh, and T. G. Park, "In vitro and in vivo anti-tumor activities of nanoparticles based on doxorubicin–PLGA conjugates", *Journal of Controlled Release*, Vol. 68, No. 3, pp. 419–431, September 2000.

296. Iyer, A. K., G. Khaled, J. Fang, and H. Maeda, "Exploiting the enhanced permeability and retention effect for tumor targeting.", *Drug Discovery Today*, Vol. 11, No. 17–18, pp. 812–8, September 2006.

297. Gurunathan, S., K.-J. Lee, K. Kalishwaralal, S. Sheikpranbabu, R. Vaidyanathan, and S. H. Eom, "Antiangiogenic properties of silver nanoparticles.", *Biomaterials*, Vol. 30, No. 31, pp. 6341–50, October 2009.

298. Koziara, J. M., T. R. Whisman, M. T. Tseng, and R. J. Mumper, "In-vivo efficacy of novel paclitaxel nanoparticles in paclitaxel-resistant human colorectal tumors.", *Journal of Controlled Release*, Vol. 112, No. 3, pp. 312–9, May 2006.

299. Larson, N. and H. Ghandehari, "Polymeric Conjugates for Drug Delivery", *Chemistry of Materials*, Vol. 24, No. 5, pp. 840–853, March 2012.

300. Gelderblom, H., J. Verweij, K. Nooter, and A. Sparreboom, "Cremophor EL; the drawbacks and advantages of vehicle selection for drug formulation", *European Journal of Cancer*, Vol. 37, No. 13, pp. 1590–1598, September 2001.

301. Tyrrell, Z. L., Y. Shen, and M. Radosz, "Fabrication of micellar nanoparticles for drug delivery through the self-assembly of block copolymers", *Progressive Polymers Science*, Vol. 35, No. 9, pp. 1128–1143, September 2010.

302. Seow, W. Y., J. M. Xue, and Y.-Y. Yang, "Targeted and intracellular delivery of paclitaxel using multi-functional polymeric micelles.", *Biomaterials*, Vol. 28, pp. 1730–1740, 2007.

303. Yang, T., Y. Wang, Z. Li, W. Dai, J. Yin, L. Liang, X. Ying, S. Zhou, J. Wang, X. Zhang, and Q. Zhang, "Targeted delivery of a combination therapy consisting of combretastatin A4 and low-dose doxorubicin against tumor neovasculature.", *Nanomedicine*, Vol. 8, No. 1, pp. 81–92, January 2012.

304. Ke, X.-Y., V. W. Lin Ng, S.-J. Gao, Y. W. Tong, J. L. Hedrick, and Y. Y. Yang, "Co-delivery of thioridazine and doxorubicin using polymeric micelles for targeting both cancer cells and cancer stem cells.", *Biomaterials*, Vol. 35, No. 3, pp. 1096–108, January 2014.

305. Hu, C.-M. J., R. H. Fang, B. T. Luk, and L. Zhang, "Polymeric nanotherapeutics: clinical development and advances in stealth functionalization strategies", *Nanoscale*, Vol. 6, No. 1, pp. 65–75, 2014.

306. Moghimi, S. . and H. . Patel, "Serum-mediated recognition of liposomes by phagocytic cells of the reticuloendothelial system – The concept of tissue specificity", *Advanced Drug Delivery Reviews*, Vol. 32, No. 1, pp. 45–60, 1998.

307. Li, J., X. Jiang, Y. Guo, S. An, Y. Kuang, H. Ma, X. He, and C. Jiang, "Linear-Dendritic Copolymer Composed of Polyethylene Glycol and All-trans-Retinoic Acid as Drug Delivery Platform for Paclitaxel against Breast Cancer.", *Bioconjugate Chemistry*, February 2015.

308. Lee, C. C., E. R. Gillies, M. E. Fox, S. J. Guillaudeu, J. M. J. Fréchet, E. E. Dy, and F. C. Szoka, "A single dose of doxorubicin-functionalized bow-tie dendrimer cures mice bearing C-26 colon carcinomas.", *Proceedings of the National Academy of Sciences U. S. A.*, Vol. 103, No. 45, pp. 16649–54, November 2006.

309. Pearson, R. M., S. Sen, H. Hsu, M. Pasko, M. Gaske, P. Král, and S. Hong, "Tuning the Selectivity of Dendron Micelles Through Variations of the Poly(ethylene glycol) Corona", *ACS Nano*, Vol. 10, No. 7, pp. 6905–6914, July 2016.

310. Ackerman, N. B. and P. A. Hechmer, "Studies on the capillary permeability of experimental liver metastases.", *Surgery, Gynecology & Obstetrics*, Vol. 146, No. 6, pp. 884–8, June 1978.

311. Hood, J. D. and D. A. Cheresh, "Role of Integrins in Cell Invasion and Migration", *Nature Reviews Cancer*, Vol. 2, No. 2, pp. 91–100, February 2002.

312. Marelli, U. K., F. Rechenmacher, T. R. A. Sobahi, C. Mas-Moruno, and H. Kessler,

"Tumor Targeting via Integrin Ligands.", *Frontiers in Oncology*, Vol. 3, p. 222, August 2013.

313. Mondal, G., S. Barui, and A. Chaudhuri, "The relationship between the cyclic-RGDfK ligand and αvβ3 integrin receptor", *Biomaterials*, Vol. 34, No. 26, pp. 6249–6260, 2013.

314. McCusker, C. F., P. J. Kocienski, F. T. Boyle, and A. G. Schätzlein, "Solid-phase synthesis of c(RGDfK) derivatives: on-resin cyclisation and lysine functionalisation", *Bioorganic & Medicinal Chemistry Letters*, Vol. 12, No. 4, pp. 547–549, 2002.

315. Wu, P., M. Malkoch, J. N. Hunt, R. Vestberg, E. Kaltgrad, M. G. Finn, V. V. Fokin, K. B. Sharpless, and C. J. Hawker, "Multivalent, bifunctional dendrimers prepared by click chemistry", *Chemical Communications*, Vol. 0, No. 46, p. 5775, December 2005.

316. Goodwin, A. P., J. L. Mynar, Y. Ma, G. R. Fleming, and J. M. J. Fréchet, "Synthetic Micelle Sensitive to IR Light via a Two-Photon Process", *Journal of the American Chemical Society*, Vol. 127, No. 28, pp. 9952–9953, July 2005.

317. Mynar, J. L., A. P. Goodwin, J. A. Cohen, Y. Ma, G. R. Fleming, J. M. J. Fréchet, K. Kataoka, and F. C. Szoka, "Two-photon degradable supramolecular assemblies of linear-dendritic copolymers", *Chemical Communications*, Vol. 47, No. 20, pp. 2081–2082, 2007.

318. Lu, J., S. C. Owen, and M. S. Shoichet, "Stability of Self-Assembled Polymeric Micelles in Serum.", *Macromolecules*, Vol. 44, No. 15, pp. 6002–6008, August 2011.

319. Pilkington-Miksa, M., D. Arosio, L. Battistini, L. Belvisi, M. De Matteo, F. Vasile, P. Burreddu, P. Carta, G. Rassu, P. Perego, N. Carenini, F. Zunino, M. De Cesare, V. Castiglioni, E. Scanziani, C. Scolastico, G. Casiraghi, F. Zanardi, and L. Manzoni, "Design, Synthesis, and Biological Evaluation of Novel cRGD–Paclitaxel Conjugates for Integrin-Assisted Drug Delivery", *Bioconjugate Chemistry*, Vol. 23, No. 8, pp. 1610–1622, August 2012.

320. Gok, O., I. Kosif, T. Dispinar, T. N. Gevrek, R. Sanyal, and A. Sanyal, "Design and Synthesis of Water-Soluble Multifunctionalizable Thiol-Reactive Polymeric

Supports for Cellular Targeting", *Bioconjugate Chemistry*, Vol. 26, No. 8, pp. 1550–1560, August 2015.

321. Carlson, C. B., P. Mowery, R. M. Owen, E. C. Dykhuizen, and L. L. Kiessling, "Selective Tumor Cell Targeting Using Low-Affinity, Multivalent Interactions", *ACS Chemistry & Biology*, Vol. 2, No. 2, pp. 119–127, February 2007.

322. Ogawa, M., N. Kosaka, C. a S. Regino, M. Mitsunaga, P. L. Choyke, and H. Kobayashi, "High sensitivity detection of cancer in vivo using a dual-controlled activation fluorescent imaging probe based on H-dimer formation and pH activation", *Molecular Biosystems*, Vol. 6, No. 5, p. 888, May 2010.

323. Magnifico, A., L. Albano, S. Campaner, D. Delia, F. Castiglioni, P. Gasparini, G. Sozzi, E. Fontanella, S. Menard, and E. Tagliabue, "Tumor-initiating cells of HER2-positive carcinoma cell lines express the highest oncoprotein levels and are sensitive to trastuzumab", *Clinical Cancer Research*, Vol. 15, No. 6, pp. 2010–2021, March 2009.

324. Baselga, J., L. Norton, J. Albanell, Y.-M. Kim, and J. Mendelsohn3, "Recombinant Humanized Anti-HER2 Antibody (Herceptin) Enhances the Antitumor Activity of Paclitaxel and Doxorubicin against HER2/neu Overexpressing Human Breast Cancer Xenografts", *Cancer Research*, Vol. 58, pp. 2825–2831.

325. Scaltriti, M., C. Verma, M. Guzman, J. Jimenez, J. L. Parra, K. Pedersen, D. J. Smith, S. Landolfi, S. Ramon y Cajal, J. Arribas, and J. Baselga, "Lapatinib, a HER2 tyrosine kinase inhibitor, induces stabilization and accumulation of HER2 and potentiates trastuzumab-dependent cell cytotoxicity", *Oncogene*, Vol. 28, No. 6, pp. 803–814, February 2009.

326. Chang, C. J., J. H. Chiu, L. M. Tseng, C. H. Chang, T. M. Chien, C. W. Wu, and W. Y. Lui, "Modulation of HER2 expression by ferulic acid on human breast cancer MCF7 cells", *European Journal of Clinical Investigation*, Vol. 36, No. 8, pp. 588–596, August 2006.

APPENDIX A: ADDITIONAL DATA

Cell viability data, DLS histograms, PBS-GPC spectra, fluorescence intensity data obtained from emisson or excitation spectra are presented in this section.

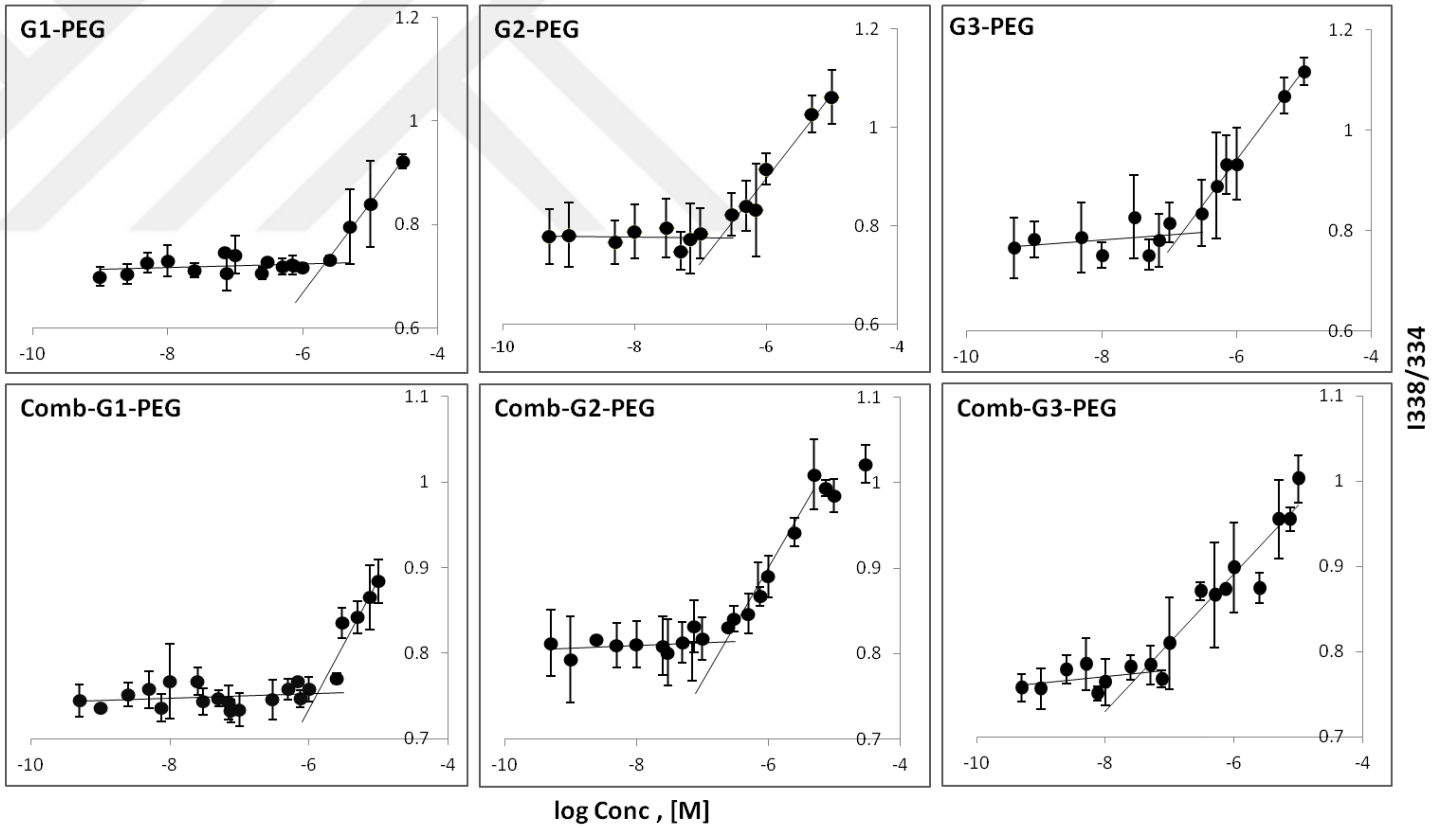

Figure A.1. The I338/334 *vs.* log Concentration graphs for DPD and Comb conjugated DPD micelles.

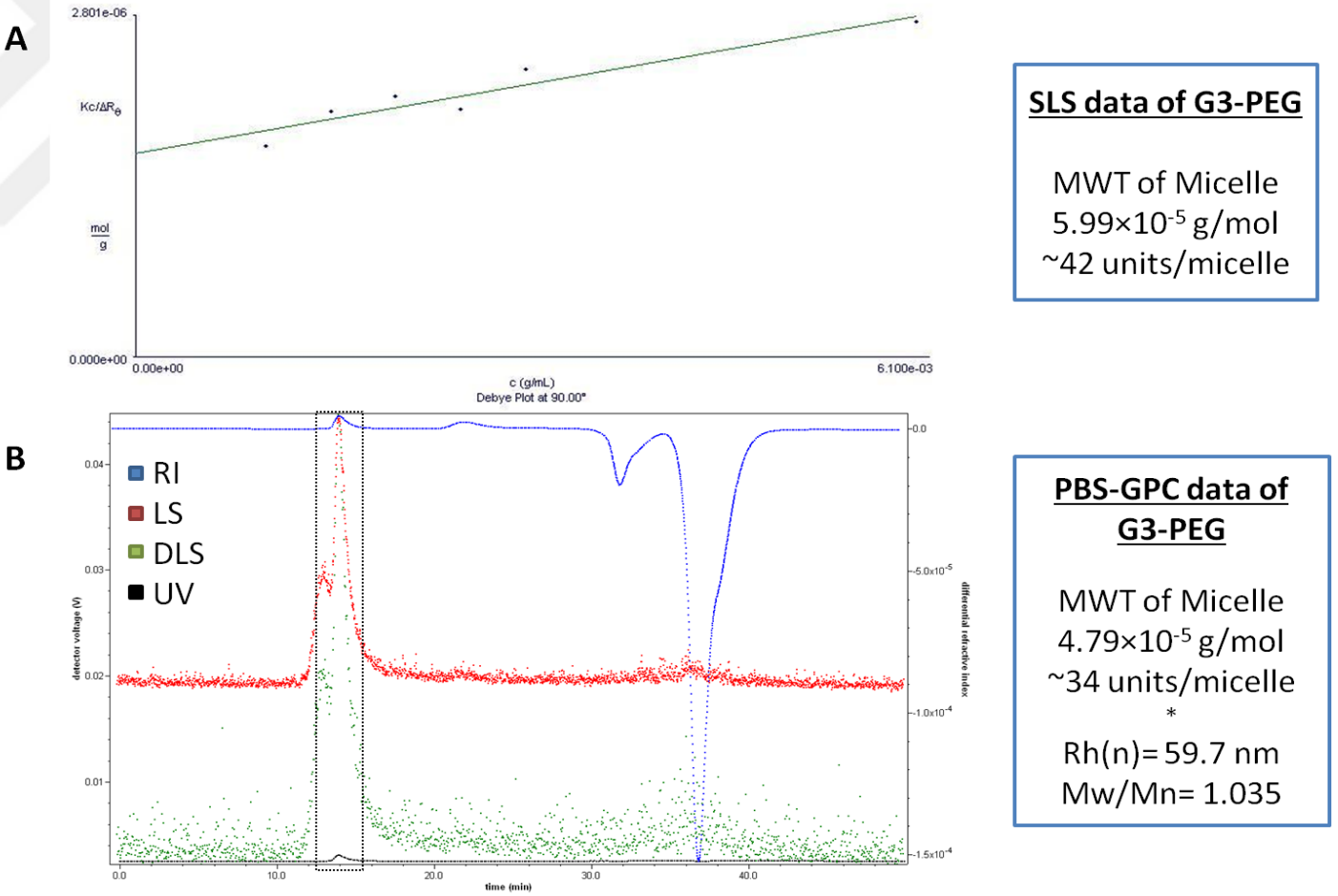

Figure A.2. (A) SLS result of G3-PEG micelles. (B) PBS-GPC results by MALLS and by in flow mode DLS of G3-PEG micelle solution.

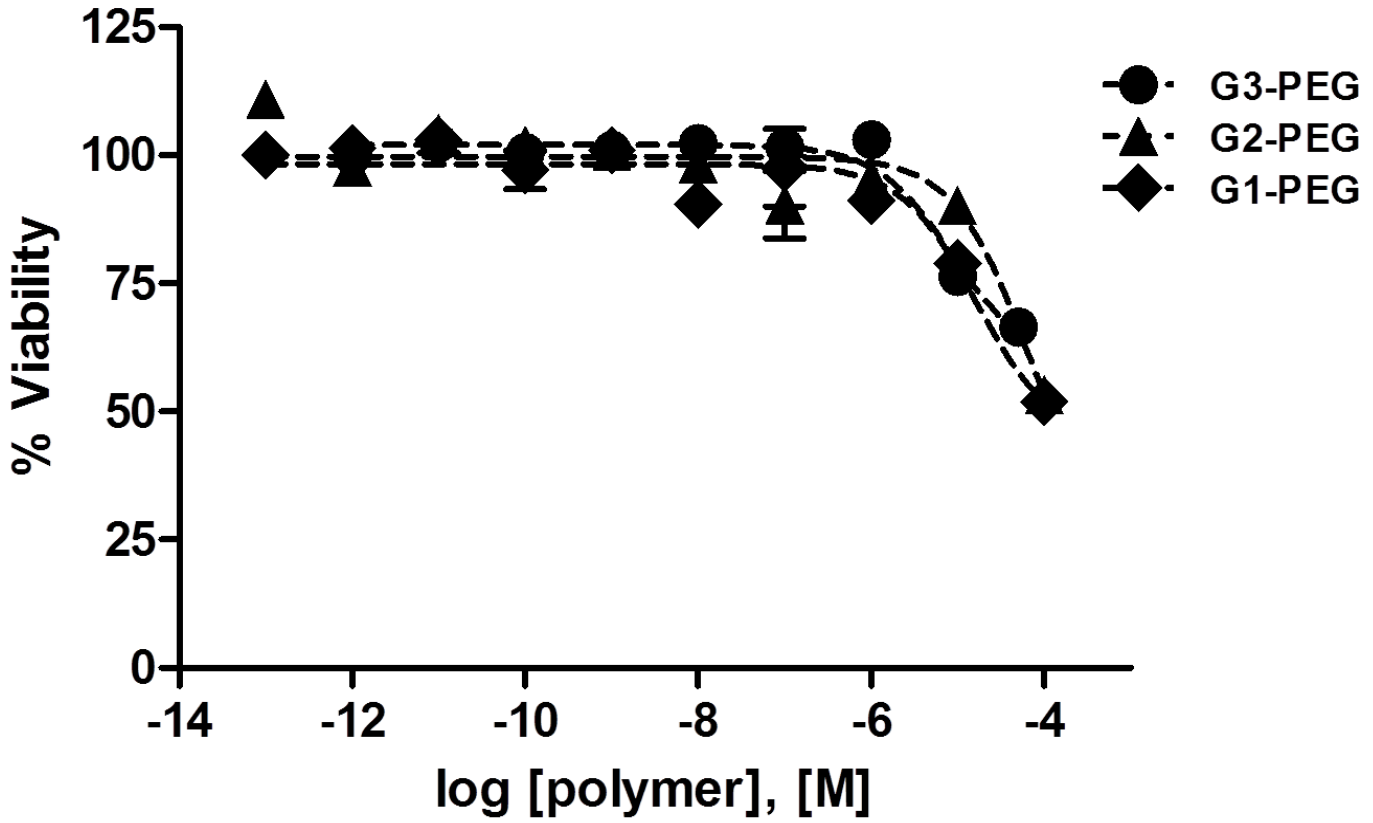

Figure A.3. HUVEC cell viabilities of DPDs after 48h continuous treatment.

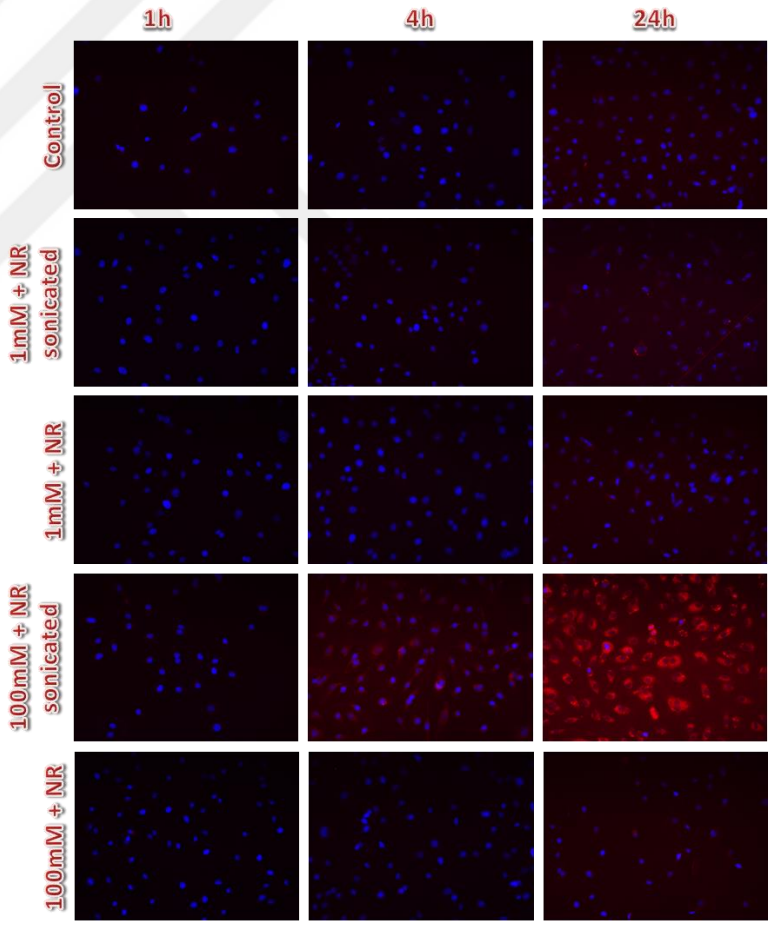

Figure A.4. Nile Red doped micelles containing 100mM and 1mM of G3-PEG,or 100mM G3-PEG polymer and Nile Red added separately without sonication

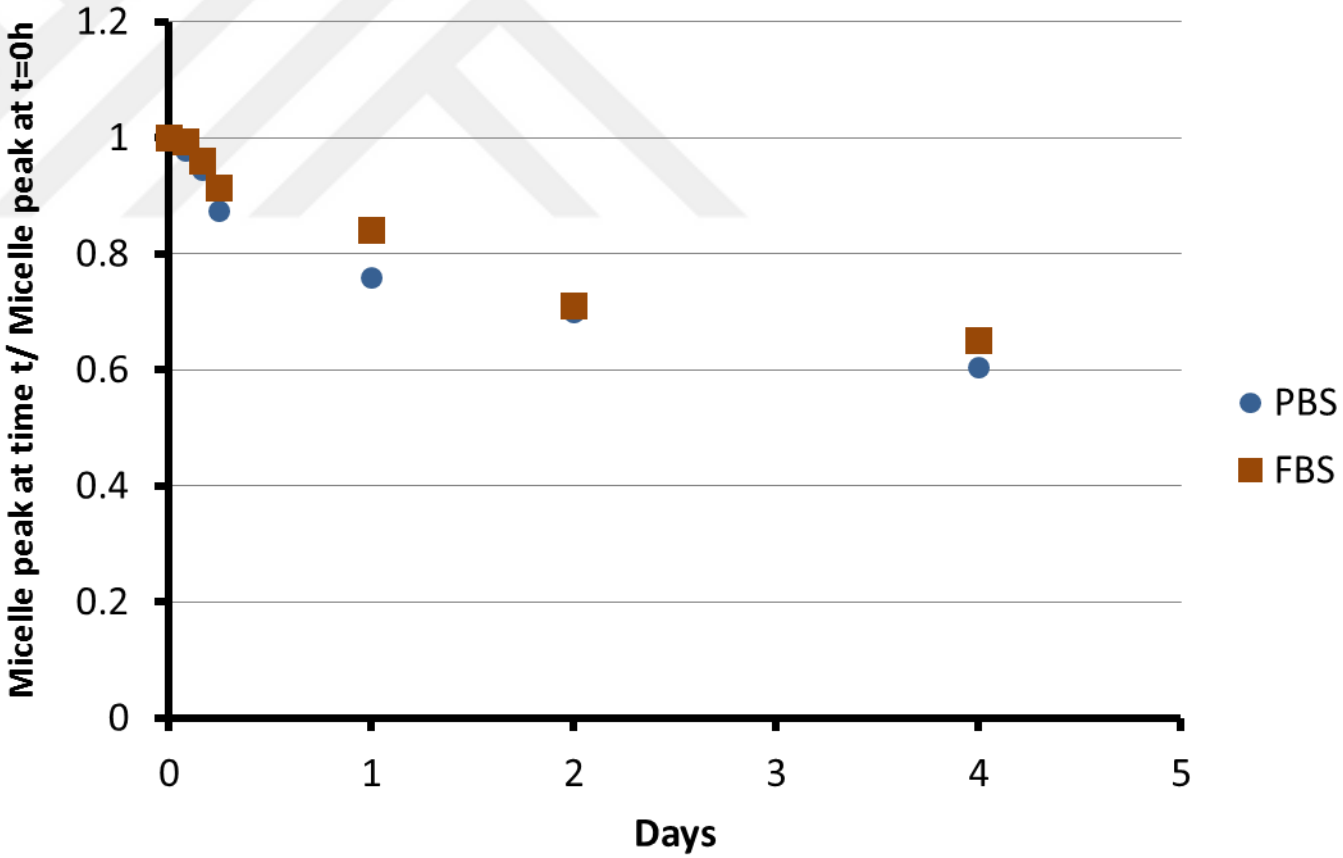

Figure A.5. Serum stability of Comb-G3-PEG micelles.

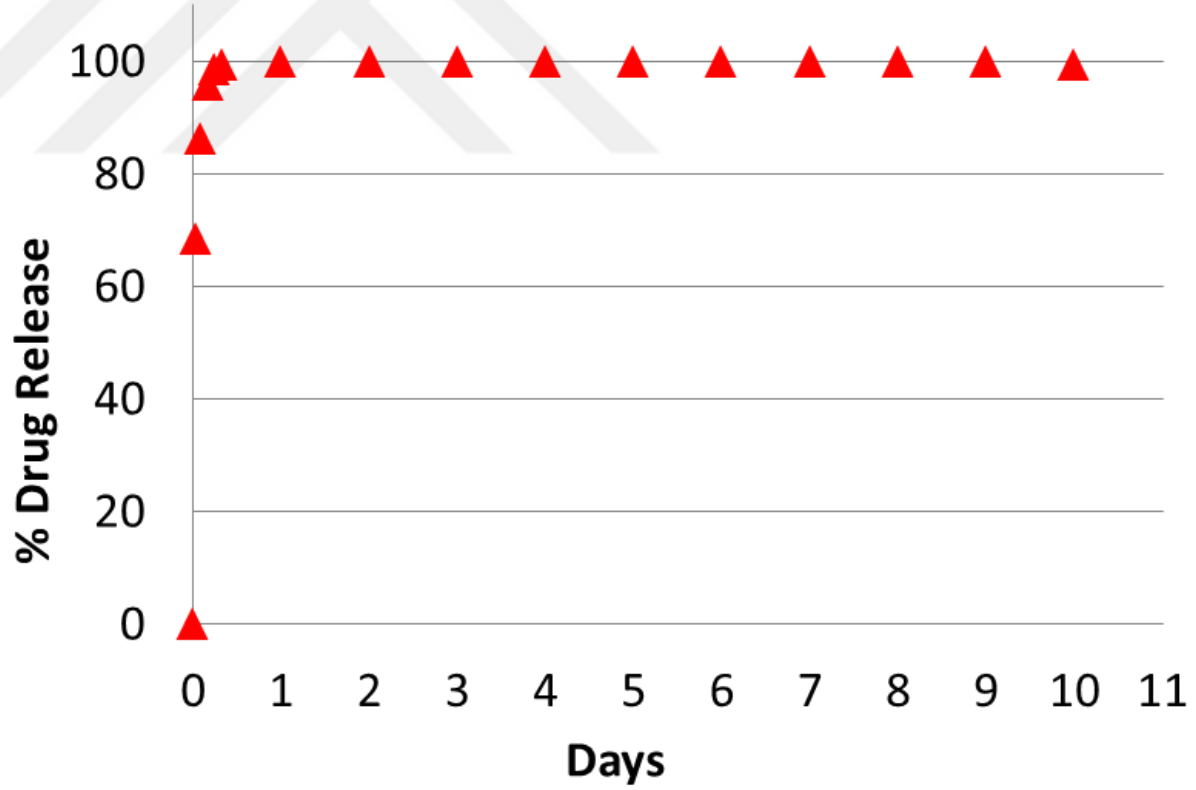

Figure A.6. Free CA4 release profile.

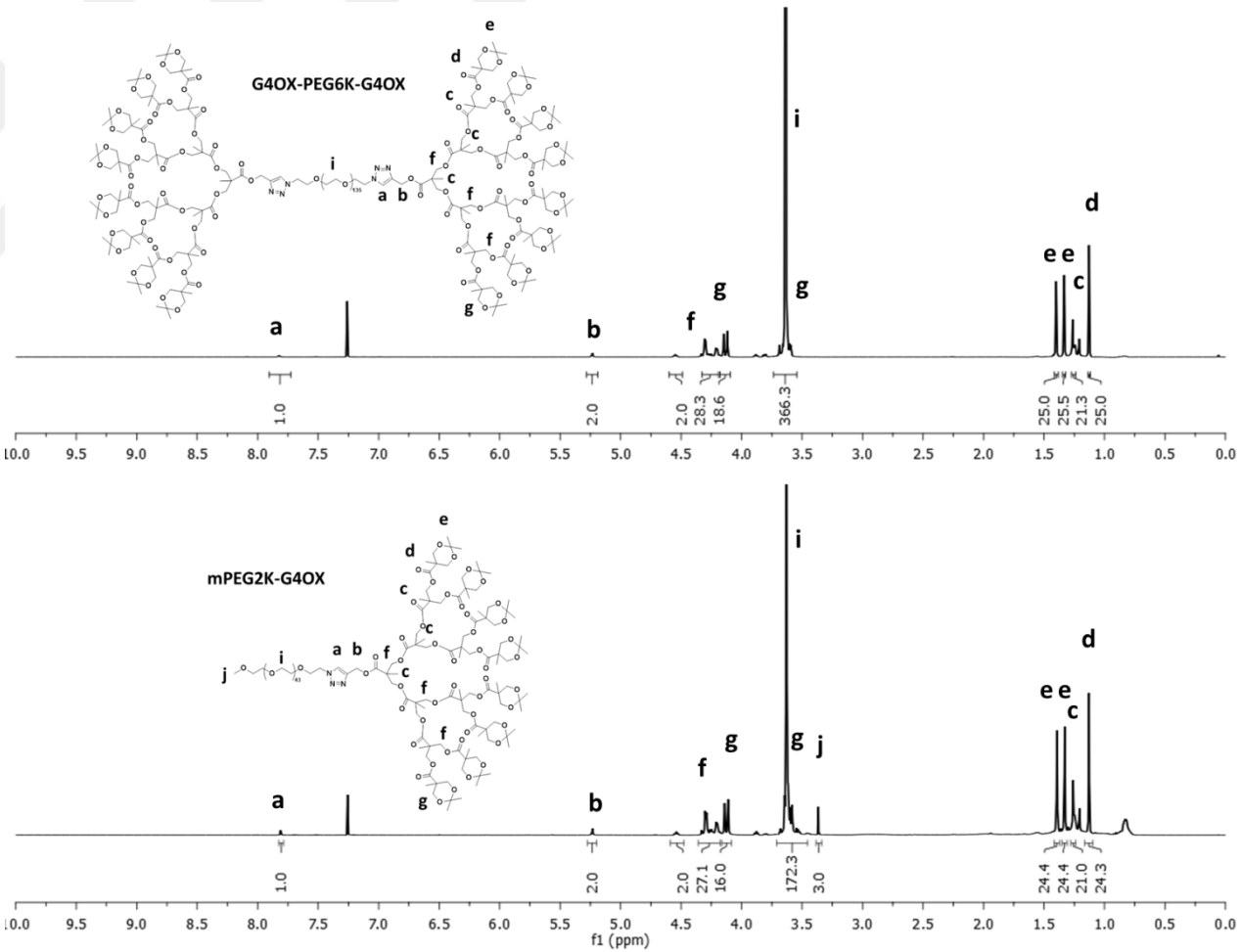

Figure A.7. ^{1}H-NMR of mPEG2K-G4OX (2K) and G4OX-PEG6K-G4OX (6K).

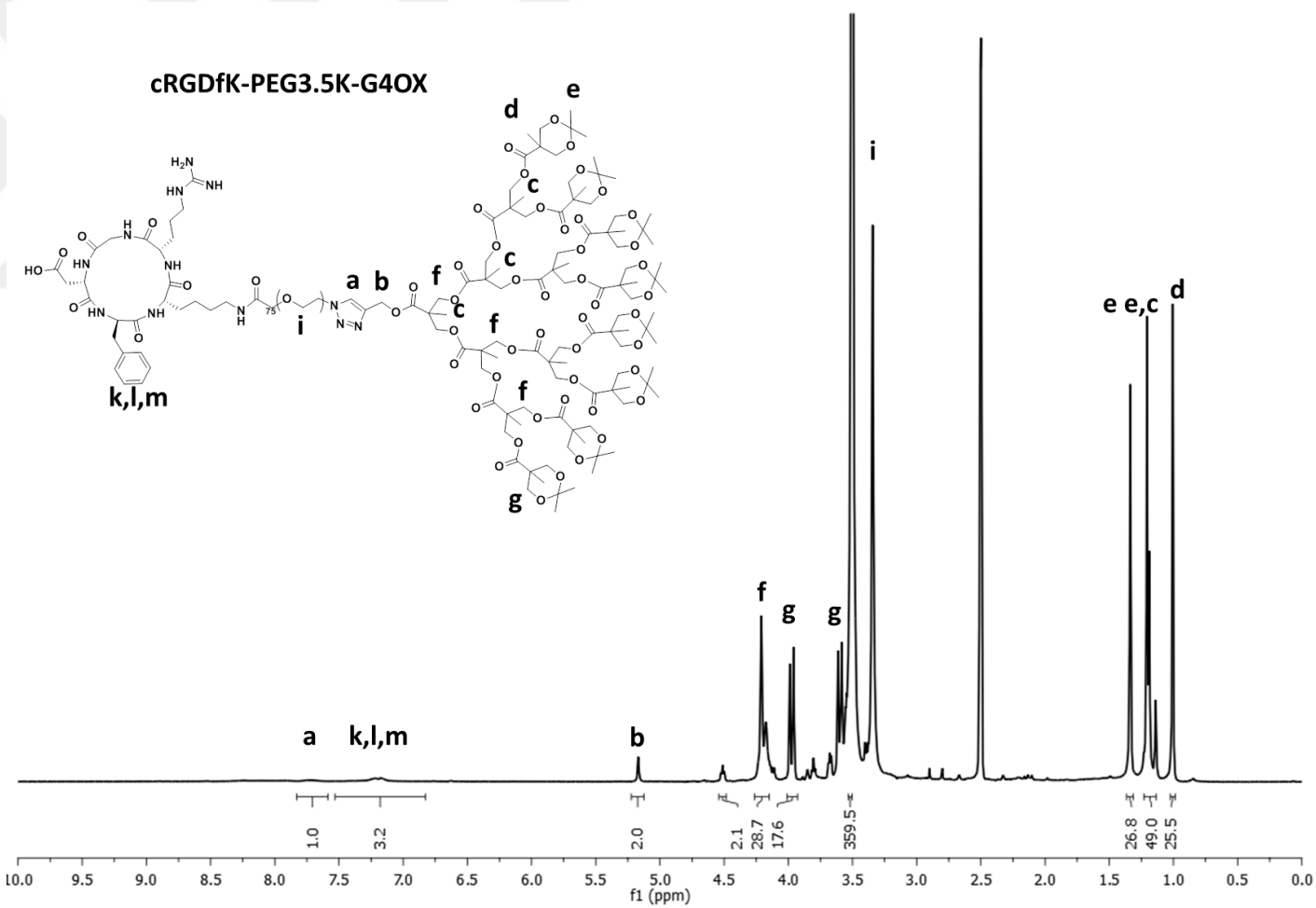

Figure A.8. ^{1}H-NMR of secondary construct cRGDfK-PEG3.5K-G4OX.

	Size*, ‡	Std ‡	PDI
2K 100-0	145.3	±63.9	0.100
2K 90-10	138.7	±63.6	0.112
2K 80-20	148.5	±71.4	0.136
2K 60-40	163.9	±72.6	0.104

*from Volume Distribution, ‡in nm

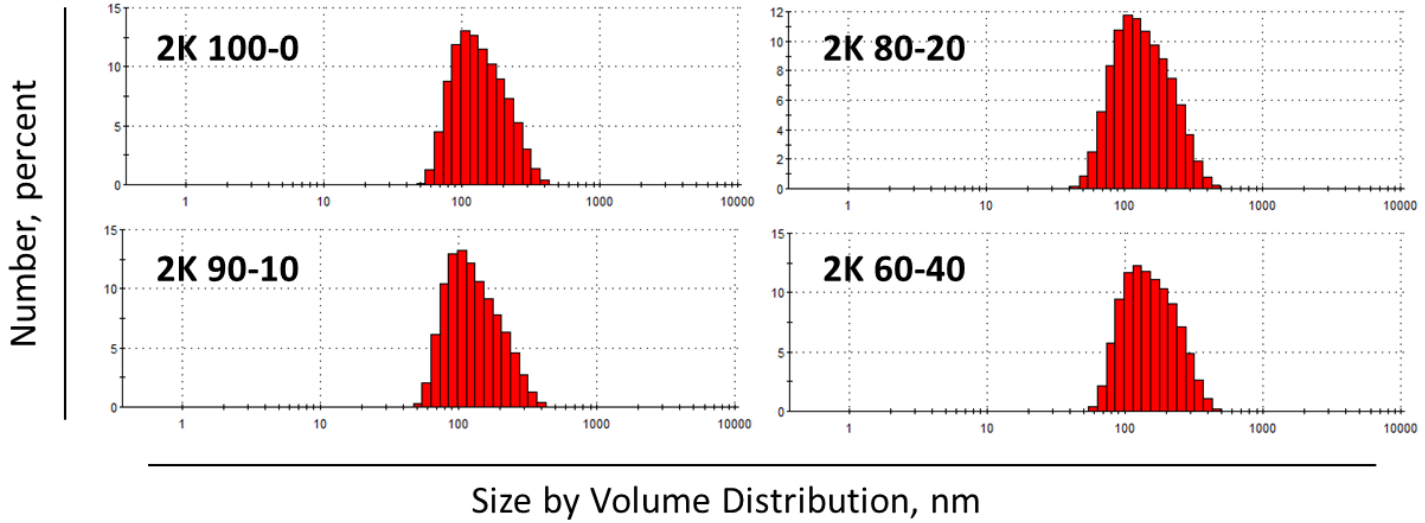

Figure A.9. DLS size and histograms of 2K micelles.

	Size*, ‡	Std ‡	PDI
6K 100-0	117.5	±51.37	0.120
6K 90-10	128.3	±56.35	0.109
6K 80-20	133.4	±58.64	0.097
6K 60-40	138.5	±102.4	0.201

*from Volume Distribution, ‡in nm

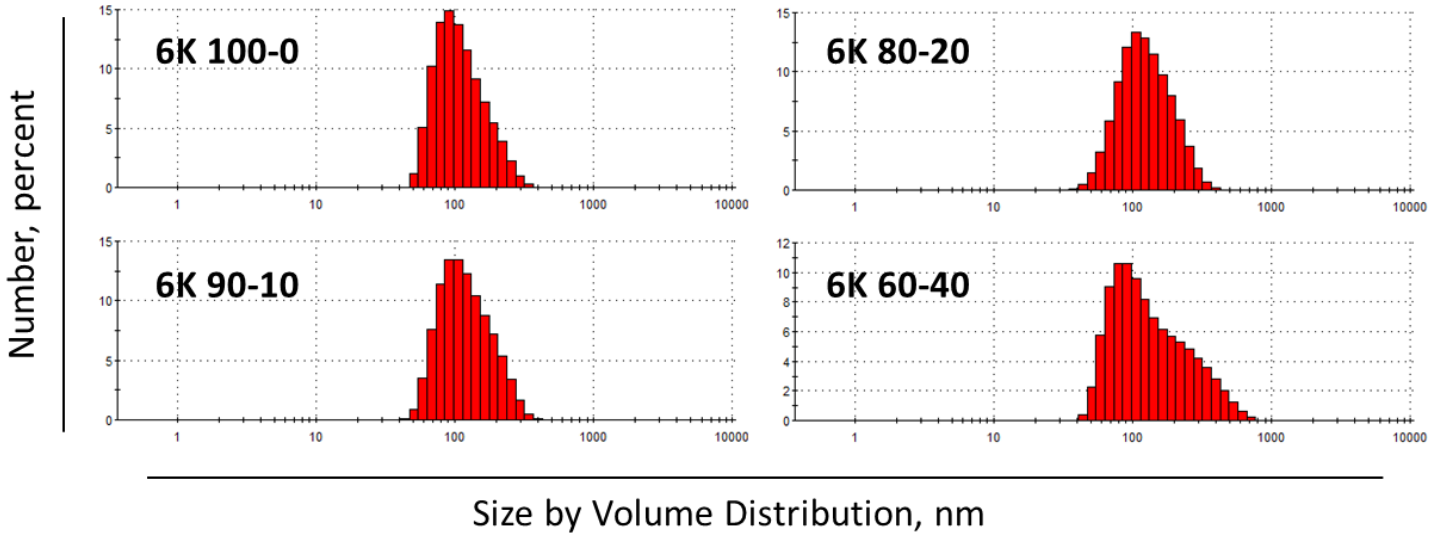

Figure A.10. DLS size and histograms of 6K micelles.

	Size*, ‡	Std ‡	PDI
2K 100-0 X	173.1	±88.2	0.212
2K 90-10 X	167.5	±78.0	0.168
2K 80-20 X	188.8	±92.0	0.198
2K 60-40 X	197.8	±107.2	0.180

*from Volume Distribution, ‡in nm

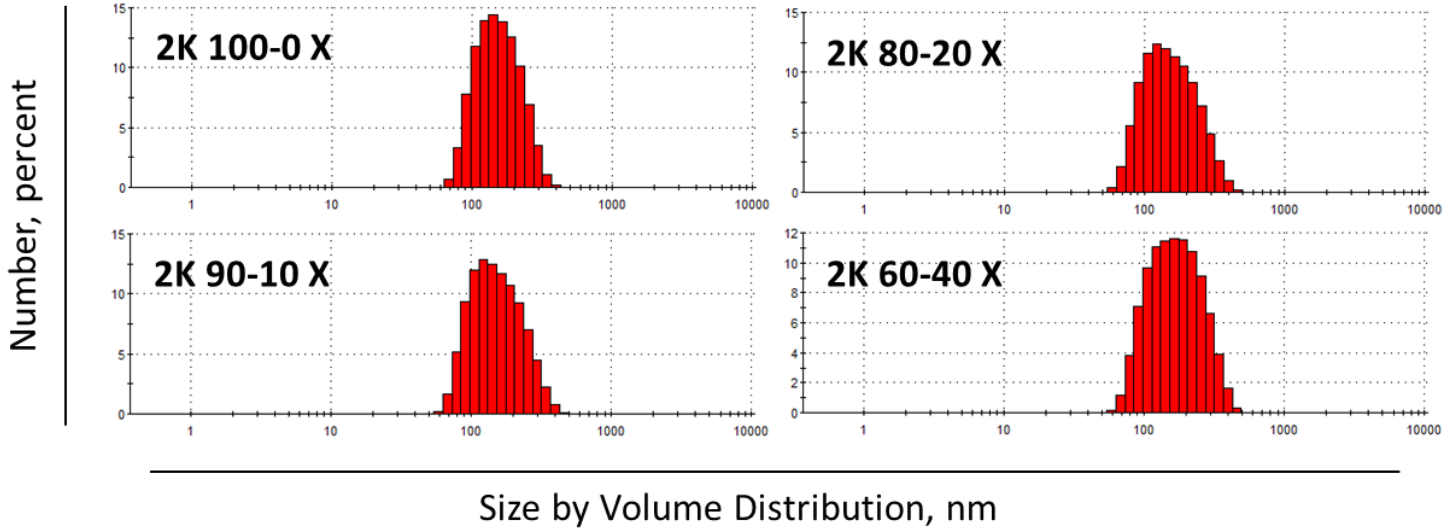

Figure A.11. DLS size and histograms of drug loaded 2K-X micelles.

	Size*, ‡	Std ‡	PDI
6K 100-0 X	226.2	±113.7	0.232
6K 90-10 X	217.7	±108.8	0.210
6K 80-20 X	182.2	±82.3	0.137
6K 60-40 X	188.0	±94.2	0.182

*from Volume Distribution, ‡in nm

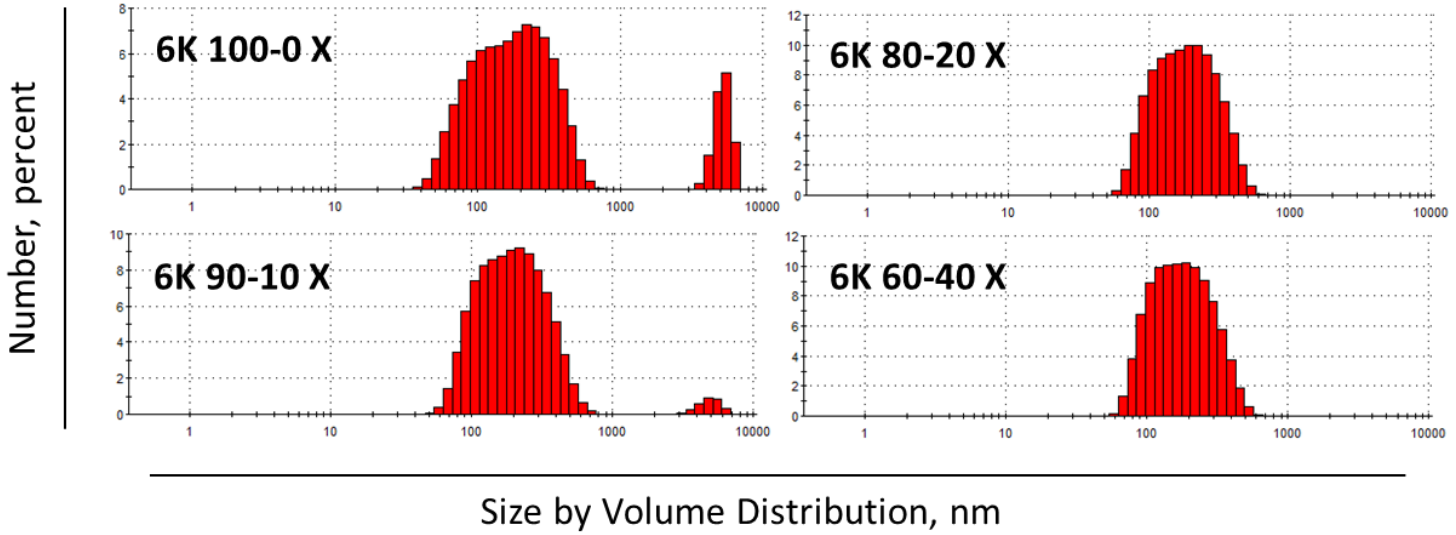

Figure A.12. DLS size and histograms of drug loaded 6K-X micelles.

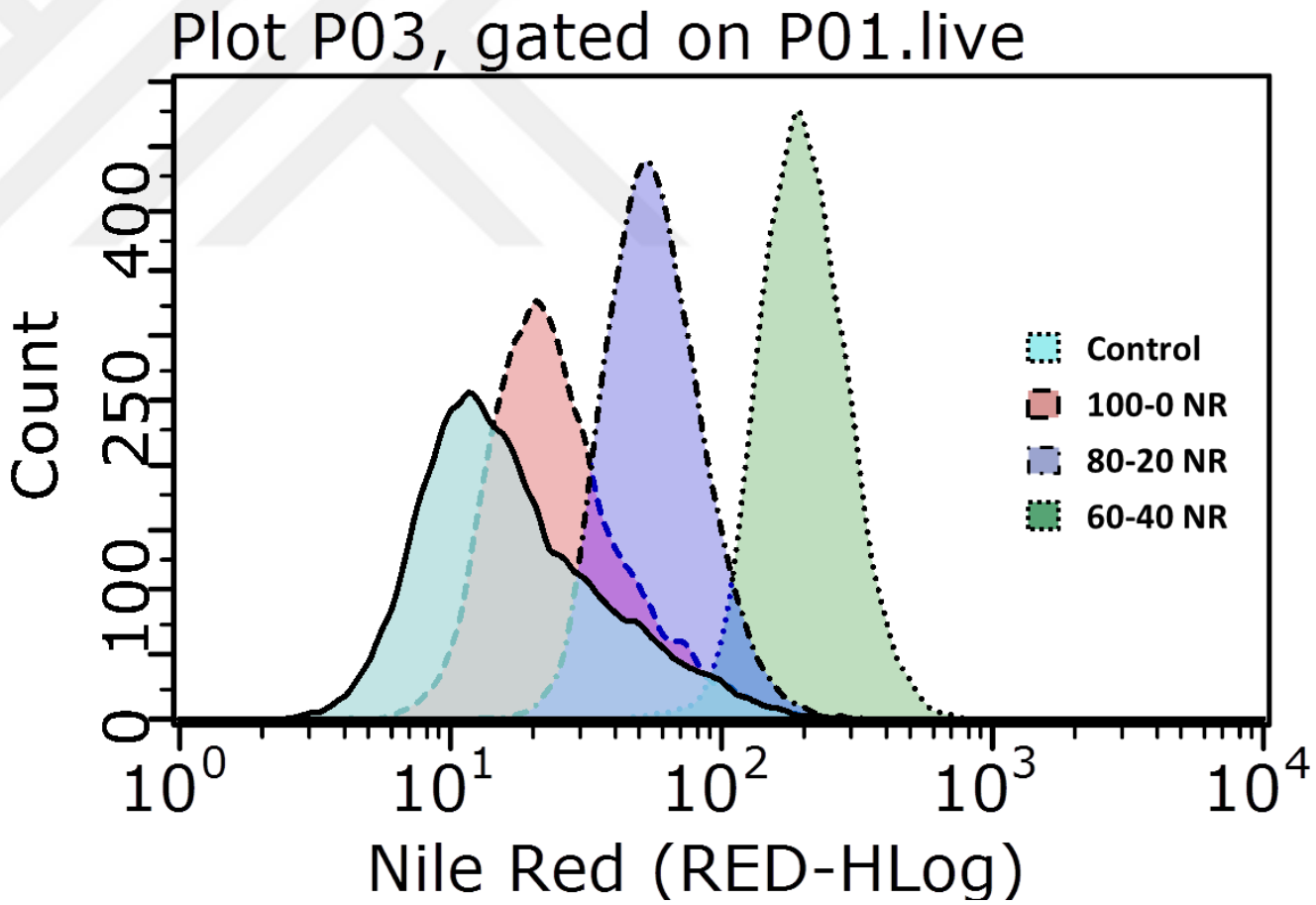

Figure A.13. Effect of secondary construct amount on MDA-MB-231 cell internalization.

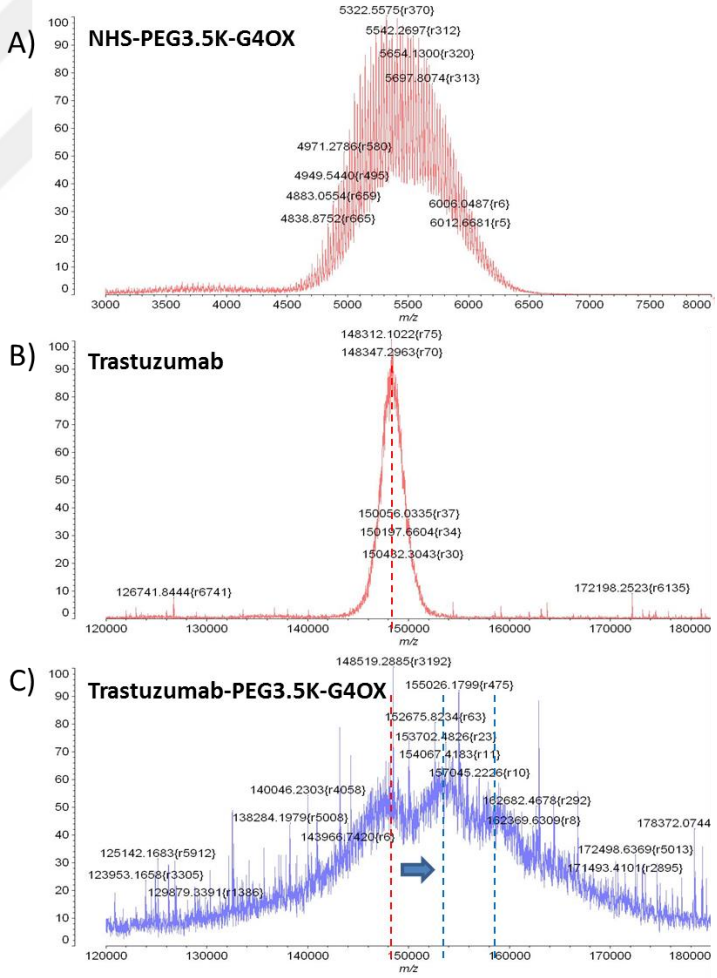

Figure A.14. MALDI-TOF analysis of A) NHS-PEG3.5K-G4OX, B) trastuzumab and C) trastuzumab-PEG3.5K-G4OX.

A)

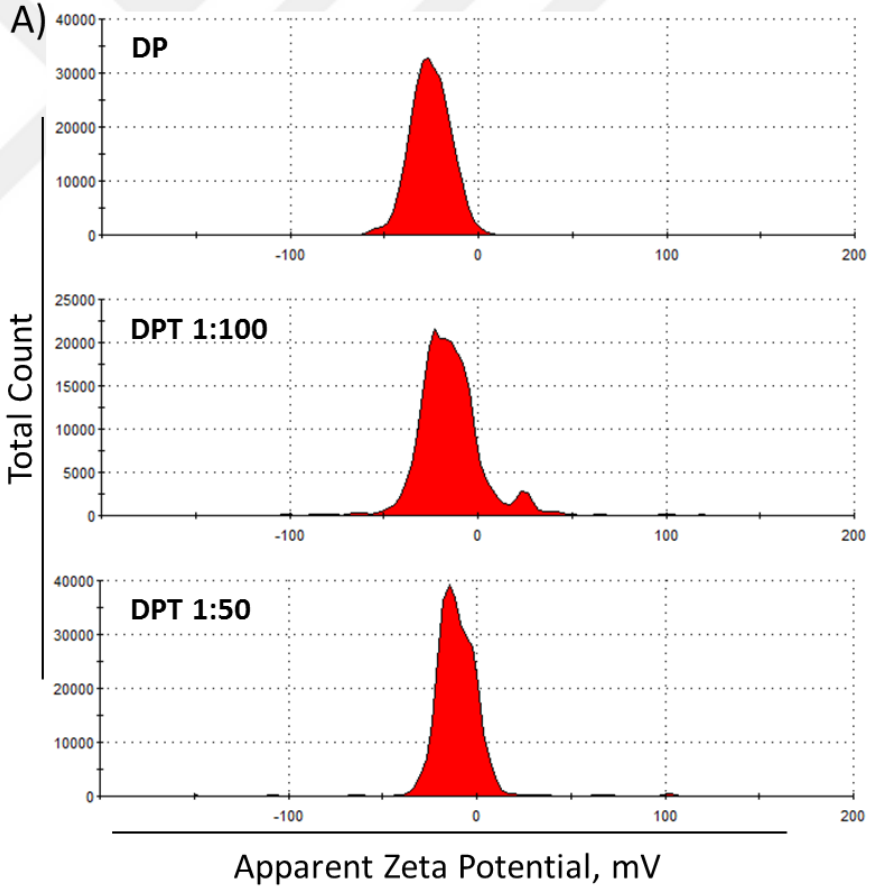

B)

Micelle	Media	ZP
DP	H_2O	-25.3 ±1.25
DPT 1:100	H_2O	-14.2 ±1.97
DPT 1:50	H_2O	-9.13 ±2.53
DP	PBS	-5.3 ±1.79
DPT 1:100	PBS	-2.6 ±1.17
DPT 1:50	PBS	-5.8 ±1.29

Figure A.15. Zeta potential A) histograms and B) values .

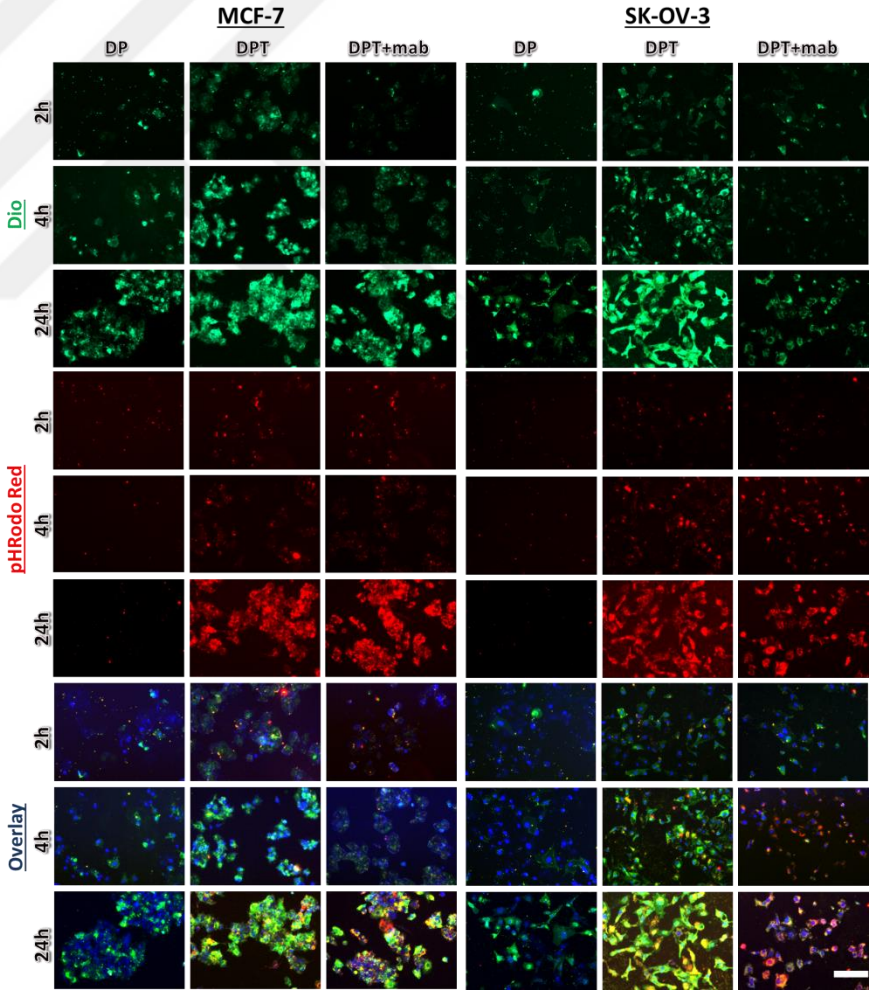

Figure A.16. Cell internalization data displaying separate channels. Scale bar 25 µm.